

KAUNAS UNIVERSITY OF TECHNOLOGY

MAKSYM TATARIANTS

**SOLVENT TREATMENT OF WASTE PRINTED
CIRCUIT BOARDS AND SUBSEQUENT
REPROCESSING INTO HIGH ADDED VALUE
PRODUCTS**

Doctoral dissertation

Technological Sciences, Environmental Engineering (T 004)

2019 Kaunas

This doctoral dissertation was prepared at Kaunas University of Technology, Faculty of Chemical Technology, Department of Environmental Technology during the period of 2016–2019. The studies were supported by Research Council of Lithuania.

Scientific Supervisor:

Prof. Dr. Gintaras DENAFAS (Kaunas University of Technology, Technological Sciences, Environmental Engineering, T 004).

Scientific Advisor:

Dr. Ahmed Samy Yousef SAED (Kaunas University of Technology, Technological Sciences, Mechanical Engineering, T 009).

Doctoral dissertation has been published in:

<http://ktu.edu>

Editor:

Dr. Armandas Rumšas (Publishing Office “Technologija”).

© M. Tatariants, 2019

ISBN 978-609-02-1614-9

The bibliographic information about the publication is available at the National Bibliographic Data Bank (NBDB) of Martynas Mažvydas National Library of Lithuania.

KAUNO TECHNOLOGIJOS UNIVERSITETAS

MAKSYM TATARIANTS

SPAUSDINTINIŲ PLOKŠČIŲ ATLIEKŲ
APDOROJIMAS TIRPIKLIAIS IR TOLESNIS
PERDIRBIMAS Į AUKŠTOS PRIDĖTINĖS
VERTĖS PRODUKTUS

Daktaro disertacija

Technologijos mokslai, Aplinkos inžinerija (T 004)

2019, Kaunas

Disertacija rengta 2016–2019 metais Kauno technologijos universiteto Cheminės technologijos fakulteto Aplinkos technologijų katedroje. Mokslinius tyrimus rėmė Lietuvos mokslo taryba.

Mokslinis vadovas:

Prof. dr. Gintaras DENAFAS (Kauno technologijos universitetas, technologijos mokslai, aplinkos inžinerija, T 004)

Mokslinis konsultantas:

Dr. Ahmed Samy Yousef SAED (Kauno technologijos universitetas, technologijos mokslai, mechanikos inžinerija, T 009).

Interneto svetainės, kurioje skelbiama disertacija, adresas:

<http://ktu.edu>

Redagavo:

Dr. Armandas Rumšas (leidykla “Technologija”)

© M. Tatarjants, 2019

ISBN 978-609-02-1614-9

Leidinio bibliografinė informacija pateikiama Lietuvos nacionalinės Martyno Mažvydo bibliotekos Nacionalinės bibliografijos duomenų banke (NBDB).

Table of Contents

List of Tables	8
List of Figures	9
Abbreviations	14
Introduction	15
1. Literature Review	21
1.1. Electrical and Electronic Waste and Waste Printed Circuit Board (WPCB) Management	21
1.1.1. Structure and composition of WPCBs	23
1.1.2. Life-cycle of WPCBs	25
1.1.3. Environmental issues caused by utilization of WPCBs	26
1.2. WPCB treatment/recycling technologies	30
1.2.1. Mechanical and physical treatment	30
1.2.2. Thermal treatment	33
1.2.3. Chemical treatment	36
1.3. Applications of secondary raw materials recovered from WPCBs	42
1.3.1. Non-metallic fraction	42
1.3.2. Metallic fraction, reprocessing into nanomaterials	43
1.4. Summary of the Literature Review	46
2. MATERIALS AND METHODS	50
2.1. Waste Printed Circuit Board samples	51
2.2. Consumable materials	56
2.3. Preliminary experiments (milled samples)	57
2.4. Indication of optimum separation conditions	58
2.5. Separation of mechanical specimens	59
2.6. Full-size WPCB experiments	60
2.6.1. Random Access Memory (RAM)	60
2.6.2. Video Card	62
2.6.3. Motherboard	63
2.7. Solvent Regeneration	65
2.8. Electrospraying	66
2.9. Synthesis of antimicrobial nanoparticles	69
2.10. Leaching and precipitation of micro/nanoparticles	72
2.11. Characterizations	74
2.12. Statistical methods and economic benefit/Carbon Footprint calculation methods	76
3. RESULTS AND DISCUSSIONS	77
3.1. Preliminary experiments (milled samples)	79
3.1.1. Solid-to-liquid ratio	79
3.1.2. Treatment time	82

3.1.3. Centrifugation	84
3.1.4. Final concentrations of Epoxy resin	84
3.1.5. Fiberglass of milled samples.....	86
3.1.6. Metal of milled samples.....	87
3.1.7. Conclusion: preliminary experiments.....	89
3.2. Indication of optimum separation conditions	89
3.2.1. Separation temperature and separation mechanism	90
3.2.2. Conclusion: optimum separation conditions.....	97
3.3. Mechanical testing of recovered fiberglass	98
3.3.1. Conclusion: Mechanical testing of recovered fiberglass	101
3.4. Full-size WPCB experiments.....	101
3.4.1. Full-size WPCBs – separation trends	101
3.4.2. Structure of full-size WPCBs.....	105
3.4.3. Recovered epoxy resin: full-size WPCBs.....	106
3.4.4. Recovered metallic components: full-size WPCBs.....	109
3.4.5. Regeneration of spent solvent	112
3.4.6. Conclusion: full-size WPCB experiments	113
3.5. Recycling rate evaluation (Solvent treatment).....	114
3.6. Preliminary economic and Carbon Footprint analysis (Solvent treatment).....	116
3.7. Indication of the material application field (Solvent treatment).....	118
3.8. Electrospraying of nanoparticles.....	120
3.8.1. Nanoparticle preparation.....	120
3.8.2. Analysis of obtained nanoparticles.....	122
3.8.3. Conclusion: Electrospraying of nanoparticles	123
3.9. Green synthesis of nanoparticles	124
3.9.1. Nanoparticle preparation and synthesis	124
3.9.2. Antimicrobial tests	126
3.9.3. Conclusion: Green synthesis of nanoparticles	127
3.10. Leaching and precipitation of micro/nano particles.....	128
3.10.1. Optimum leaching conditions	128
3.10.2. Analysis of Micro-fraction.....	129
3.10.3. Analysis of Nano-fraction.....	131
3.11. Recycling rate evaluation (Reprocessing)	132
3.12. Preliminary economic and Carbon Footprint analysis (Reprocessing)	134
3.13. Indication of the material application field (Reprocessing)	136
CONCLUSIONS	140
REFERENCES	141
LIST OF SCIENTIFIC PUBLICATIONS ON THE DISSERTATION TOPIC	159

ANNEXES160

List of Tables

Table 1.1.1. Characterization of materials embedded into generic WPCBs	24
Table 1.1.2. Exposure sources of heavy metals from e-waste	28
Table 1.4.1. Generalized comparison of current WPCB treatment/recycling technologies (based on the technology comparisons done by Awasthi <i>et al.</i> (2017) and Ning <i>et al.</i> (2017)	46
Table 2.1.1. Selected WPCBs and their properties	55
Table 2.2.1. Properties of the used solvent	56
Table 2.3.1. WPCB models and sample codes	57
Table 2.4.1. WPCB models and sample codes	58
Table 3.5.1. General recycling rates for all sample types.....	114
Table 3.6.1. Summary of preliminary economic analysis for solvent treatment of WPCBs (calculated for one tonne of waste)	117
Table 3.6.2. GHG emissions from waste Motherboard recycling by the developed approach	118
Table 3.11.1. General recycling rates of the used reprocessing methods	133
Table 3.12.1. Summary of preliminary economic analysis for reprocessing of WPCBs (calculated for 100 kg of waste)	135
Table 3.12.3. GHGE from Leaching treatment of Through-Hole Solder Joints	136

List of Figures

Figure 1.1.1. Examples of PCB types	22
Figure. 1.1.2. WEEE collection system in Finland	25
Figure 1.1.3. Formal and informal E-waste treatment routes in China	26
Figure 1.1.4. Waste PCBs from all kinds of electronic equipment	27
Figure. 1.1.5. Environmental risks of primitive WPCB recycling techniques: (a) precious metals recovery by acid leaching; (b) unprotected WPCB dismantling; (c) open burning of WPCBs	27
Figure 1.1.6. WEEE-generated pollution in China	28
Figure 1.2.1. Hammer milling of WPCBs	31
Figure 1.2.2. Corona electrostatic separator	32
Figure 1.2.3. Eddy Current separator	33
Figure 1.2.4. Flow of heavy metals from the WEEE dismantling residues in the incinerator	34
Figure 1.2.5. Setup for pyrolysis process	35
Figure 1.2.6. Typical scheme of a leaching reactor: for WPCBs 1) mechanical stirrer; (2) propeller; (3) leaching pulp; (4) sampler; (5) thermometer; (6) feeder; (7) water thermostat; (8) crushed PCBs	37
Figure 1.2.7. Bioleaching unit for WPCB treatment	38
Figure 1.2.8. Experimental setup for solvent treatment of WPCBs	41
Figure 1.3.1. Example of metallic and non-metallic fractions recovered from WPCBs	42
Figure 1.3.2. Recovered fiberglass for sound insulation application	43
Figure 1.3.3. Pyrolysis products: A) WPCBs before treatment, B) Carbon-rich slug, C-D) Metal-rich phases E) Copper-rich metallic phase obtained after heat treatment at 1150 °C	44
Figure 1.3.4. Metallic foils obtained after solvent treatment	44
Figure 2.1. Structure of the experiments in the thesis (the numbered boxes correspond to the subsections in the materials and methods Section).....	50
Figure 2.1.1. WPCB powder after the milling process (sample codes in Table 2.1.1., section “Powder”)	52
Figure 2.1.2. WPCB samples (10 mm) after cutting (sample codes in Table 2.1.1., section “Separation specimens”)	52
Figure 2.1.3. Images of: A) blank PCB; B) red; C) green; D) yellow; E) violet; and F) blue mechanical specimens (sample codes in Table 2.1.1., section “Mechanical specimens”)	53
Figure 2.1.4. Image of a waste RAM card with its dimensions	53
Figure 2.1.5. Image of waste Video Card with dimensions	54

Figure 2.1.6. Image of: A) Waste motherboard and B) Motherboard layout according to manufacturer manual	54
Figure 2.3.1. Five WPCB models used in the present research	57
Figure 2.3.2. WPCB powder: (A) before ultrasonication and (B) after ultrasonication	58
Figure 2.4.1 Schematic flow chart for the separation process experiments	59
Figure 2.5.1. A) Developed WPCB separator and B) separation unit	60
Figure 2.6.1. Schematic flowchart of waste RAM separation and liberation of precious metals	60
Figure 2.6.2. Two-unit reactor for simultaneous dissolution and ultrasonic treatment of RAMs	61
Figure 2.6.3. Steps followed to liberate gold from contacts: A) recovered contacts; B) pure nitric acid; C) dissolution of copper and nickel; D) liberation of gold; and E) obtained gold powder	62
Figure 2.6.4. Schematic flowchart of the waste video card separation experiments	62
Figure 2.6.5. Development of the traditional ultrasonic bath (reactor) for Video Card separation	63
Figure 2.6.6. Schematic flowchart for motherboard (MB) separation and liberation of metals	64
Figure 2.6.7. Schematic drawing of the developed reactor	65
Figure 2.7.1. Schematic sketch of the solvent regeneration and epoxy resin extraction process	66
Figure 2.8.1. Schematic flowchart for the synthesis and characterization of Cu-NPs	66
Figure 2.8.2. A) Modified WPCB separator, B, C, D, E) Recovered layers and components of WPCBs (Compound unit, Substrate, Recovered metal, and fiberglass respectively)	67
Figure 2.8.3. Steps followed to produce copper (II) acetate	68
Figure 2.8.4. Composite NP synthesis mechanism for Electrospraying process	69
Figure 2.9.1. Schematic flowchart for green synthesis and characterization of Cu-NPs	70
Figure 2.9.3. Images illustrating Cu-NPs preparation steps: (A) Copper Sulfate water solution; (B) Ascorbic Acid/ β -cyclodextrin water solution; (C) Beginning of the reduction process; (D) End of the reduction process; and (E) Final shape of the produced powder	71
Figure 2.9.4. Images of the prepared Cu-NPs suspensions (A) at the beginning and (B) after 22hrs.	72
Figure 2.10.1. Schematic flowchart of the micro/nanoparticle preparation and copper recovery	73

Figure 2.11.1. A) Fixation of a mechanical sample in the Universal Testing Machine and B) image of full-size mechanical samples at the end of the test	75
Figure 3.1. Structure of the results and discussions Section (the numbered boxes correspond to the subsections in the results Section)	77
Figure 3.1.1. Metallographic images of some of milled WPCB samples (sample codes in Tab. 2.3.1.)	79
Figure 3.1.2. Effect of solid-to-liquid ratio on Epoxy Resin concentration (generalized results obtained from tests on all sample types): A) Experimental results and B) Derived linear regression dependencies	80
Figure 3.1.3. Dependence between solid-to-liquid ratio and the respective Epoxy Resin concentrations linear regression slope coefficients and the derived cubic polynomial regression	81
Figure 3.1.4. Dependence between BER concentration (C_{BER}), time (t), and solid-to-liquid ratio (s/l) as calculated by using the specified equation	82
Figure 3.1.5. Effect of treatment time on Epoxy Resin concentration (sample codes in Table 2.3.1.): A) Experimental results; B) Derived cubic polynomial regressions	83
Figure 3.1.7. WPCB structure; (B) milled WPCBs; and (C) Layers of milled WPCBs after the centrifugation of powder: (A) before ultrasonication and (B) after ultrasonication	84
Figure 3.1.8. Absorbance of BER/DMF samples before centrifugation (sample codes in Table 2.3.1.)	85
Figure 3.1.9. Very fine fiberglass particles dispersed in BER/DMF samples: (a) Red; (b) Violet; (c) Blue; (d) Green; and (e) Yellow (sample codes in Table 2.3.1.)	85
Figure 3.1.10. A) Absorbance of BER/DMF samples after centrifugation and B) Concentration of BER in DMF (sample codes in Table 2.3.1.)	86
Figure 3.1.11. Purification steps of recovered milled fiberglass at different treatment times: A) 30 min.; B) 60 min.; C) 90 min.; D) 120 min.; E) 150 min.; F) 180 min.; G) 210 min.; H) 240 min.	87
Figure 3.1.12. SEM images of recovered metal powder: lamella-like particles of (A) Blue sample and (B) Violet sample (sample codes in Table 2.3.1.)	88
Figure 3.1.13. Chemical composition of recovered metal powder samples (sample codes in Table 2.3.1.)	89
Figure 3.2.1. Separation time of WPCB samples (sample codes in Table 2.4.1.)	90
Figure 3.2.2. Regression modeling of the dependencies between separation time (t) and temperature (T): A–E) Graphical representation of regression models for individual samples; F) Graphical representation of regression models for average data; G) Regression equations and R^2 coefficients	91
Figure 3.2.3. Brominated Epoxy Resin concentration trends for: A) Yellow; B) Red sample (sample codes in Table 2.4.1.)	92
Figure 3.2.4. Linear regression models of BER concentration trends for: A) Yellow sample; B) Red sample (sample codes in Table 2.4.1.)	93

Figure 3.2.5. Linear regression models of BER concentration trends based on the average of all experimental values	94
Figure 3.2.6. Dependence between regression slope coefficients (of BER concentration trends regression models) and temperature	94
Figure 3.2.7. Dependence between concentration of epoxy resin (C_{BER}), time (t) and temperature (T), calculated by using the specified equation	95
Figure 3.2.8. Concentration of BER in DMF of WPCB samples (sample codes in Tab. 2.4.1.)	95
Figure 3.2.9. Regression modeling of the dependencies between concentration of Epoxy Resin (C_{BER}) time and temperature (T): A–E) Graphical representation of regression models for individual samples; F) Graphical representation of regression model for average data; G) Regression equations and R^2 coefficients	96
Figure. 3.2.10. WPCB separation mechanism	96
Fig. 3.2.11. Relation between average separation time and final BER concentration in respect to the treatment temperature	97
Figure 3.3.1. Stress-strain curves of plain woven fiberglass samples extracted from WPCBs in: A) Plain; B) single-notched; and C) multi-notched cases (sample codes in Table 2.5.1.)	99
Figure 3.4.1. Separation time: Random Access Memory (RAM), Video Card (VC), and Motherboard (MB)	101
Figure 3.4.2. Correlation between surface area and separation time for cut specimens, Random Access Memory (RAM), Video Card (VC), and Motherboard (MB)	102
Figure 3.4.3. Correlation between mass and separation time for Cut specimen, Random Access Memory (RAM), Video Card (VC), and Motherboard (MB)	103
Figure 3.4.4. Types and number of complete layers found inside Random Access Memory (RAM), Video Card (VC), and Motherboard (MB)	103
Figure 3.4.5. Regression models for determining the separation time of WPCB specimen (t) under the developed treatment based on: A) sample surface area (S), B) sample mass (m)	104
Figure 3.4.5. Random Access Memory: a reconstruction of layers and elements ...	105
Figure 3.4.6. Video Card: a reconstruction of layers and elements	106
Figure 3.4.7. The reconstruction of layers and elements of cut WPCB samples (the cut samples were originally prepared from motherboard specimens)	106
Figure 3.4.8. Typical FTIR spectra of thin epoxy residue film	107
Figure 3.4.9. Typical SEM-EDS analysis of recovered epoxy resin	108
Figure 3.4.10. Typical TGA-DTG analysis of recovered epoxy resin	108
Figure 3.4.11. Typical DSC curve of recovered BER sample	109
Figure 3.4.12. SEM-EDS analyses of recovered copper layers from (A) MB, (B) VC, and (C) RAM samples	109
Figure 3.4.13. SEM-EDS analysis of recovered Gold	111
Figure 3.4.14. Structure of Through-Hole Solder Joints	112

Figure 3.4.15. Average weight percentage of metals in the liberated THSJ	112
Figure 3.4.16. FTIR spectra of unused and regenerated DMF	113
Figure 3.6.1. Boundaries and economic performance of the developed technique (example of milled samples, calculations for 1 ton of input WPCBs)	116
Figure 3.8.1. Composite NP synthesis mechanism for Electrospraying process ...	120
Figure 3.8.2. SEM images of nanoparticles synthesized at A) 23 kV; B) 25 kV; C) 27 kV; and 29 kV	121
Figure 3.8.3. SEM images of Cu-NPs with scale A) 1 mm; B) 500 nm; and C) 300 nm (Electrospraying).....	122
Figure 3.8.4. A) SEM-EDS mapping of Cu-NPs, B, C) EDS analyses at points “1” and “2” (Electrospraying).....	122
Figure 3.8.5. HRTEM images of Cu-NPs (Electrospraying)	123
Figure 3.9.1. Copper (II) Sulfate solution produced from: (A, B, C) MB, VC, RAM; The obtained Copper (II) Sulfate from: (D, E, F) MB, VC, RAM sample	124
Figure 3.9.2. SEM-EDS images of Cu-NPs synthesized from: (A) MB; (B) VC; and (C) RAM	125
Figure 3.9.3. HRTEM images of Cu-NPs synthesized from: (A–C) MB; (D–F) VC; and (G–I) RAM	125
Figure 3.9.4. Representative batch growth profile in the presence of varying concentrations of synthesized Cu-NPs for: A) <i>E. coli</i> ; B) <i>P. aeruginosa</i> ; and C) <i>S. aureus</i> ; D) Optical density of <i>E. coli</i> culture grown overnight	126
Figure 3.10.1 Relation between solid-to-liquid ratio, temperature and THSJ leaching time	128
Figure 3.10.2. Images illustrating the leaching steps at different periods of time ...	129
Figure 3.10.3. SEM-EDS images of the Micro-fraction of THSJ _M (A ₁ –A ₂) and THSJ _V (B ₁ –B ₃)	130
Figure 3.10.4. A) SEM-EDS mapping of precipitated powder; B, C) EDS analysis	131
Figure 3.10.5. TEM images of (a) THSJ _M and (b) THSJ _V samples	132
Figure 3.12.1. Boundaries of the developed reprocessing technique (Leaching used as example)	135
Figure 3.13.1. The developed WPCB recycling/remanufacturing technology as a part of Circular Economy system (example of Copper nanoparticles)	137
Figure 3.13.2. Industrial technology for mass production of Micro/nano products from WPCBs	138

Abbreviations

BER – Brominated Epoxy Resin;
CE – Circular Economy;
CMOS - Complementary Metal Oxide Semiconductors;
DMF – Dimethylformamide;
DMSO – Dimethylsulfoxide;
DSC – Differential Scanning Calorimetry;
EEE - Electrical and Electronic Equipment;
EU – European Union;
FTIR - Fourier-Transform Infrared Spectroscopy;
GGE, GHGE – Greenhouse Gas Emissions;
HAVPs - High Added Value Products;
HRTEM – High-Resolution Transmission Electron Microscopy;
ICP-OES – Inductively Coupled Plasma;
LCCA - Life-Cycle Cost Analysis;
LED - Light-Emitting Diode;
MB – Motherboard;
MB – Video Card;
β-NCD - Native Beta-Cyclodextrin;
NMF – Non-Metallic Fraction;
NMP - *N*-Methyl-2-pyrrolidone;
NMR – Nuclear Magnetic Resonance;
PBBs - Polybrominated Biphenyls;
PBDEs - Polybrominated Diphenyl Ethers;
PMC - Phenolic Moulding Compound;
PP – Polypropylene;
PVA - Polyvinyl Alcohol;
RAM – Random Access Memory;
RoHS – Restriction of Hazardous Substances;
SCF – Supercritical Fluid;
SCM - Supercritical Methanol;
SCWO - Supercritical Water Oxidation;
SEM-EDS – Scanning Electron Microscopy – Energy Dispersive X-Ray Spectroscopy
StEP – Solving the E-Waste Problem;
TBBPA - Tetrabromobisphenol-A;
TEM - Transmission Electron Microscopy
TGA-DTG - Thermal Gravimetric Analysis - Differential Thermal Gravimetric;
THSJ – Through-Hole Solder Joints;
UV-VIS – Ultraviolet-Visible Spectroscopy;
WEEE – Waste Electrical and Electronic Equipment;
WPCBs – Waste Printed Circuit Boards;
XRD – X-ray Diffraction.

Introduction

We may wonder what are the words most associated with the 21st century. We can name a few of them: overpopulation, global warming, resource scarcity, global crisis, technological advance. All of these factors are interconnected:

- Technological advance improves conditions for living, which creates THE problem of Overpopulation;
- Overpopulation multiplied by Technological advance creates a huge Demand for resources;
- Intense Consumption of resources leads to the Resource scarcity and enormous Waste generation;
- Finally, Waste generation is the factor which results in Negative environmental impact; THIS can be best illustrated with the issue of Global warming.

Therefore, a question arises: are there any ways to solve these problems? The answer is: yes, there are. Talking globally, they are Sustainable Development, Low Carbon Economy, Resource Efficiency, Green Technology and Zero Waste approaches (Baker, 2005; Kooroshy, 2015; Mulvaney, 2011; Zaman, 2014). They aim towards reducing or completely removing the anthropogenic waste stream and optimizing the current use of resources and energy while employing such methods as renewable (wind, solar, bio-, tidal, wave, and hydro-) energy usage, waste recycling, reuse, reprocessing, designing eco-friendly products, etc.

All of these concepts are particularly relevant in the case of Waste Electrical and Electronic Equipment (WEEE). The end of the 20th century and the beginning of the 21st century were marked by major breakthroughs and overall advance in both industrial and scientific aspects. Among these achievements, the progress in electronics is worth to be distinguished since it is specifically electronics that caused the most significant impact on the human society during the abovementioned period. Internet, mobile networks and cell phones, personal computers – all of these as well as many other products of electronic technology became objects of the highest demand, which induced the respective growth of the electronic production industry. For this reason, large scale manufacturing quickly worsened the issue of WEEE – it is estimated that 50 million tons of E-waste could have been generated in 2018, and this amount is expected to increase progressively in the coming decades as a result of the technological progress and growing consumption rate (Pomponi & Moncaster, 2017). This type of waste is rich in many metals such as Copper (Cu), Tin (Sn), Lead (Pb), Aluminum (Al), etc. as well as precious metals like Gold (Au) and Palladium (Pd) (Chauhan, Jadhao, Pant, & Nigam 2018; Guo, Zhang & Xu, 2016; Zhang & Xu, 2016). This fact as well as the necessity to decrease the environmental risks and address the shortage of resources were the main drivers for many researchers to start developing techniques for extraction of these metals through various recycling routes (Dimitrakakis, Janz, Bilitewski & Gidarakos, 2009; Zhang, Ding, Liu & Chang, 2017).

Waste Printed Circuit Boards (WPCBs), being a type of WEEE, contain most of these metals; WPCBs themselves represent 10 wt.% of THE E-waste stream and

are composed of ~30 wt.% metallic fraction and ~70 wt.% non-metals (fiberglass and epoxy resin) (Jianbo Wang & Xu, 2015). Since the non-metallic fraction (NMF) represents the biggest part of WPCB mass while also containing some hazardous materials like Bromine (Br), a number of technologies were developed to recycle this type of waste, e.g., float-sink and triboelectric separation, etc. (Rajagopal, Rajarao, Cholake & Sahajwalla, 2017; Haifeng Wang *et al.*, 2018; Zhang *et al.*, 2017). However, due to the low economic return of NMF recycling, most of the developed studies focused on direct recovery of metals while using several techniques, such as supergravity separation, pyrometallurgical processing, pyrolysis, leaching, etc. (Evangelopoulos, Kantarelis & Yang, 2017; Meng *et al.*, 2017; Rocchetti, Amato & Beolchini, 2018; Huaidong Wang *et al.*, 2017; Žiukaitė, Ivanauskas, Tatarianis & Denafas, 2017).

It is worth mentioning that some techniques, especially bioleaching, employ low temperature treatment for extraction of metals from WPCBs, for instance, Kumar *et al.* (2017) used bioleaching at 30 °C in order to recover gold and silver from WPCBs (Kumar, Saini, & Kumar, 2017). Similarly, Gu *et al.* (2017) employed bioleaching enhanced by a nitrogen-doped carbon nanotubes modified electrode to recover copper from WPCB while the processing temperature was 28 °C (Gu *et al.*, 2017). Moreover, another bioleaching process reported by Wang *et al.* (2017) was also performed at a low temperature of 30 °C while achieving a high copper extraction rate (Gu *et al.*, 2017). However, a disadvantage of such techniques is, in some cases, the extensive use of various chemicals, a low extraction rate, or focus on only one or two metals while not addressing the issue of non-metals.

In order to avoid the abovementioned problems, a group of Chinese researchers employed a new type of chemical treatment using Dimethylsulfoxide (DMSO) to dissolve epoxy resin of WPCBs and TO separate metal from non-metal (Zhu, Chen, Wang, Qian *et al.*, 2013; Ping Zhu *et al.*, 2013). Despite the promising results, the temperature of the dissolution process was relatively high (130–170 °C), while the size of the separated samples did not exceed 2–3 cm². Verma *et al.* (2016, 2017b, 2017c) increased the size of samples up to 16 cm² and also selected a more efficient solvent, Dimethylformamide (DMF) instead of DMSO (Verma, Singh & Mankhand, 2016, 2017a, 2017b). Another trending research direction in WPCB treatment is reprocessing the waste into high added value materials. Researchers investigated the possibility of reprocessing WPCBs into nano-sized particles (Moriwaki, Yamada & Usami, 2017; Zhan, Xiang, Xie & Sun, 2016). The results of these studies were promising, however, such reprocessing technologies require well-thought integration into the overall scheme of WPCB recycling in order to be sustainable.

Therefore, the focus of the current doctoral dissertation was on the investigation of using solvent treatment for the separation of all the components of WPCBs and reprocessing of the extracted materials into high added value products. Firstly, experiments on WPCB separation were performed to find the optimum process conditions, to characterize the recovered materials, to adapt the technology for full-sized WPCBs (e.g., motherboard), etc. The second part of experiments was concerned

with the additional purification of the recovered metallic fraction and the production of various micro- and nanomaterials by several methods, their characterization and evaluation of the economic and environmental benefits.

Aim of the Doctoral Thesis

The thesis is aimed at developing a solvent treatment approach for the recovery of materials from WPCB that would provide tangible benefits compared to the approaches traditionally used in this field (incineration, pyrolysis, acid leaching, etc.).

Objectives

1. To conduct preliminary experiments on the separation of WPCBs by solvent in order to study the fiberglass purification mechanism and indicate the preferable initial condition of WPCBs (milled or non-milled);
2. To find the optimum solvent separation conditions for WPCBs of the selected initial condition by evaluating the effect of temperature, solid-to-liquid ratio, and the WPCB type on the separation time;
3. To assess the recycling rate, economic performance and carbon footprint of the treatment through investigation of the recovered materials – their quality, properties, and potential applications;
4. To close the loop of solvent treatment by studying possibilities of using the extracted materials as precursors for manufacturing of added value products while suggesting several approaches based on the recent advances in this area and the types of the materials.

Scientific Novelty

1. ***Optimum process conditions for several most common WPCB types found.*** Our investigation revealed that solvent treatment can still be efficient at low temperatures if assisted by ultrasound treatment. Low temperature solvent treatment of WPCBs has not been reported before since other groups of researchers focused on separation at higher temperatures, for instance, Zhu *et al.* (2013) conducted experiments with solvent temperatures up to 135 °C. Similarly, Verma *et al.* (2016) worked in an even higher temperature range of 80–170 °C. The obtained experimental data was supported with models of the process which showed that even the biggest types of WPCBs can still be separated within a relatively short treatment period (<85 hrs.). It is worth noting that previously reported works on this topic dealt with experimental analysis of the solvent treatment process, while process optimization supported by modeling was used for the first time in the research conducted in the framework of this dissertation;
2. ***The size of treatable Waste Printed Circuit Boards increased.*** Previously reported works on solvent treatment demonstrated only separation of size-reduced WPCBs. Verma *et al.* (2016) managed to separate 100–1,600 mm² samples, while Zhu *et al.* (2013) reported separation of cut specimens with size reaching only 100–300 mm². At the same time, in the present research, based on the optimized process, the separation of a full-sized Video Card, a

Random Access Memory module, and a Motherboard (up to 70,000 mm²) was achieved;

3. ***Options to increase the added value of the recovered products found.*** The materials recovered at the end of separation, namely, high purity copper foils and through-hole pad solder joints, were successfully reprocessed into added value products – Copper nanoparticles (size 5–7 nm), Tin Oxide nanoparticles (size ~7 nm) and Lead Oxide microparticles (size ~1 µm). It is important to note that, to the best of our knowledge, the relevant literature does not mention obtaining such products from WPCBs; for instance, only Copper Oxide, Copper-Tin and Lead nanoparticles synthesized from WPCBs have been reported.

Defended Proposition

1. An environmentally friendly solvent treatment method can be successfully used for the recovery of valuable metallic and non-metallic materials from waste multilayer composites, such as Waste Printed Circuit Boards while using processing at optimized conditions – solvent type Dimethylformamide, temperature 50°C, solid-to-liquid ratio 3:10 (wt./v), separation time ~20 hrs./8,000 mm² sample;
2. Metals recovered by solvent treatment can be reprocessed into high added value products in the form of nanoparticles, for example, 5–7 nm sized Copper nanoparticles, 7 nm sized Tin Oxide nanoparticles.

Structure

This doctoral thesis consists of the following segments: introduction, literature review, materials and methods, results and discussions, conclusions, acknowledgements, reference list, publications list, and appendices. The thesis is comprised of 177 pages, 106 figures, 12 tables, and 29 appendices.

Publications

The results of the research work used for the preparation of the current dissertation were presented in 9 articles published in the journals registered in the *Web of Science* database. Additionally, the research results were presented at 3 conferences.

Practical Significance

During the research on this topic, several laboratory prototypes of separation reactors were constructed with modifications for each type of WPCB treated. Based on the obtained data on material flows in the technology, a layout of an industrial recycling line that includes pre-treatment, separation in a specifically designed reactor, classification, and a number of steps for the production of added value materials have been suggested. Applications of all the materials recovered from WPCBs, including Epoxy Resin, Fiberglass, and Metals, were reviewed, and at least several applications were recommended for each material. Overall, the obtained data can be very useful for technologists working in both science and engineering, and it

will help to better understand the WPCB separation mechanism, the strengths and opportunities of the solvent treatment approach, and it will facilitate the transfer of the technology from the laboratory to the industrial scale.

Author's Contribution

The research results presented and discussed in this work were originally collected and analyzed by the author. Part of material characterizations was handled by co-authors of the published articles from the Lithuanian Energy Institute (Vidas Makarevičius and Stasė-Irena Lukošius). Co-authors from the Center for Physical Sciences and Technology (Martynas Skapas and Remigijus Juškėnas) assisted with the characterizations of the produced nanoparticles. The antimicrobial behavior of nanoparticles was investigated by co-authors from Vytautas Magnus University (Sandra Sakalauskaitė and Rimantas Daugelavičius). Part of the experimental work was assisted by co-authors from KTU, Faculty of Chemical Technology (Rūta Sidaravičiūtė and Martynas Tichonovas). The published papers were prepared by the author under the guidance of a supervisor (Gintaras Denafas) and a scientific advisor (Samy Yousef) from Kaunas University of Technology. Additional supervision for article preparation was provided by Regita Bendikienė (KTU, Faculty of Mechanical Engineering and Design). It should be noted that all the above-listed co-authors have no intent of using the published data for preparation of other dissertations.

Use of Data and Text of Published Articles in the Dissertation

Throughout the dissertation, a significant amount of the presented material was extracted directly from the articles published by the author during his PhD studies. The following list shows the chapters and the corresponding articles, the text of which was used in the specific chapter (only article titles, see the full article data in the respective section).

Articles:

Article 1. Separation and purification of metal and fiberglass extracted from waste printed circuit boards using milling and dissolution techniques;

Article 2. Recovery of gold, other metallic and non-metallic components of full-size waste random access memory;

Article 3. Antimicrobial copper nanoparticles synthesized from waste printed circuit boards using advanced chemical technology;

Article 4. Characterization of waste printed circuit boards recycled using a dissolution approach and ultrasonic treatment at low temperatures;

Article 5. Industrial technology for mass production of SnO₂ nanoparticles and PbO₂ microcube/microcross structures from electronic waste;

Article 6. Mechanical and thermal characterizations of non-metallic components recycled from waste printed circuit boards;

Article 7. A strategy for synthesis of copper nanoparticles from recovered metal of waste printed circuit boards;

Article 8. Recycling of bare waste printed circuit boards as received using an organic solvent technique at a low temperature;

Article 9. Feasibilities for hydrometallurgical recovery of precious metals from waste printed circuit boards in Lithuania.

Chapters and subchapters:

Introduction: *Article (9)*

1. Literature review: **1.1.** – *Articles (1–4, 6, 8)*, **1.2.** – *Articles (2, 6, 8, 9)*, **1.3.** – *Articles (3, 7)*;

2. Materials and Methods: **2.1.** – *Articles (1, 4, 8)*, **2.2.** – *Article (3)*, **2.3.** – *Article (1)*, **2.4.** – *Article (4)*, **2.5.** – *Article (6)*, **2.6.** – *Articles (2, 8)*, **2.7.** – *Article (8)*, **2.8.** – *Article (7)*, **2.9.** – *Article (3)*, **2.10.** – *Article (5)*, **2.11.** – *Articles (1, 6, 7)*;

3. Results and Discussions: **3.1.** – *Article (1)*, **3.2.** – *Article (4)*, **3.3.** – *Article (6)*, **3.4.** – *Articles (2, 3, 4, 7, 8)*, **3.5.** – *Articles (1, 2, 4)*, **3.6.** – *Articles (1, 2)*, **3.7.** – *Article (6)*, **3.8.** – *Article (7)*, **3.9.** – *Article (3)*, **3.10.** – *Article (5)*, **3.11.** – *Articles (3, 5, 7)*, **3.12.** – *Article (5)*, **3.13.** – *Articles (3, 5, 7)*.

1. Literature Review

1.1. Electrical and Electronic Waste and Waste Printed Circuit Board (WPCB) Management

In the recent years, the issue of Waste Electrical and Electronic Equipment (WEEE) has been attracting the attention of many researchers due to the constantly growing amounts of the abovementioned waste and its potentially harmful impact both on the environment and the human health (Lu & Xu, 2016). The global generation of Electronic Waste (or E-waste) was targeted with the *Solving the E-Waste Problem* (StEP) initiative as a highly considerable value of 65.4 million tonnes was obtained in 2017, which is a sharp increase compared to 20 million tonnes of E-waste generated in 2000 (Yoshida *et al.*, 2016). This dramatic increase in the generation of waste electrical and electronic equipment (WEEE) is a result of the integration of electronic devices into almost every sphere of human life and the appearance of completely new electronic products denoted by high popularity, especially computers and mobile phones. Altogether, this leads to the accumulation of high amounts of WEEE (Guanghan, Zhu, Wenyi, Chenglong & Wen, 2016; Huang, Guo & Xu, 2009; Veit & Bernardes, 2015; Yoshida *et al.*, 2016).

Environmental and health concerns related to WEEE are caused by the usually ineffective and inappropriate management and disposal of this type of waste. The situation is worsened by the fact that a significant share of E-waste is treated ‘informally’ by burning it in open areas, which leads to the release of various harmful substances including dioxins, furans, heavy metals, etc. into the environment (Chi, Streicher-Porte, Wang & Reuter, 2011). This makes recycling of E-waste a categorical imperative imposed on researchers and entrepreneurs who are interested in this field, and steps must be made towards the fastest possible transition from the laboratory to the industrial scale technology while taking the cost, the environmental impact and the recycling rate into account (Guanghan *et al.*, 2016).

Naturally, these issues were not unnoticed, and various legislations as well as environmental policies have been implemented over the course of the last decades around the world. In the European Union, there are two main regulations of this kind, namely, the *Directive on the Restriction of the Use of Certain Hazardous Substances in Electrical and Electronic Equipment* (the RoHS Directive) and the *Directive on Waste Electrical and Electronic Equipment* (the WEEE Directive) (European Parliament, 2003; The European Parliament & The Council of the European Union, 2003). Since their first introduction, both directives have been updated over the years, for instance, in the WEEE Directive, the collection target for 2016 was defined as 45% from all the Electric and Electronic Equipment (EEE) put on the market, and it is planned to increase this percentage up to 65% in 2019 to address the growing rate of electronics manufacturing (Van Eygen, De Meester, Tran & Dewulf, 2016).

Waste Printed Circuit Board (WPCBs), being a particular type of WEEE, represents a relatively small share of ~3–10% from the total mass of WEEE; however, WPCBs have been receiving notable attention from the researchers and recycling companies (Fogarasi, Imre-Lucaci, Egedy, Imre-Lucaci & Ilea, 2015). Printed Circuit

Boards (PCBs) may have different designs (**Fig. 1.1.1.**), however, the function of all the PCB models is similar – to support a number of electronic components mounted on them (transistors, integrated circuits, capacitors, etc.) and provide electrical connection as well as insulation between the components if needed.

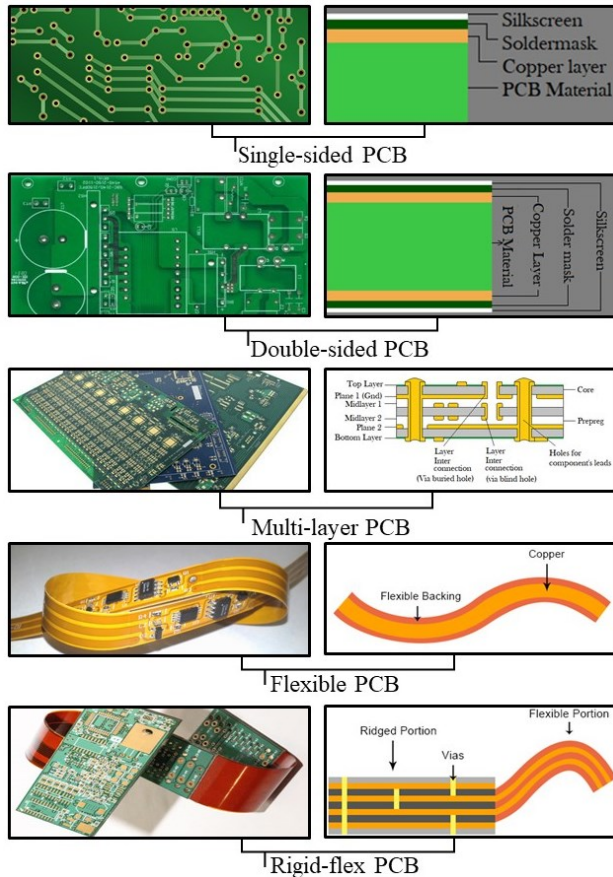


Figure 1.1.1. Examples of PCB types (Agarwal, 2015; Kansagara, 2018; Printed Circuit Board Introduction & PCB Types, 2018)

Virtually every type of electric devices, except for the simplest ones, nowadays contains one or more specific models of PCB. Over the recent years, the average rate of the worldwide Printed Circuit Boards manufacturing has been increasing in the range of 7.04–21.3% annually (depending on the product type, e.g., TV, PC or mobile phones) (Lu & Xu, 2016). This percentage may further grow during the following years due to the significant and rapid progress in electrical industry, shortening life expectancy of Electrical and Electronic Equipment (EEE), technological advancement and because of the increased company competition (Kolias, Hahladakis & Gidarakos, 2014; Umair, Björklund & Petersen, 2015).

During the last decade, the recycling of waste printed circuit boards (WPCBs) has increasingly been taken seriously for two main reasons. The first reason is that WPCBs contain a considerable amount of metallic and non-metallic components, such

as Copper (Cu), Iron (Fe), Tin (Sn), Nickel (Ni), Lead (Pb), Zinc (Zn), Silver (Ag), Gold (Au), Palladium (Pd) and fiberglass encapsulated in resins; WPCBs could be used as a source of valuable raw materials for recycling. The second reason is that WPCBs are classified as hazardous waste, and the environment needs protection from the harmful substances contained inside WPCBs; these substances can be released as a result of landfilling the abovementioned waste or treating it with the traditional methods, such as incineration, which may produce toxic gases and result in carbon dioxide emissions (Zhou, Guo, Lin, Huang & Deng, 2013).

1.1.1. Structure and composition of WPCBs

E-waste including PCBs is well-known as an important source of secondary raw materials (Cucchiella, D'Adamo, Rosa & Terzi, 2016). In the case of WPCBs, the content of non-metals (woven fiberglass and epoxy resin) represents 70% of their weight, while the remaining weight is constituted from various metals (Cayumil, Khanna, Rajarao, Mukherjee & Sahajwalla, 2016). According to other evaluations, WPCBs consist of 40% of organic substances (epoxy resin, brominated flame retardants, curing agents, curing accelerators, etc.) and 60% of inorganic substance (glass fiber made from various oxides, usually SiO_2 , CaO and Al_2O_3) (Lin & Chiang, 2014). In terms of the metal content, the average percentage of Cu in WPCBs fluctuated between 5.10% in 1980 and 12.8% in the mid-1990s and has been decreasing afterwards. The decreases in Ag and Cu amounts could possibly be associated with the thinner layers of these metals in the newer models of PCBs (Adie *et al.*, 2017).

Regardless of the composition, the metal recycling rates remain rather low – in 2011, they were reported to be below 15% (Graedel *et al.*, 2011). This can be explained by the complex design of printed circuit boards (PCBs) and their characteristics: they are designed to feature high mechanical properties, considerable chemical and thermal resistance. Usually the main part of PCBs is the so-called substrate – several layers of woven fiberglass impregnated with epoxy resin (Longobardo, 2010). The top and bottom surfaces of the substrate are used as a support for conductive tracks and mounted components, such as resistors, capacitors, and so forth. Conductive tracks, in turn, are covered with a thin protective layer of lacquer-like solder mask. It can be stated that the recycling of PCBs is a challenging task since Brominated Epoxy Resin (BER), which adheres all the layers of WPCB, can be a source of toxic and carcinogenic materials that may lead to environmental and health problems (Ikhlail, 2017; Verma *et al.*, 2016; Verma, Singh & Mankhand, 2017c; Verma *et al.*, 2017a, 2017b). Similarly, solder mask is used to isolate specific layers in PCBs. This can be another source of toxins, and a few studies have been conducted to eliminate or reduce toxic emissions occurring during the treatment of electronic waste (Raele *et al.*, 2017, Saini *et al.*, 2017).

The typical composition of WPCB was evaluated by Cucchiella (2016) by analyzing a number of sources and splitting WPCBs into categories (Cat1–4) according to the type of WEEE that contained the WPCBs (Cat1 – bulky household appliances (e.g., fridges, washing machines, air conditioners, etc.); Cat2 – small-sized

household appliances (e.g., vacuum cleaners, toasters, fryers, etc.); Cat3 – IT and telecommunication equipment (e.g., PCs, tablets, notebooks, smartphones, etc.), and Cat4 – consumer equipment (e.g., TVs, stereo systems, digital cameras, etc.)) (Cucchiella, D’Adamo, Lenny Koh & Rosa, 2016). The exact numbers, including the potential price of materials, can be seen in **Table 1.1.1**. We should take note that the percentages of materials presented in the table can be highly variable across different WPCB types. For example, one study reported that the content of Copper in WPCBs reached 32.5 wt.% (Silvas *et al.*, 2015).

Table 1.1.1. Characterization of materials embedded into generic WPCBs (Cucchiella, D’Adamo, Rosa *et al.*, 2016)

Materials	Cat1 WPCBs	Cat2 WPCBs	Cat3 WPCBs	Cat4 WPCBs	
	p_{rm}^* (%)	p_{rm} (%)	p_{rm} (%)	p_{rm} (%)	pr_{rm}^{**} (€/kg)
Selling materials					
Iron (Fe)	15.45	12.00	14.10	6.93	0.05
Copper (Cu)	13.00	11.00	20.00	17.25	5.13
Silver (Ag)	0.01	0.02	0.17	0.08	480
Gold (Au) ^{***}	0.003	0.002	0.04	0.01	32,500
Palladium (Pd)	0.003	0.001	0.01	0.002	29,000
Aluminum (Al)	7.65	8.60	3.38	10.05	1.5
Beryllium (Be)	0	0	0.002	0	850
Bismuth (Bi)	0	0	0.02	0.03	11.4
Chromium (Cr)	0.02	0.02	0.54	0.02	1.75
Tin (Sn)	1.49	2.70	0.69	0.73	16
Zinc (Zn)	1.94	1.40	1.35	1.17	1.6
Hazardous materials					
Antimony (Sb)	0.08	0.06	0.13	0.16	
Arsenic (As)	0	0	0.0005	0	
Bromine (Br)	0.16	0.01	0.82	0.39	
Cadmium (Cd)	0	0	0.000001	0	
Chlorine (Cl)	0.20	0.43	0.01	0.31	
Lead (Pb)	1.25	3.00	0.79	1.09	
Nickel (Ni)	0.07	0.11	1.13	0.26	
Conferred materials					
Plastics	41.50	46.00	30.20	25.00	
Epoxy	8.50	16.00	0.92	14.75	
Ceramics	7.00	0	15.02	13.60	
Glass	0	0	2.00	0	
Others	2.20	0	8.38	8.50	
Liquid crystals	0	0	0.16	0	

* p_{rm} - % of metal or non-metal in 1 kg of WPCB

** pr_{rm} - price of recycled metal

*** 0.003% of Au means 30 ppm of Au or 30 g of Au in 1 tonne of PCBs

From Table 1.1.1., it is clear that special attention should be given to the WPCBs with a high precious metal content because of their high market value. Random Access Memory (RAM) modules, being a type of Printed Circuit Boards (PCBs), are essential components of Personal Computers (PCs) and laptops that perform a function of

volatile memory storage and are usually based on Complementary Metal Oxide Semiconductors (CMOS) (Haraszti, 2002). Just like the usual WPCBs, RAMs contain non-metals (fiberglass/epoxy resin composite) as well as metals, e.g., copper (Cu) and, what is more important, precious metals (Akcil *et al.*, 2015; Zhu, Zhou, Guo & Sun, 2015). Therefore, waste RAMs were classified as one of the primary metal sources in the overall stream of Waste Printed Circuit Boards (WPCBs) (Bidini *et al.*, 2015).

1.1.2. Life-cycle of WPCBs

In the general case, Electronic Waste, including PCBs, passes through five main stages over the course of its lifecycle: Manufacturing, Consumption, Collection, Recycling, and Disposal (Islam & Huda, 2018). However, the structure of this chain and its material flow may vary greatly depending on the country. For example, in Finland, there is a well-established national collection system for E-waste that mainly operates through permanent collection points funded through producer associations; in addition, there are alternatives for private households, such as collection through reception in stores and mobile collections, as shown in **Fig. 1.1.2**.

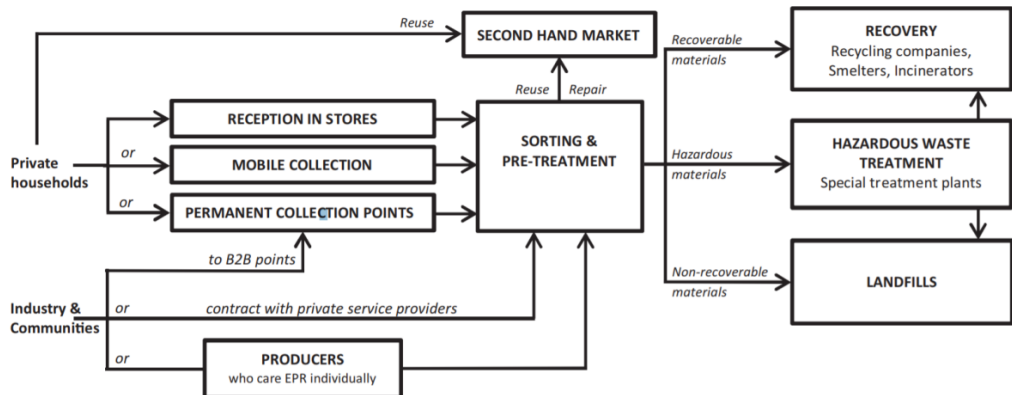


Figure. 1.1.2. WEEE collection system in Finland (Ylä-Mella, Poikela, Lehtinen, Keiski & Pongrácz, 2014)

The implementation of this approach allowed to increase the collection rates of WEEE up to 9 kg/inhab./year thus reaching the average E-waste recovery rate of 91.5% and the average reuse/recycling rate of 88.5% (Ylä-Mella *et al.*, 2014). Similar collection systems are being run in other European countries, such as Sweden (Bernstad, la Cour Jansen & Aspegren, 2011), Denmark (Grunow & Gobbi, 2009), Portugal (Gomes, Barbosa-Povoa & Novais, 2011), etc.

Unfortunately, on the global scale, the situation with E-waste is far from being taken under strict control. This is a result of tendencies across many developed countries when the country itself does not develop its infrastructure for the treatment of the waste – instead it relies on the export of waste to the developed countries due to economic reasons. Such countries as Canada, USA and Japan have been reported to dump significant quantities of E-waste in the Eastern European and developing countries (Afroz, Masud, Akhtar & Duasa, 2013). For instance, it was estimated that

in the USA 50–80% of E-waste is not treated in recycling facilities but is instead sold to other countries, such as China (Puckett *et al.*, 2002).

At this point, a new problem arises because of the fact that E-waste recycling sectors in such countries as India and China strongly or completely relies on the imported waste streams while having none or limited access to proper recycling technologies. Coupled with low income rates in the above mentioned countries, their high population and high market prices of metals, this leads to high rates of informal recycling when up to 95% of E-waste can be treated by the unauthorized sector (Awasthi, Wang, Wang, Awasthi & Li, 2018; Pradhan & Kumar, 2014).

In China, which is the world's largest endpoint of E-waste, it is reported that only 25% of E-waste are recycled formally while 75% is treated through the informal way (Perkins, Brune Drisse, Nxele & Sly, 2014). Formal and informal sectors coexist; formal industries are attracted by the potential benefits stemming from the recovered materials but require large volumes of waste, while the informal sector benefits from the advantage of informal collection when collectors can collect and repair electronic devices in informal workshops with cheaper labor costs than the official sector. Both sectors are being stimulated by the high demand for metals as well as plastics, as shown in **Fig. 1.1.3**.

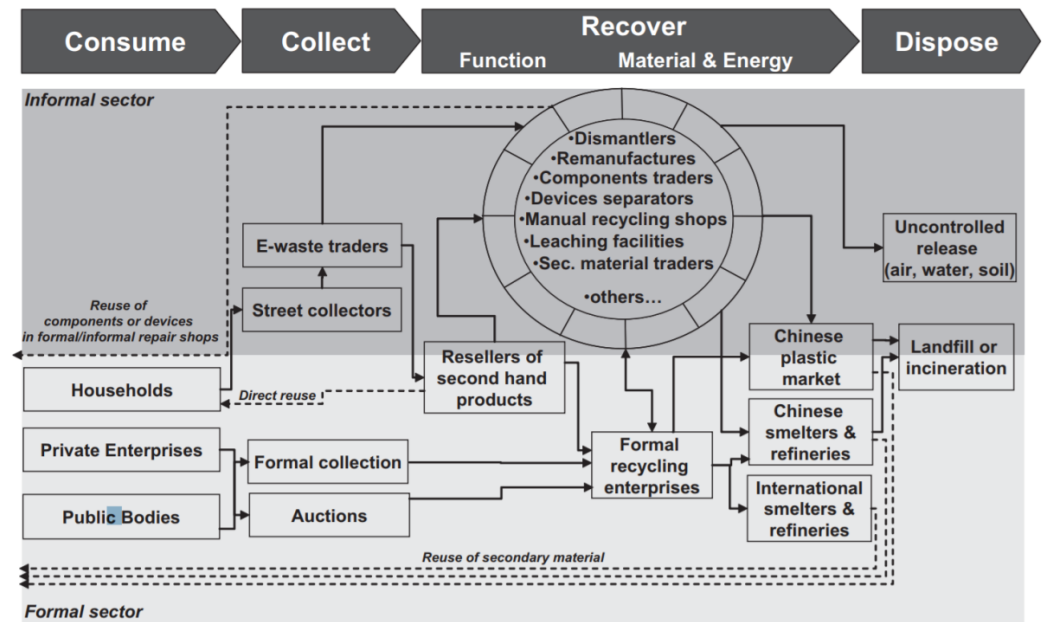


Figure 1.1.3. Formal and informal E-waste treatment routes in China (Chi *et al.*, 2011)

1.1.3. Environmental issues caused by utilization of WPCBs

A summary of the information outlined in the previous section is that millions of tonnes of E-waste generated around the world eventually end up in the informal recycling sectors of the developing countries, especially in China (Song & Li, 2015). Unauthorized recyclers operate mainly by using the most accessible and simple techniques, such as manual dismantling followed by burning in open areas or leaching with strong acidic solutions in order to obtain precious and base metals contained in E-waste and especially WPCBs (Bi *et al.*, 2010; Chehade *et al.*, 2014; Leung *et al.*, 2011). During the treatment process, E-waste cannot be sorted properly, which further decreases the efficiency of unapproved recycling (Fig. 1.1.4. (Huang *et al.*, 2009)). The inevitable result is the release of large quantities of hazardous metals, toxic organic compounds and other pollutants into the atmosphere, soil and water in the form of various emissions as demonstrated in Fig. 1.1.5. (Fu *et al.*, 2011; Gullett *et al.*, 2007; Hischer, Wäger & Gaughhofer, 2005).



Fig. 1.1.4. Waste PCBs from all kinds of electronic equipment (Huang *et al.*, 2009).



Figure. 1.1.5. Environmental risks of primitive WPCB recycling techniques: (a) precious metals recovery by acid leaching; (b) unprotected WPCB dismantling; (c) open burning of WPCBs (Huang *et al.*, 2009)

It needs to be noted that environmental pollution from E-waste and WPCBs treatment in China is mostly localized in three regions – Guiyu, Taizhou and Qingyuan, as presented in Fig. 1.1.6.



Figure 1.1.6. WEEE-generated pollution in China (Song & Li, 2015)

It has been reported that only in the city Guiyu, Guangdong Province, illegal E-waste recycling has been conducted for over 10 years with 60–80% of local population and ~100,000 migrant workers being involved in such activities, which leads to significant pollution of the surrounding areas by dumped E-waste and residues left after E-waste processing (Huo *et al.*, 2007; Wong, Duzgoren-Aydin, Aydin & Wong, 2007).

Research papers published in 2008–2013 revealed all the seriousness of environmental and human health consequences stemming from illegal and uncontrolled WEEE treatment. **Table 1.1.2.** outlines the main findings of these studies focused on the groups of the exposed people (residents and workers who were directly or indirectly coming into contact with WEEE-emanating pollutants) and the concentrations of heavy metals in the blood of people belonging to the above listed groups.

Table 1.1.2. Exposure sources of heavy metals from e-waste (Song & Li, 2015)

Location	Sampling time	Exposure ways	Exposure groups	Concentrations	References
Taizhou	Nov 2005	Rice	Residents	As: 0.8; Cd:0.7; Hg: 0.1; Pb: 3.7 $\mu\text{g}/(\text{day}\cdot\text{kg bw})$.	(Fu <i>et al.</i> , 2008)
Longtang	Sept 2007	Vegetables	Residents	Cd: 1.36 $\mu\text{g}/(\text{day}\cdot\text{kg bw})$; Cu: 10.6 $\mu\text{g}/(\text{day}\cdot\text{kg bw})$; Pb: 3.00 $\mu\text{g}/(\text{day}\cdot\text{kg bw})$; Zn: 69.8 $\mu\text{g}/(\text{day}\cdot\text{kg bw})$.	(Luo <i>et al.</i> , 2011)
Rural region in South China	—	Food (vegetables, rice, pork, chicken and	Residents (adults, and children)	Adults: Cd: 5.28; Pb: 54.2; Cu: 155; Zn:228; Ni: 15.7 $\mu\text{g}/(\text{day}\cdot\text{kg bw})$; Children: Cd: 8.95; Pb:81.2; Cu:	(Zheng <i>et al.</i> , 2013)

		fish); House dust; Groundwater		316; Zn: 502; Ni: 26 $\mu\text{g}/(\text{day}\cdot\text{kg bw})$.	
Guiyu	Dec 2004	Dust	Workers and children	Workers: Pb: 175.7; Cu: 13.2; Cd: 0.043; Cr: 0.11 $\mu\text{g}/(\text{day}\cdot\text{kg bw})$; Children: Pb: 1421; Cu: 106.8; Cd: 0.34; Cr: 0.93 $\mu\text{g}/(\text{day}\cdot\text{kg bw})$.	(Leung, Duzgoren-Aydin, Cheung & Wong, 2008)
Jiangsu (Formal)	—	Air	Workers	ADD _{ing} : Cr: 49.1; Cu 20,900; Cd 16; Pb: 4930 $\text{ng}/(\text{day}\cdot\text{kg bw})$; ADD _{inh} : Cr: 0.0055; Cu: 2.33; Cd: 0.0018; Pb: 0.013 $\text{ng}/(\text{day}\cdot\text{kg bw})$; ADD _{derm} : Cr: 0.22; Cu: 94; Cd: 0.072; Pb: 22.2 $\text{ng}/(\text{day}\cdot\text{kg bw})$.	(Xue, Yang, Ruan & Xu, 2012)
Shanghai (Formal)	—	Air (PM2.5)	Workers	Mechanical workshop: ADD _{ing} : Cr: 1,371; Cu: 2,652; Cd: 37.7; Pb: 23,345 $\text{ng}/(\text{day}\cdot\text{kg bw})$; ADD _{inh} : Cr: 0.15; Cu: 0.48; Cd: 0.0032; Pb: 2.61 $\text{ng}/(\text{day}\cdot\text{kg bw})$; ADD _{derm} : Cr: 6.18; Cu: 1.932; Cd: 0.17; Pb: 105.53 $\text{ng}/(\text{day}\cdot\text{kg bw})$; Manual dismantling workshop: ADD _{ing} : Cr: 1,083; Cu: 592; Cd: 107; Pb: 7,910 $\text{ng}/(\text{day}\cdot\text{kg bw})$; ADD _{inh} : Cr: 0.12; Cu: 0.15; Cd: 0.012; Pb: 2.39 $\text{ng}/(\text{day}\cdot\text{kg bw})$; ADD _{derm} : Cr: 4.89; Cu: 0.62; Cd: 0.48; Pb: 35.65 $\text{ng}/(\text{day}\cdot\text{kg bw})$.	(Fang, Yang & Xu, 2013)

As it can be seen, in many cases, the quantities of the mean estimated Lead (Pb) intake notably exceeded the tolerable daily intake ($3.6 \mu\text{g}/(\text{day}\cdot\text{kg bw})$) for both adults and children who were consuming contaminated food or inhaled contaminated air, whereas Pb is a commonly used component of soldering in electrical and electronic equipment or EEE (Menon, George, Osterman & Pecht, 2015). A similar situation was observed for more metals, such as Cadmium (Cd), Arsenic (As), Copper (Cu), Chromium (Cr), Mercury (Hg) and others (Song & Li, 2015).

The overall E-waste contamination accumulates in three environmental systems before reaching the human population: waters and aquatic systems, air, and soils and terrestrial environments (Robinson, 2009). A list of main potential contaminants including not only heavy metals but also organic compounds and their sources in E-waste is presented in **Annex 1**. Some organic pollutants, such as Polybrominated Diphenyl Ethers (PBDEs), Tetrabromobisphenol-A (TBBPA) and Polybrominated Biphenyls (PBBs) are specifically produced from WPCBs during burning since they are major components of many commercially used epoxy resins, whereas brominated epoxy resins are commonly used for the production of PCB laminates (Alaee, Arias, Sjödin & Bergman, 2003; Hongtao Wang, Hirahara, Goto & Hirose, 2004).

Summarizing the information given above, it can be concluded that environmental pollution problems and human health hazards associated with E-waste

and WPCBs are, more often than not, directly caused by the technology that is being used to treat this type of waste. Obviously, a number of indirect factors (e.g., E-waste-related legislation, the efficiency of national waste collection systems, etc.) play a serious role, however, without a proper waste treatment technology, all other steps would not be fruitful. Therefore, in the next sections, our review will be focused on the current technical possibilities of WPCB treatment/recycling.

1.2. WPCB treatment/recycling technologies

Landfilling is considered to be the main way for the disposal of non-metallic components of WPCBs; it is commonly used after the extraction of the valuable copper and other metal components by incineration techniques (Hall & Williams, 2007). As discussed above, these methods may cause serious problems directly related to the environment and human health, such as: large areas of land wasted, destruction of the microbial balance of soil, negative effects on the groundwater quality and plant growth by diffusion and infiltration into the soil, harm to the atmospheric environment as a result of volatilization of lead and arsenic (metals which are used as fillers and coloring agents in WPCBs) as well as non-metallic materials into the atmosphere (Huang *et al.*, 2009). Currently, recycling of E-waste has become a necessity in terms of not only addressing the shortage of mineral resources for the industry of electronics but also in order to decrease environmental pollution and human health-related risks (Zeng, Yang, Chiang & Li, 2017). Closed-loop recycling of electronics can be a valuable tool to sustain the future development of the flourishing electronics industry (Zeng & Li, 2016). Furthermore, recycling processes have been developed in order to avoid the above mentioned problems; these processes can be classified into three categories: mechanical and physical treatment, thermal treatment, and chemical treatment (Guanghan *et al.*, 2016; Ning, Lin, Hui & McKay, 2017).

1.2.1. Mechanical and physical treatment

Mechanical or physical treatment is likely the most straightforward approach compared to other techniques; it includes the following techniques as well as their combinations: size reduction, size/density-based separation, electrostatic separation, and magnetic separation (Ghosh, Ghosh, Parhi, Mukherjee & Mishra, 2015). This group of treatment methods mainly relies on the mechanical properties of materials contained in WPCBs and the morphology of crushed particles as a means for separation of the metallic fraction of WPCBs from the Non-Metallic Fraction (NMF).

Hammer milling. Virtually any technology of this type requires size reduction as a first step. Milling with a hammer mill, as shown in **Fig. 1.2.1.**, is one of the most commonly used solutions for such a task even though there are other suitable options, e.g., ball milling, disc milling, etc. For example, Yang *et al.* (2015a) used ball milling, pan milling and jet milling of WPCBs to compare pulverized products while employing these approaches and to evaluate the quality of the produced Polypropylene (PP) composites reinforced by milling products (Yang, Bai & Wang, 2015). Yang *et al.* (2015a) found that the powder produced after 15 cycles of pan

milling featured the best properties in terms of the particle size ($61\text{ }\mu\text{m}$) and offered better properties to the reinforced composite. Nekouei *et al.* (2018a) applied two milling steps (knife milling and ring milling) to obtain powder of various fractions (from $-25\text{ }\mu\text{m}$ to $+450\text{ }\mu\text{m}$) by separation with sieves in two steps, and, finally, the powder was separated into two phases (metal and non-metal) by using a bromoform-based heavy liquid; the results indicated that the separation was successful in terms of the enrichment of the metallic faze (75% metal content increase) and the removal of metal from NMF (Nekouei, Pahlevani, Rajarao, Golmohammadzadeh & Sahajwalla, 2018a).

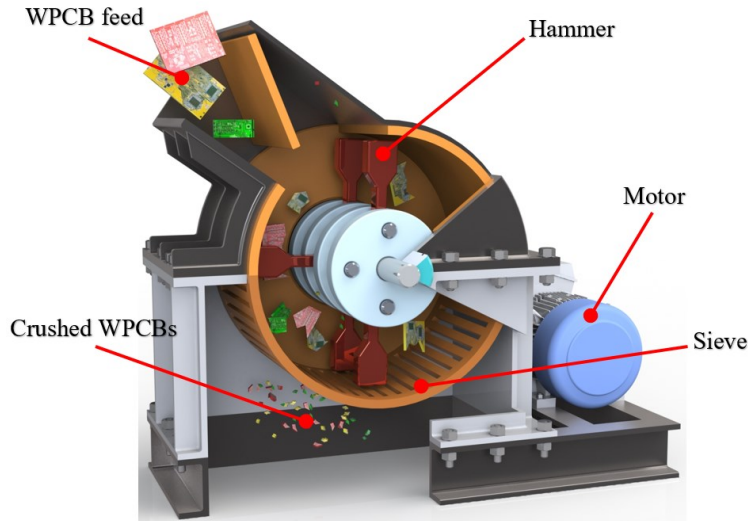


Figure 1.2.1. Hammer milling of WPCBs

Density or size-based separation is an extremely widespread approach used not only in recycling but also, for instance, in virgin mining (Wills & Napier-Munn, 2006). As the name suggests, size-based separation techniques take into account that various materials contained in WPCBs take a different shape after crushing, and therefore sieves or other barriers with a specific opening size and shape are used to separate the fractions in the WPCB powder into metallic and non-metallic powder (Verma, Singh, & Basha 2018). Verma *et al.* (2018) produced a $\sim 87\text{ wt.}\%$ copper-containing fraction from WPCBs milled at the optimum feed rate of 3 kg/hr. , crushing time 7 min , and the sieve size of BSS 100 (0.15 mm opening size). As for the density-based separation, it can be performed in several ways. The most popular option is the usage of water or heavy liquids (e.g., Bromoform, Dibromoethane, etc.) to separate light non-metallic and heavy metallic fractions in milled WPCBs through a float-sink mechanism. Another option is the usage of air classification to separate WPCB powder into fractions (Cui & Forssberg, 2003). Hanafi *et al.* (2012) conducted a research regarding the separation of pulverized WPCBs by using a mixture of Tetrabromomethane and acetone so that to obtain a heavy copper-rich fraction and eventually produce pure ($98.82\text{ }\%$) Copper Sulfate Hydrate ($\text{CuSO}_4 \cdot 5\text{H}_2\text{O}$) (Hanafi *et al.*, 2012).

Electrostatic separation is another widespread technology which found its use in not only recycling but also in virgin mining operations due to its relatively low energy consumption and environmental friendliness (Jordens, Cheng & Waters, 2013). Commonly encountered types of electrostatic separators are Corona Electrostatic (**Fig. 1.2.2.**) and Eddy Current (**Fig. 1.2.3.**) separators (Cui & Forssberg, 2003). Corona electrostatic separators operate by using corona charging to obtain conductive and non-conductive fractions of ground materials. Eddy Current separation uses a magnetic rotor composed of powerful constant magnets to generate an induction field at the end of a moving belt. Non-ferrous metals that are fed via a belt become magnetized after reaching the induction field, which causes ejection of the above mentioned metals. Li *et al.* (2007) studied the separation of WPCBs via Corona Electrostatic separation; his findings indicated that particles with sizes of 0.6–1.2 mm can be separated in industrial conditions after two-step crushing with a low risk for environment (Jia Li, Xu & Zhou, 2007).

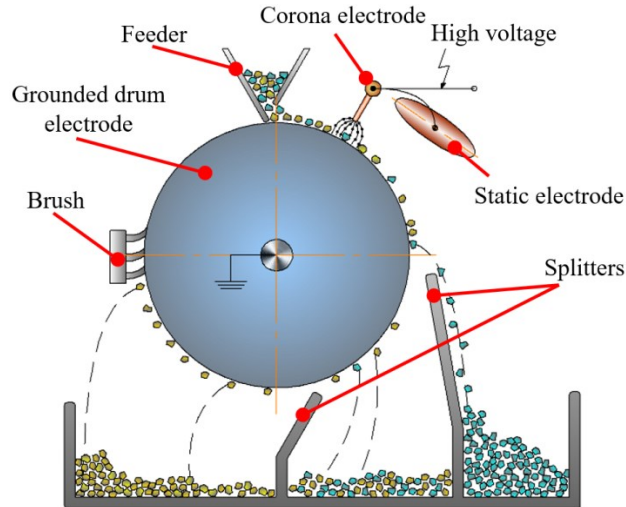


Figure 1.2.2. Corona electrostatic separator

Another researcher, He *et al.* (2010), focused his studies on **Eddy Current separation** in the context of WPCB recycling; after a series of experiments, it was found that Eddy Current separation can achieve efficiency of >92% with concentrate enrichment at a level of >95% with a rotor speed 5–15 Hz and a belt speed of 7–9 Hz (He, He, Ge, Duan & Wu, 2010)

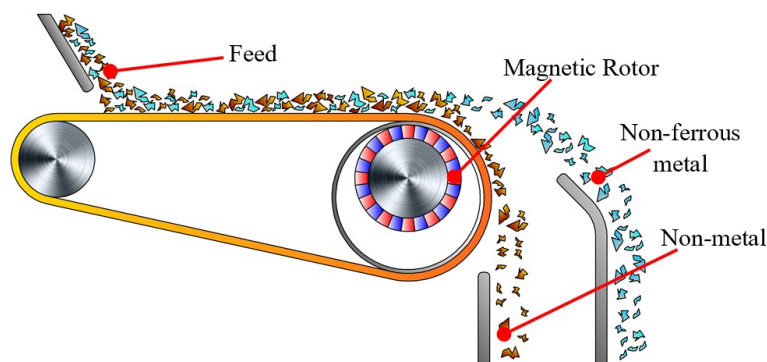


Figure 1.2.3. Eddy Current separator

Magnetic separation has a limited function in WPCB recycling due to mainly being used for removal of ferromagnetic materials from a WPCB stream before other processing steps (Goosey & Kellner, 2003). For instance, a dry magnetic separator was used by Veit *et al.* (2006) at a magnetic field intensity of 6000–6500G in order to separate the magnetic fraction of WPCBs with subsequent electrowinning of copper from the non-magnetic fraction with a purity of >98% (Veit, Bernardes, Ferreira, Tenório & Malfatti, 2006).

It is evident that mechanical treatment is extremely useful in the processing of WPCBs, however, the usage of only mechanical treatment does not allow to fully recover all the components in WPCBs in the light of focusing mainly on Copper recovery while other materials are not given proper attention; in addition, overreliance on mechanical treatment definitely results in the loss of materials due to their volatilization during the milling operations. To avoid the arising issues, mechanical treatment should be supplemented with other treatment technologies that are discussed in the following sections.

1.2.2. Thermal treatment

Thermal treatment of WPCBs is based on using heat to decompose the organic constituents of WPCBs thus reducing their volume and liberating the most valuable part of WPCBs – metals (Cui & Zhang, 2008). Thermal treatment includes some of the simplest treatment techniques as well as some of the most advanced ones. Among the simple techniques, combustion and incineration take a central place and are used almost universally (Shen, Chen, Ge & Chen, 2018a).

Combustion and incineration. Uncontrolled combustion is chiefly used in the developing countries for the treatment of E-waste including WPCBs and is associated with a multitude of health risks (e.g., the release of harmful Volatile Organic Compounds (VOCs) and the pollution of soil/air/water) due to the low burning temperatures as discussed previously in **Section 1.1.3**. At the same time, Incineration, unlike combustion, is a controlled process performed at a high temperature (>800°C) while the input material and the output gases are thoroughly monitored (Batnasan, Haga & Shibayama, 2018). WPCBs with their calorific value of $\sim 9.9 \times 10^4$ kJ/kg are a good material for incineration and significantly shrink in volume ($\sim 50\%$) after the

incineration process (Jie, Ying-Shun & Mai-Xi, 2008; De Marco *et al.*, 2008). Unfortunately, incineration is far from being a perfect solution for the treatment of WPCBs because of several reasons. After the process, the NMF of WPCBs (up to 70% of the original weight) is usually lost whereas such modern strategies as Circular Economy set a goal of maximizing the recycling rate (Pomponi & Moncaster, 2017). Another problem arising from incineration is the high concentrations of heavy metals in fly and bottom ash. Long *et al.* (2013) performed a series of experiments conducted in a pilot-scale incineration plant for WEEE residues and reported elevated concentrations of Cu, Zn, Pb, Ni and Cd both bottom and fly ash as shown in **Fig. 1.2.4.** (Long, Feng, Cai, Ding & Shen, 2013). Lastly, the metals which are concentrated in the bottom ash after incineration still require an additional enrichment procedure in order to be used again, for example, leaching by acids or density classification (Gurgul, Szczepaniak & Zabłocka-Malicka, 2018).

Therefore, more advanced **pyrolytic techniques** were developed and tested by a number of researchers. The main difference between pyrolysis and incineration is that pyrolysis is conducted in the oxygen-depleted inert atmosphere; this allows avoiding combustion and triggering decomposition of organic materials in WPCBs so that to obtain various new compounds including fuels (Quan, Li, Gao & Dan, 2010). The typical conditions of WPCB pyrolysis are Nitrogen or Argon atmosphere and a temperature of 400–700 °C, whereas the reaction products are H₂, CO₂, CO, and CH₄ (Gurgul *et al.*, 2018; Yang, Sun, Xiang, Hu & Su, 2013).

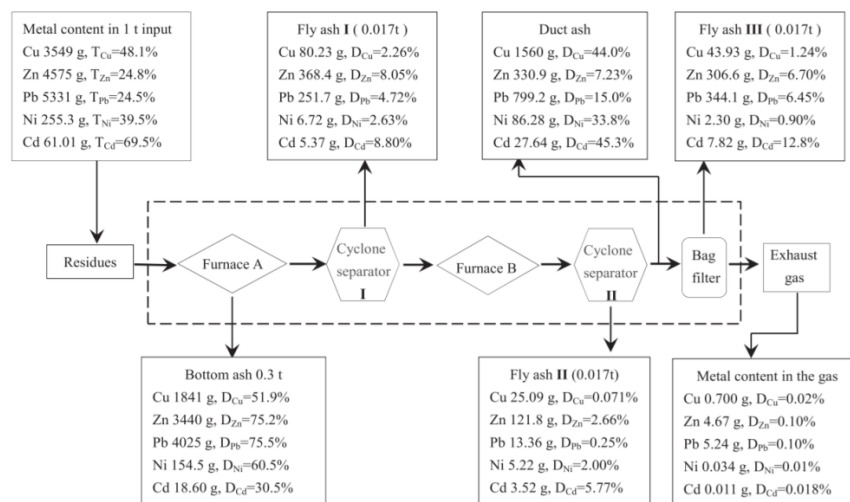


Figure 1.2.4. Flow of heavy metals from the WEEE dismantling residues in the incinerator (Long *et al.*, 2013)

Researchers working on this topic pay special attention to the toxicity and debromination of pyrolysis-generated compounds since Bromine is a major component of Brominated Flame Retardants used for manufacturing of PCBs (Alaee *et al.*, 2003).

Chien *et al.* (2000) found that, after pyrolysis at 823K (550°) for 30 min., 40.6 wt.% of the reaction product was composed of oils (light naphtha and heavy gas oil),

34.5 wt.% was constituted of solid residues, and 24.9 wt.% were non-conductible gases while Bromine was mainly found in the off-gas stream and oils in the form of HBr and Bromobenzene (Chien, Paul Wang, Lin, Huang & Yang, 2000). Cayumil *et al.* (2016) used a horizontal tube furnace (Fig. 1.2.5.) to conduct pyrolysis of precious metal-containing samples of WPCBs at high temperatures (800–1350 °C); as a result, the generation of harmful substances was minimized; thus concentrated Pd, Ag, Au and Pt were found in the recovered metallic fractions while the original NFM was converted into slag residue (Cayumil *et al.*, 2016).

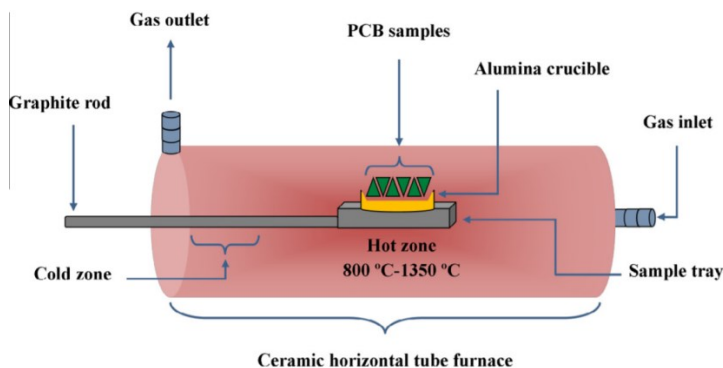


Figure 1.2.5. Setup for pyrolysis process (Cayumil *et al.*, 2016)

According to the results reported by Ye *et al.* (2018), the content of Bromine in the pyrolysis oil obtained after treatment at 500 °C could be reduced from 59.07 wt.% to 4.68 wt.% by using compound additive Fe_3O_4 and catalysts (Ye *et al.*, 2018). Shen *et al.* (2018b) studied the possibility of combining chemical pre-treatment with pyrolysis and came to the conclusion that leaching by HCl could provide removal of 92.4 wt.% of Cu in the raw feedstock, alkali (NaOH, KOH) pre-treatment notably improved the fixation of Br in char up to 53.6 %, and the overall environmental friendliness of the pyrolysis was significantly improved (Shen, Chen, Ge & Chen, 2018b).

Pyrometallurgy is another variation of thermal treatment, an approach aiming for recovery of metals from E-Waste (including WPCBs) by smelting the waste in plasma arc furnaces or smelters after mechanical-physical pre-treatment (Zhang & Xu, 2016). Such treatment can be highly efficient in terms of base and precious metals recovery, and it already has industrial applications, for instance, in the state-of-the-art plants of the *Umicore* company with an integrated smelter and a refinery which are able to recover both base (copper, etc.) and precious metals (Ag, Au, Pt, Pd, Rh, Ru and Ir) (Tuncuk, Stazi, Akcil, Yazici & Deveci, 2012). However, this approach has its disadvantages as well. Among them there are high capital investments in the equipment, inability to recover or separate epoxy resin and fiberglass (which make up to 70% of the WPCB weight), and high risks of hazardous emissions requiring installation of expensive monitoring and control systems (Ebin & Isik, 2016).

Given the points above, we can see that thermal treatment may be a good solution for some types of WEEE with a high plastic content and in cases of absence of hazardous Bromine; however, WPCBs should be treated more selectively since low

temperatures during the pyrolysis allow for NMF recovery but produce harmful compounds, whereas high temperatures eliminate the unwanted compounds but also degrade the NFM beyond recovery. As many researchers have suggested, Chemical treatment can provide such a selective approach and become the optimum solution of this problem.

1.2.3. Chemical treatment

Probably the most diverse and widely researched set of WPCB processing techniques at the moment is Chemical treatment – and there are a number of reasons for this popularity. Chemical techniques, for example, Hydrometallurgy, are well-suited for the recovery of metal from WPCBs, can be controlled with relative ease and potentially are less harmful for the environment in comparison with pyrometallurgy or heat treatment (Ghosh *et al.*, 2015).

Hydrometallurgy is an extremely widespread set of techniques which has a solution for the recovery of each metal or a combination of metals found in WPCBs. The core principle of Hydrometallurgy is the dissolution of the target metals with the suitable reagents (usually, acidic solutions) so that to later recover the metals or metal-based compounds in the concentrated form which already have a market value (Žiukaitė *et al.*, 2017).

Copper as a major constituent of WPCBs accounting for up to ~33% of its weight can be leached by acidic or ammoniac solutions (Chehade *et al.*, 2014). Behnamfarad *et al.* (2013) used two-step Sulfuric Acid (H_2SO_4) leaching with Hydrogen Peroxide (H_2O_2) as an oxidant to extract 99% of Copper from WPCBs (Behnamfard, Salarirad & Veglio, 2013). A combination of H_2SO_4 and H_2O_2 is useful not only in Copper recovery; these chemicals are also capable of extracting other base metals from WPCBs. To confirm that, Oh *et al.* (2003) treated rushed WPCBs by 2M H_2SO_4 and 0.2M H_2O_2 solution thereby successfully achieving 95% extraction of Cu, Fe, Zn, Ni and Al after 12 hrs. of leaching at 80 °C (Oh, Lee, Yang, Ha & Kim, 2003).

Chemical treatment can be combined with other treatment types in order to achieve the optimum performance. Havlik *et al.* (2010) used pyrolysis at 300–900 °C as a pre-treatment before leaching WPCBs with Hydrochloric Acid (HCl) in the leaching reactor (**Fig. 1.2.6.**); high pyrolysis temperatures resulted in Copper extraction rates of up to 98% (Havlik *et al.*, 2010).

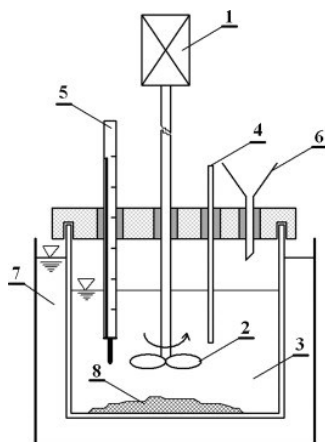


Figure 1.2.6. Typical scheme of a leaching reactor: for WPCBs 1) mechanical stirrer; (2) propeller; (3) leaching pulp; (4) sampler; (5) thermometer; (6) feeder; (7) water thermostat; (8) crushed PCBs (Havlik *et al.*, 2010)

Special attention is given by researchers to the topic of precious metals leaching from WPCBs due to the high concentrations of such metals in WPCBs (e.g., 35–50 times higher Gold content than in ores or concentrates) and high market values of the obtained metals (Akcil *et al.*, 2015; Cui & Zhang, 2008). Normally, there are three target precious metals in WPCBs: Gold (Au), Silver (Ag), and Palladium (Pd); thus extraction technologies focus on simultaneous recovery of all the three or at least two types of them. Petter *et al.* (2014) employed a commercial cyanide-based leaching agent for Gold and Silver extraction thus recovering ~60% of the leachable Gold (500 g/tonne of WPCBs) and 100% of leachable Silver (3,494 g/tonne of WPCBs) (Petter, Veit & Bernardes, 2014). Focusing on the development of an environmentally friendly technique, Jing-ying *et al.* (2012) used thiourea ($\text{SC}(\text{NH}_2)_2$) as a leaching agent and a solution with ferric ions (Fe^{+3}) as an oxidant to dissolve 90% of Gold and 50% of silver contained in crushed WPCBs of mobile phones after 2 hrs. of treatment (Jing-ying, Xiu-li & Wen-quan, 2012).

From the information given above, we can see that Hydrometallurgy can be extremely useful for selective and efficient metal extraction/recovery from WPCBs, whereas its clear weakness is the lack of NMF recovery possibilities and environmental risks of acid-polluted wastewater release into the environment as well as low sustainability of strong acids used in high quantities.

As a response to sustainability and environmental risks of Hydrometallurgy, a new branch of metal recovery technology, Biometallurgy, appeared (Kaksonen *et al.*, 2018). Biometallurgy includes two main research directions – Biological leaching (Bioleaching) which deals with leaching of metals while using various microorganisms and products of their activity, and Biosorption which is focused on the extraction and concentration of previously dissolved metals by the means of biological materials (Gadd, 2009; Mishra & Rhee, 2010; Zhang & Xu, 2016).

Bioleaching relies on acidophilic bacteria (e.g., *Acidithiobacillus* and *Leptospirillum ferrooxidans*, *Acidithiobacillus thiooxidans*, etc.) which are able to

produce sufficiently strong oxidizing and promote the dissolution of metals (Liang, Mo & Zhou, 2010). A specialized bioleaching unit (**Fig. 1.2.7.**) was constructed by Chen *et al.* (2015) to study the copper bioleaching kinetics by *Acidithiobacillus ferrooxidans*; the results indicated that 94.8% copper recovery could be reached after 28 days of bioleaching through Fe^{2+} – Fe^{3+} cycle (Chen, Yang, Liu, Dong & Liu, 2015).

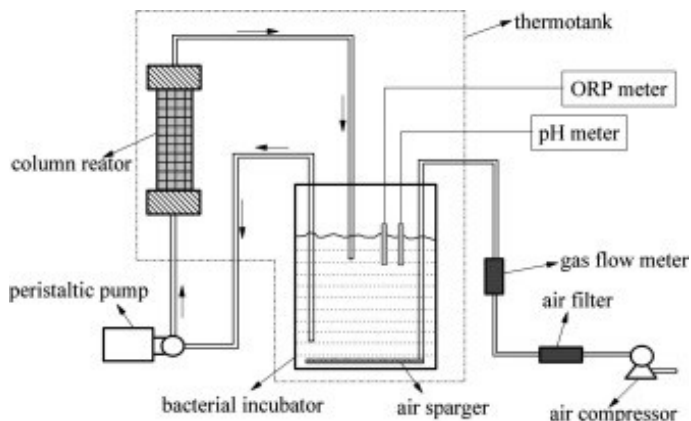


Figure 1.2.7. Bioleaching unit for WPCB treatment (Chen *et al.*, 2015)

One of the major challenges of WPCB bioleaching is the long leaching time of up to several weeks. Zhu *et al.* (2011) found that mixed cultures of bacteria obtained from acid mine drainage can be highly efficient; under the optimum conditions, the process took only 45 hrs. to leach 96.8% of copper, while 98 hrs. were needed to leach 88.2% of aluminium and 91.6% of zinc (Zhu *et al.*, 2011). The efficiency of WPCB bioleaching still requires improvements, especially for precious metals that are highly resistant to chemical treatment. Işıldar *et al.* (2016) came to a decision to conduct bioleaching of WPCBs in two steps, firstly by extracting base metals and then focusing on gold in order to increase the metal mobilization efficiency; as a result, 98.4% of copper (leaching with *A. ferrivorans* and *A. thiooxidans*) and 44% of gold (leaching with *P. putida*, strain WCS361) were leached after 48 hrs. of treatment (Işıldar, van de Vossenberg, Rene, van Hullebusch & Lens, 2016). Currently, Bioleaching is being considered a very promising technology that requires low energy consumption, capital investments, and labour intensity; the main challenges come from its long treatment time as the technology is still under development (Guo *et al.*, 2016).

As for **Biosorption**, it can be done by using several types of microorganisms – fungi, algae, bacteria as well as waste biomaterials in order to accumulate the metals inside the biomass for later collection instead of the traditional approach using reagents for metal precipitation (Gadd, 2009). Potentially, a combination of bioleaching or another environmentally-friendly leaching approach and biosorption can be a highly effective solution for E-waste recycling; Gurung *et al.* (2013) tried to demonstrate this by using sustainable acidothiurea leaching combined with biosorption by agricultural waste – persimmon tannin-based gel (Gurung *et al.*, 2013). The investigation showed that this technique was suitable for the recovery of gold and

silver. Another researcher, Côrtes *et al.* (2015), investigated biosorption of gold recovered from gold-plated microprocessor pins by chitin; as a result, ~80% of gold was recovered by using two-step precipitation followed by biosorption with a chitin concentration level of 20 g L⁻¹ at 298 K for 4 hrs. (Côrtes, Tanabe, Bertuol & Dotto, 2015).

Supercritical technology. As mentioned above, one of the key issues of Hydrometallurgy is its inability to properly treat the NFM of WPCBs containing potentially hazardous organic compounds. Researchers have recently introduced a new technology, Supercritical Fluid treatment, which could be extremely useful in the utilization of WPCBs. Supercritical Technology requires high pressure and temperature (e.g., for water, it is 374 °C and 22.1 MPa), under the effect of which, fluids gain an unusual combination of properties of both liquid (the ability to dissolve substances) and gas (the ability to effuse through solid materials); this enables Supercritical Fluids to be extremely efficient at decomposing organic substances (Zhang & Xu, 2016).

As shown by Matsumoto *et al.* (2014), Supercritical Water Oxidation (SCWO) can be a good alternative to pyrolysis of WPCBs with the objective of epoxy resin removal (Matsumoto & Oshima, 2014). Matsumoto *et al.* (2014) managed to reach 99 wt.% recovery of metallic Au and Cu, while also simultaneously removing 90% of organics from WPCBs by treating it in a batch-type reactor with a reaction chamber size of 10.5 cm³, sample weight of 30 mg, pressure equaling 25 MPa and temperature being set at 380 °C. The applicability of Supercritical Methanol (SCM) for WPCB treatment was shown by a group of Chinese researchers (Xiu & Zhang, 2010). Xiu *et al.* (2010) discovered that the usage of SCM can be more favourable compared to SCWO since it does not decompose organics, but instead it can be used to produce oils. The experiments in a 200-ml high pressure supercritical reactor on WPCBs at 350 °C produced phenol with 58% purity while Bromine was recovered from such gaseous products as HBr; up to 62% of metals including Cu, Fe, Sn, Pb, Zn were recovered as well.

Supercritical Technology appears to be an extremely effective WPCB treatment approach, although the main challenge for this technology is the increase of the scale of supercritical devices for industrial use. As the literature suggests, laboratory reactors used for this purpose are very small, and bigger high-pressure prototypes or full-size industrial equipment would be quite expensive in manufacturing (special materials needed) and operation (sustained treatment at 350–450 °C).

Solvent treatment

Finally, a new technology in the field of WPCB recycling was developed recently. An organic solvent treatment method has been lately employed as a new environmentally friendly recycling technique with a significant reduction in the emission of toxic gases and a high efficiency for WPCB separation (Huang, Yu, Dai & Wang, 2011). The focal point of the new technique is that its main principle lies in the dissolution of brominated epoxy resin (BER) by using various solvents to break the internal van der Waals' bonds between BER and other components of WPCB; hence, BER is gradually dissolved in the solvent, and the delamination of the WPCBs

followed by complete separation takes place (Wath, Katariya, Singh, Kanade & Vaidya, 2015). *N*-Methyl-2-pyrrolidone (NMP), dimethyl sulfoxide (DMSO) and Dimethylformamide (DMF) are common solvents used in this separation approach due to their high boiling point, relatively high viscosity, and high thermal stability with ability at high efficiency levels to dissolve numerous organic and inorganic chemicals without corroding metals (Verma *et al.*, 2016; P. Zhu *et al.*, 2012; Zhu, Chen, Wang, Qian *et al.*, 2013).

Based on the results obtained by Zhu *et al.* (2013), chemical treatment using Dimethylsulfoxide (DMSO) can be effectively used to dissolve epoxy resin of WPCBs and separate metal from non-metal. Despite the promising results, the temperature of the dissolution process was relatively high (130–170 °C), whereas the size of the separated samples did not exceed 2–3 cm². It is worth highlighting that the recovered metal elements according to the reported results can be used for several applications, while the recovered woven fiberglass layers only have limited application since fiberglass was recovered in the form of small pieces. Such a material can be used as a filler after milling in order to improve the mechanical behavior of plastic, wood, and concrete composites. Moreover, the recovered epoxy resin can be applied for the production of composite structural materials in marine, automotive and various other industries after some additional treatment since, according to the literature, cured epoxy resin can still be repolymerized and recycled (Dang, Kubouchi, Yamamoto, Sembokuya & Tsuda, 2002; Iji, 1998; Jin, Li & Park, 2015; La Rosa, Banatao, Pastine, Latteri & Cicala, 2016).

The physical and chemical properties of NMP and DMSO were discouraging in the view of commercial viability as well as in terms of public health since DMSO is classified as a highly hygroscopic solvent with high specific heat, high viscosity, and an ability to penetrate human skin; furthermore, its vapours are heavier than air. Dimethyl formamide (DMF) is a colourless aprotic solvent, and it is relatively cheaper when compared with DMSO and NMP. Also, DMF is more stable up to its boiling point of 153 °C; its evaporation rates are low. This motivated Verma *et al.* (2016) to replace DMSO and NMP with (DMF) so that to achieve the dissolution of BER in WPCBs and the separation of its components (Verma *et al.*, 2016). The scholars investigated the effect of various parameters on the optimum dissolution time and the concentration of BER in DMF. The results obtained by using the experimental setup (shown in **Fig. 1.2.8.**) highlighted that the technique was most effective with the following parameters: WPCB sample size of 1 cm × 1 cm, separation time of 4 hours with the temperature being set at 135 °C.

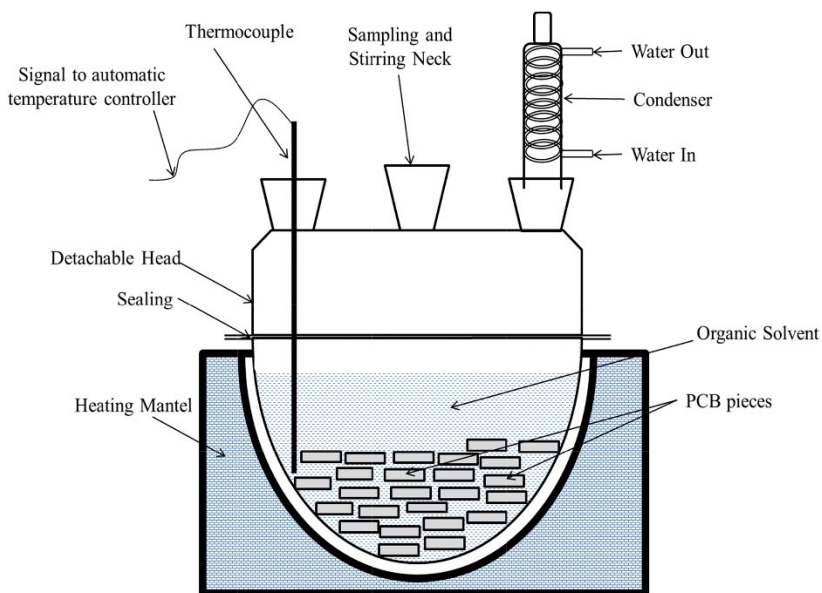


Figure 1.2.8. Experimental setup for solvent treatment of WPCBs (Verma *et al.*, 2016)

However, the size of the separated samples still did not exceed 16 cm², also, all the experiments were performed inside a flask placed in a heating mantle, which has several disadvantages – first of all, the heating mantle is only suitable for round-shaped flasks, and it can cause local superheating and decomposition of heated chemical substances due to the probability of the glass of the flask being at significantly higher temperatures than the chemical substances contained inside the flask. In addition, it is very hard to combine the reported system with other techniques so that to accelerate the recycling process. Besides, the volume of the flask is small, which does not allow to use it for the separation of full-size WPCBs. In addition, this technology still requires relatively high energy consumption (due to the need to reach 135 °C), which is difficult to apply on the industrial scale. It was also noted that most of the WPCB recycling techniques focused on the development of the approach and were applied only on one type of the WPCB model despite each model having a different configuration, e.g., different numbers and structures of woven fiberglass layers, the presence or absence of filler materials inside the substrate, different solder mask types, the size and shape of conductive tracks, etc. (Singho, Lah, Johan, & Ahmad, 2012).

1.3. Applications of secondary raw materials recovered from WPCBs

1.3.1. Non-metallic fraction

Non-Metallic Fraction, or NMF, recovered from WPCBs by the means of one of the appropriate recycling techniques, can usually be obtained separately from the metallic fraction as shown in **Fig. 1.3.1**.

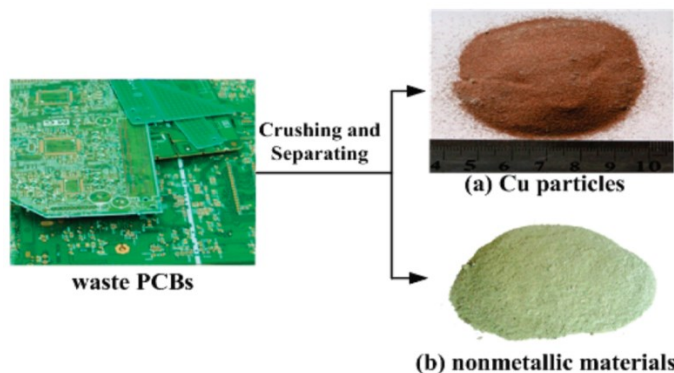


Figure 1.3.1. Example of metallic and non-metallic fractions recovered from WPCBs (Guo, Cao, Guo & Xu, 2008)

This fraction containing Fiberglass, Epoxy Resin and other organic components can be used in the following applications (Hadi, Xu, Lin, Hui & McKay, 2015):

- Phenolic moulding compounds;
- Filler for construction industry;
- Polymer composite filler;
- Porous material for sound absorption;
- Adsorbent production.

Phenolic Moulding Compound (PMC) produced by Guo *et al.* (2008) from pulverized phenolic WPCBs contained 20% of recycled NMF that was used to replace the traditional wood flour filler (Guo, Li, Rao & Xu, 2008). The resulting properties of the composite (Flexural strength 70 MPa, HDT 168 °C, charpy V-notch impact strength 2.4 KJ/m², dielectric strength 3.9 MV/m, and fluidity (Raschig) 103 mm) were all in the range of the standard data, which suggests that the composite containing recycled materials had sufficient quality to match the original PMCs.

The construction industry, as reported in researches, can make use of recovered NMF by using it as a filler in asphalt or concrete (Guo, Guo, Wang & Xu, 2009; Panyakapo & Panyakapo, 2008). Guo *et al.* (2009) showed improvements in high temperature performance of asphalt by adding 25 wt.% of NMF; the parameters were as follows: viscosity (1225 cP at 135 °C), $G^*/\sin \delta$ (3995.27 Pa at 60 °C), upper limit temperature (69.4 °C), etc. According to Wang *et al.* (2012), fresh cement mortar with NMF additives is denoted by better water retention, while hardened mortar has higher bulk density; such cement mortar is a green building material with a wide variety of applications (Wang, Zhang & Wang, 2012).

A significant amount of work has been done in the production of various polymer composites from the recycled NMF; fiberglass was used to reinforce Polypropylene (PP), Polyester, and other polymers (Hong & Su, 1996; Zheng, Shen, Cai, Ma & Xing, 2009a). Zheng *et al.* (2009a) reported that the presence of fiberglass in PP composite inhibits the formation of big cracks but instead triggers the formation

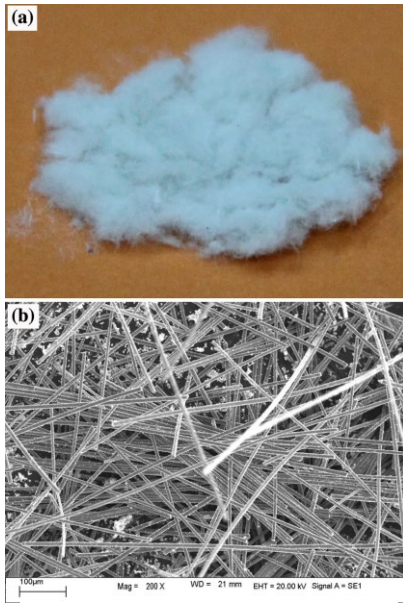


Figure 1.3.2. Recovered fiberglass for sound insulation application (Sun *et al.* (2015))

of micro-cracks consuming a prohibitively high amount of energy; as a result, NMF-reinforced composites are denoted by significantly improved flexural strength and modulus. In another study presented by Xu *et al.* (2016), a composite containing β -nucleated polypropylene and nonmetallic particles was prepared; the additives greatly increased the impact strength (205.3%) and the flexural modulus (61.8%) of the final product (Xu *et al.*, 2016).

Sound insulation is another application where recycled fiberglass can be efficiently used (Hadi *et al.*, 2015). Sun *et al.* (2015) used recovered fiberglass (**Fig. 1.3.2.**) to produce a sound insulation material with a thickness of 30 mm and the average sound absorption coefficient of >0.8 in the 100–6,400 Hz frequency range (Zhixing Sun, Shen, Ma & Zhang, 2015).

Lastly, the possibility of using recycled NMF for the production of a chemically activated adsorbing agent or an exchange type resin is studied (Hadi, Gao, Barford & McKay, 2013).

Hadi *et al.* (2013) showed that the chemical activation of NMF with potassium hydroxide (NaOH) can produce a good absorbent of toxic heavy metal (tests done for Cu and Pb) ions with the positive charge which demonstrated properties similar to commercial adsorbents. Such a functionalized NMF-based adsorbent may even deliver a better removal efficiency than industrial resins and selectively extract metals in multi-metallic solutions (Hadi, Barford & McKay, 2014).

1.3.2. Metallic fraction, reprocessing into nanomaterials

Metals recovered at the end of WPCB processing are represented with main elements denoted by sizable weight percentages – Cu, Sn, Pb, Zn, Fe and the precious ones, i.e. metals of highest value – Ag, Ag, Pd (Park & Fray, 2009). The shape and condition of metals may depend on the type of the recycling technology in use – it may be metal-rich droplets or wires after pyrolysis (**Fig. 1.3.3.**), pulverized material (**Fig. 1.3.1.**), metal foils after solvent treatment (**Fig. 1.3.4.**), etc.

Having obtained concentrated metals, it is relatively easy to treat them while using traditional metal refining technologies in order to obtain raw material for manufacturing new products (Zhang & Xu, 2016). However, these recycled metals do

not possess much added value; therefore, a number of researchers tried to address this problem and find routes for reprocessing metals recovered from WEEE and WPCBs into products with a high added value (Xiu & Zhang, 2009).

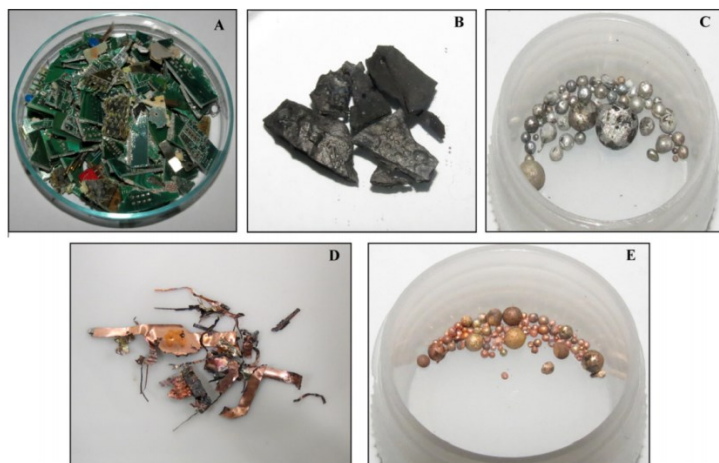


Figure 1.3.3. Pyrolysis products: A) WPCBs before treatment; B) Carbon-rich slug; C–D) Metal-rich phases; E) Copper-rich metallic phase obtained after heat treatment at 1150 °C (Cayumil *et al.*, 2016)

Currently, the concept of Circular Economy (CE) has been receiving increasing attention worldwide as a way to overcome the issues of the current production and consumption model that is based on the continuous growth and the increasing resource throughput; with special focus being on urban and industrial waste mining, the purpose of CE is to make economic systems and industrial processes more environmentally friendly and sustainable. This can be achieved through long-lasting design, maintenance, repair, reuse, remanufacturing, refurbishing, and recycling (Geng, Fujita, Park, Chiu & Huisingsh, 2016; Ghisellini, Cialani & Ulgiati, 2016).

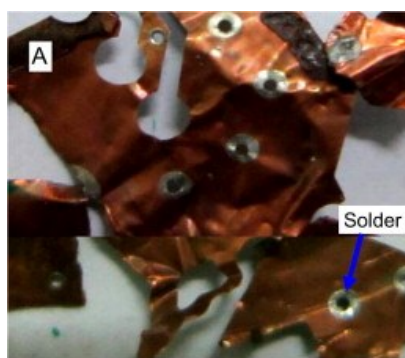


Figure 1.3.4. Metallic foils obtained after solvent treatment (Zhu, Chen, Wang, Zhou & Zhou, 2013)

Recently, a Chemical WPCB treatment technique has been developed to apply the CE-Remanufacturing concept for the metallic fraction of WPCBs in order to

produce High Added Value Products (HAVPs) from the recovered Cu. Copper Nanoparticles (Cu-NPs) are considered as the most appropriate choice for HAVP production, especially since Cu-NPs are widely used in a variety of fields, such as photochemistry, catalysis, electronics, optics, biosensing, gas sensors, electrochemical sensing, solar/photovoltaic energy conversion, lubrication, nano-fluids, etc. (Gawande *et al.*, 2016; Gurav *et al.*, 2014; Khodashenas & Ghorbani, 2014; Zin *et al.*, 2013). In order to satisfy the excessive demand for Cu-NPs, several production techniques have been developed, e.g., chemical reduction, sonochemical reduction, thermal reduction, γ -radiation, laser ablation, reverse micelles, electron beam irradiation, micro-emulsion techniques, wire explosion, etc. (Din & Rehan, 2017; Rafique *et al.*, 2017).

Recently, there have also been some attempts to produce Cu-containing nanoparticles from WPCBs, for example, Xiu and Zhang, 2009, Shokri *et al.* (2017), and Xiu *et al.* (2017) used electrokinetic, thermal micronizing, and supercritical methanol processes for this purpose, respectively (Shokri, Pahlevani, Levick, Cole & Sahajwalla, 2017; Xiu *et al.*, 2017; Xiu & Zhang, 2009). Although the results were promising and nanoparticles with the average size of <500 nm were produced, various restrictions related to energy consumption, process efficiency, recovery yield or recycling rate, economic profitability, pollution rate, and focus on metals recovery only emerged during the nanoparticles preparation processes. In addition, the prepared nanomaterials were not only pure Cu-NPs, but also Cu-Tin alloy and nano-Cu₂O, which indicates the difficulty of producing pure Cu-NPs from WPCBs since Cu can oxidize or dissolve other metals inside itself during the treatment process if WPCBs are treated as received without separation into fractions. In addition, the reported techniques did not recover most of the non-metallic components of WPCBs; therefore, such methods may encounter difficulties in terms of the residue disposal. Accordingly, the liberation of Cu foils from WPCBs at the beginning and preparation of Cu-NPs from the recovered foils may be a promising way to increase the yield and purity of the synthesized Cu-NPs. Besides Cu-NPs, there were some attempts to produce other types of nanomaterials from WPCBs, such as lead nanoparticles and carbon nanotubes (Quan, Li & Gao, 2010; Zhan *et al.*, 2016).

Recently, two promising techniques for Cu-NPs synthesis have been reported which could be applied for WPCB reprocessing. Khalil *et al.* (2014) employed the Electrospraying technique to produce Cu-NPs by using a precursor composed of copper acetate and poly(vinyl) alcohol and setting the voltage in the range of 20–29 kV (Khalil, Jouiad, Khraisheh & Hashaiekh, 2014). The results showed that the obtained Cu-NPs had an average diameter between 30 nm and 70 nm while still demonstrating a good yield and size distribution.

The second technique involved using Green Chemistry as an advanced eco-friendly synthesis method to prepare Cu-NPs while employing environmentally benign non-toxic solvents (Nasrollahzadeh, Momeni & Sajadi, 2017). Native Cyclodextrins (NCDs) proved to be highly effective in the field of green chemistry; they are used in many applications related to pharmaceutical, food, and cosmetic industry (Davis & Brewster, 2004; Szejtli, 2005). NCDs are circular-shaped

molecules with a relatively simple structure whose main feature is the ability to form inclusion complexes by hosting small molecules within their hydrophobic cavity at basic pH. Native Cyclodextrins are soluble in water due to the presence of primary and secondary hydroxyl groups. In addition, NCDs are non-toxic by their nature; therefore, their usage can be highly recommended above other more hazardous chemicals (Loftsson & Duchêne, 2007). Therefore, Suárez-Cerda *et al.* (2016) used NCDs (α -, β -, and γ -NCD) as a stabilizing agent to synthesize Cu-NPs through the chemical reduction of aqueous solutions of Copper (II) Sulfate (CuSO_4) with ascorbic acid (Suárez-Cerda *et al.*, 2016). The results showed that the nanoparticles synthesized via the developed method were stable for several months without physical or chemical changes and had the size range of 2–23 nm. The optimum stabilizing agent was β -NCD, which facilitated the production of nanoparticles with minimum size distribution due to its rigid structure and low water solubility, which makes the nanoparticle complex precipitate easily.

1.4. Summary of the Literature Review

As it has been shown in the previous Sections, in many countries, environment and human health are being put in great risk due to the improper recycling of E-waste and particularly WPCBs. Although rich in metals, this type of waste requires special treatment in order to fully recover the contained materials without creating waste fractions. Thus a current challenge is to find and develop a proper treatment approach towards this type of waste. Having reviewed the relevant WPCB recycling technologies, we can now perform their side-by-side comparison and indicate the most promising direction of research. The generalized evaluation results are summarized in **Table 1.4.1**. As it can be seen, the more traditional treatment approaches, such as mechanical treatment and thermal treatment, appear to be less favorable options for WPCB recycling. The core issues of Mechanical Treatment are the inability to purify metallic and non-metallic fractions beyond a certain degree, to separate all individual metals in the metallic fraction, as well as the inability to separate fiberglass from epoxy resin. An additional downside is the inevitable generation of dust during the treatment, which negatively affects the environmental and treatment efficiency (loss of volatilized metals) scores; unfortunately, it also results in high capital cost (Cui & Forssberg, 2003).

Table 1.4.1. Generalized comparison of current WPCB treatment/recycling technologies (based on the technology comparisons done by Awasthi *et al.* (2017) and Ning *et al.* (2017) (Awasthi, Zlamparet, Zeng & Li, 2017; Ning *et al.*, 2017))

Criteria Technology	Efficiency	Environmental Risk	Technology Cost	Treatment Time	Recoverables
Mechanical Treatment	Medium (✓✓)	Medium (✓✓**)	High (✓*)	Low (✓✓✓***)	<ul style="list-style-type: none"> • Non-metallic fraction; • Metallic fraction.

Thermal treatment	High (✓✓✓)	High (✓)	High (✓)	Low (✓✓✓)	<ul style="list-style-type: none"> • Energy; • Oils; • Metallic fraction.
Hydrometallurgy	Medium (✓✓)	Medium (✓✓)	Low (✓✓✓)	Medium (✓✓)	<ul style="list-style-type: none"> • Pure metals or metallic compounds.
Biometallurgy	Low (✓)	Low (✓✓✓)	Medium (✓✓)	Long (✓)	<ul style="list-style-type: none"> • Pure metals or metallic compounds.
Supercritical Fluid	High (✓✓✓)	Low (✓✓✓)	High (✓)	Low (✓✓✓)	<ul style="list-style-type: none"> • Oils; • Fiberglass; • Metallic fraction.
Solvent Treatment	High (✓✓✓)	Low (✓✓✓)	Medium (✓✓)	Medium (✓✓)	<ul style="list-style-type: none"> • Pure metals; • Epoxy resin; • Fiberglass.

*, **, *** - Ticks represent how beneficial the reviewed aspect of the technology is. For example, **Low environmental risk** has ✓✓✓ rating, which means that it is very beneficial, whereas **Low efficiency** has ✓ rating, which means that it is a weak point of the technology.

Thermal treatment, similarly to Mechanical treatment, cannot recover both metals and nonmetals; it produces mainly a concentrated metallic fraction and oils or energy. Operation at high temperatures imposes specific requirements on the equipment as well as on the materials it is manufactured from; as a result, the technology costs are high. Furthermore, such a technology is associated with high environmental risks as organic decomposition products can be extremely hazardous, thus emission control and treatment systems are needed within the technology, therefore additionally increasing its cost (Yang *et al.*, 2013).

Hydrometallurgy, as proven by many studies, can be a solid approach to the recovery of metals (including precious ones) from WPCBs with high purity, however, the method does not offer a possibility to recover NMF, it pollutes the treatment residue with various chemical agents and consumes high amounts of strong acids/bases (Tuncuk *et al.*, 2012). Biometallurgy solves some problems of hydrometallurgy as it does not require such high reagent consumption and is more environmentally benign as the technology can produce the needed reagents by means of biological organisms. Despite the high potential, as for now, biometallurgical WPCB treatment is far from being industrially feasible (especially for precious metal extraction) due to its long metal extraction times and low efficiency (Ilyas & Lee, 2014).

Furthermore, we can evaluate the Supercritical Fluid Technology. This approach is perhaps the most efficient one among all the reviewed technologies; moreover, it has a potential to completely eliminate the environmental risks of toxic

organic compounds by oxidizing them to basic organic compounds and producing flame retardant-free oils. The drawbacks of the approach stem from its reaction conditions – high pressure and temperature make the construction of industrially-sized equipment difficult and costly, whereas the reactors used for studies feature very small reaction chambers (10–200 ml) (Xing & Zhang, 2013).

Finally, it should be highlighted that it was found that the newly-emerged Solvent Treatment can be seen as the optimum choice when considering all the above-mentioned approaches. It can provide both high efficiency and low environmental risks, at the same time featuring a moderate technology cost and treatment time. Most importantly, Solvent Treatment can recover all the components of WPCBs, including metals, fiberglass, and epoxy resin, simultaneously generating a minimum amount of waste and thus going along with the Zero Waste and Circular Economy concepts (Korhonen, Nuur, Feldmann & Birkie, 2018; Song, Li & Zeng, 2015; Verma *et al.*, 2017b). Given all the points reviewed during the literature analysis, we may observe that Solvent Treatment is a very promising recycling approach with many benefits compared to the other approaches (recovery of all the original materials from WPCBs, no high pressure or temperature needed) that needs to be improved in the following ways in order to become more competitive:

- We need to find such process conditions that would provide the optimum separation efficiency not only for size-reduced WPCBs but also for full-sized samples, while the process should occur below the boiling temperature of the solvent in order to decrease the potential hazardous gas emissions and solvent degradation;
- Preliminary economic and environmental performance analysis of the process should be done to better reveal the benefits of using the new process conditions. The obtained materials should be thoroughly analyzed to indicate their quality, potential applications and to discover whether any additional purification is needed;
- Ways of reprocessing the recovered materials into products with a high added value should be suggested since it has been reported that specific materials in WPCBs have a potential for such a step. This can help to close the loop of the technology and increase the sustainability of the approach.

Additionally, based on our literature analysis in terms of discussion of the currently used and researched practices, pre-dismantling was selected as a necessary step to increase the flexibility and efficiency of the developed approach. An extremely extensive investigation done by Rocchetti *et al.* provided a review of >200 international patents on the topic of PCB recycling registered within the period of 1990–2017; it was indicated that virtually all the recycling approaches employed some way of dismantling necessary for the removal of reusable and hazardous components mounted on the PCB substrate (see Chapter 2 and Fig. 1 in the referenced article) (Rocchetti *et al.*, 2018). Researchers working on the development of new WPCB treatment technologies also suggest that disassembly is an essential part of the WPCB recycling process as different types of mounted components (capacitors, batteries, etc.) require dedicated treatment (see Chapter 5.1.1. in the reference) (Ghosh *et al.*,

2015). While some recycling approaches (e.g., some types of pyrometallurgical treatment) may not require pre-dismantling of WPCBs prior to processing, the information discussed above was sufficiently convincing to implement pre-dismantling in the current work. In addition, inclusion of pre-dismantling in the developed technology was supported by the fact that, currently, there is a number of highly promising dismantling technologies such as semi/fully automatic dismantling, chemical/thermal desoldering followed with automated sorting of components which would be a great addition to the solvent treatment and would provide a significant advantage compared to the treatment of non-dismantled WPCBs (Jianbo Wang, Guo & Xu, 2015; Zhang *et al.*, 2015).

Thus a decision was made to focus on the development of the Solvent Treatment approach in this thesis while using the specific solvents reported in the literature since the reviewed researches on this subject revealed certain weak and not-yet-addressed sides of the approach.

2. MATERIALS AND METHODS

Structure of the research

The overall structure of the research may be split into two major sections: *Solvent Treatment* and *Reprocessing into High Added Value Products* as shown in **Fig. 2.1.** with the layout box numbers corresponding to the respective sections in the materials and methods Chapter.

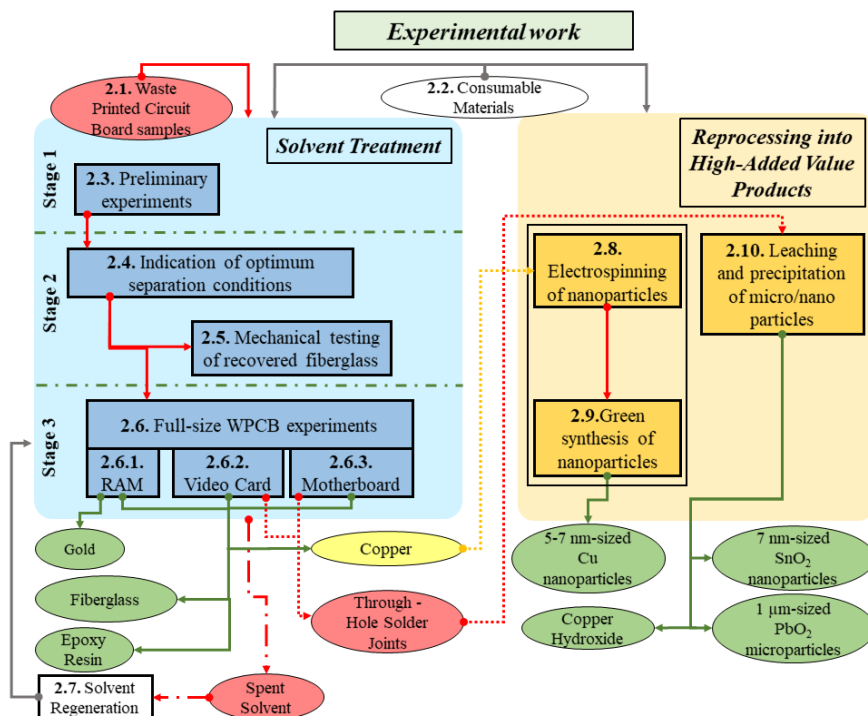


Figure 2.1. Structure of the experiments in the thesis (the numbered boxes correspond to the subsections in the materials and methods Section)

Solvent Treatment, as the main focus of the thesis, included most of the experimental work and was split into three stages. A number of WPCB samples (**box № 2.1.**) was selected and prepared specifically for each stage. Both solvent treatment and Reprocessing sections also required certain consumable materials (**box № 2.2.**).

During the first stage, initial solvent treatment experiments (**box № 2.3.**) were conducted on milled WPCB samples.

After the results had been achieved, work progressed into the second stage when experiments were already conducted on cut 10 mm-sized specimens (**box № 2.4.**). When the optimum conditions had been created, mechanical specimens with specific dimensions were cut from WPCBs, separated into layers, and the quality of the recoverable fiberglass was tested in order to indicate/define its possible applications (**box № 2.5.**).

During the third stage, three common full-sized types of WPCBs (RAM, Video Card, Motherboard) were separated by using the conditions found previously (**box № 2.6.**). The spent solvent received during all the steps of solvent treatment was regenerated (**box № 2.7.**). Three materials were received from all the three types of WPCBs, specifically, Epoxy Resin, Fiberglass, and Copper. While Epoxy Resin and Fiberglass were confirmed to be ready for use in several applications, the recovered Copper was found to have a potential for reprocessing into nanoparticles with a higher added value. Nanoparticles were produced from the recovered copper by employing the Electrospraying approach (**box № 2.8.**). However, the yield of the nanoparticles was found to be very low; thus a decision was made to try another green synthesis production approach; as a result, a bigger amount of nanoparticles was received, and the obtained particles were tested for antimicrobial behavior (**box № 2.9.**).

Finally, it needs to be noted that, during the separation of the motherboard and the video card, through-hole solder joint components were recovered (**boxes № 2.6.2 and 2.6.3.**). These components were composed of several metals and metallic alloys and therefore were not ready to be used in any application thus leaving the loop of the solvent treatment open and requiring additional processing. To solve this issue, acid leaching followed by precipitation was performed, and several types of particles were separately received (**box № 2.10.**).

Additionally, the materials and methods Section includes two more subsections not shown in **Fig. 2.1.**, namely, Subchapter **2.11. Characterizations** dealing with the instruments used in this work, and Subchapter **2.12. Statistical methods and carbon footprint/economic benefit calculation methods**. A detailed description of each experimental step can be found in the subsections below.

2.1. Waste Printed Circuit Board samples

In the present research, in total, 6 different types of WPCBs specimens were prepared, specifically, milled WPCBs, cut 10 mm sized WPCBs, 170 x 30 mm-sized WPCB stripes for mechanical tests (all of these three types were prepared from motherboards as the motherboard is the most common type of WPCB), a full-size Random Access Memory (RAM) card, a full-size Video Card (VC), and, finally a full-size Motherboard (MB). Detailed specifications of each WPCB type can be found in **Table 2.1.1**. All the investigated WPCBs were collected from local electronic repair shops in Lithuania.

At the beginning, the preparation procedures were similar for all the WPCBs: all the mounted electronic components, such as resistors, integrated circuits, capacitors, relays, and transformers, slots, and so forth were removed from the boards by using the appropriate mechanical tools (e.g., pliers), then the dismantled boards were cleaned with compressed air and kept in a desiccator. After that, the preparation was different (i.e., specific) depending on the experiment.

For the **milled samples**, it was taken into account that copper is considered to be the main metallic element in the typical WPCBs that represents up to ~33 % of the total weight (Xiu *et al.*, 2017), while the other metallic elements, such as aluminum, zinc, calcium, iron, manganese, lead and so forth can be found in the solder and

through hole-pad components. Since the amount and distribution of the solder and through hole-pad components in each PCB model are dissimilar, the recovery experiments should be carried on only one model of WPCB so that to determine the optimum recovery conditions. However, the process conditions defined in this case may not be optimal for other types of WPCB. Therefore, during the cutting of samples for milling from WPCBs of different models, an effort was made to avoid the places with drilling holes, notches, and solder joints in order to ensure that all the samples feature a similar structure (copper foil, fiberglass, and epoxy resin).

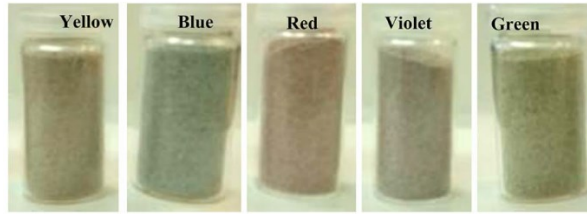


Figure 2.1.1. WPCB powder after the milling process (sample codes in Table 2.1.1., section “Powder”)

Five samples of the size equivalent to the weight of 3 grams (each board had a different density and color) were cut from the tested boards, then ball milling was used to produce a powder denoted by a high degree of fineness from the crushed WPCBs of five types (**Fig. 2.1.1.**); the milling conditions were as follows: 60 min. grinding at the frequency of 20 Hz.

The **cut samples for the separation experiments** were prepared in the following way: three samples with a surface area of 100 mm² were cut from each WPCB model by using a hand cutter (the size was chosen according to the optimum results reported by Verma *et al.* (Verma *et al.*, 2016). It is worth mentioning that, during the cutting of samples from each WPCB, an effort was made to avoid the places with the drilling holes, notches, and solder joints to be sure that all the samples have a similar structure as shown in **Fig.2.1.2**. Then, the WPCB samples were washed and rinsed with distilled water and acetone and subsequently dried for 24 hrs. at room temperature.

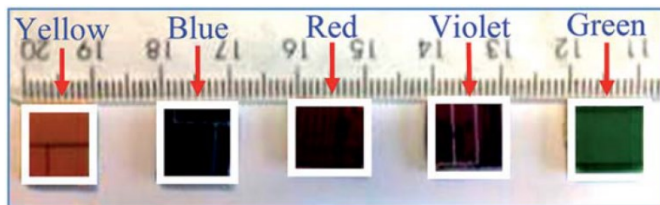


Figure 2.1.2. WPCB samples (10 mm) after cutting (sample codes in Table 2.1.1., section “Separation specimens”)

The **samples cut for mechanical testing** were prepared in a similar way, the only difference was that three samples with the dimensions of 170 x 30 mm were cut from each WPCB model with a manual cutter according to ASTM D5035 Standard as shown in **Fig. 2.1.3.** (Methods, 2015).

The procedures for **RAM** preparation were conducted in a similar way to the previously described steps for other WPCBs, and the RAM substrate after the removal of all the attached components can be seen in **Fig. 2.1.4**.

A **Waste Video Card** (model *Trident-TVGA9000i 3*, Taiwan) was sourced from a local shop in Lithuania. This type of waste video cards was mainly used in desktop computers produced in 1994 (*VGA Legacy MKIII – graphic cards since 1981!*, 2015).

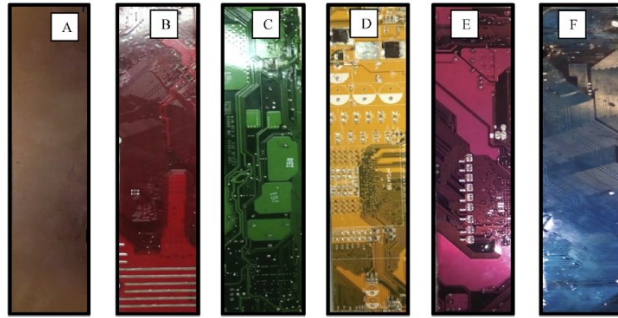


Figure 2.1.3. Images of: A) blank PCB; B) red; C) green; D) yellow; E) violet; and F) blue mechanical specimens (sample codes in Table 2.1.1., section “Mechanical specimens”)

All the electronic components mounted on the board, such as resistors, integrated circuits, capacitors, relays, and transformers, slots, etc. were removed manually by using the appropriate mechanical tools; then, the bare board was cleaned with compressed air, and the final shape of the card is shown in **Fig. 2.1.5**.

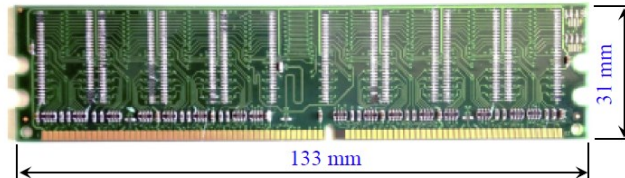


Figure 2.1.4. Image of a waste RAM card with its dimensions

The type of **motherboard** studied in this work was mostly used in desktop computers produced in 1996. **Figure 2.1.6.A.** features a picture of the waste motherboard (WMB), whereas **Fig. 2.1.6.B.** illustrates the distribution of the electrical components on the fiberglass/epoxy resin composite substrate in accordance with the manual of the producing company. In order to prepare the WMB for the separation process, all the electronic components mounted on the motherboard substrate, such as resistors, integrated circuits, capacitors, relays, transformers and slots, etc., were separated by using the appropriate mechanical tools. During the next step, the bare WMB was cleaned with compressed air, washed in warm distilled water followed by acetone bath and finally kept in a desiccator after drying.



Figure 2.1.5. Image of Video Card card with dimensions

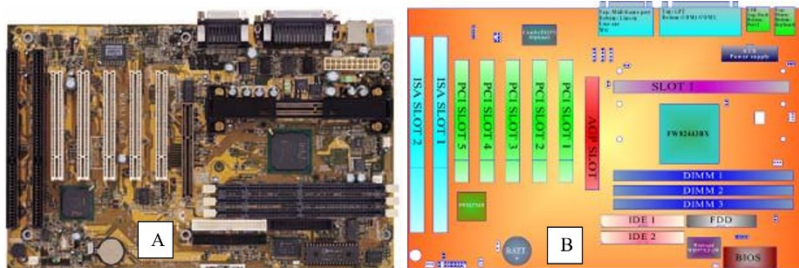


Figure 2.1.6. Image of: A) Waste motherboard and B) Motherboard layout according to the manufacturer's manual (*MSI MS-6163 Motherboard Manual, MSI Computer Corp., 2001*)

Table 2.1.1. Selected WPCBs and their properties

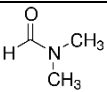
Motherboard	Video Card	Random Access Memory	Cut pieces		Powder	WPCB type/condition
			Mechanical	Separation		
70,400	10,400	4,120	5,100	100	~ 20 – 100 (particles)	Surface area or particle size, mm ² or
320 x 220	168 x 62	133 x 31	170 x 30	10 x 10	-	Dimensions, mm
226	41	13	16	0.7	3	Single specimen weight, gram
<ul style="list-style-type: none"> MS-6163 ATX BX13 	<ul style="list-style-type: none"> Trident-TVGA9000i 3, Taiwan 	<ul style="list-style-type: none"> Apacer 512MB UNB PC3200 CL2.5 400MHz Non-ECC Unbuffered 184-Pin DIMM 	<ul style="list-style-type: none"> Same models and codes as for powder specimens Bare PCB substrate (Code: Blank PCB) 	<ul style="list-style-type: none"> Same models and codes as for powder specimens 	<ul style="list-style-type: none"> Compaq DeskPro EN Socket 370 AGP Motherboard 187498-001 010630-101 (Code: Green) Gigabyte GA-8IG1000-G (Code: Blue) 845GV-MLV (Code: Yellow) MSI PT880 Neo (V2.0) MS-7043 (v1.00) ATX Mainboard (Code: Red) Soltek SL-75DRV5 (Code: Violet) 	Model(s)
1	2	3	6	5	5	Total amount of samples

2.2. Consumable materials

Solvent

Dimethylformamide (DMF) is an aprotic solvent, it is colorless and is relatively cheaper when compared with other similar solvents. Also, DMF is more stable up to its boiling point of 153 °C with low evaporation rates. The main idea behind using an organic solvent in this work lies in the dissolution of Brominated Epoxy Resin (BER) through breakage of Van der Waals' bonds thus separating metal and non-metal components of WPCBs. The main parameters of the solvent are listed in **Table 2.2.1.** below:

Table 2.2.1. Properties of the used solvent

	Dimethylformamide (DMF)
Structure	
IUPAC Name	N,N-dimethylformamide
CAS Number	68-12-2
Molecular formula	C ₃ H ₇ NO
Molar mass, g/mol	73.095
Solubility in water	Miscible
Boiling Point, °C	153
Density, g/mL ⁻¹	0.948

Chemicals for sample cleaning

Pure 96% Ethanol (CH₃CH₂OH) and 97% Acetone (CH₃COCH₃) were used in the present work to remove any dust, grease, chemicals, adhesive, smudges, etc. from the surface of the prepared WPCB samples before the solvent treatment.

Metal leaching

Concentrated Nitric Acid (HNO₃), as a highly efficient oxidizing agent, was used in multiple stages of this work to perform leaching of metals for the purification of gold from gold-plated contacts and leaching of copper from copper foils so that to prepare copper sulfate, and the leaching of tin and lead from through-hole solder joints.

Electrospun copper nanoparticles

Firstly, Acetic Acid ((CH₃)₃COOH) was used to prepare Copper Acetate (Cu(CH₃COO)₂) for the Electrospaying process.

Polyvinyl Alcohol (PVA) was used to produce sol-gel from previously obtained Copper Acetate needed for Electrospaying.

Green synthesis copper nanoparticles

At the beginning, Sulfuric Acid (H₂SO₄) was used to produce Copper Sulfate (CuSO₄) needed for the synthesis of nanoparticles.

After that, Ascorbic Acid was used to synthesize antimicrobial Cu-NPs through the chemical reduction of aqueous solutions of Copper (II) Sulfate (CuSO_4).

Native Beta-Cyclodextrin (β -NCD) was used to stabilize antimicrobial particles during the reduction by Ascorbic Acid. In general, NCDs are circular-shaped molecules with a relatively simple structure whose main feature is the capacity to form inclusion complexes by hosting small molecules within their hydrophobic cavity at basic pH. Native Cyclodextrins are soluble in water due to the presence of primary and secondary hydroxyl groups. In addition, NCDs are non-toxic by their nature; therefore, their usage can be highly recommended above other more hazardous chemicals (Loftsson and Duchêne, 2007).

Finally, Sodium Hydroxide (NaOH) was used as a reagent for intermediate reactions during the synthesis of copper nanoparticles via both routes and for obtaining Copper Hydroxide ($\text{Cu}(\text{OH})_2$) precipitate from leached Through-Hole Solder Joints.

2.3. Preliminary experiments (milled samples)

As mentioned above, in this part of our study, 5 types of WPCBs shown in **Fig. 2.3.1.** were assigned specific codes (see **Table 2.3.1.**) and pulverized. Pulverization was followed by dissolution of BER in organic solvent DMF to break the internal van der Waals' bonds of BER; the dissolution was conducted with the objective to separate the metal particles and the milled fiberglass from BER.

Table 2.3.1. WPCB models and sample codes

Item	WPCB model	Sample code
1	Compaq DeskPro EN Socket 370 AGP Motherboard 187498-001 010630-101	Green
2	Gigabyte GA-8IG1000-G	Blue
3	845GV-MLV	Yellow
4	MSI PT880 Neo (V2.0) MS-7043 (v1.00) ATX Mainboard	Red
5	Soltek SL-75DRV5	Violet

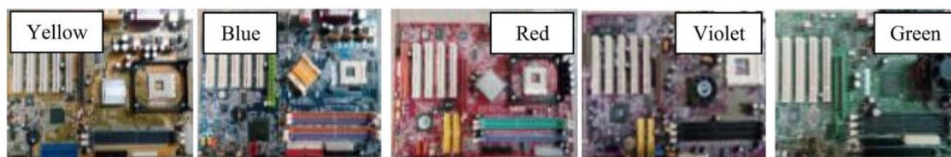


Figure 2.3.1. Five WPCB models used in the present research

Dissolution was performed in standard laboratory-type wide mouth glass bottles (an individual bottle for each sample) which were placed in an ultrasonic bath (tank volume 6L, max. ultrasound frequency 40 kHz) filled with distilled water at a temperature of 50 °C, whereas the optimum treatment time was 4 hrs., and the solid-to-liquid ratio (WPCB powder/DMF) was 3:10 (wt./v). The samples before and after the treatment are shown in **Fig. 2.3.2.** The optimum sonication time was determined based on the purity of the recovered fiberglass particles and on the time required to dissolve all the epoxy resin remaining on fiberglass. The dissolution process was repeated several times at a constant temperature and solid-to-liquid ratio with different durations of sonication (1, 2, 3, 4, 5

hrs.) so that to determine the optimum sonication time limited by the maximum feasible purification degree of fiberglass. The fiberglass-solvent suspension was periodically examined with an optical microscope, and the purity degree of the fiberglass was inspected.

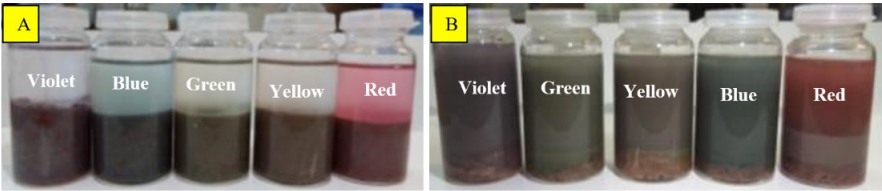


Figure 2.3.2. WPCB powder: (A) before ultrasonication and (B) after ultrasonication

2.4. Indication of optimum separation conditions

Each prepared sample was assigned a code according to the WPCB color and separation temperature, as illustrated in **Table 2.5.1**. **Fig. 2.5.1**. shows the procedures which were followed to separate all the components of the WPCB by using the new technique.

Table 2.4.1. WPCB models and sample codes

No.	WPCB Model specifications	WPCB color	Separation temperature	Sample code
1	Compaq DeskPro EN Socket 370 AGP Motherboard 187498-001 010630-101	Green “G”	25	G/25
			50	G/50
			75	G/75
2	Gigabyte GA-8IG1000-G	Blue “B”	25	B/25
			50	B/50
			75	B/75
3	845GV-MLV	Yellow “Y”	25	Y/25
			50	Y/50
			75	Y/75
4	MSI PT880 Neo (V2.0) MS-7043 (v1.00) ATX Mainboard	Red “R”	25	R/25
			50	R/50
			75	R/75
5	Soltek SL-75DRV5	Violet “V”	25	V/25
			50	V/50
			75	V/75

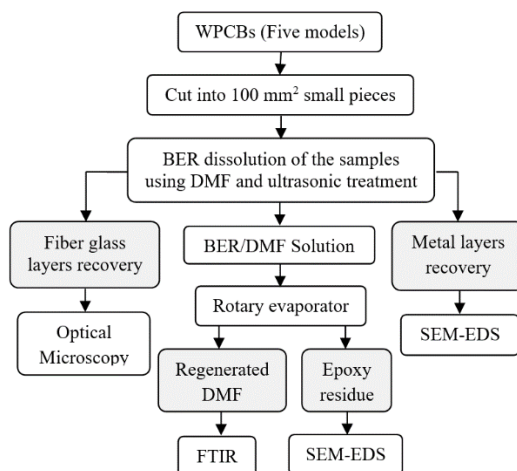


Figure 2.4.1 Schematic flowchart for the separation process experiments

At the beginning, each WPCB sample was placed in an individual flask containing DMF with a solid-to-liquid ratio (i.e., WPCB : DMF ratio) of 300 g L^{-1} . Then, the flasks (containing DMF and WPCB samples) were submerged in a sonication bath filled with a vibrating fluid (distilled water). Each sample was separated at different temperature values: 25, 50 and 75 °C. At the end of the sonication process, two main types of material were received: fiberglass and conductive metals. In addition, BER dissolved in DMF was obtained; then, a rotary decompression evaporator was used to extract BER and regenerate the used DMF. Finally, B/25, G/25, R/25, V/25, and Y/25 samples were prepared to be used as reference samples for comparison with the separated samples at the end of the process. To examine the recovered fiberglass layers and to study the mechanism of the separating process, Optical Microscopy was employed. Absence of significant degradation of regenerated DMF was confirmed by FTIR analysis. Epoxy residue recovered in the form of small particles was examined by SEM to indicate its morphology and EDS in order to determine its chemical composition (most importantly, the share of Bromine in the mass of samples). Similarly, the morphological features of the recovered metallic layers were studied by SEM, while the purity of the obtained metal was studied by EDS.

2.5. Separation of mechanical specimens

The samples cut for mechanical testing were assigned specific codes as shown in **Table 2.1.1.**, section “mechanical specimens”. The separation process was conducted in a simple reactor (a WPCBs separator) designed specially for this purpose under the following conditions: temperature 50 °C, solid-to-liquid ratio 300 g/L. In the developed separator, the main body of the traditional ultrasonic bath containing a vibrating fluid (distilled water) was used at the same time as a base of the separator and the source of high frequency ultrasonic waves as shown in **Fig. 2.5.1.A.**, whereas a glass vessel divided into 6 chambers containing DMF was used as a separation unit. The unit was closed with a glass cover to prevent evaporation of DMF and also to hold the WPCB samples inside the chambers individually as shown in **Fig. 2.5.1.B.** The separation unit, supported with four flexible wires (fixed in the outer frame of the separator), was floating in the vibrating

fluid so that to increase the contact area between the the water and the separation unit as well as to transfer vibration and thus increase the separation rate. In addition, a suction system was installed to prevent any emissions of harmful fumes.

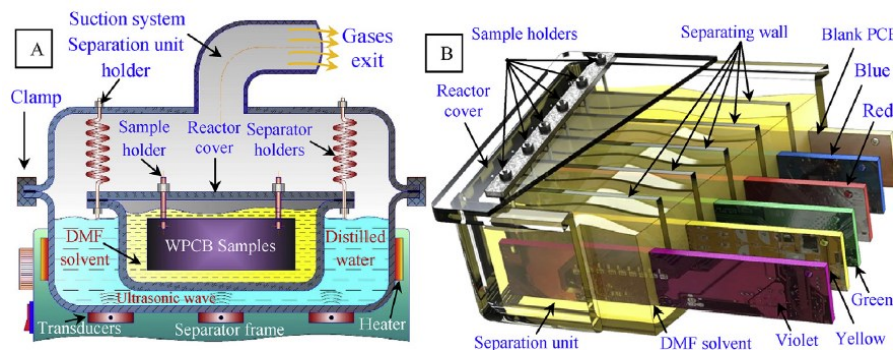


Figure 2.5.1. A) Developed WPCB separator and B) separation unit

2.6. Full-size WPCB experiments

2.6.1. Random Access Memory (RAM)

Fig. 2.6.1. shows the procedures which were followed to separate all components of RAM.

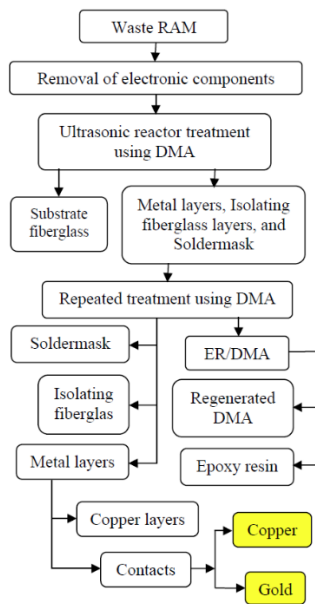


Figure 2.6.1. Schematic flowchart of waste RAM separation and liberation of precious metals

In the general case, the structure of PCBs, including RAMs, is comprised of a so-called substrate which is normally presented by woven fiberglass/epoxy resin (ER) laminate. This laminate can also contain inner metal foil layers that are usually referred to as *signal layers*. Finally, the outer surface of the substrate contains conductive tracks

that are, in turn, coated with a protective solder mask layer (Lewis & Ryan, 2010). In the present research, separation by solvent is used as a tool for reverse engineering of RAMs through dissolution of ER by solvent and liberation of metal components from non-metal components.

The dissolution was conducted in a developed reactor which was designed specially for this purpose. The developed reactor was comprised of two units: dissolution and ultrasonic units as shown in **Fig. 2.6.2**. The dissolution unit is represented by three cylindrical glass reaction chambers containing RAMs and filled with solvent, with each chamber having the inner diameter of 35 mm and the length of 150 mm. The dissolution unit was placed inside the ultrasonic unit which was a standard ultrasonic bath filled with heated vibrating fluid (distilled water) and covered with a glass cover. The high frequency impulses generated by the ultrasonic unit led to an acceleration of the breakage rate of the internal van der Waals' bonds of ER, which resulted in the formation of hydrogen bonding between the hydroxyl moiety of ER and the carbonyl moiety of the solvent thus decreasing the dissolution time (Verma *et al.*, 2017a, 2017c).

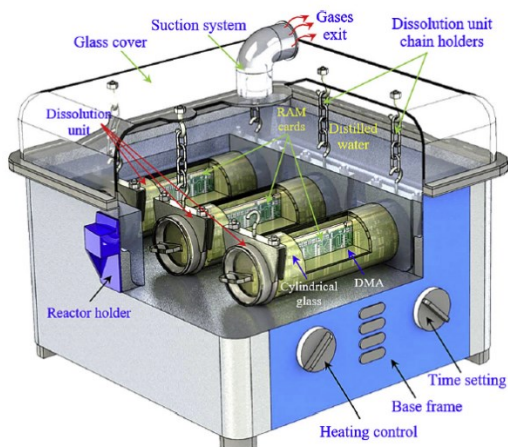
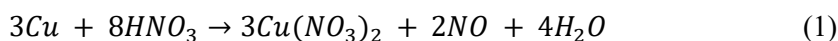
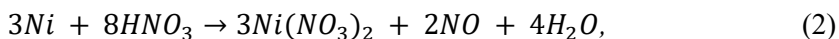


Figure 2.6.2. Two-unit reactor for simultaneous dissolution and ultrasonic treatment of RAMs

It is worth mentioning that the glass cover in the ultrasonic unit was used to prevent leakage of any harmful fumes and to hold the dissolution unit inside the system by chains. Lastly, a suction system was installed at the top of the glass cover so that to remove the evaporated water and any other fumes from the ultrasonic bath. The experiments were carried out under constant conditions with the solid-to-liquid ratio of 3:10 (i.e., WPCB : solvent ratio was 300 g/L) and at a temperature of 50 °C.

The recovered contacts contained three main metallic elements – copper, nickel and gold. Accordingly, based on its dissolution properties, nitric acid was used to dissolve all the metallic elements of contacts except for gold that was left as solid residue. Gold was obtained according to the following chemical reactions (Eqs. (1) and (2)). **Fig. 2.6.3.** shows the steps that were followed to prepare gold as well as the changes in the color and consistency of the solution after the reactions.





where Cu, HNO_3 , $\text{Cu}(\text{NO}_3)_2$, NO, H_2O , Ni, $\text{Ni}(\text{NO}_3)_2$, and are Copper, Nitric Acid, Copper Nitrate, Nitric Oxide, Water, Nickel and Nickel Nitrate respectively.

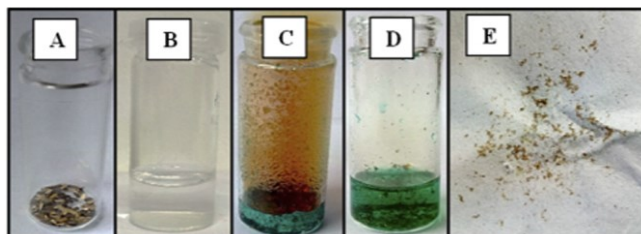


Figure 2.6.3. Steps followed to liberate gold from contacts: A) recovered contacts; B) pure nitric acid; C) dissolution of copper and nickel; D) liberation of gold; and E) obtained gold powder

2.6.2. Video Card

The steps needed to separate all the components of the WPCB by using the new technique are shown in **Fig. 2.6.4**. The separation process was performed in two phases: the first phase focused on developing a simple reactor in order to dissolve BER in DMF thus separating all the fiberglass layers while the second phase concerned with the extraction of BER and regeneration of the used DMF by using a rotary decompression evaporator.

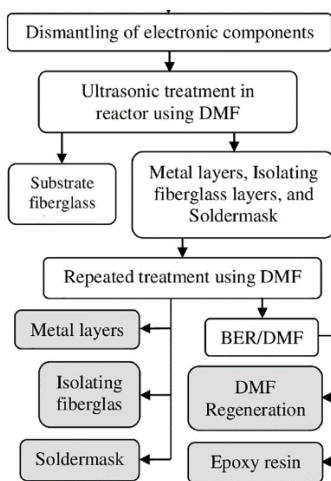


Figure 2.6.4. Schematic flowchart of the waste video card separation experiments

Fig. 2.6.5. shows the developed reactor which was used in the present study to separate the components of the waste video card. As shown in the figure, the traditional ultrasonic bath filled with distilled water was used as the main body of the reactor. A glass vessel containing DMF and a waste video card served as the reaction chamber. The reaction chamber was submerged in the main body and supported by four flexible wires. The top sides of the wires were completely fixed on a safety cover, while the other sides

had a possibility to move freely together with the reaction chamber in the vibrating fluid (distilled water). High frequency ultrasonic waves were used to generate vibratory motion thus facilitating the breakage of the internal Van der Waals' bonds of BER and consequently accelerating the penetration of DMF inside the board and increasing the separation rate. Also, the reaction chamber was closed with a glass cover to prevent any leakage of harmful fumes and to collect the condensed DMF by returning it back again to the reaction chamber. The experiments were carried out under the constant conditions with a solid to liquid ratio 3:10 (i.e., WPCB: DMF ratio 300 g/L) and a temperature of 50 °C. Finally, a suction system was used to remove the evaporated water and any harmful fumes from the ultrasonic bath. A silicone sealant glue (Permatex® *Clear RTV Silicone Adhesive Sealant*) was used as a sealant between the main body and the suction cover to prevent possible leakage or evaporation of DMF (Permatex, n.d.).

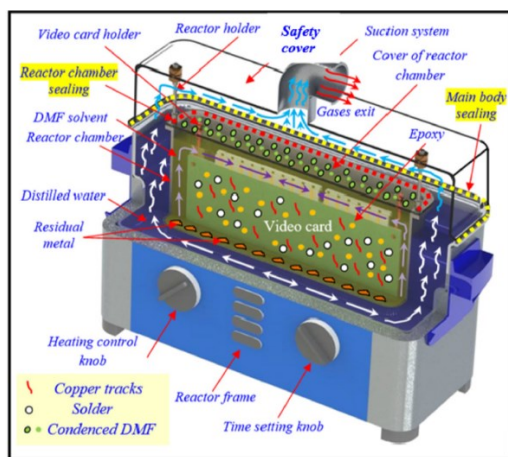


Figure 2.6.5. Development of the traditional ultrasonic bath (reactor) for Video Card separation

Silicone was chosen for sealing since its bonds can be much stronger than the traditional physical sealing systems which rely on bolting or welding; this is especially important in the case of glass. In addition, silicone sealant is denoted by good chemical resistance to solvents as well as resistance to temperature extremes (180 °C) in addition to water resistance as well as absence of weakening if exposed to either moisture or UV irradiation (Pantaleo, 2013).

2.6.3. Motherboard

Fig. 2.6.6. shows the procedures which were followed to separate all the components of a Waste Motherboard (MB) while using the newly developed approach.

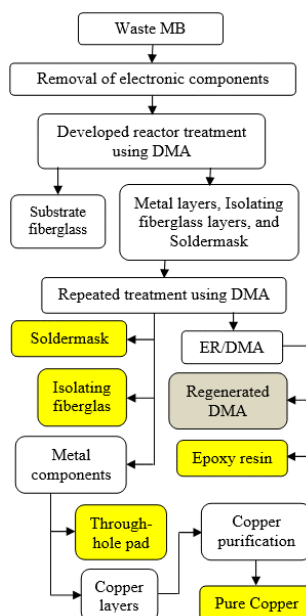


Figure 2.6.6. Schematic flowchart for motherboard (MB) separation and liberation of metals

Motherboard separation was done in a specifically designed glass chamber (reaction chamber) containing solvent with solid: liquid ratio 3:10 (i.e., mass of WMB: volume of solvent). The motherboard sample was positioned in a way so that to have clearance with respect to the walls of the chamber, which facilitated the penetration of the solvent into WMB layers. **Figure 2.6.7.** shows the complete design of the developed WMB separation system based on dissolution supported by ultrasonic-mechanical treatment. As it can be seen, the main component of the new reactor was an actual ultrasonic bath due to its capacity to accommodate the full-size WMB (320mm x 220mm). The bottom of the dissolution chamber freely floated in the vibrating liquid (distilled water), whereas the other side was supported with four wires fixed onto the cover of the ultrasonic bath. The ultrasonic bath together with the cover and the reaction chamber inside were referred to as the *Ultrasonic unit*. To facilitate the separation process even more, the Ultrasonic unit was fixed onto the shaker plate with several bolts. Each unit (Ultrasonic and Shaker) had a separate control unit for adjusting the handle frequency, the heating rate, and the treatment time.

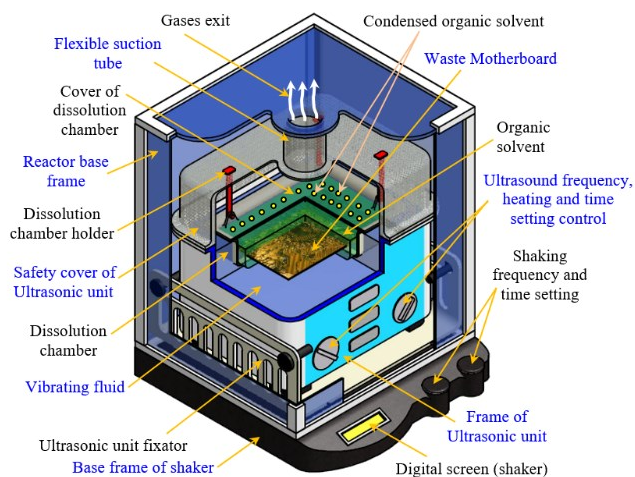


Figure 2.6.7. Schematic drawing of the developed reactor

The separation was done according to the optimum temperature reported by Tatariants *et al.* (2017) (50 °C) in order to obtain a high concentration of epoxy resin in the solvent, to decrease the consumed energy and to decrease the probable emissions of harmful gases (Tatariants, Yousef, Sidaraviciute, Denafas & Bendikiene, 2017). The solid-to-liquid ratio (i.e., MB: DMA ratio 300 g/L) was selected based on the data reported by Verma *et al.* (2017c). To avoid the saturation of the solvent with epoxy resin, the spent solvent was regenerated after the dissolution of 25 wt.% from Minimum Separation Concentration (MSC) of BER had been reached. Afterwards, the regenerated solvent was returned into the dissolution chamber so that to continue the extraction of BER, and the procedure was repeated 4 times in total. Since the exact MSC was not known at the beginning of the treatment process, a small piece (100 mm²) was cut from it and fully separated under the optimum conditions (50 °C, 300 g/L). At the end of separation, the concentration of BER inside the solvent was measured by Ultraviolet-Visible spectroscopy with regard to the absorbance curve of BisPhenol-A as plotted by Verma *et al.* (2017a).

2.7. Solvent Regeneration

At the end of the separation process for every WPCB type (powder, RAM, Motherboard, etc.), a certain amount of BER was dissolved in a solvent. Therefore, a rotary decompression evaporator was used to regenerate the spent solvent and extract the epoxy resin. **Fig. 2.7.1.** shows a schematic drawing of the process resulting in the extraction of BER and the regeneration of the solvent. As shown in the figure, the used solvent inside the flask was submerged in heated mineral oil (above the boiling point of DMF ~153 °C) (Long, Meek, 2001) in order to vaporize the solvent (green points); the escaping vapors were condensed back to obtain the regenerated liquid which also had the same colorless appearance as the unused solvent. At the same time, epoxy residue was produced in the flask in the form of a thin film (yellow points).

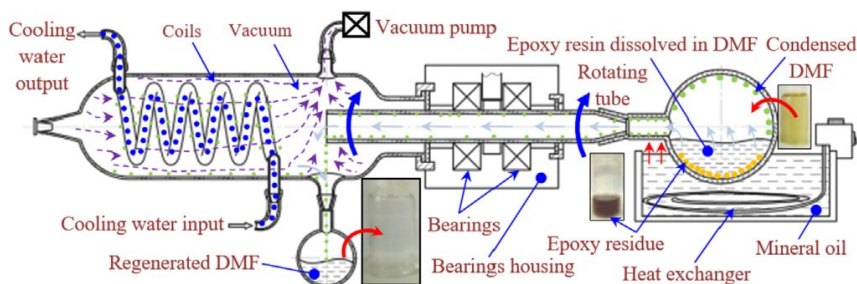


Figure 2.7.1. Schematic sketch of the solvent regeneration and epoxy resin extraction process

2.8. Electrospaying

Fig. 2.8.1. shows the procedures which were followed to liberate Cu foils from WPCBs and subsequently prepare Cu-NPs by using the Electrospaying technique.

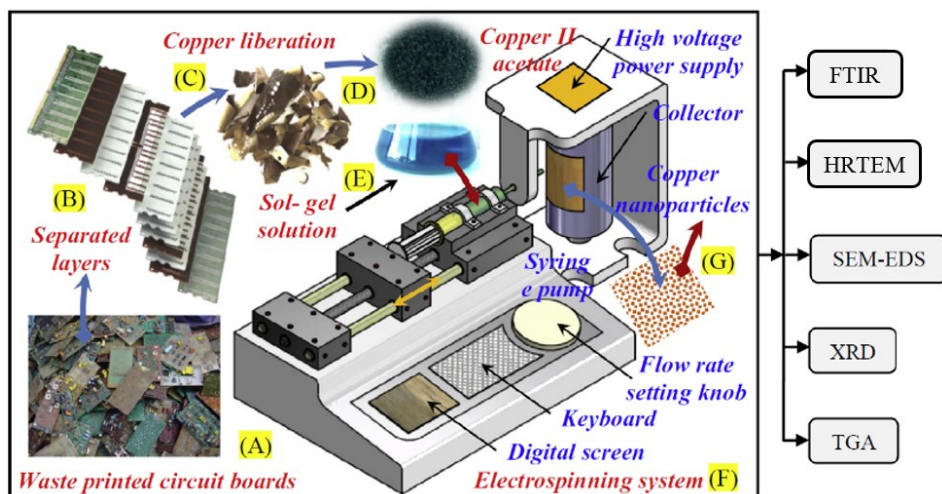


Figure 2.8.1. Schematic flowchart for the synthesis and characterization of Cu-NPs

The experimental work performed in the main stages of the Electrospaying, namely, Liberation of copper foils (**Fig. 2.8.1.C.**), Copper acetate preparation (**Fig. 2.8.1.D.**); synthesis of copper nanoparticles (**Fig. 2.8.1.F., G.**) is explained below

Liberation of copper foils

The WPCB separator, which was designed specially for this purpose as described in the previous Chapters, was used to liberate copper foils and other metal components from non-metallic components. In order to increase the safety and improve the performance of the reactor, some modifications related to the sealing system were made in the old design.

Figure 2.8.2.A. shows the final reactor design after the modification. As shown in the figure, the developed reactor consisted of: a) the main body containing a vibrating fluid (distilled water) and several transducers which generate high frequency ultrasonic waves; b) the reaction chamber containing an organic solvent and WPCB samples with

the standard solid-to-liquid ratio of 3:10 (i.e., WPCB: solvent 300 g/L) at 50 °C. The new design was provided with a new sealing system (graphite rings) instead of the old silicone glue sealing system in order to avoid any leakage of harmful gases or fluids and make the developed reactor eco-friendlier. The graphite rings were installed between the main body and the suction cover, also, between the reactor chamber and the reactor cover. Graphite rings were chosen due to their good resistance to the solvent and lower permeability than the traditional sealing, especially at higher temperatures.

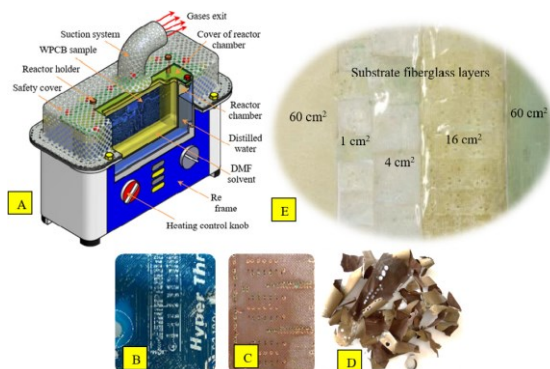
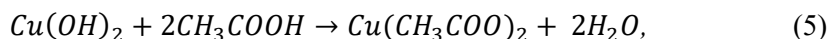
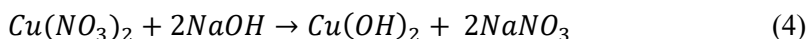
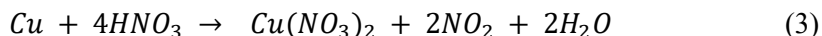


Figure 2.8.2. A) Modified WPCB separator; B, C, D, E) Recovered layers and components of WPCBs (Compound unit, Substrate, Recovered metal, and fiberglass, respectively)

Regarding the process of copper foils liberation, it was performed in three parallel steps: a) dissolution of BER in DMA; b) separation of upper and lower compound units against the substrate; and c) separation of all the layers of the main structure (substrate) which previously consisted of five layers of substrate fiberglass and four layers of copper. After 6–10 hrs., all the layers were separated, and the copper layers were collected. It was clear that the recovered copper layers were contaminated, and, in order to ensure the accuracy of our experiments, they were additionally purified. The purification process was performed in the same reactor by returning the copper foils again to the reaction chamber and processing them for 4 h at 80 °C. A metallographic microscope was used to examine the copper layers' surface before and after the purification process.

Copper (II) acetate preparation

Copper (II) acetate $Cu(CH_3COO)_2$ is widely used as a reagent and catalyst for the synthesis of various inorganic and organic compounds (Biffis, Gardan & Corain, 2006; Kuang, Michaels, Simmons, Clark & Zhu, 2010; Lago, Carballo, Rodríguez-Hermida & Vázquez-López, 2014). In the present research, $Cu(CH_3COO)_2$ was prepared from purified copper foils and used as a precursor for the synthesis of Cu-NPs. $Cu(CH_3COO)_2$ was produced according to the following chemical reactions (Eqs. 3–5):



where HNO_3 , NO_2 , $Cu(NO_3)_2$, $NaOH$, $NaNO_3$, $Cu(OH)_2$, CH_3COOH and H_2O are Nitric Acid, Nitrogen Dioxide, Copper Nitrate, Sodium Hydroxide, Sodium Nitrate, Copper Hydroxide, Acetic Acid and Water, respectively.

Figure 2.8.3. illustrates the steps followed to prepare $Cu(CH_3COO)_2$ as well as the changes in the color and consistency of the solution after each reaction. As shown in the Figure, the color of the solution changed to blue after purified copper foils had been added to HNO_3 ; also, during this reaction, some organic materials appeared in the solution (**Pic. 2.8.3.B.**).

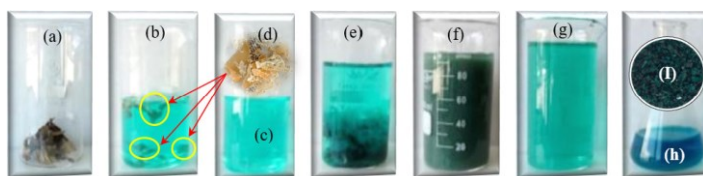


Figure 2.8.3. Steps followed to produce copper (II) acetate

The presence of these materials means that there was a small amount of epoxy resin (thin film) not exceeding $\sim 3\text{--}5\%$ wt. remaining on the outer surface of the recovered Cu foils; it was removed by filtering as shown in **Fig. 2.8.3.C., D.** After this step, the filtered solution was mixed with $NaOH$ in order to obtain $Cu(OH)_2$. After the reaction, the viscosity of the solution began to increase gradually until reaching the maximum and then decreased again until completely stabilizing after two hours as shown in **Fig. 2.8.3.E., F.** Finally, the solution was mixed with CH_3COOH to produce an aqueous $Cu(CH_3COO)_2$ solution which was left for drying at $50^\circ C$ for 3 hrs. in order to obtain crystallized $Cu(CH_3COO)_2$ as shown in **Fig. 2.8.3.I.** The produced Copper acetate was analyzed by Fourier Transform Infrared Spectroscopy and X-Ray Diffraction to confirm its purity.

Synthesis of copper nanoparticles

Copper nanoparticles were synthesized through two steps: firstly, a sol-gel was prepared from copper (II) acetate, and then Electrospraying with high voltage was used to produce Cu-NPs.

The sol-gel was prepared from copper (II) acetate salt (prepared from recovered copper foils) as follows: 0.5 g of salt was mixed with 1ml of water via vigorous magnetic stirring for 30 min. Then, 1 mL of acetic acid was added, and vigorous magnetic stirring for 30 min. was applied again. The addition of acetic acid was important in order to avoid the hydrolysis of PVA during the Electrospraying process. After this, 5 g of 15 wt.% aqueous PVA solution was added, and the solution was left overnight with magnetic stirring. These steps resulted in the formation of highly viscous and uniform sol-gel denoted by the polymer-to-salt weight ratio of 1.5:1.

The prepared homogeneous sol-gel was fed into a plastic syringe installed in the Electrospraying system featuring a gauge 20 (internal dia. = 0.603 mm) stainless steel needle at its end. The synthesis process was carried out at room temperature and at a relative humidity of 65% and a constant distance between the nozzle and the collector (10 cm); the flow rate was set at 0.2 ml/h, while the applied voltage was varied between

23 and 29 kV. **Fig. 2.8.4.** elucidates the possible Cu-NP growth mechanism for the Electrospaying process.

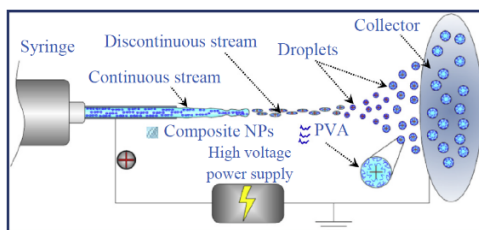


Figure 2.8.4. Composite NP synthesis mechanism for Electrospaying process

As shown, the prepared solution is extruded from the syringe in a continuous stream in the form of laminar flow. When the solution passes through the needle, a high voltage is applied, which causes the solution to become charged. At this point, the forces of electrostatic repulsion begin to counteract the forces of the surface tension acting in sol-gel (Cheng *et al.*, 2011). An evaporation process begins on the surface of the sol-gel immediately after it has left the syringe; this leads to the increase of the PVA concentration in this area consequently resulting in the formation of the gel layer when the concentration has exceeded the coagulation threshold (Yang, Wang, Wang & Yan, 2017). The formed gel-layer becomes a grid which maintains the morphology and prevents the sol-gel from distortion and oxidation. As a result of the liquid phase evaporation under the atmospheric ambient, the viscosity of the solution decreases significantly, which causes the charged jet to become discontinuous, and the stream of sol-gel breaks into droplets (Liu, Zhu, Zhang & Qiu, 2018). The synthesized composite particles were collected on aluminum foil as a substrate. The collected particles were then left overnight in a furnace at 70 °C to remove any unwanted moisture. Finally, SEM was used to determine the optimal synthesis conditions in terms of voltage.

Therefore, the samples prepared at the optimum voltage were dried and then calcined in a furnace at 475 °C for 2 hrs. The calcination temperature was based on the PVA decomposition temperature, as determined with TGA analysis. The calcined particles were then reduced in hydrogen atmosphere at 300 °C so that to obtain pure Cu-NPs.

2.9. Synthesis of antimicrobial nanoparticles

Figure 2.9.1. shows the procedures that were followed to liberate Cu foils from WPCBs and later prepare Cu-NPs by using a green technique.

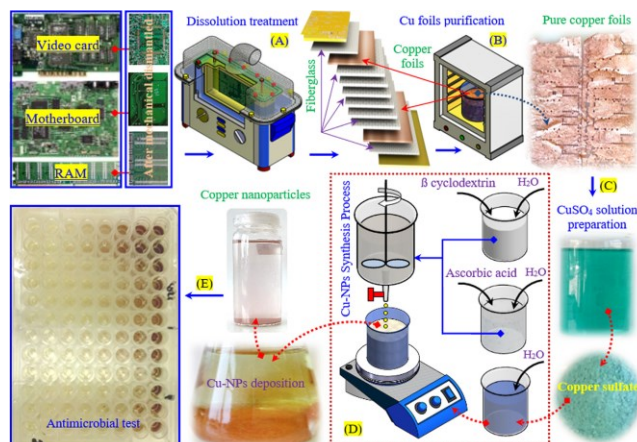


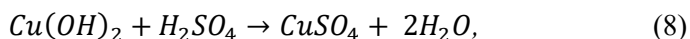
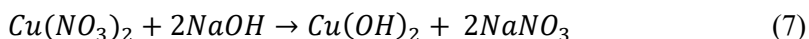
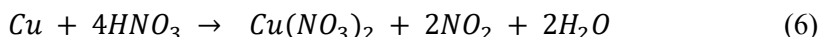
Figure 2.9.1. Schematic flowchart for green synthesis and characterization of Cu-NPs.

The obtained Cu foils were inspected by conducting SEM-EDS analysis to indicate their purity. Since EDS is quantitative analysis and is thus not suitable for materials with low concentrations, additional Inductively Coupled Plasma-Optical Emission Spectroscopy measurements were performed on the recovered metal foils. The samples for ICP analysis were digested by aqua regia under microwave treatment according to Kim, Lee, Yu & Han (2018).

The preparation of Cu-NPs was performed in two stages. Firstly, aqueous solutions of Copper (II) Sulfate were produced from the recovered Cu of each WPCB sample. Afterwards, Cu-NPs were synthesized by using b-NCD.

Copper (II) Sulfate preparation

Copper (II) Sulfate ($CuSO_4$) is an inorganic compound which has found extensive usage in pigments, plating and surface treating agents, surface active agents, agricultural products, water treatment products, blood testing for anemia, etc. (Moroydor Derun, Tugrul, Senberber, Kipcak & Piskin, 2014). In the present research, $CuSO_4$, used as a precursor for the synthesis of Cu-NPs, was prepared from the recovered copper foils of WPCB samples. $CuSO_4$ was produced according to the following chemical reactions Eqs. (6–8):



where HNO_3 , $Cu(NO_3)_2$, NO_2 , $NaOH$, $Cu(OH)_2$, $NaNO_3$, H_2SO_4 , and H_2O are Nitric Acid, Copper (II) Nitrate, Nitrogen Dioxide, Sodium Hydroxide, Copper (II) Hydroxide, Sodium Nitrate, Sulfuric Acid and water, respectively.

It should be mentioned that, during the reaction described by Eq. (6), some organic residue started to appear in the solution as Cu gradually dissolved in HNO_3 ; therefore, a filtering process was employed to remove it. The organic residue obtained from each WPCB type was dried, collected, and analyzed by EDS. Carbon (C), Oxygen (O) and

Bromine (Br) were the main elements in the residue of all the samples, which means that all Cu was dissolved, and the residue contained only epoxy resin.

To confirm that there was no contamination with other elements, ICP analysis was employed to check the chemical composition of the prepared reagents. Also, Raman Scattering Spectroscopy and X-Ray Diffraction (XRD) were used to analyze and identify the chemical compounds of the obtained dried powder. Raman Scattering measurements were performed by using a Raman microscope *inVia* (Renishaw). The excitation beam from a diode laser of 532 nm wavelength was focused on the sample while using a 50× objective (NA = 0.75, *Leica*). The laser power at the sample surface was 0.24 mW. For all the measurements, the integration time was 5–10 s, and the signal was accumulated once. The Raman Stokes signal was dispersed with a diffraction grating (2400 grooves/mm), and the data was recorded by using a Peltier cooled charge-coupled device (CCD) detector (1024 × 256 pixels). This system yields a spectral resolution of about 1 cm⁻¹. Silicon was used to calibrate the Raman setup in both Raman wavenumber and spectral intensity.

Preparation of Cu-NPs

The Cu nanoparticles were prepared via the same route that was developed by Suárez-Cerda *et al.* (2016). Three separate aqueous solutions were prepared for each waste sample (MB, VC, and RAM); the solutions were CuSO₄·5H₂O (0.3975 g/25 mL H₂O), ascorbic acid (1.09 g/25 mL H₂O) and β cyclodextrin (0.25 g/25 mL H₂O). After that, the ascorbic acid and β cyclodextrin solutions were mixed and added dropwise to the CuSO₄·5H₂O solution. The final solution was heated and stirred at 80 °C and 700 rpm for five hours. Once the reduction process had started, the light blue color of the solution changed to light green, and the formation of a solid precipitate began. After a certain period, the color of the solution changed again to dark yellow with a significant increase in the amount of a brown-colored precipitate as shown in **Fig. 2.9.3**. At the end of the synthesis process, the solution was left for cooling and stabilization of the precipitate. Afterwards, the liquid was carefully extracted and removed by pipette, whereas the remaining powder was washed several times and kept in ethanol in order to avoid possible oxidation.

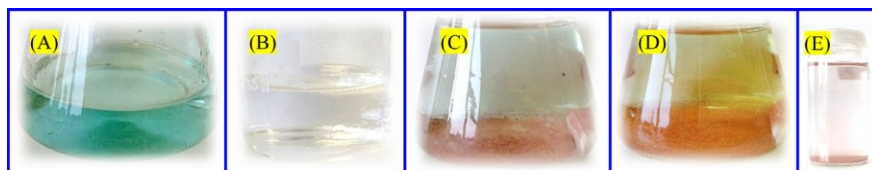


Figure 2.9.3. Images illustrating Cu-NPs preparation steps: (A) Copper Sulfate water solution; (B) Ascorbic Acid/ β-cyclodextrin water solution; (C) Beginning of the reduction process; (D) End of the reduction process; and (E) Final shape of the produced powder

Antimicrobial test of the synthesized copper nanoparticles

The Disc diffusion and the Broth dilution method (standard microdilution method) are the common techniques which are usually applied to evaluate the antibacterial activity of the synthesized nanoparticles including Cu-NPs (Argueta-Figueroa, Morales-Luckie,

Scougall-Vilchis & Olea-Mejia, 2014; Hajipour *et al.*, 2012). In the present research, the conventional broth microdilution method based on the Clinical and Laboratory Standards Institute (CLSI M100-S25, January 2015) was selected for the evaluation of the antimicrobial activity of the produced Cu-NPs due to its simplicity and sufficient accuracy (CLSI, 2013). Microdilution experiments were conducted in 96-well plates as shown in **Fig. 2.9.4.** with the primary concentration of copper particles at 6% for three different bacterial cultures: Gram-negative (*E. coli* and *P. aeruginosa*) and Gram-positive (*S. aureus*) bacteria. The added concentration of bacteria was at a level of (5×10^5 CFU/ml) in each well. The bacterial cells (105 CFU/mL) were incubated into Mueller-Hinton broth at 50 μ L per well in 96-well microtiter plates (Dealba-Montero *et al.*, 2017). After well mixing, the inoculated 96-well plate was incubated without agitation under 37 °C temperature for 22 hrs. As the next step, the absorption data of the tested Cu-NPs samples was monitored at 600 nm wavelength with an absorbancy reader (Ruparelia, Chatterjee, Duttagupta & Mukherji, 2008). It is worth noting that the plate was being shaken for 5 s before each registration point. The bacterial strains used in the present research were obtained from the stock-culture collection of the Biological Laboratory of the School of Chemistry, Vytautas Magnus University, Kaunas, Lithuania.

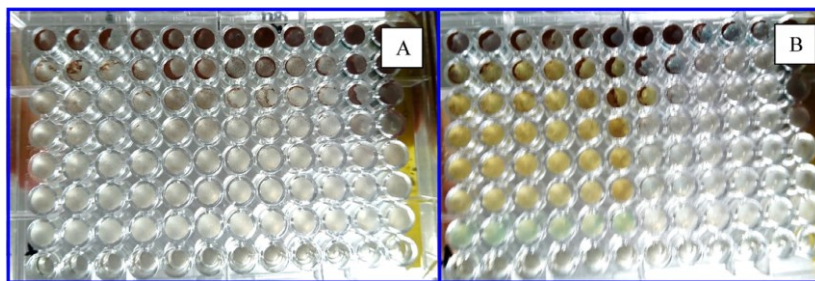


Figure 2.9.4. Images of the prepared Cu-NPs suspensions (A) at the beginning and (B) after 22hrs.

2.10. Leaching and precipitation of micro/nanoparticles

Liberation of through hole solder joints from WPCBs

All the experimental procedures conducted in this section are illustrated in **Fig. 2.10.1.**

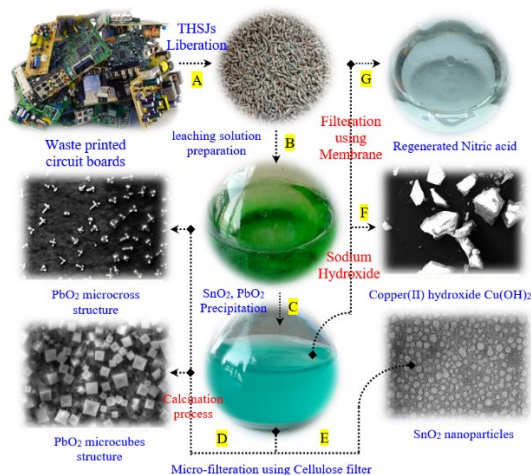


Figure 2.10.1. Schematic flowchart of the micro/nanoparticle preparation and copper recovery

Through Hole Solder Joint (THSJ) components employed in this research were liberated from two different WPCBs (a Motherboard (THSJ_M) and a Video Card (THSJ_V)) in order to improve the accuracy of the final results and to study the variations in the chemical composition. Due to the complex structure of the liberated THSJ_s, Scanning Electron Microscopy (SEM) was used to examine the liberated THSJ samples and determine their dimensions, structural components, and other morphological features with a scale of 700 μm at 20 kV and at Magnification 80X.

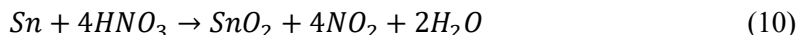
To complement the SEM data, Energy Dispersive Spectrometry (EDS) was used to analyze the chemical composition of the samples. Inductively Coupled Plasma-Optical Emission Spectroscopy (ICP-OES) measurements were used to precisely determine the chemical composition of the samples. The ICP analysis was done for 0.5g of each sample after grinding into micronized powder with a Planetary Ball Mill for 15 minutes at 300 rpm digested by aqua regia under microwave treatment (Kim *et al.*, 2018).

The THSJ treatment consisted of four approaches that are widely used in the industry: leaching of THSJ by Nitric Acid (Priya & Hait, 2018), micro/nanoparticle precipitation by ultrasonic treatment (Cerchier, Dabalà & Brunelli, 2017), micro/nanoparticle control and morphology refining by Ni, Fe, Al and Pd as catalysts or doping agents (Hu *et al.*, 2018; Lin, Li, Chen & Fu, 2017; Mavrokefalos *et al.*, 2017; Mei *et al.*, 2017), and, finally, pH control to extract copper in the hydroxide form (Yang, Li, Tan, Liu & Dong, 2017).

Leaching and micro/nanoparticle synthesis

The main experiments were conducted on 25g of liberated THSJ_s from each WPCB type. Such an amount can be extracted from one full-size motherboard (12% of its total weight) or from five full-size Video Cards. To determine the optimum leaching conditions, 0.5g of THSJ_M and THSJ_V was digested by concentrated Nitric Acid in spherical glass vessels under ultrasonic treatment at different temperatures. Pretreatment, in particular milling, was not conducted to avoid losses of metal and dust emissions as well as to decrease energy consumption. Preliminary leaching conditions were selected

according to the results reported in the literature; after several tries, the conditions were adjusted to ensure the minimum dissolution time. In the literature, dissolution conditions were mostly in the temperature range of 40–80 °C and within the solid to liquid ratio of 1:15 to 1:40 (Yang *et al.*, 2017; Yousef *et al.*, 2018). Based on these results, the preliminary leaching experiments were conducted in the same range by using an ultrasonic bath; **Eqs. (9–11)** show the main chemical reactions that took place in our experiment (reactions of those metals which are only present in minor quantities, such as Ni, Al and Fe, are discussed further in our thesis).

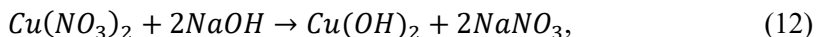


where *Pb*, *HNO₃*, *Pb(NO₃)₂*, *NO₂*, *H₂O*, *Sn*, *SnO₂*, *Cu* and *Cu(NO₃)₂* are Lead, Nitric Acid, Lead(II) Nitrate, Nitrogen Dioxide, Water, Tin, Tin Dioxide (Tin(IV) Oxide), Copper, and Copper(II) Nitrate, respectively.

The morphology and size of the particles precipitated from the solutions were observed and measured by SEM to indicate the meshing size of the filter needed to separate the precipitate (the solid phase) from acidic solutions (the liquid phase). The micro-filtration process using a cellulose filter with a mesh size of 0.5 µm was employed to separate the micro-fraction followed by the calcination process at 500 °C for 2 hrs. for purification and for the improvement of the morphology of the obtained particles. The remaining solution containing the nano-fraction was left for 2 hrs. until obtaining full precipitation of solid particles, then the liquid phase was carefully removed by pipette, and the remaining powder was calcined and kept in ethanol in order to avoid contamination.

Recovery of copper from the prepared THSJs solution

To recover the copper from the solution after the extraction of Tin and Lead, Sodium Hydroxide was added to the solution until pH 8 was reached; thus Copper Hydroxide was obtained as a result of the chemical reaction illustrated in **Eq. (12)**. The pH value of the solution was measured with a pH meter.



where *Cu(NO₃)₂*, *NaOH*, *Cu(OH)₂* and *NaNO₃* are Copper(II) Nitrate, Sodium Hydroxide, Copper(II) Nitrate and Sodium Nitrate, respectively. Copper Hydroxide was later collected by filtration through a cellulose filter, dried and kept in a desiccator.

2.11. Characterizations

The concentration of BER in the solvent was measured by using Ultraviolet-Visible Spectroscopy (UV-VIS: model GENESYS 8). Fourier Transform Infrared Spectroscopy (FTIR, *Vertex70 spectrometer*) and Nuclear Magnetic Resonance Spectroscopy (NMR) were used to analyze and identify the chemical compounds of the regenerated DMF for each sample; the results for the samples were compared with the unused DMF. The

morphology and the purification degree of the recovered milled fiberglass were examined by using a metallographic microscope (model *Orchid MCX300*). Additionally, a Scanning Electron Microscope (SEM: model *BPI-T*) and Energy-dispersive X-ray spectroscopy (EDS) were used to investigate the chemical composition of the recovered metal. Ball milling (model *Fritsch P-5*) was used to produce powder samples with a high degree of fineness for the experiments. An Ultrasonic bath (*GT SONIC-T6*) was used for solvent treatment of the samples. A *Mettler Toledo Five Easy FP20* pH meter was used to inspect the pH of the prepared acidic and base solutions.

Mechanical tensile properties of plain woven fiberglass of blank PCB and five WPCB specimens were measured with a Lloyd Universal Testing Machine (model *LR10K*), with a loading rate for the five specimens being set at 300 ± 10 mm/min. All the tests were conducted at the ambient temperature. To be sure that the tension on the specimen was uniform across the clamped width, the tested samples were mounted between two rubber jaws as shown in **Fig. 2.11.1.A.**, whereas **Fig. 2.11.1.B.** shows the full size of the mechanical samples at the end of the test.

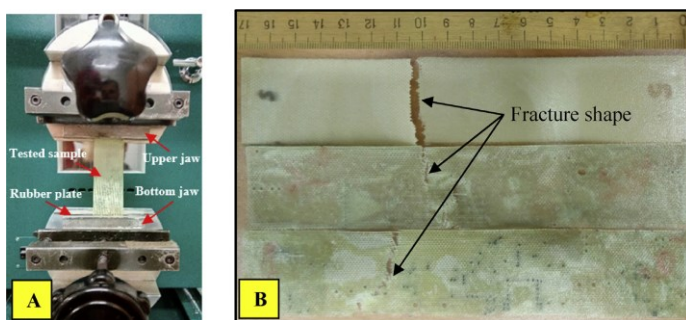


Figure 2.11.1. A) Fixation of a mechanical sample in the Universal Testing Machine and B) image of full-size mechanical samples at the end of the test

The thermal stability of the recovered epoxy resin of blank PCB and WPCB samples was determined by Thermogravimetric/Derivative Thermogravimetric analysis (TGA-DTG), TA instruments *TGA Q500*. Finally, changes in the crystallinity content and the melting temperature were assessed by heating the samples in a Differential Scanning Calorimeter (DSC model *Q-100* supplied by *TA Instruments*). The sample was heated until 200 °C at a rate of 10 °C per minute in nitrogen ambient and then cooled with water. The crystallinity of blank PCB and WPBC samples was calculated according to Eq. (13) (Guo, Harrats, Groeninckx & Koch, 2001).

$$X_c(\%) = \frac{\Delta H_c}{\Delta H_m^0}, \quad (13)$$

where ΔH_c is the apparent entropy of the crystallization of the sample, and ΔH_m^0 is the melting enthalpy of 100% crystalline epoxy resin. Since bromine is considered to be the main constituent of the epoxy resin polymer, so ΔH_m^0 is equal to 81 J/g (Chang, 1988; Verma *et al.*, 2017a)

The crystal structure and the chemical composition of the synthesized nanoparticles were characterized by X-ray Powder Diffraction (XRD) while using a SmartLab

diffractometer (*Rigaku*) and Fourier Transform Infrared Spectroscopy (FTIR, *Nicolet iS10*). The morphology and purification degree of the synthesized nanoparticles were examined by using a High-Resolution Transmission Electron Microscope (HRTEM: Model *JEM-2100*) and a Scanning Electron Microscope (*Zeiss EVO/MA15*, *HITACHI SU8200* Series) as well as Inductively Coupled Plasma-Optical Emission Spectroscopy (ICP-OES). It is worth mentioning that the *SEM-Zeiss EVO/MA15* device (1) was used to determine the optimal synthesis conditions in terms of voltage; then, *SEM-HITACHI SU8200* (2) was employed to obtain the final images of the nanoparticles. In addition, Energy-dispersive X-ray Spectroscopy (EDS) was used to investigate the chemical composition of the synthesized nanoparticles. The absorbance of antimicrobial samples was monitored with a *TECAN GENios Pro*TM instrument. Finally, the thermal stability of the particles was determined by using Thermogravimetric Analysis (TGA) with a heating rate of 20 °C/min from room temperature to 550 °C in nitrogen atmosphere.

2.12. Statistical methods and economic benefit/Carbon Footprint calculation methods

The statistical methods used throughout this work were implemented by using *Microsoft Excel 2016* and included linear regressions suitable for describing most of the reaction kinetics data. However, linear regressions were not suitable for all the datasets, therefore, cubic polynomial regressions, power regressions, and exponential regressions were also used. The average or arithmetic mean values were used throughout the work to generalize the obtained data. Finally, the coefficient of determination (R^2) was used to determine the accuracy of our regression models.

The economic benefit was calculated by using the principles of Life Cycle Cost Analysis (LCCA) while following specific guidelines (Ozbay, Jawad, Parker & Hussain, 2003). The cost of consumable materials and energy was considered as the factual expenditures, while the cost of the recovered materials (i.e., costs estimated as based on the price of similar scrap materials on the market) was considered to be treated as the benefits. The profit was calculated as the difference between the expenditures and the benefits.

The climate change impact in terms of Greenhouse Gas Emissions (GGE) of the solvent treatment was studied based on the case of motherboard separation as it was the most difficult to separate among all of the treated WPCBs (thus its recycling generates the highest environmental impact). In addition, the Carbon Footprint was calculated for reprocessed Through-Hole Solder Joints (THSJs) as this process was very complex and necessary due to THSJs consisting of three base metals requiring separation. The calculations were done according to *ISO 14040* Standard (The International Standards Organization, 2006; Turner, Williams & Kemp, 2015). The GGE values were calculated according to the recovered materials (epoxy resin, fiberglass and metals (recovered foils or nano/microparticles)); each material had a different GGE value determined according to various literature sources (EEA, 2014).

3. RESULTS AND DISCUSSIONS

Structure of the research

Similarly to the Materials and Methods section, the content of the Results and Discussions section can be split into Solvent Treatment and Reprocessing parts with Solvent Treatment being the main focus and Reprocessing being additional treatment so that to improve the value of the recovered materials as shown in **Fig. 3.1**.

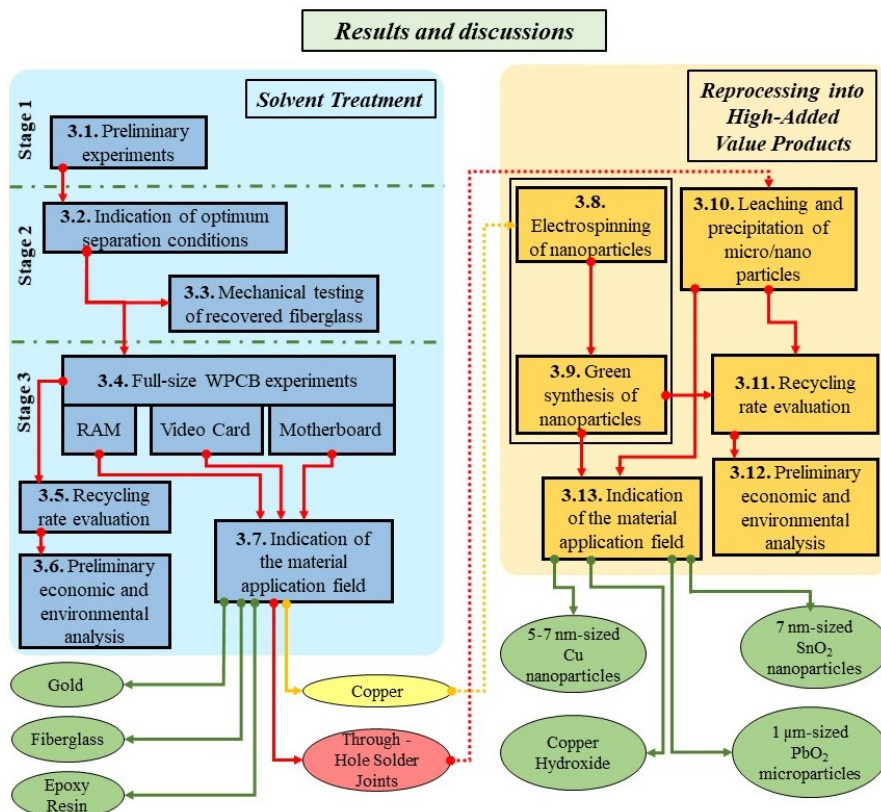


Figure 3.1. Structure of the results and discussions Section (the numbered boxes correspond to the subsections in the results Section)

The first results section was concerned with preliminary experiments on milled WPCB samples (**box № 3.1.**). The results of this Section indicated that the solvent treatment of milled samples was not the optimum approach due to the higher solvent consumption and because of the difficulties in the separation of the obtained fiberglass and metal fractions from each other with a high recycling rate.

Therefore, the optimum separation conditions (**box № 3.2.**) were determined on cut (non-milled) WPCB samples. The conditions were determined as follows: temperature 50 °C, solid-to-liquid ratio 3:10 (wt./v.), and average separation time ~15 hrs. for 100 mm² samples. The next step was concerned with the investigation of the

mechanical properties of the recovered fiberglass so that to later indicate its possible applications (**box № 3.3.**).

With the mechanical properties of fiberglass having been determined, the discussions proceed to experiments on Full-size WPCB experiments (**box № 3.4.**). It was found that the relation between the surface area of WPCB and the separation time could be well described by linear dependence. Also, this section provided a discussion on the properties of the recovered materials – Through-Hole Solder Joints, Gold, Copper, and Epoxy Resin; it also offered some highlights regarding the internal structure of the separated WPCBs and its effect on the separation time.

The Recycling rate evaluation (**box № 3.5.**) Section showed that the recycling rates of the treatment were rather high by reaching 99% in laboratory conditions. Also, it was shown that the solvent can be regenerated with a high recycling rate as well (~98%), thus suggesting that the solvent treatment can efficiently operate as a closed-loop system. By knowing the material recovery rates, preliminary economic and environmental analysis was done (**box № 3.6.**) thus indicating that the solvent treatment is denoted by good potential for upscaling due to the significant economic/environmental benefits it provides.

After that, a conclusion on the reusability of the materials recovered from WPCBs was drawn (**box № 3.7.**). It was found that most materials – Fiberglass, Epoxy Resin, and Gold were in proper condition to be reused in their respective applications, whereas Copper was found to have a greater value if reprocessed into a high added value product; one more component of WPCBs, namely, Through-Hole Solder Joints was not found to be ready for leaving the loop of the system without additional reprocessing.

Moving on to the reprocessing Section, we begin from the first Copper reprocessing attempt into nanoparticles by Electrospraying (**box № 3.8.**). Overall, the results indicated that small-sized nanoparticles could be produced; however, the major flaws of the approach were a prohibitively low production rate and a difficult preparation procedure. Therefore, a different approach involving Green synthesis was applied (**box № 3.9.**), which resulted in the production of a higher amount of nanoparticles. It was also discovered that some of the produced nanoparticles manifested antimicrobial behavior. Leaching followed by precipitation (**box № 3.10.**) was used as a reprocessing approach for Through-Hole Solder Joints, which resulted in the production of Lead Oxide microparticles, Tin Oxide nanoparticles, and Copper Hydroxide powder.

Our Recycling (or, rather, reprocessing) rate evaluation (**box № 3.11.**) pointed out that the reprocessing of Copper and Through-Hole Solder Joints both exhibited low losses with the respective recycling rates of 90% and 96%. From the economic and environmental perspective (**box № 3.12.**), reprocessing was found to offer certain benefits, especially in the case of Copper nanoparticle synthesis. Finally, potential applications were successfully found for all the reprocessed materials in the respective section (**box № 3.13.**).

3.1. Preliminary experiments (milled samples)

The WPCB powder produced by milling for preliminary experiments was micro-scale (particle size $\sim 20\text{--}100\text{ }\mu\text{m}$) and consisted of three phases: metal particles (some of them still featured adhered fragments of epoxy resin), fiberglass particles (partially covered with epoxy resin), and fiberglass-metal-epoxy composite agglomerations as shown in **Fig. 3.1.1**.

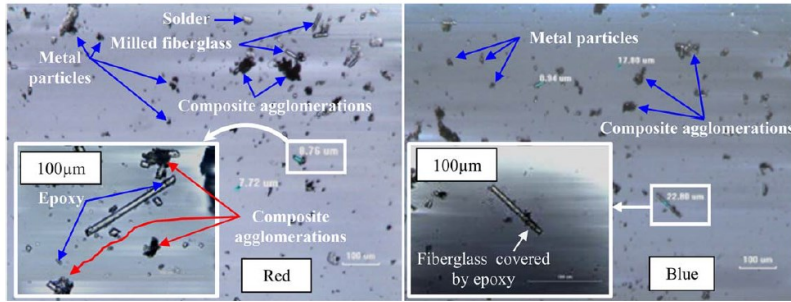


Figure 3.1.1. Metallographic images of some of milled WPCB samples (sample codes in **Table 2.3.1.**)

The dissolution process in the developed technique was constrained by two variables: the solid-to-liquid ratio and the treatment time. As for the temperature, since the experiments were conducted as preliminary and focused mostly on the fiberglass purification mechanism, it was selected as $50\text{ }^{\circ}\text{C}$ and maintained a constant level throughout the experiments.

3.1.1. Solid-to-liquid ratio

Initially, it was planned to use the standard w/v ratio of 300 g/L that was already used by Verma *et al.* (2016) for the separation of the cut WPCB samples. However, due to the pulverization, all the powderized samples increased their volume by 2 times while retaining the same weight, and the initial ratio set at 1:3 did not provide full sample submersion into the solvent. Therefore, a decision was taken to conduct a series of experiments where w/v ratios 300, 250, 200, 150, 100 and 50 g/L were tested as illustrated in **Fig. 3.1.2.A**.

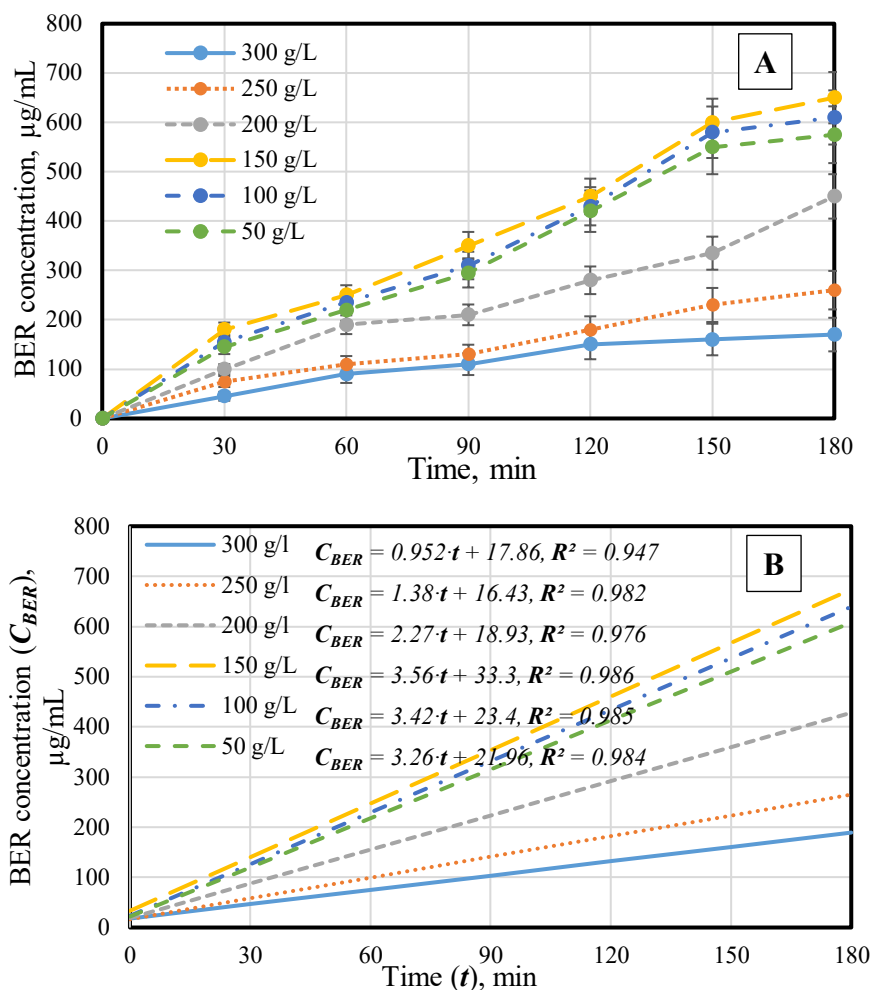


Figure 3.1.2. Effect of solid-to-liquid ratio on Epoxy Resin concentration (generalized results obtained from tests on all sample types): A) Experimental results and B) Derived linear regression dependencies

As it was expected, the original solid-to-liquid ratio of 300 g/L was not effective in the dissolution of BER due to providing only $\sim 170 \mu\text{g/mL}$ BER concentration after 3 hrs. of dissolution. By decreasing the amount of the solid material until 250 and 200 g/L, a progressive improvement in the BER extraction rate was observed, reaching its maximum at a solid-to-liquid ratio of 150 g/L. After that point, a further decrease of the solid material amount resulted in lower concentrations of BER in solution due to the insufficient amount of the available-for-dissolution Epoxy Resin. The excessive volume of the solvent diluted the solution, resulted in a higher swelling of samples and did not provide any additional benefits in terms of BER extraction. To better understand the role of the solid-to-liquid ratio in BER dissolution kinetics, linear regression equations were found for each tested solid-to-liquid ratio (Fig. 3.1.2B.). Linear regression was selected since it corresponded well to the pattern observed in the experimental dataset and was

capable of describing the data with a high coefficient of determination R^2 (>0.94). The shape of the linear regression curves suggested that the maximum concentration efficiency was reached at a solid-to-liquid ratio of 150 g/L. This fact is even more evident if the slope coefficients of linear regressions are compared as shown in **Fig.3.1.3**. While 150 g/L shows the highest corresponding slope coefficient, it was noted that the increasing solid-to-liquid values had a much more pronounced effect on the slope coefficient compared to the decreasing solid-to-liquid ratio. This dependence can be well described by cubic polynomial regression with an R^2 coefficient of 0.95.

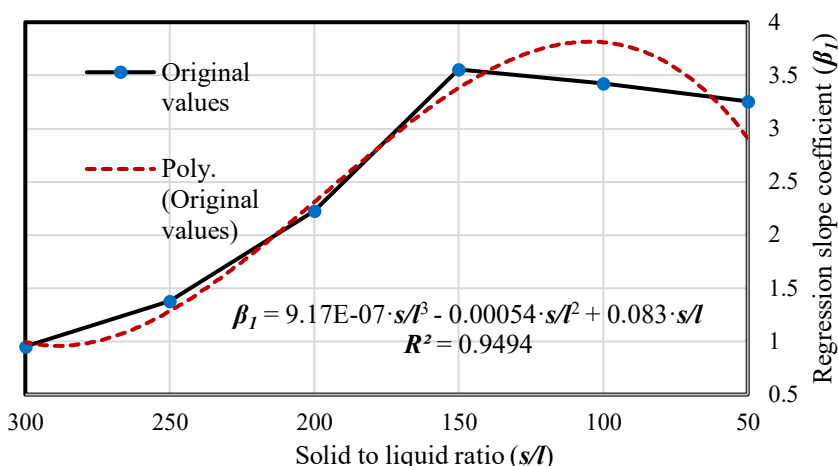


Figure 3.1.3. Dependence between solid-to-liquid ratio and the respective Epoxy Resin concentrations linear regression slope coefficients and the derived cubic polynomial regression

By using a regression equation from **Fig. 3.1.3.**, it was now possible to combine it with the regression equation from **Fig. 3.1.2.** in order to obtain a single formula allowing to calculate the BER concentration based on time (0–180 min.) and solid-to-liquid variables (50–300 g/L) as shown in **Fig. 3.1.4**. The coefficient of determination was calculated by using the original data (**Fig. 3.1.2.A.**) for each s/l ratio. It was found to be in the range of (0.947–0.986), which suggests that the derived formula was fairly accurate in the prediction of the original data variability.

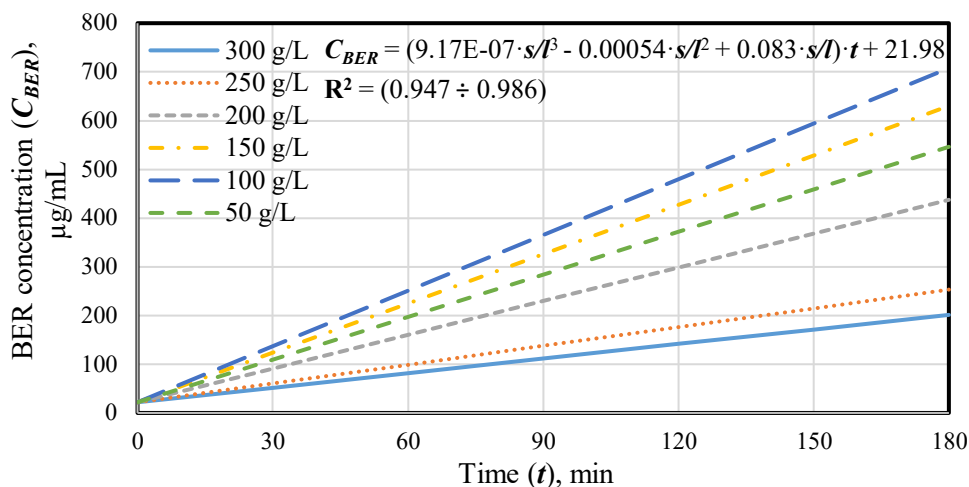
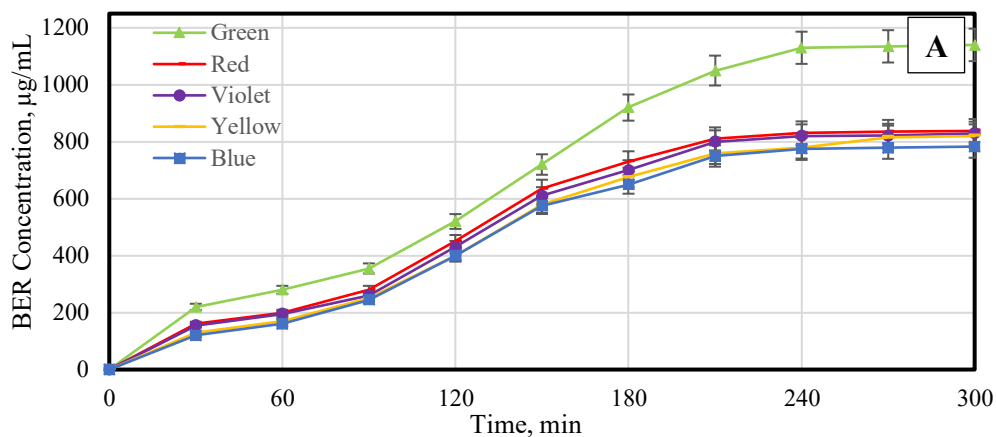


Figure 3.1.4. Dependence between BER concentration (C_{BER}), time (t), and solid-to-liquid ratio (s/l) as calculated by using the specified equation

The obtained dependencies were different from the results reported by Verma *et al.* in his work, where solid-to-liquid ratios higher than the optimum resulted in the overall lower concentrations of BER compared to the solid-to-liquid ratios lower than the optimum. This difference was most likely caused by the fact that this work treated milled WPCBs by solvent unlike Verma *et al.* who focused on the treatment of cut WPCB pieces. Based on the obtained data, the optimum ratio of 150 g/L, or 1:6, was selected for the following experiments.

3.1.2. Treatment time

The data used to determine the optimum treatment time can be seen in **Fig. 3.1.5.A**. Interestingly, the Green sample showed significantly higher BER concentrations throughout all the treatment period, and, as the final measured concentrations showed (**Fig. 3.1.10.**), the concentration of BER from the samples extracted at optimum conditions exceeded the concentration of BER from the other samples by ~25%.



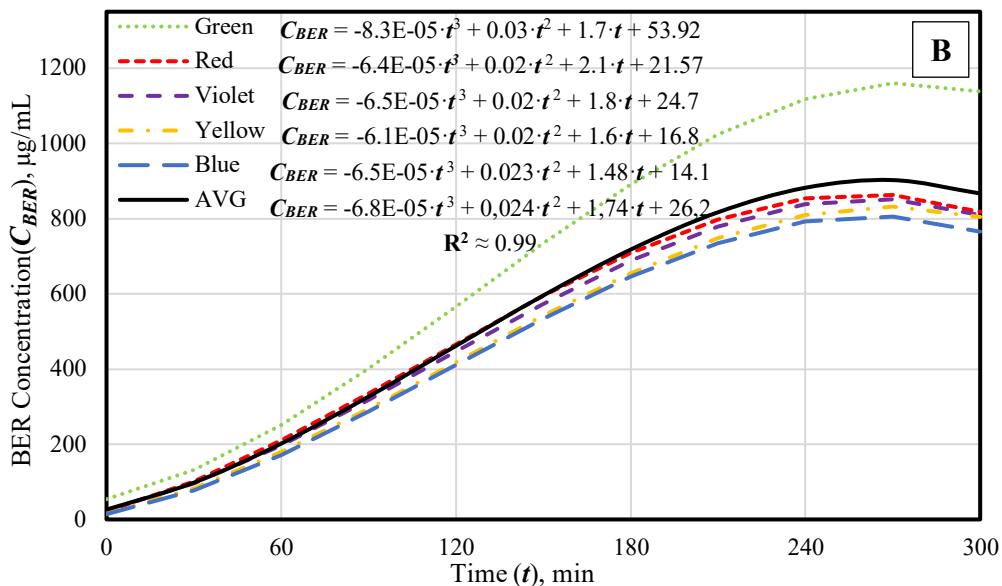


Figure 3.1.5. Effect of treatment time on Epoxy Resin concentration (sample codes in Table 2.3.1.): A) Experimental results; B) Derived cubic polynomial regressions

This can be explained by the fact that the overall fineness of the particles from the Green samples was higher than the fineness of the particles from the other samples due to the Green samples having the lowest mechanical properties and thus being easier to comminute (confirmed in Section 3.3. **Mechanical testing of recovered fiberglass**). After the initial 30 min., a sharp increase in the concentration of Epoxy Resin in the solvent was observed for the samples as the DMF quickly dissolved the finest-crushed particles. The BER dissolution speed slightly decreased during the following time interval up until 90 min. since the finer particles had already been dissolved, and the contact area between the solvent and Epoxy Resin therefore decreased as only the bigger particles were left. After 90 min., the dissolution rate increased again and became stable up until 180 min. (for the Green samples) or 150 min. (for the rest of the samples) as a result of the bigger Epoxy Resin particles splitting into smaller particles under the effect of solvent treatment and ultrasound thus increasing the BER/DMF contact area. After that point, the amount of BER available for dissolution started to deplete as reflected by the rapidly decreasing dissolution rate. Finally, after 4 hrs. (240 min.), the BER concentration plateau was observed for all the WPCBs; the concentrations did not significantly change for 5 hrs.-treated samples; therefore, the 4 hrs. treatment was selected as the optimum time. Such a treatment time is very similar to the treatment time of other approaches applied for WPCB recycling. For instance, acid leaching of a single metal (typically, Copper) from WPCBs may take 2–4 hrs. depending on the leaching agent and the input material pre-processing (Chen, Huang, Ogunseitan, Zhu & Wang, 2015; Maguyon, Alfara, Migo, Movillon & Rebancos, 2012). However, if more metals are targeted for recovery, the treatment time increases dramatically and may reach >18 hrs. (Zhou *et al.*, 2013). At the same time, solvent treatment offers a possibility to recover

the main metallic fraction as well as non-metals within a relatively short timeframe. By using the experimental data, cubic polynomial regressions were found for each sample type as shown in **Fig. 3.1.5.B**. This type of regression provided high R^2 values for all the datasets with the only drawback being a slightly less apparent concentration plateau. Finally, to provide an equation suitable for determining the concentration of BER regardless of the sample type, a regression based on the average concentration values was performed, and the respective regression coefficients were defined. The ultimate BER concentrations for all the samples are shown in **Fig. 3.1.8.B**.

3.1.3. Centrifugation

Generally, WPCBs consist of many components, such as metal tracks, solder mask, and through-hole pads. Additionally, fiberglass layers and copper foil layers are stacked together by BER as shown in the reconstruction **Fig. 3.1.7.A**. (Jia Li, Lu, Guo, Xu & Zhou, 2007). Therefore, after milling, all of these components and elements are mixed together in the form of powder that contains a variety of different fractions with dissimilar specific weights (**Fig. 3.1.7.B**). Therefore, a centrifuge was employed to separate the liquid phase (BER dissolved in DMF) against the solid phase (metal particles and milled fiberglass) with a separation time of 5–10 minutes. After the centrifugation, samples with four layers (**Fig. 3.1.7.C**) were obtained, namely: a BER/DMF solution, a milled fiberglass layer, an overlap zone (containing both fiberglass and metal), and a metal particle layer.

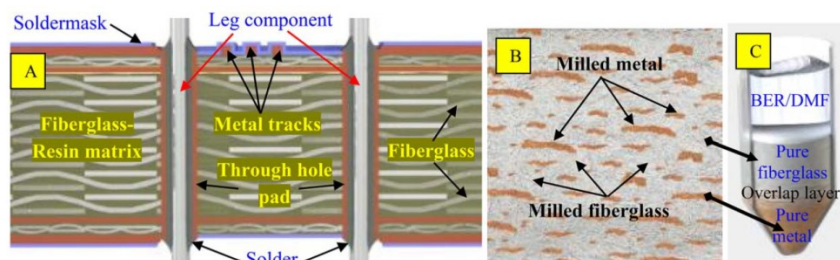


Figure 3.1.7. WPCB structure; (B) milled WPCBs; and (C) Layers of milled WPCBs after the centrifugation of powder: (A) before ultrasonication and (B) after ultrasonication

The overlap zone appeared since some finer metal particles featured a weight close to the weight of fiberglass particles. Thus, during the separation by density, a mixed layer formed. The material from the overlap layer was centrifuged again to liberate metal particles from milled fiberglass.

3.1.4. Final concentrations of Epoxy resin

During the measurements for determining the optimum treatment time, all the samples were diluted according to the optimum dilution conditions, and the absorbance data is shown in **Fig. 3.1.8**. However, the absorbance data of the Red, Yellow, and Blue samples was still located in the nonlinear zone due to the presence of very fine fiberglass and solder mask particles non-uniformly dispersed in the BER/DMF solution samples leading to inflated UV readings. Metallographic microscopy was used to confirm the

presence of suspended particles inside the used DMF. **Fig. 3.1.9.** shows the metallographic photography of used DMF; as it can be seen, the Red and Violet liquid samples contained a very small amount of micro-size milled fiberglass and metal particles; they are clearer if compared to the Blue, Green, and Yellow liquid samples contain not only large amounts of fine fiberglass and metal particles but also composite particles and agglomerations.

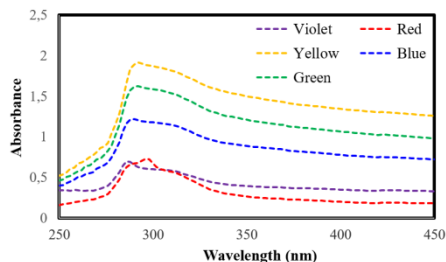


Figure 3.1.8. Absorbance of BER/DMF samples before centrifugation (sample codes in Table 2.3.1.)

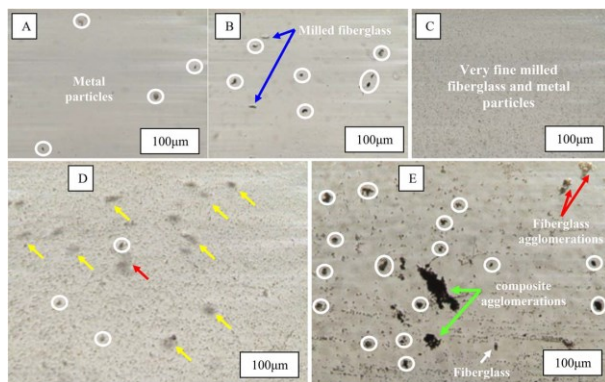


Figure 3.1.9. Very fine fiberglass particles dispersed in BER/DMF samples: (a) Red; (b) Violet; (c) Blue; (d) Green; and (e) Yellow (sample codes in Table 2.3.1.)

Moreover, evident correlation between the amounts of solid particles (**Fig. 3.1.9.**) and the absorbance data (**Fig. 3.1.8.**) can be seen for each sample with a higher quantity of particles resulting in significantly higher absorbance. Therefore, UV measurements were repeated again for all the samples after the centrifugation to ensure that the samples are not contaminated by solid particles. Finally, **Fig. 3.1.10.A.** shows the absorbance data against the ultraviolet light for BER/DMF samples diluted by ethanol with a volume ratio of 0.1:4 (mL) after centrifugation. It is clear that the centrifugation had a positive effect on the accuracy of the results since all the treated samples had the peaks at the same wavelength, and also the absorbance data became lower than 0.85, varying from 0.5 to 0.7. **Fig. 3.1.10.B.** shows the final concentration of BER in DMF for the five samples of different WPCBs at the wavelength of 282 nm.

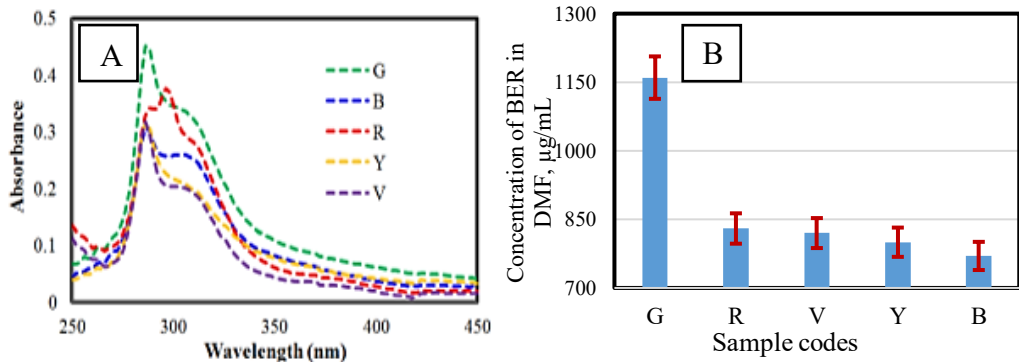


Figure 3.1.10. A) Absorbance of BER/DMF samples after centrifugation and B) Concentration of BER in DMF (sample codes in Table 2.3.1.)

3.1.5. Fiberglass of milled samples

Currently, milled fiberglass is commonly used as a filler material in many critical applications related to aerospace, automotive industry, etc. due to its good strength, corrosion resistance, low thermal expansion, and high in-plane properties compared with the traditional materials (Jingjing Li, Zhao, Gao, Wan & Zhou, 2014). Meanwhile, Recovered Milled Fiberglass (RMFG), especially the one recycled from WPCBs, is still used to a limited extent or only in traditional applications, such as wood-based products, concrete, asphalt, plastic and so forth due to its low purity. The RMFG from WPCBs is usually contaminated with BER which is considered a toxic organic material (Yin, Li, He, Huang & Xu, 2011). In the present part of the thesis, DMF was used to dissolve BER and to improve the purity of RMFG. To determine the optimum dissolution time limited by the required purity of RMFG, a metallographic microscope was used to examine the fiber subjected to purification every 30 minutes during the ultrasonication treatment. **Figure 3.1.11.** shows all the steps of BER dissolution, starting from the original WPCB powder until the pure RMFG was obtained.

Figure 3.1.11.A. illustrates the crushed section of plain woven type fiberglass (this type is commonly used in the manufacturing of WPCBs) (Jinlian, Yi & Xueming, 2004); such woven fiberglass commonly consists of two types of yarns (weft and warp) interlaced at a certain angle so that to obtain the matrix. During the initial 30 minutes of sonication, the fiberglass-DMF suspension mainly contained composite agglomerations, while DMF only started to strip epoxy. During the following 30 minutes, the reversible breaking of the internal van der Waals' bonds occurred, and the BER bond started to vibrate with a higher energy; the process was facilitated by ultrasonication treatment and finally resulted in the dissolution of BER (Haugan & Dalsjø, 2014); then DMF started to penetrate between the interlaced weft and warp yarns until the complete separation of the yarns occurred as shown in **Fig. 3.1.11.B.**

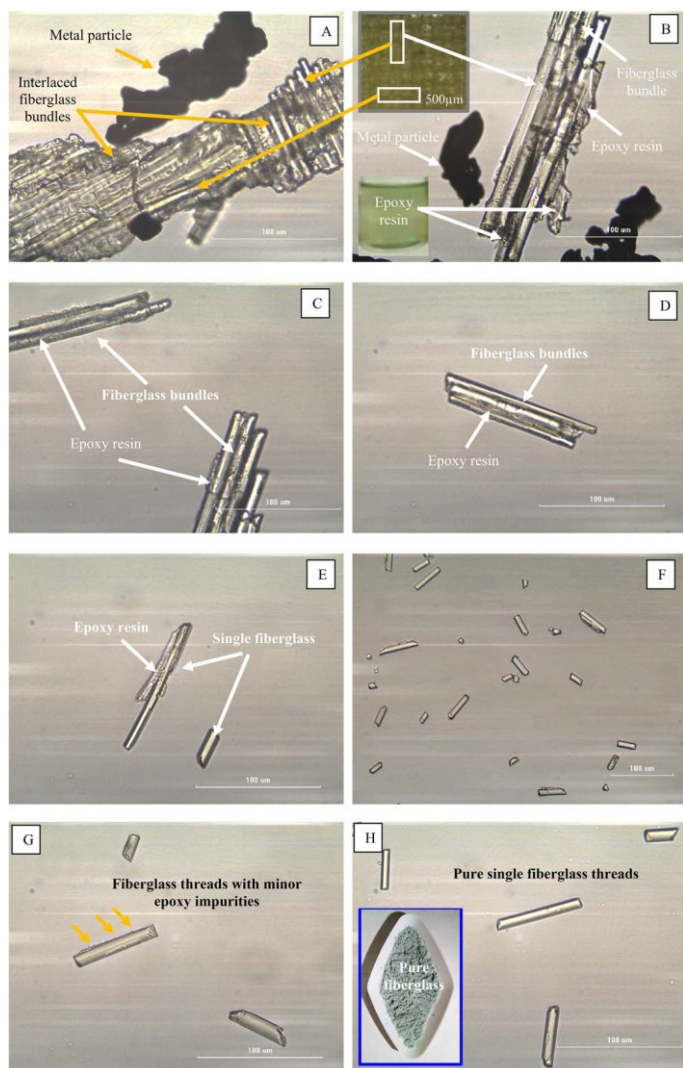


Figure 3.1.11. Purification steps of recovered milled fiberglass at different treatment times: A) 30 min.; B) 60 min.; C) 90 min.; D) 120 min.; E) 150 min.; F) 180 min.; G) 210 min.; H) 240 min.

After a further 120 minutes, DMF started to weaken the internal van der Waals' bonds of BER located inside fiberglass yarns separating each fiberglass yarn into smaller bundles; however, the fiberglass bundles were still encapsulated or covered with epoxy as shown in **Fig. 3.1.11.C–G**. To break the remaining bonds between epoxy and fiberglass, the treated RMFG was again subjected to ultrasonication for another 30 minutes for additional purification. Finally, pure milled fiberglass applicable for the production of high quality composite materials was obtained after 4 hrs. of ultrasound treatment in total, as shown in **Fig. 3.1.11.H**.

3.1.6. Metal of milled samples

In the past, multiple studies were performed to determine the chemical composition of the recovered metals and the location of each element inside WPCBs; these studies can be classified according to the amount of elements they are focused on, i.e., multiple element studies or single element studies (as in the current case of copper in WPCBs). Atomic absorption spectroscopy (AAS) is necessary in cases of multiple element studies to determine their weight fraction inside the tested sample. Also, AAS is recommended for chemical elements present in small concentrations, especially in precious metal recovery (Yazici & Deveci, 2015). At the same time, scanning electron microscopy-energy-dispersive X-ray spectroscopy (SEM-EDS) is widely used in cases of one main element being present due to the simplicity and the fact that the tested sample does not require special preparation like for AAS. Therefore, in the present research, SEM-EDS was used to study the purity of the recovered copper particles. **Figure 3.1.12.** shows SEM images (scale ranges (200, 300 mm)) of the recovered metal powder of the Blue and Violet samples with the average observed particle size of 122 mm after cleaning the samples with an ultrasound cleaner.

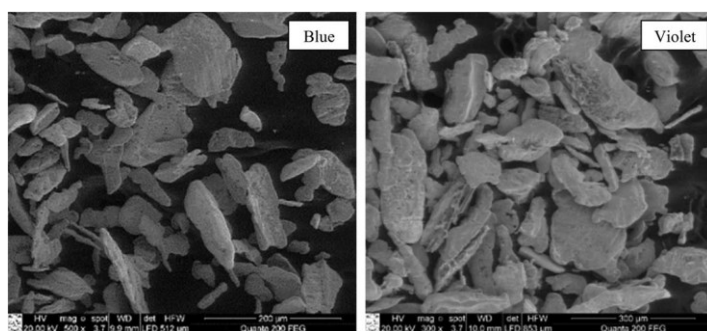


Figure 3.1.12. SEM images of recovered metal powder: lamella-like particles of (A) Blue sample and (B) Violet sample (sample codes in Table 2.3.1.)

As shown in the Figure, the particles were lamella-like (flake-shaped); this shape was a result of continuous milling. Also, SEM-EDS was used to observe the morphology and element distribution of each milled metal sample (**Fig. 3.1.13.**). Detailed results of our analysis can be found in **Annex 2**. It was found that Carbon (C) and Oxygen (O) were present in all the samples having weight percentages of 5–8 wt.% and 2.5–5.9 wt.%, respectively, which could be a result of the corrosion that could have taken place during the storing or functioning of PCBs. Similarly, a high content of Cu was observed for all the samples since Cu is used as a main component of all the conducting elements of PCB due to its good electrical properties (Duan *et al.*, 2009); however, its share varied in the range of 86–93 wt.%. Also, a very small amount of Aluminum (Al) was found only in the Green and Yellow samples representing 1 and 2.4 wt.%, respectively. These results give strong evidence that the chemical composition of each sample is notably different in terms of the presence of elements and their mass weight. Finally, it can be concluded that Cu can be considered the main metallic element in all the WPCB samples.

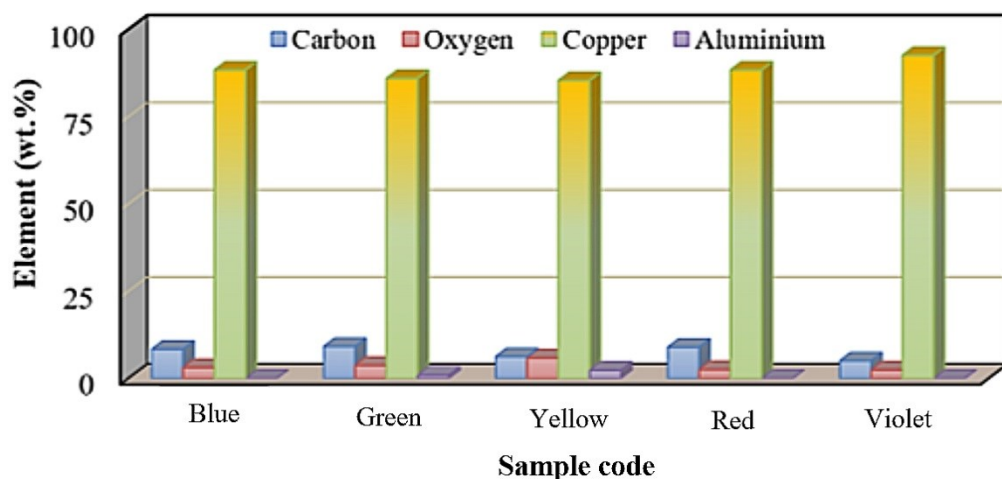


Figure 3.1.13. Chemical composition of recovered metal powder samples (sample codes in Table 2.3.1.)

3.1.7. Conclusion: preliminary experiments

As a result of studies on ultrasound-assisted solvent treatment of milled WPCBs, it was found that solvent DMF can efficiently extract Epoxy Resin from the samples within ~4 hours of processing at 50 °C. However, the approach had major disadvantages originating from the nature of the input material. Firstly, it was found that milled WPCB samples required a two-times-higher amount of the solvent for effective treatment compared to the non-milled samples. Secondly, after Epoxy Resin extraction, the product was obtained as a mixture of metal and non-metal particles. Attempts to separate this mixture into the respective fractions by centrifugation indicated that the efficiency of the process was not very high with the total recycling rate of ~92% (the rates are discussed in Section 3.5. **Recycling rate evaluation**) when compared to the results reported for solvent treatment of non-milled WPCBs. Therefore, a decision was taken to avoid milling of specimens and to continue experiments in order to indicate the optimum conditions of solvent treatment on cut samples.

3.2. Indication of optimum separation conditions

The primary focus of the optimum separation condition experiments was on finding the optimum treatment temperature for the separation of non-milled WPCB specimens. Unlike the case of the milled samples, separation in the current experiments meant not the point when the full extraction of BER from the samples had been achieved but rather the point when all the layers of different materials inside WPCB had been split from each other under the effect of the treatment.

Achievement of the splitting of layers is very important from the recycling perspective since, after that, non-metallic layers can be separated from metallic foils, and specific purification procedures can be conducted for each fraction based on the planned application. For example, if it is planned to reuse recovered fiberglass for the production of an Epoxy

Resin-based composite material, there is no need for full purification of the substrate from residual non-dissolved BER; thus cost savings can be achieved.

As for the other separation conditions, the solid-to-liquid ratio was selected based on the previously reported ratio for cut WPCB specimens, i.e., 3:10 wt./vol. (Verma *et al.*, 2016)). The treatment time was a derived parameter defined by being based on the point in time when the separation of specimens occurred at a specific treatment temperature.

3.2.1. Separation temperature and separation mechanism

Fig. 3.2.1. shows the effect of WPCB models on the final dissolution time. It can be seen that, at the lowest temperature of 25 °C (without heating, only ultrasonic treatment), the yellow, green, and violet samples showed the shortest separation time, while the blue and red samples demonstrated the longest time. Also, it was noted that the difference between the maximum and minimum dissolution times was ~53% (32–68 hrs.) since the quantity of BER in the WPCBs was not the same, nor was its spatial configuration and distribution. With increasing the heating rate to 50 °C, significant acceleration was noted for the separation process of all the WPCB samples, and the same trend was present as at 25 °C; i.e., the separation time for the sample types was yellow < green < violet < blue < red. The difference in the separation time between the samples was ~66, 68, 69, 73, and 74%, respectively. This may be associated to strong hydrogen bond formation affinity of DMF leading to the breakage of the internal van der Waals’ bonds of BER and the acceleration of this phenomenon with the increasing temperature (Haugan & Dalsjø, 2014).

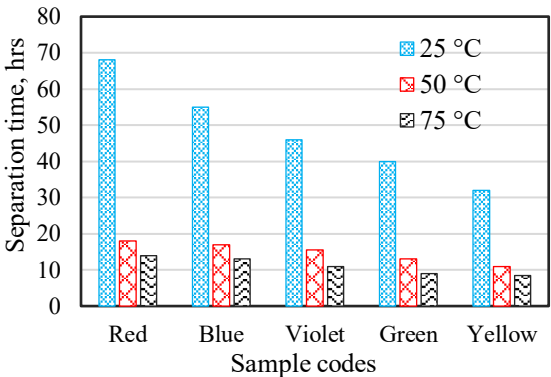


Figure 3.2.1. Separation time of WPCB samples (sample codes in Table 2.4.1.)

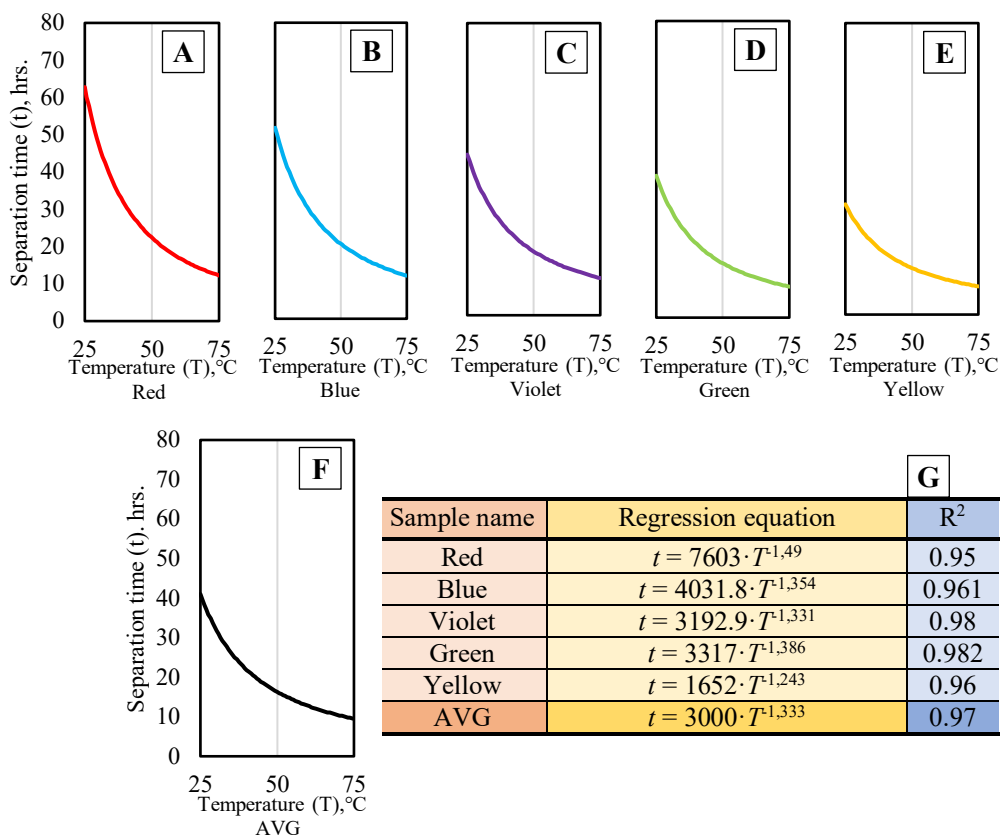


Figure 3.2.2. Regression modeling of the dependencies between separation time (t) and temperature (T): A–E) Graphical representation of regression models for individual samples; F) Graphical representation of regression models for average data; G) Regression equations and R^2 coefficients

As proof of the above-outlined statements, with a further increase of the heating rate to 75 °C, the separation time decreased again, and the trend in the separation time of yellow < green < violet < blue < red was observed once more. Also, the elevated temperature enhanced by vibrations led to the formation of hydrogen bonding between BER and DMF, and thus the dissolution of BER improved the efficiency of delamination and separation of WPCB samples. This was the main reason to use the ultrasonication process in the present work (Wath *et al.*, 2015).

The experimental results shown in **Fig. 3.2.1.** clearly exhibited a certain pattern as, regardless of the sample type, the ratio between the separation time at 25, 50 and 75 °C remained very similar for all specimens. To better illustrate that, a number of power regression equations was determined as shown in **Fig. 3.2.2.** As the similarity between all the samples became much more apparent (the main difference was a slight variation in power coefficients), one final equation was determined based on the average separation time values (**Fig. 3.2.2.F.**) for a posterior use in determining the optimum separation conditions. Overall, it must be noted that the prediction accuracy was fairly high, reaching 0.97 for the average values prediction.

According to the obtained results, the separation of WPCBs by using a solvent contains three main steps: the penetration of DMF inside the layers, the dissolution of BER between the layers, and the delamination of the layers. The contact areas between DMF and WPCB layers can be considered as the starting points of the separation process, and their increase leads to the acceleration of the separation. The sizes of the contact areas are affected by the solder mask layer, copper tracks and solder which hinder the progress of DMF penetration inside the matrix. However, the separation time does not count as conclusive evidence for whether each element inside the matrix is fully separated or not for the particular BER type.

The Brominated Epoxy Resin concentration trends of the Yellow and Red samples at 25, 50, and 75 °C can be seen in **Fig. 3.2.3**. The Yellow and Red samples were selected as the most representative ones as Yellow had the shortest separation time while Red had the longest time. Both samples show similar trends at all temperatures. At 25 °C, the concentration curve showed sharp growth only at the initial one or two observation points as a result of DMF dissolving easily accessible Epoxy Resin from the perimeter of WPCBs. After that, the curve became more sloped as the solvent had to penetrate deeper between the layers of the sandwiched composite structure.

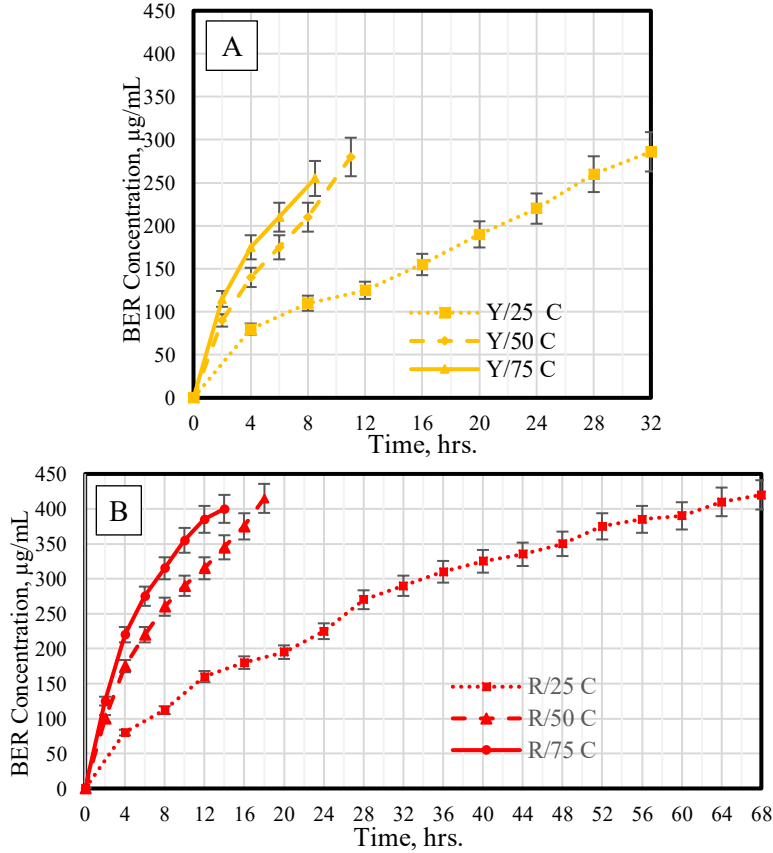


Figure 3.2.3. Brominated Epoxy Resin concentration trends for: A) Yellow; B) Red sample (sample codes in Table 2.4.1.)

This sloped curve shape with some deviations was maintained throughout the entire separation process at 25 °C for both samples. Moving on to the concentration trends at 50 and 75 °C, a different, more rapid, concentration growth can be seen throughout the entire separation process. In this regard, 50 and 75 °C trends are very similar, with the main difference being that 75 °C treatment resulted in somewhat higher BER concentrations at all equal observation points as well as in slightly shorter separation times. With the experimental data being obtained, a regression model was determined to provide a tool for the BER concentration prediction. As shown in **Fig. 3.2.4.**, the observed trends can be fairly easy to describe with simple linear regression models. As the regression coefficients suggest, the 25 °C separation process is set apart from the treatment at 50 and 75 °C, which can be easily seen by comparing the slope coefficients.

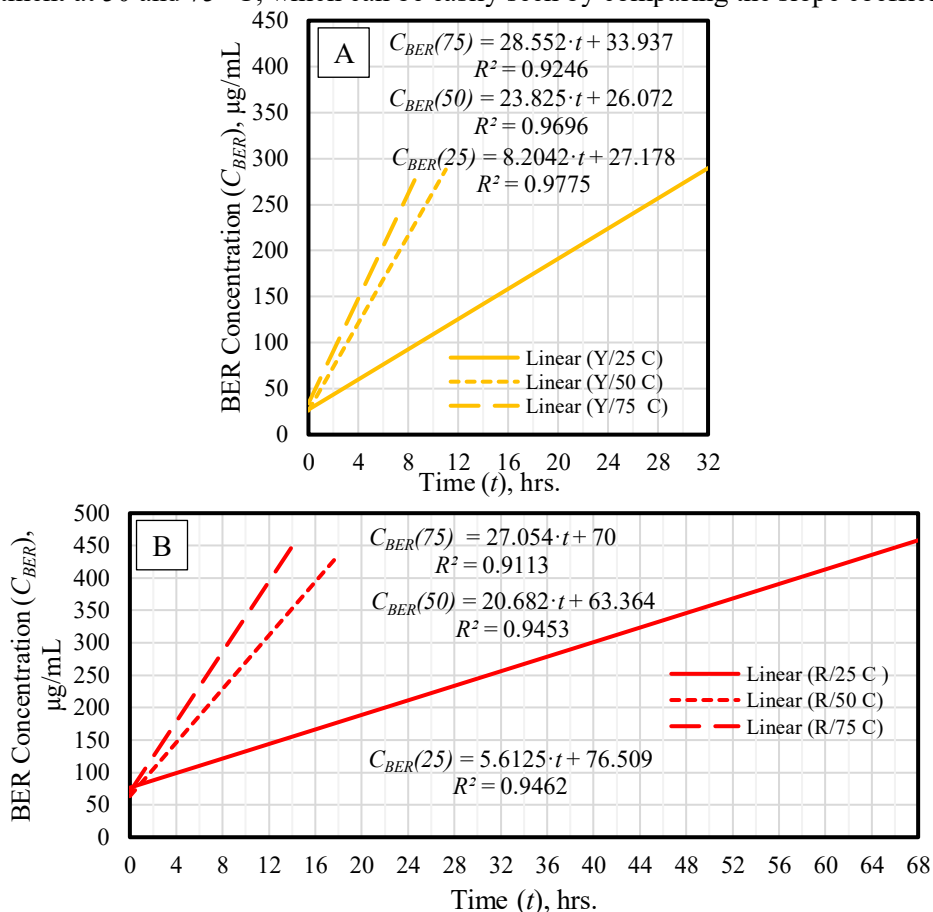


Figure 3.2.4. Linear regression models of BER concentration trends for: A) Yellow sample; B) Red sample (sample codes in Table 2.4.1.)

However, modeling based on the Epoxy Resin concentration data obtained from specific sample types may not be very effective in terms of prediction due to the fact that, as experiments showed, there may be a high degree of variety between different samples.

Therefore, it was considered more appropriate to use the average values of BER concentrations in order to obtain the regression model as shown in **Fig. 3.2.5**.

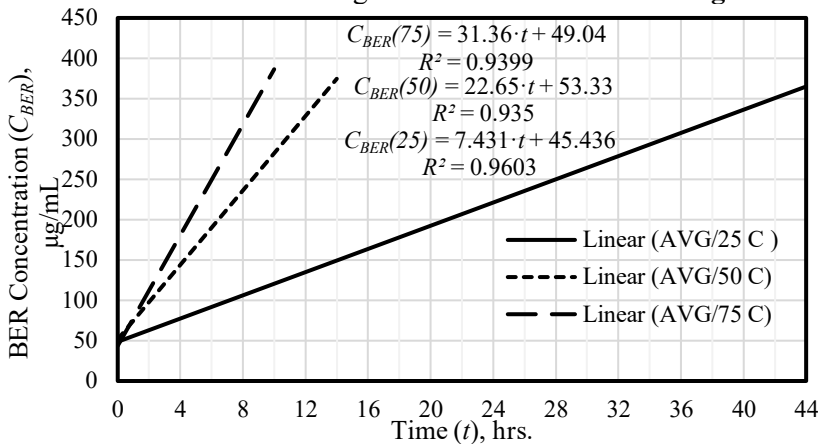


Figure 3.2.5. Linear regression models of BER concentration trends based on the average of all experimental values

Since the slope coefficients were the main variable factor that differentiated the regression equations, another regression model was created, as in the case of milled samples, to establish dependencies between the temperature and the coefficients as shown in **Fig. 3.2.6**. As it was found, the dependence between the coefficients was essentially linear, and the respective regression equation managed to describe the coefficient very well with $R^2 = 0.99$.

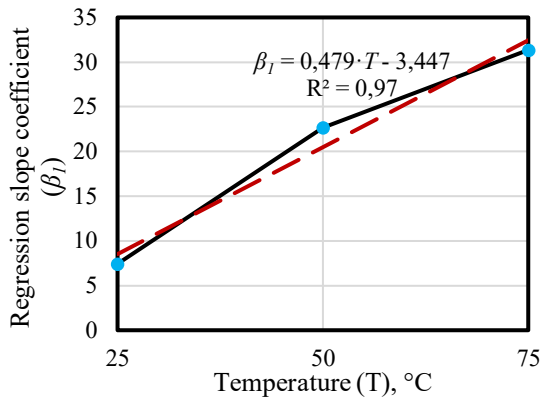


Figure 3.2.6. Dependence between regression slope coefficients (of BER concentration trends regression models) and temperature

After the equation showing correlation between the temperature and the regression slope coefficients in **Fig. 3.2.5**. had been defined, this data was used to obtain the final equation allowing to calculate the BER concentrations for the average WPCB separation process lasting for 8.5–44 hrs. as shown in **Fig. 3.2.7**. The input parameters included two variables: time and temperature. It is worth noting that, as R^2 coefficients suggest, the prediction model was more accurate at the lower temperatures where the BER

concentration growth was slower and therefore easier to predict by linear regression resulting in $R^2 \approx 0.97$, while, at the higher temperatures ($>50^\circ\text{C}$), the growth pattern showed a slightly less linear behavior. However, the suggested equations remained fairly accurate even in this area, suffering only a minor decrease in R^2 coefficient (0.91).

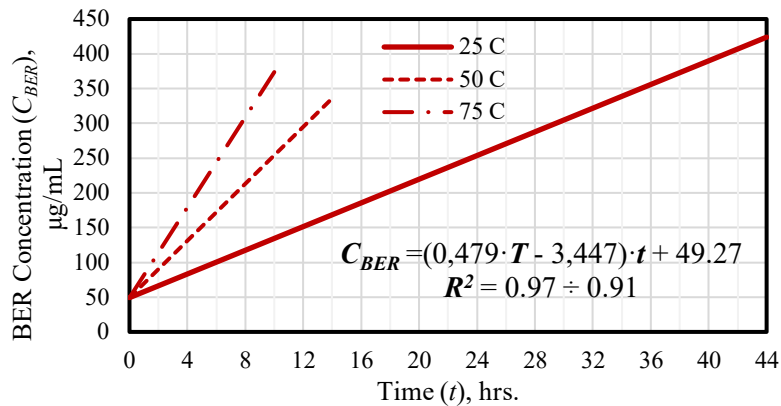


Figure 3.2.7. Dependence between concentration of epoxy resin (C_{BER}), time (t) and temperature (T), calculated by using the specified equation

Fig. 3.2.8. shows the final concentrations of BER in DMF for all the samples at 25, 50, and 75 °C. As shown in the Figure, at all temperatures, the red, blue, and violet samples had the highest concentrations of BER, while the green and yellow samples had the lowest concentrations, respectively. Also, it can be seen that the concentrations of BER were directly proportional to the separation time; for instance, the red sample (the longest separation time as shown in **Fig. 3.2.1.**) had the highest concentration of BER, while the yellow sample, with the shortest separation time, featured the lowest BER concentration. The main reason for this was that, with a longer separation time, DMF had more time to penetrate inside the WPCBs layers and break the internal van der Waals’ bonds of BER, as shown in **Fig. 3.2.10.**

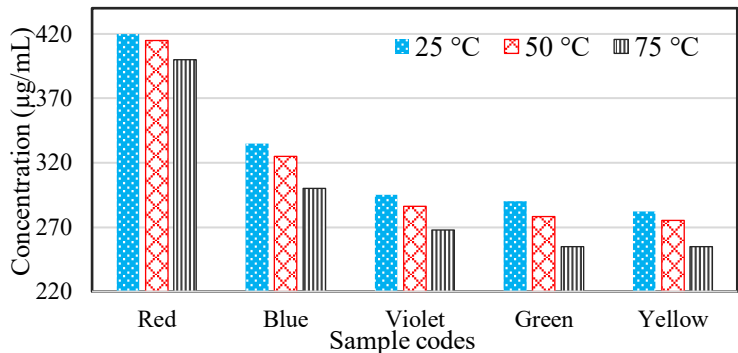


Figure 3.2.8. Concentration of BER in DMF of WPCB samples (sample codes in **Table 2.4.1.**)

It was evident that the final concentrations of BER, presented in **Fig. 3.2.8.**, had evident correlation with the treatment temperature that was observed for all the samples.

It was found that, as shown in **Fig. 3.2.9.**, this correlation could be expressed with linear regressions.

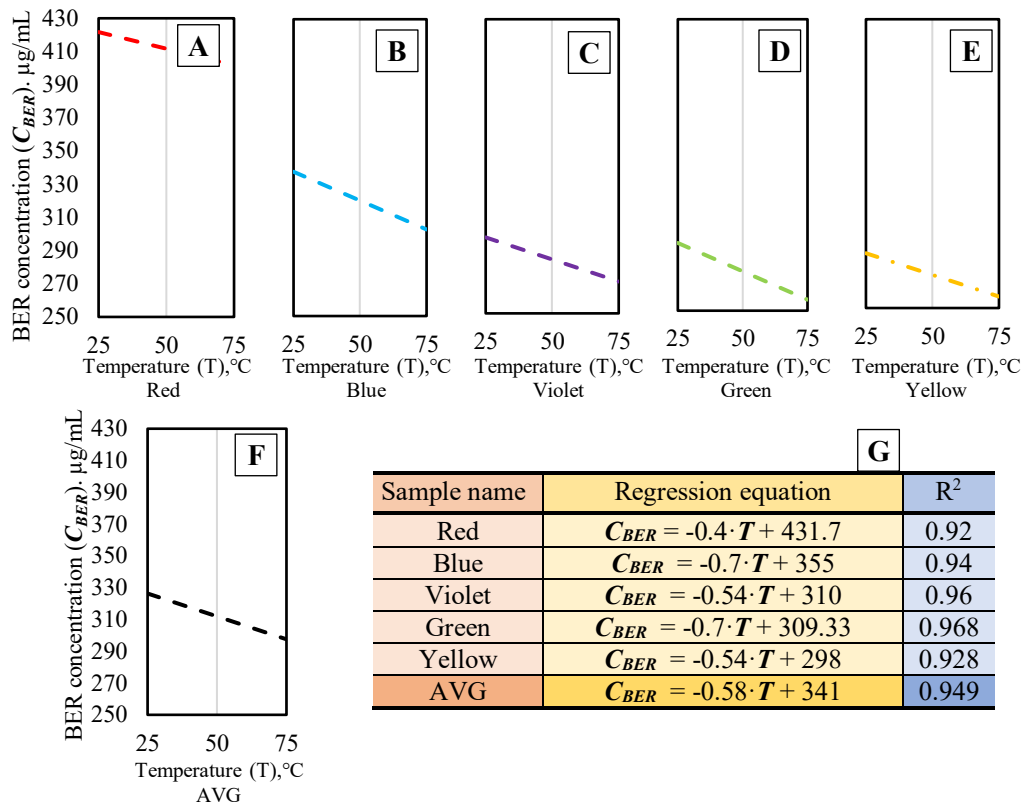


Figure 3.2.9. Regression modeling of the dependencies between concentration of Epoxy Resin (C_{BER}) time and temperature (T): A–E) Graphical representation of regression models for individual samples; F) Graphical representation of regression model for average data; G) Regression equations and R^2 coefficients

Such a prediction method was less accurate for the Yellow and Red samples (as they exhibited a higher BER concentration variation degree), where R^2 was below 0.93, whereas, for the rest of the samples, it was >0.94 . Moreover, in the case of long separation times, DMF (indicated by green circles) can additionally dissolve BER particles directly adhered to the lower or upper layers of fiberglass (indicated by a blue circle), while the short separation time only allows DMF to split the layers by dissolving BER in the middle of the layers (indicated by yellow circles) thus leaving more BER adhered to fiberglass (Verma *et al.*, 2017b).

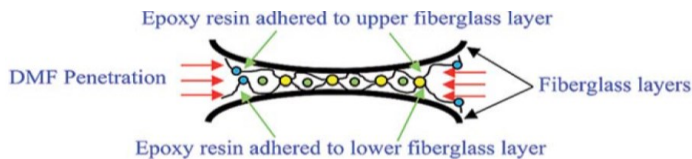


Figure. 3.2.10. WPCB separation mechanism

Regarding the influence of the temperature, it is clear that the concentration of BER in DMF in all the samples showed the same trend, as temperatures of 25 °C provided the highest, 50 °C provided the medium, and 75 °C provided the lowest concentration. These results came in contrast to those expected for the reason that, at lower temperatures, DMF alone does not have the capacity to quickly break the bonds of BER and thus needs another source to accelerate the dissolution process. Accordingly, ultrasonic treatment was used in the developed technique as a dissolution enhancer to accelerate the dissolution process by generating high-frequency sound waves (by means of vibration transducers) with frequencies higher than the upper bonding limit of BER. The summary effect of these waves increases by increasing the operation time (the separation time in our case), which leads to an increase in the shear rate of BER thus raising the final concentration of BER in the DMF solution (Dean, Krstina, Tian & Varley, 2007; Yuhana, Ahmad & Bahri, 2012). Therefore, the samples subjected to ultrasound treatment for a longer time due to a longer separation had higher concentrations of BER also because of the ultrasound treatment.

During the separation, two main factors were considered in order to indicate the optimum conditions: the separation time and the final BER concentration. While it was preferable to shorten the separation time as much as possible, it was also noted that a short separation time resulted in lower final concentrations of the extracted BER. To establish balance between these two parameters, two models for the separation time and BER concentrations that were described in Fig. 3.2.2. and 3.2.9. were compared as shown in Fig. 3.2.11. The resulting data suggested that, compared to treatment at 25 and 75 °C, 50 °C could offer the right balance between the separation time and the BER extraction.

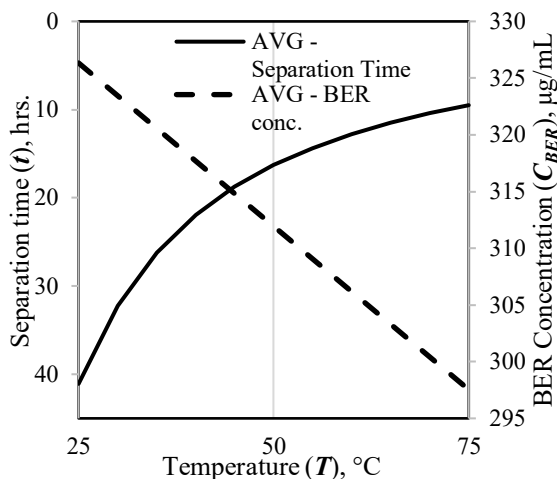


Figure 3.2.11. Relation between average separation time and final BER concentration in respect to the treatment temperature

3.2.2. Conclusion: optimum separation conditions

Finally, given the points that BER is a base element in WPCBs, and that the concentrations of BER at 25 °C and 50 °C were almost the same yet significantly lower at 75 °C, it can be concluded that 50 °C was the optimum separation temperature in terms

of the reaction time and BER removal rate since quickly separated layers of WPCBs at 75 °C still contained a considerable amount of adhered BER, while a slightly slower separation at 50 °C produced purer fiberglass and metal; this data was confirmed from the modeling perspective, as in was shown in the models for the separation time/BER extraction rate (Figs. 3.2.2., 3.2.9.) and their comparison (Fig. 3.2.11.).

3.3. Mechanical testing of recovered fiberglass

Stress–strain curves were composed to investigate the effect of the WPCB structure on the mechanical properties of the recovered woven fiberglass. Generally, during the manufacturing of PCBs, Epoxy Resin/fiberglass laminate (base of PCB) is subjected to drilling operations in order to create through holes which are later used for the mounting of electrical components, for providing electrical connection, etc. (Hirai, Hamada & Kim, 1998). These openings and notches can still be found after the recycling process in all fiberglass layers; they are randomly distributed depending on the model of WPCB and the specific area of WPCB, from where the sample was taken.

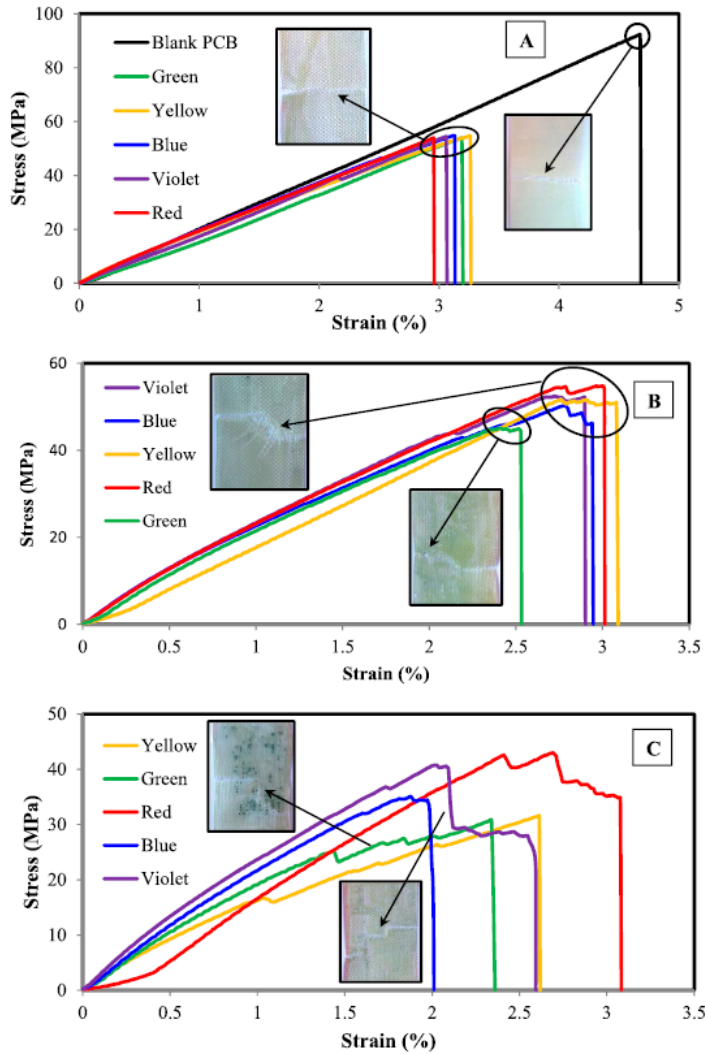


Figure 3.3.1. Stress-strain curves of plain woven fiberglass samples extracted from WPCBs in: A) Plain; B) single-notched; and C) multi-notched cases (sample codes in Table 2.5.1.)

It is certain that the location, size and quantity of these holes will affect the final mechanical behavior of the recovered fiberglass layers in terms of strength (σ_f), strain (ϵ_f), and modulus (E). To overcome all of these obstacles and reduce the variation of the final results, three samples in total were cut from each WPCB: one plain sample without holes (the minimum possible amount and size of holes), and two samples from different places having a different amount of holes (determined by the amount of solder joints on the outer surface of WPCBs). The results of mechanical tests were classified according to the amount of holes in the samples into: a) plain, b) single-notched, and c) multi-notched. After that, the average values of these three cases were calculated in order to get the final mechanical parameters. Also, another sample having no holes or any other structural features that could have possibly affected its mechanical properties during the

strength testing was cut from blank PCB in order to provide a reference for WPCB fiberglass samples. The first case of plain samples is illustrated in **Fig. 3.3.1.A.** showing measured mechanical properties of the Blue, Green, Yellow, Violet, Red WPCB and blank PCB samples.

As it can be seen in the Figure, the blank PCB sample had the highest σ_f (92 MPa), while for the WPCB samples it was lower, remaining in the range from 53 to 55 MPa. Similarly, ϵ_f values showed a similar trend for blank PCB and WPCB samples – the measurements for the blank samples resulted in ϵ_f (4.7%), whereas for WPCB samples it was in the range of 3–3.3%. This significant reduction in the s_f and ϵ_f values of the WPCB samples (~41% and ~1.55% for σ_f and ϵ_f , respectively, when compared with the blank PCB sample) might partly have been a result of minor degradation caused by storage for a long time, since WPCB samples were produced between 1995 and 2004. Also, the σ_f and ϵ_f value reduction may have been observed due to the use of mechanical tools during the assembly process for mounting the electronic components on bare boards. This caused residual stress which increases with time and leads to a decrease in the strength (Longobardo, 2010; Al-Kuwaiti, Mourad, 2015; Rath & Sahu, 2011).

In addition, thermal degradation may also influence the final properties of the extracted fiberglass since, during the service time, PCBs are exposed to the influence of thermal sources (e.g., CPU, resistors, and other electrical components) as well as environmental effects. Fiberglass is sensitive to temperature variations inducing thermal stresses between fiberglass and the polymer matrix due to their distinct thermal expansion coefficients. At elevated temperatures, the differential thermal expansion of the fiber and the matrix may lead to the formation of micro-cracks in the fiber/polymer interface (Deng & Chawla, 2008; Etches, Potter, Weaver & Bond, 2009).

Similarly to the σ_f and ϵ_f values, E also showed the same trend as for blank PCB and WPCB samples, but with a minor percentage difference, unlike s_f and ϵ_f ; E for blank samples E was 29.3 MPa, whereas E for WPCB samples was in the range of 22–28 MPa, which may have been due to a certain amount of epoxy still remaining attached to the fiber and leading to higher E values, especially because epoxy resin is denoted by good Young's modulus (Suresha, Chandramohan, Renukappa & Siddaramaiah, 2007).

In the second case of single-notched samples, the σ_f of the Blue, Yellow, Red, and Violet samples were similar and equal to ~50 MPa, while the σ_f of the Green sample was 45 MPa as shown in **Fig. 3.3.1.B.** This means that the presence of a single hole in the fiberglass layer decreased σ_f by 8% for the Blue, Yellow, Red, and Violet samples and by 16% for the Green sample in comparison to the plain samples from the first case. This phenomenon can be explained by the difference in the hole sizes – drilling holes cause stress concentration which is higher in the case of holes with a higher diameter (Das Chakladar, Pal & Mandal, 2012; Chang, Yau & Chou, 1987; Hwan, Tsai, Chiu & Huang, 2014; Naik & Shembekar, 1992). This was the main reason for a significant reduction in σ_f in the Green sample where the average diameter of a drilling hole was 0.7 mm, while for other samples it was 0.3 mm. Also, the E -values of single-notched WPCB samples were in a similar range with small deviations; they were equal to ~30 MPa.

Finally, in the third case of multi-notched samples, a significant drop in s_f was detected – s_f decreased in average value of 35 MPa with a sizable variation range of 31–

43 MPa; the same trend was observed for ϵ_f and E due to the increase of stress concentrators as shown in **Fig. 3.3.1.C**. It needs to be noted that a major variation range was a result of the random distribution of drilling holes, their location, size and numbers (Ghasemi Nejhad & Chou, 1990; Khashaba, 2003).

The average σ_f , ϵ_f and E for each WPCB sample where the average values were calculated for the three cases: A) plain, B) single-notched, and C) multi-notched can be found in **Annexes 3–5**.

3.3.1. Conclusion: Mechanical testing of recovered fiberglass

Mechanical tests confirmed that recovered fiberglass sheets still retained a significant fraction of their strength (up to ~60%) as well as other properties. The main reason for the decrease of the properties was the presence of drilling openings. Additionally, phenomena with a high concentration of BER extracted from the Green sample during the preliminary experiments (3.1.3.) was explained, as the Green sample was found to feature the lowest mechanical properties; therefore, the size of particles produced during the milling of this sample was the smallest, which resulted in a higher BER extraction rate.

3.4. Full-size WPCB experiments

Since the optimum conditions had been found (Section 3.2.) as a solid-to-liquid ratio of 3:10 (wt./v.) and a temperature of 50 °C, a decision was made to conduct experiments while using these conditions on the three most common types of WPCBs (Random Access Memory – RAM, Video Card – VC, and Motherboard – MB) in order to study the process efficiency and applicability for large specimens. This chapter focuses on the analysis of the separation process and materials recovered from the three types of WPCBs.

3.4.1. Full-size WPCBs – separation trends

As a result of solvent treatment at optimum conditions, all the three WPCB types were separated after the time intervals shown in **Fig. 3.4.1**.

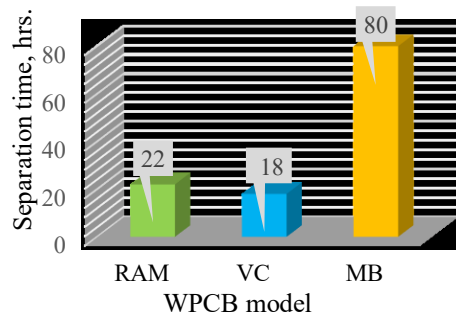


Figure 3.4.1. Separation time: Random Access Memory (RAM), Video Card (VC), and Motherboard (MB)

To explain such significant differences in separation times, we need to investigate dependencies between the separation times, mass, surface area, and the structure of the

specimens. Naturally, the separation time is greatly affected by all of these parameters. For example, a larger surface area greatly increases the distance that the solvent has to penetrate inside the sample in order to reach its center. **Figure 3.4.2.** shows the correlation between the sample surface area and the separation time.

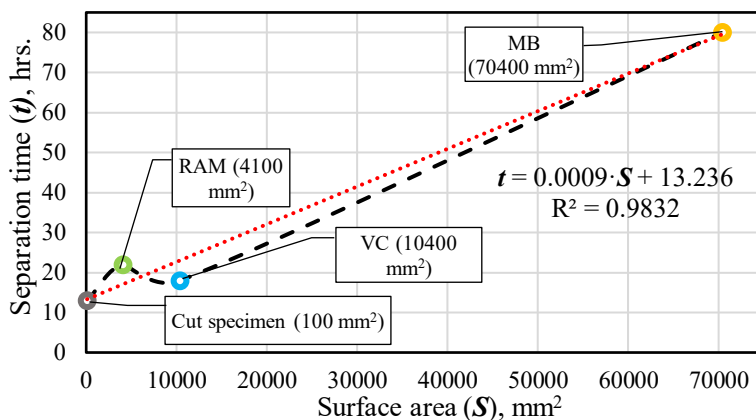


Figure 3.4.2. Correlation between surface area and separation time for cut specimens, Random Access Memory (RAM), Video Card (VC), and Motherboard (MB)

As it can be seen, nearly linear dependence of separation time on surface area was observed for the cut specimens, Video Card, and Motherboard. Firstly, an increase of the surface area of the sample by ~100 times (cut specimens to VC) resulted in an increase of the separation time only by ~40%. However, when the surface area was increased again by ~7 times (VC to MB), the separation time already grew by 450%. This shows us that the separation of WPCBs with a solvent is much more efficient for the treatment of smaller-sized specimens while treating samples with sizes beyond 100,000 mm² may not be feasible as the estimated separation time will exceed 100 hours, thus a size reduction operation may be needed.

The next important point that needs to be addressed is the separation time of RAM. According to the general trend, it should have been ~15–16 hrs., whereas, in the real case, the separation time was 22 hrs., which is bigger than the time needed for a larger-sized VC. There are several possible reasons for such a deviation in the separation time – the difference between the chemical composition of epoxy resin in RAM and other specimens, the difference in the masses of specimens, and the difference in the internal structure of the samples. The relation between the mass of the specimens and the separation time is shown in **Fig. 3.4.3.**

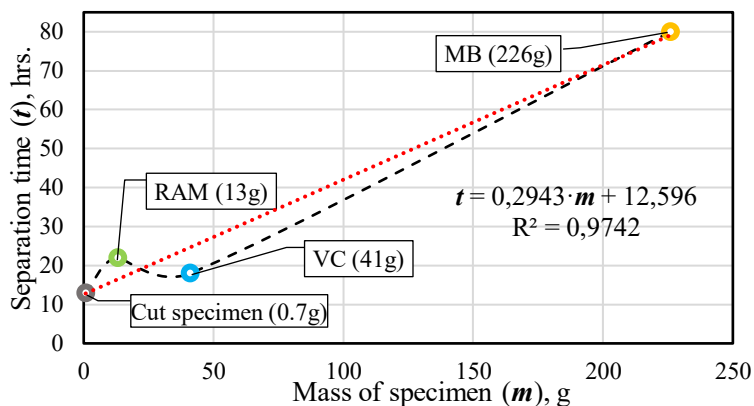


Figure 3.4.3. Correlation between mass and separation time for Cut specimen, Random Access Memory (RAM), Video Card (VC), and Motherboard (MB)

A trend that is very similar to **Fig. 3.4.2.** can be seen again, where RAM had a 3 times lower mass than the VC while requiring a longer time for separation. Based on this data, a conclusion can be drawn that the mass is not the factor which caused deviations in the trend. The chemical composition of Epoxy Resin from all the WPCB types is another important point of the study. While more detailed analysis can be found in the respective chapter below, the general conclusion was that all the samples contained Brominated Epoxy Resin with similar transmittance in the infrared spectra and with a similar thermal behavior.

Thus, having two parameters ruled out, we should focus on the internal structure of the specimens. The number and type of the layers contained in WPCBs of specific types is summarized in **Fig. 3.4.4.**

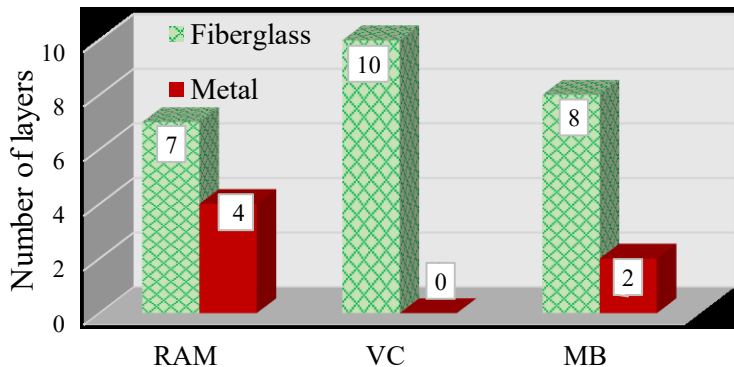


Figure 3.4.4. Types and number of complete layers found inside Random Access Memory (RAM), Video Card (VC), and Motherboard (MB)

The provided data can finally explain the deviation noted in the separation time of RAM. When comparing all the three types of WPCBs, RAM can be remarked as the type featuring the biggest amount of metallic layers. Metallic and woven fiberglass layers possess a crucial difference in the way the solvent interacts with them inside the WPCB matrix. Fiberglass layers consist of individual glass fibers that are encapsulated in Epoxy

Resin which is gradually removed by the solvent as it penetrates inside the layers. At the same time, the encountered metal layers become a non-permeable barrier for the solvent thus limiting its penetration to only the horizontal direction and greatly hindering the separation of the WPCB composite. Therefore, this was a primary reason for the unexpectedly long RAM separation time.

Based on the obtained data, four prediction models suitable for determining the separation time of solvent-treated WPCB were created. As shown in **Fig. 3.4.5.**, the models use linear and exponential regressions to predict the desired parameters.

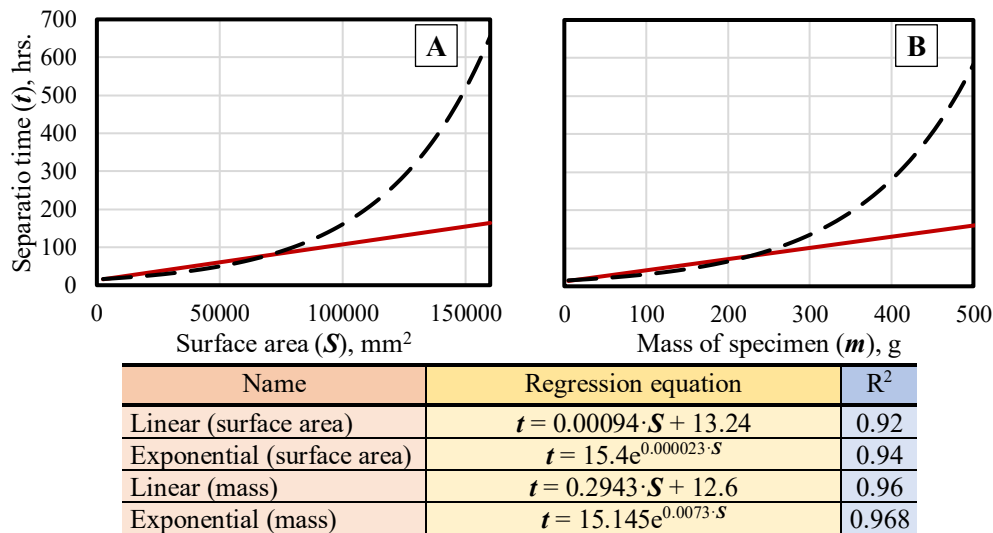


Figure 3.4.5. Regression models for determining the separation time of WPCB specimen (*t*) under the developed treatment based on: A) sample surface area (*S*), B) sample mass (*m*)

The models were selected according to the two separation scenarios: the more and less optimistic ones. The more optimistic scenario suggests that the separation time linearly increases by increasing the surface area or the mass of specimens and relies on the experimental data, which demonstrated mostly linear dependence between these parameters in the measured range. Such a linear pattern was observed by other researchers and is not uncommon for various dissolution processes (Verma *et al.*, 2016). However, only the linear model cannot be relied on; therefore, a less optimistic variant of the separation process where the dependence of the separation time on the surface area and the mass is exponential was developed. For example, Zhu *et al.* reported a dramatic increase in the separation time from 90 to 480 min. by doubling the sample size from 100 mm² to 200 mm² (Ping Zhu *et al.*, 2013). Although the used solvent was different, the fact that non-linear dependence may be determined needs to be accounted for. It is worth mentioning that both models (linear and exponential) describe the experimental data well with the exponential dependence being slightly more accurate. Since the exponential scenario is highly likely, it can be seen that with the sample surface area of >100,000 mm², the separation time may progressively increase thus consuming more and more resources for the treatment as the deviation from the linear scenario will continue to

increase. Thus the suggestion would be to avoid treatment of such large specimens as the separation may take 160 hrs. and more.

3.4.2. Structure of full-size WPCBs

Since the internal structure of WPCBs played a great role in the separation process (as mentioned previously), its detailed investigation was done within the scope of this work.

Our waste RAM had a sandwich-type structure which is shown in **Fig. 3.4.5**. As it can be seen, it contained in total 5 layers of woven fiberglass (3 layers of the base structure and 2 isolating ones), 2 internal track layers, 2 metal foil layers and 2 compound units, while the epoxy resin acted as an adhesive agent fastening the structure.

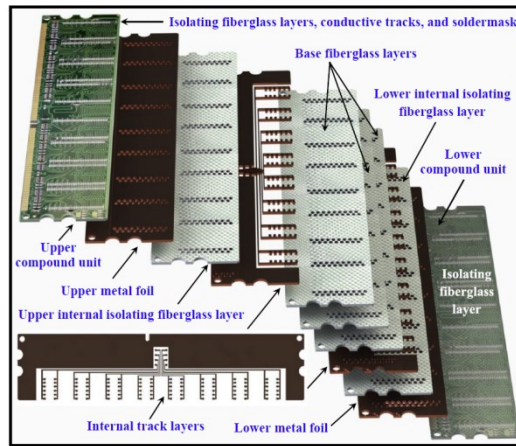


Figure 3.4.5. Random Access Memory: a reconstruction of layers and elements

All the layers had their specific purpose, for instance, three woven fiberglass layers of base structure in the middle of separated RAM had a function to increase the strength of the final board. The base structure was covered with two internal track layers (upper and lower ones). In addition, two woven fiberglass layers were used to isolate the internal track layers from the two metal foil layers. Finally, two more woven fiberglass layers isolated the metal foil layers from the compound units which can be defined as an assembly of isolating fiberglass layers, solder joints, conductive tracks, contacts, and solder mask

What regards the Video Card, it consisted of the following main components: a) substrate fiberglass layers (layers b–g), b) isolating fiberglass layers (layers a and h), c) conductive tracks, d) connectors, and e) solder mask as shown in **Fig. 3.4.6**. All the above mentioned layers and components were adhered together by BER. It can be seen that the substrate fiberglass components consist of six plain-woven fiberglass layers with each layer having different thickness in the range of 0.4–1 mm. Also, it was noted that each layer of the initially recovered isolating fiberglass layers (layers a and h) was a double layer. Finally, the separation process was conducted in three stages: a) dissolution of BER in DMF, b) Separation of substrate fiberglass layers, and c) Separation of isolating fiberglass layers, conductive tracks, connectors, and solder mask as one unit.

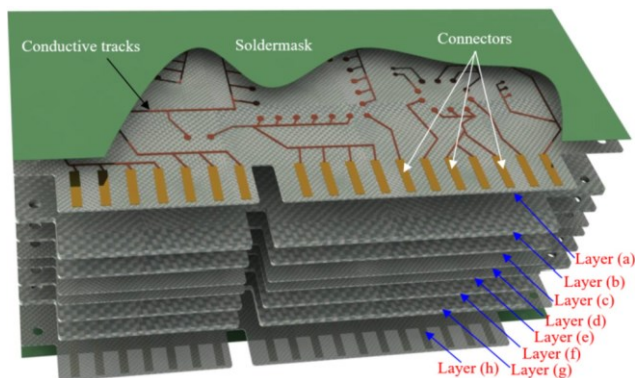


Figure 3.4.6. Video Card: a reconstruction of layers and elements

Finally, the structure of the Motherboard consisted of six layers of fiberglass (representing the WPCB substrate), two copper foil layers (the upper and lower layers), two fine-woven fiberglass layers (the upper and lower isolating layers), copper tracks, and two solder mask layers (the upper and lower layers). All the layers of WPCBs and tracks were glued together by BER, as shown in Fig. 3.4.7.

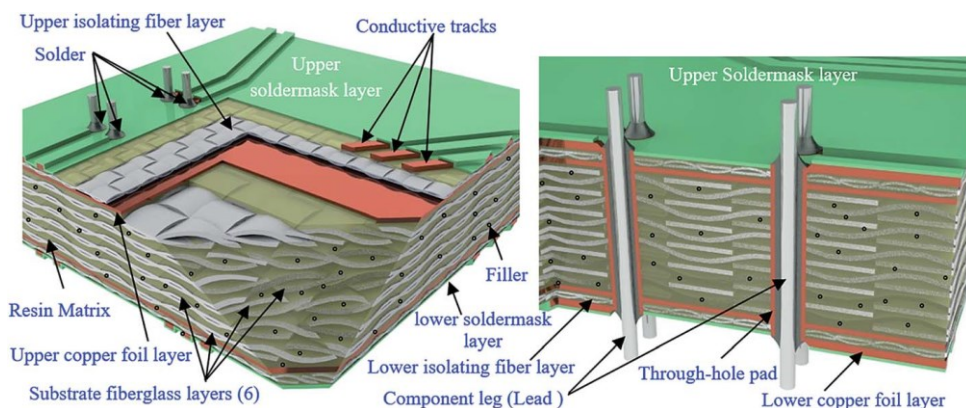


Figure 3.4.7. The reconstruction of layers and elements of cut WPCB samples (the cut samples were originally prepared from motherboard specimens)

In addition, the boards contained a certain amount of through-hole pads and leg components for mounting electronic components. It is worth noting that the amount and distribution of the through-hole pads and leg components in each sample depended on the WPCB model and the location on the WPCB from where the prepared sample was taken. Also, it was noted that the separation of substrate fiberglass layers was much easier than the separation of isolating fiberglass layers, where the isolating fiberglass layers, conductive tracks, and solder mask were separated as one unit (a compound unit).

3.4.3. Recovered epoxy resin: full-size WPCBs

In order to investigate if Brominated Epoxy Resin recovered from different types of WPCBs featured significant differences in the chemical composition and to investigate

its quality, a number of tests using FTIR, SEM-EDS, TGA, and DTG were conducted. It was found that all the recovered resins were very similar chemically and thermally, while the main varying factor was the percentage of Bromine (Br) that varied from 10 to 28%. The results of typical sample analysis are shown below.

Figure 3.4.8. shows the FT-IR spectra of a recovered thin epoxy resin film that was prepared from the residue recovered after the vacuum evaporation of a solvent. The found vibrations corresponded to a paradistributed aromatic compound and C-H, C-C, C=C stretching of the aromatic ring, bend and rock of alkane, O-H stretch, C-O, C-O-C stretch of ether and stretch of C-Br bonds. Therefore, the data of FT-IR confirms the presence of phenol, alcohol, hydroxyl, and ether groups in the thin film that are the major constituents of the BER polymer chain (Verma *et al.*, 2016; Yung, Zhu, Wu, Yue & Xie, 2007).

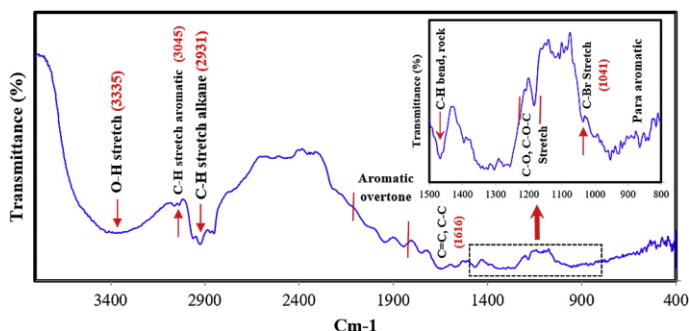


Figure 3.4.8. Typical FTIR spectra of thin epoxy residue film

Figure 3.4.9. shows the results of SEM-EDS analysis of the recovered epoxy resin. As shown, the recovered epoxy resin shows a slightly different surface morphology for each given particle due to the broad size range and the adhesive nature of BER particles. The analysis revealed that the residue contained Carbon (C), Oxygen (O), and Bromine (Br). The composition of the samples provides strong evidence that BER was successfully extracted by evaporation, and this result is similar to the result obtained by Zhu, Chen, Wang, Qian *et al.*, (2013) and Ping Zhu *et al.* (2013).

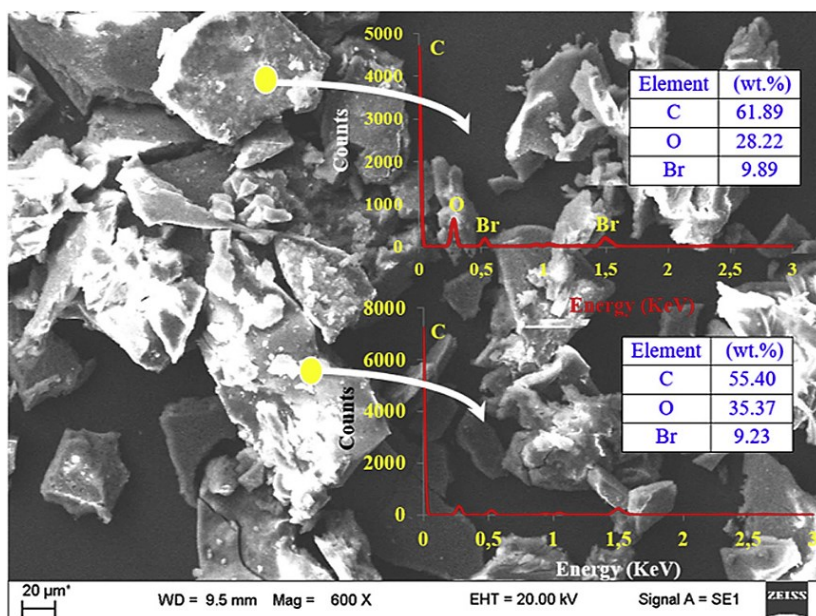


Figure 3.4.9. Typical SEM-EDS analysis of recovered epoxy resin

Figure 3.4.10. shows the results of TGA-DTG analysis for the recovered epoxy resin residue obtained from waste RAM. As illustrated in the Figure, the thermal degradation profile demonstrated significant weight loss in the 260–380 °C range and the maximum instantaneous weight loss at 330 °C. Moreover, it is clear that the thermal stability in terms of weight loss was 68%. The obtained results are fairly similar to the results reported in other literature covering pure cured epoxy resin (resin decomposition range 260–400 °C and weight loss 75%) (Lin & Chiang, 2014).

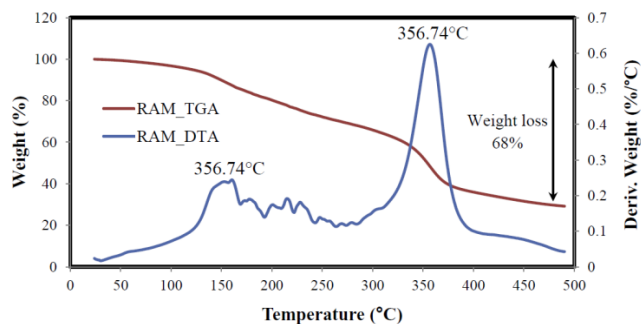


Figure 3.4.10. Typical TGA-DTG analysis of recovered epoxy resin

Figure 3.4.11. shows a typical DSC curve of the of epoxy resin recovered in the temperature range 120–190 °C. As shown in the Figure, the DSC curve contains two regions which are the melting and cure regions, respectively. In the melting region, endothermic behavior was observed for BER with the melting temperatures of 156 °C and the melting enthalpy in the range of (12.76 J/g), while the cure zone exhibited exothermic behavior, and these results are similar to the ones given in works of Smith

and Sichina (Sichina, 2000; Smith, 1985). Also, the results showed that the crystalline degree of the recovered BER decreased until approx. 17% due to the thermal degradation and polymer chain disruption at an elevated temperature during the chemical treatment process and thermal degradation stemming from a relatively high temperature of >165 °C which was used for the extraction of epoxy resin (Ellis, 1993).

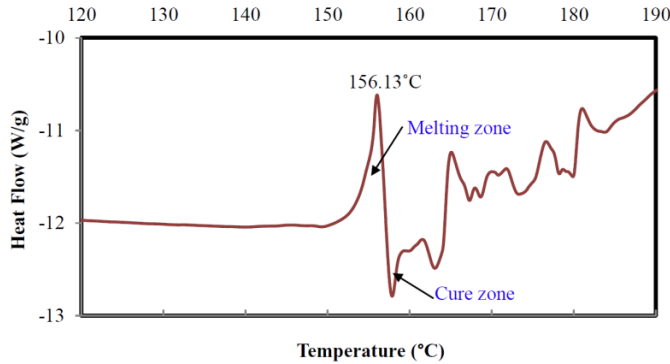


Figure 3.4.11. Typical DSC curve of recovered BER sample

More data on instrumental analyses of recovered BER from different WPCB types can be found in **Annexes 6–10**.

3.4.4. Recovered metallic components: full-size WPCBs

Copper

Figure 3.4.12. shows the EDS-Mapping analysis of the Cu foils recovered from WPCBs with the analysis made at the cross-section of each sample. As shown in the Figure, the chemical analysis (of the entire scanned area) confirmed that Cu had a strong presence in all the samples, and RAM demonstrated its highest percentage (98.2%), whereas Cu of VC had lower (92.4%), and MB showed the lowest purity (87.7%).

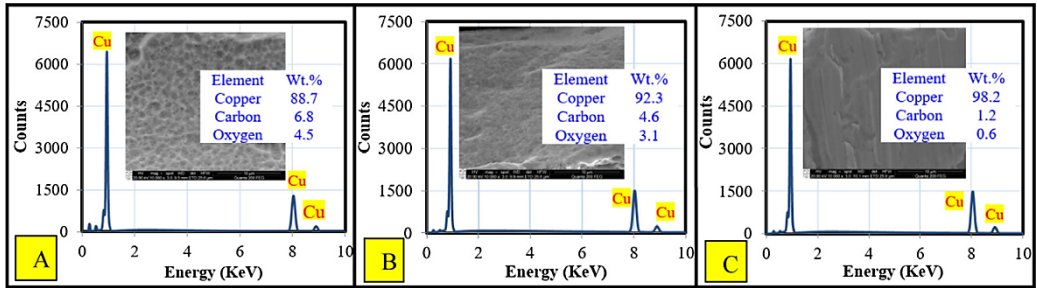


Figure 3.4.12. SEM-EDS analyses of recovered copper layers from (A) MB, (B) VC, and (C) RAM samples

Since EDS is quantitative analysis and is not suitable for materials with low concentrations, additional Inductively Coupled Plasma-Optical Emission Spectroscopy (ICP-OES) measurements were performed on the recovered metal foils. The samples for ICP analysis were digested by aqua regia under microwave treatment according to Kim

et al. (2018). The results showed (**Annex 11**) that all the copper samples had impurities represented by such metals as Al, Cd, Co, Fe, Mg, Mn, Ni, Pb, and Zn with the respective difference in the amount of metal inclusions for RAM, VC, and MB, as RAM had the highest purity (with the total metal impurities of <0.5 wt.%), followed by VC (total metal impurities of <1.2 wt.%), and MB (total metal impurities of ~1.5 wt.%). Impurities containing similar elements can also be found in laboratory-grade copper supplied by Sigma Aldrich. Since the target elements of impurities are C and O (as they represent contamination by organic compounds and oxidation), ICP is not suitable for determining the accurate concentrations of these elements in samples, and thus all the produced materials were analyzed by EDS. Finally, it was noted that the recovered copper foils were not contaminated with Silicon because, in the PCB structure, copper foils and woven fiberglass layers (the main source of the Si element) were completely isolated from each other by the layers of epoxy resin.

Gold

By the means of the developed technique, 0.1659 g (the total number of contacts per card 184×0.0009 g – the weight of a single contact) of contacts was extracted from the RAM module. SEM-EDS images of the contact at base metal, coating metal, and cross section sides can be found in **Annex 12**. The base metal of the contact was composed mostly of Cu (~88 wt.%) with a small amount of BER particles on the surface that were not dissolved during the treatment. Furthermore, Nickel (Ni) (72–86 wt.%) and Au (14–28 wt.%) were the main elements of coating, which is a typical case for the electrical industry where Ni-Au alloys are often used for contact plating due to their increased durability in comparison to pure Au (Materion Corporation, 2011). It needs to be noted that the typical thickness of Au coatings can be within the range of 0.8–2.5 μm , due to which, its identification and analysis in the cross-section was problematic (Christie & Cameron, 1994). Nickel was the main element of the undercoating layer (99.66 wt.%), while Cu was the main element of the base (99.28 wt.%).

Finally, **Fig. 3.4.13.** illustrates the SEM-EDS analysis of the metallic powder recovered after the leaching process. It can be seen that the recovered powder was composed of thin foil-shaped layers (indicated by yellow arrows) as shown in **Fig. 3.4.13.A**. The elemental analysis **Fig. 3.4.13.B** showed that three elements were present in the sample: C, O, and Au. Gold represented the most sizable part (94 wt.%) of the mass of the sample, which indicates that the developed recycling technique is efficient in terms of gold recovery.

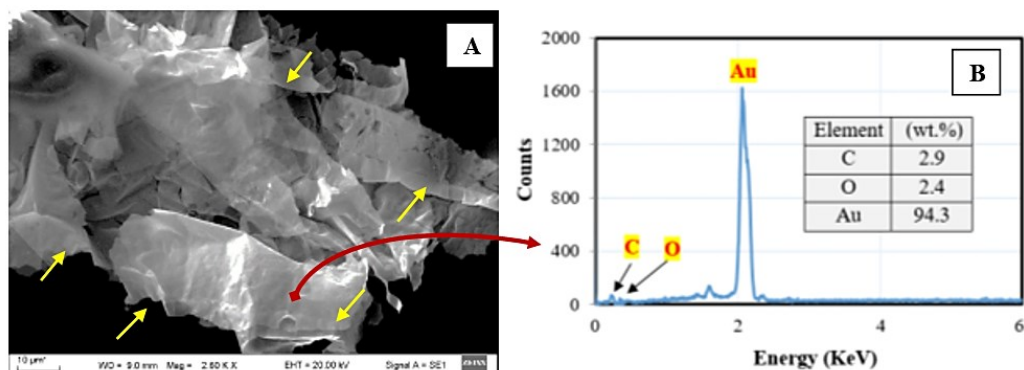


Figure 3.4.13. SEM-EDS analysis of recovered Gold

Through-hole solder joints

One more type of a metallic component, Through Hole Solder Joint (THSJ), was liberated from the Motherboard (THSJ_M) and the Video Card (THSJ_V), whereas it was not found in RAM. The components can be seen in **Fig. 3.4.14.A₁, B₁**. As shown in the SEM images **Fig. 3.4.14.A₂, B₂**, the samples were composed of a copper core (a leg with an average diameter of 600 μ m) fitted in a metallic cylinder (a through-hole pad with the outer diameter of \sim 1.2mm) and joined together at both ends by solder with the total sample length of 3.5–4.6 mm and the average weight of \sim 20 mg/THSJ. To complement the SEM data, Energy Dispersive Spectrometry (EDS) was used to analyze the chemical composition of the samples; Line Scanning of the full length of the THSJ components is shown in **Fig. 3.4.14.A₃, B₃**. The elemental analysis showed that Tin, Copper, and Aluminum represented the main elements of the legs, while Tin and Lead were the main elements of the solder. Meanwhile, Copper, Tin, Lead, and several low-concentration additives, such as Iron, were the main elements of through-hole pads. Overall, the recovered THSJs were composed only of various metallic elements with different weight percentages as EDS Area Scanning showed in **Fig. 3.4.14.A₄, B₄**. Although the elemental composition data obtained by EDS was similar to the results reported in the literature, the analysis was performed only for the outer surface; moreover, EDS is considered to be quantitative analysis, and it is not suitable for materials with low concentrations (Cheng, Huang & Pecht, 2017). Thus Inductively Coupled Plasma-Optical Emission Spectroscopy (ICP-OES) measurements were used to precisely determine the chemical composition of the samples. The results showed that the liberated THSJs were composed mainly of three metals: Cu, Sn, and Pb. In addition, small amounts of Pd, Ni, Fe, and Al were detected. It was noted that Fe was present in the THSJ_M sample only (with the detailed sample analysis presented in **Annex 13**).

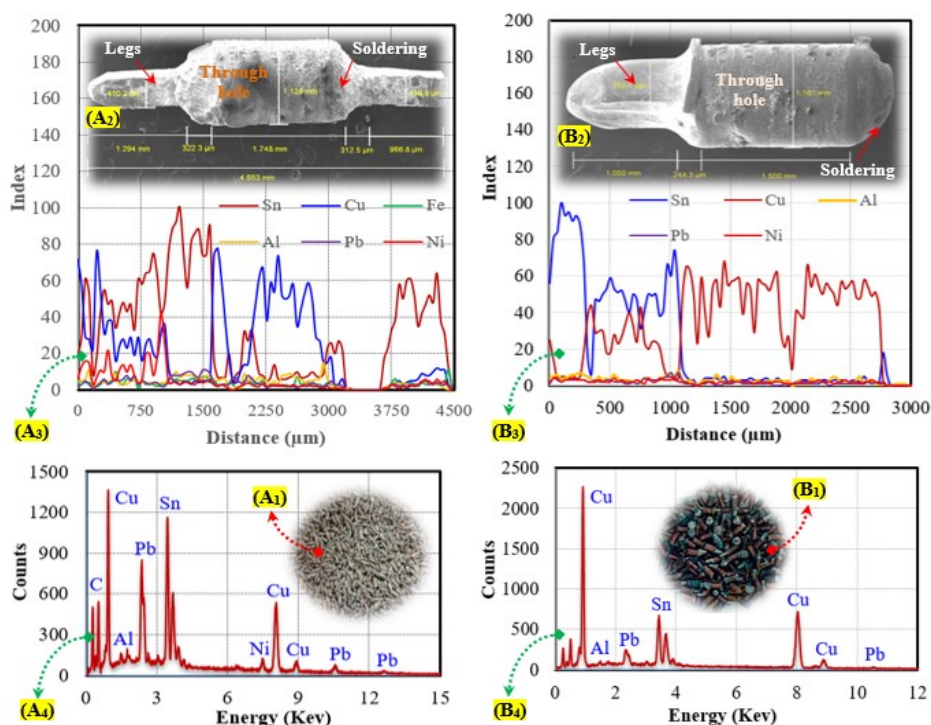


Figure 3.4.14. Structure of Through-Hole Solder Joints

Figure 3.4.15. shows the average weight percentage of each metal in the liberated THSJs. It is clear that Sn, Pb, and Cu had a strong presence in all the samples with the average weight percentage of 43.2 wt.%, 28.7 wt.%, 26.6 wt.% (in total, 98.5 wt.%) respectively, while other metals (Ni, Fe, Al, and Pd) represented ~1.4wt%.

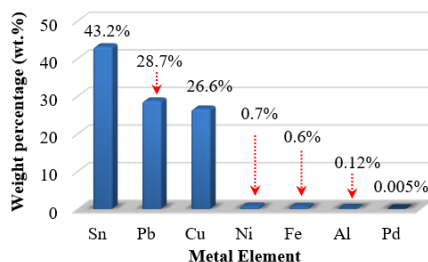


Figure 3.4.15. Average weight percentage of metals in the liberated THSJ

3.4.5. Regeneration of spent solvent

Since solvent was regenerated several times during this work, verification that it retained its original properties was needed. For that purpose, the FT-IR spectra of unused and regenerated DMF were performed, as illustrated in **Fig. 3.4.16**. It can be seen that the FT-IR spectra of the regenerated DMF were almost the same as that of the original DMF, and the two samples featured approximately the same bands. The spectral analysis

of unused and regenerated DMF showed vibrations corresponding to the C-H stretch ($3000\text{--}2850\text{ cm}^{-1}$), C=O stretch (1670 cm^{-1}), C-N stretch ($1250\text{--}1020, 657\text{ cm}^{-1}$), which is identical to the FT-IR spectra of pure DMF (Khandpur, 2006).

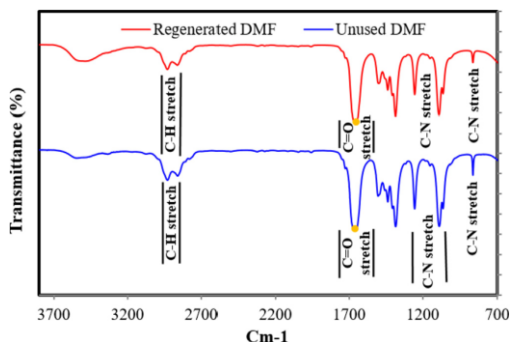


Figure 3.4.16. FTIR spectra of unused and regenerated DMF

The FT-IR analysis validated that the regenerated liquid was DMF, and an evaporation technique can be used to recover the spent DMF, which is beneficial from both economic and environmental points of view. Also, besides FTIR, NMR was used to confirm the identity of a small molecule. **Annex 14** shows the ^1H -NMR (solution in CDCl_3) and ^{13}C -NMR (solution in CDCl_3) spectra of the unused DMF and regenerated liquid. The position of hydrogen and carbon atoms after regeneration was unaltered, whereas the ^1H -NMR signal was at 7.88, 2.84, 2.75 ppm, and the ^{13}C -NMR signal was at 162.43, 36.35, 31.24 ppm, which is identical to the standard proton and carbon chemical shift spectra of pure DMF (Silverstein, Webster, Kiemle & Einholm, 2005). The similarity in the chemical structure of the regenerated liquid and pure DMF validated the regeneration of the spent solvent.

3.4.6. Conclusion: full-size WPCB experiments

In this section, it was shown that the separation of typical full-sized WPCB types at optimum conditions can be achieved within 18–80 hrs. The analysis of separation trends showed that the surface area of WPCB was a crucial factor affecting the separation time. Based on the virtually linear dependence between these two parameters, it can be concluded that the separation of specimens with a surface area of $>100,000\text{ mm}^2$ may not be effective, and a size reduction operation will be required in this case. Moreover, various materials from the treated RAM, Video Card, and Motherboard were extracted and investigated. Epoxy Resin with a very similar chemical structure and a low degradation degree was recovered from all the WPCB types. Copper of varying purity was also recovered from all the WPCB types with the Motherboard providing the least pure (88%), and RAM providing the purest (98%) metal. In addition, relatively pure Gold (94%) was produced from gold-plated contacts separated from RAM. A specific type of metal components, Through Hole Solder Joints (THSJs), was recovered from the Video Card and the Motherboard. These components contained a number of metals in the alloyed form, with the main elements being Sn and Pb. Finally, to improve the sustainability of the approach, the spent solvent was regenerated, and the absence of thermal degradation was investigated.

3.5. Recycling rate evaluation (Solvent treatment)

The evaluation of the recycling rate is a very important step for determining the economic and environmental performance of any recycling approach; therefore, in the current work, it was assessed according to the mass balances of the initial samples and recovered/regenerated materials/solvent as illustrated in **Table 3.5.1**.

Tab. 3.5.1. General recycling rates for all sample types

Sample code	Initial mass, g		Recovered materials, g				Regener. solvent, g	Recycling rate, (Initial mass / Σ Masses of recov. mat.)	
	Sample	Solvent	Fiberglass	Epoxy Resin	Copper	Trough-Hole Solder Joints		WPCB	Solvent
Milled samples (preliminary experiments, sample codes in Tab. 2.3.1.)									
Blue	3	-	1.63	-	0.81	-	-	92%	-
Green		-	1.87	-	0.88	-	-		
Yellow		-	1.95	-	0.89	-	-		
Red		-	1.99	-	0.93	-	-		
Violet		-	2.15	-	0.65	-	-		
Avg.		-	1.918	-	0.832	-	-		
Total: 1.918 + 0.832 = 2.75									
Separation specimens (optimum condition experiments, sample codes in Tab. 2.4.1.)									
Blue	0.667	1.889	0.262	0.223	0.1644	-	1.851	97.5%	98%
Green	0.635	1.798	0.272	0.144	0.2064	-	1.762	98%	98%
Yellow	0.685	1.94	0.263	0.127	0.288	-	1.882	99%	97%
Red	0.692	1.96	0.276	0.239	0.177	-	1.90	99%	97%
Violet	0.673	1.91	0.266	0.181	0.22	-	1.868	98%	98%
Avg.	0.67	1.899	0.268	0.183	0.211	-	1.853	98.3%	97.6%
			Total: 0.268+0.183+0.211 = 0.662						
Random Access Memory (RAM, Gold mass balance not included, see subchapter below)									
RAM	12.73	40.06	6.32 (50%)	1.56 (12%)	4.76 (38%)	-	32.05	99.9%	98%
			Total: 6.32 + 1.56 + 4.76 = 12.64						
Video Card (VC)									
VC	41	126	28 (70%)	4.1 (10%)	4.92 (12%)	3.28 (8%)	123.7	99%	98.2%
			Total: 28 + 4.1 + 4.92 + 3.28 = 40.6						
Motherboard (MB)									
MB	225.6	709.9	132.7 (60%)	18.4 (8%)	43.8 (20%)	27.4 (12%)	694.3	98.6%	97.8%
			Total: 132.7 + 18.4 + 43.8 + 27.4 = 222.3						

Firstly, evaluation was done for the milled samples. The weight of the recovered metal varied; it was 0.65–0.93 g (~28 wt.% of the initial WPCB mass), whereas the weight of the recovered fiberglass was 1.63–2.15 g (~64 wt.% of the initial WPCB mass), which is similar to the results reported in the recent literature (Fogarasi, Imre-Lucaci, Imre-Lucaci & Ilea, 2014; Yang *et al.*, 2015). However, the average recycling rate was only 92%. The losses occurred mainly due to the loss of epoxy resin and other organic materials which represented the remaining part of the WPCB mass and were not recovered in this part of the work (Long *et al.*, 2010).

The second section of evaluation was concerned with cut specimens for the optimum separation conditions. As illustrated, the recycling rate was relatively high, being, for all the WPCBs, in the range of 97.5–99%, while for DMF these values were 97–98%. There were some variations observed in the weight of the recovered metal – the amount varied from 0.164 to 0.288 g (~43% variation); the same deviation could be seen in the weight of non-metals (fiberglass and epoxy resin) 0.42–0.51 g (~17% variation). The recycling rate was notably higher compared to the milled samples since, this time, the solvent was regenerated, and epoxy resin was successfully extracted.

Finally, we can compare the RAM, VC, and MB recycling rates. The Random Access Memory module was separated with the highest recycling rate among the other full-size WPCBs at 99.3%. This can be associated with the RAM having the lowest weight share of Fiberglass. During the separation process, a small quantity of fiberglass shows a tendency to separate from sheets into individual fibers which are very difficult to collect after the end of the treatment. At the same time, Copper is not affected by the solvent, and Epoxy Resin can be completely dissolved to be later collected after the solvent evaporation. It is worth noting that only VC and MB were found to contain Through-Hole Solder Joints, which accounted for 8 wt.% in VC and 12 wt.% in MB. Lastly, a clear dependence between the number of specific layers (as illustrated in **Fig. 3.4.4.**) and the mass of the respective recovered materials can be seen. This explains dissimilarities in the weight shares of the recovered materials for different WPCBs. For instance, VC had the biggest number of Fiberglass layers (10) as well as the highest wt.% of Fiberglass (70%).

Losses during the separation process were mainly a result of fiberglass splitting into poorly collectable microfibers, micronization of the solder mask layer under the effect of the solvent, and the degradation of organic materials during the dissolution by solvent and its regeneration.

Gold recovery from RAM

Since the mass of gold represents a very small fraction of the total RAM weight, its balance was not included in **Table 3.5.1.**, and all the discussions are instead done in this Section. The results showed that 0.028 g of gold could be recovered from the contacts of one RAM, which means that one kg of RAMs contains 2.2 g of gold (about 2 kg/tonne of RAMs). These results are more academically valuable when compared to the studies reported in the literature, where the maximum amount of recovered gold was 1 kg/tonne (Bidini *et al.*, 2015). Also, the yield of the recovered gold in most of the previous studies was calculated based on the initial weight of the samples which were mainly represented

by solid residue (sludge) or sections with a high gold concentration cut from WPCBs (including non-metal components) (He & Xu, 2015; Imre-Lucaci, Nagy, Imre-Lucaci & Fogarasi, 2017; Torres & Lapidus, 2016). In order to calculate the final yield with a high accuracy and compare it with the results reported in the literature, a section with a high gold concentration was cut from one full-size waste RAM by using a manual cutter and weighted (1134 mg) by using digital scales. The yield of gold from the section with a high gold concentration was determined to be $28 \text{ mg}/1134 \text{ mg} \times 100\% = 2.45 \text{ wt.}\%$. These results can be compared with some previously performed studies, for instance, one of them had a starting concentration of gold of 0.2339 wt.%, whereas gold recovery yield was 90%; therefore, the final yield was $0.002339 \times 0.9 = 0.21\%$ (He & Xu, 2015). Therefore, the developed technique exceeds (in terms of the gold yield) the previously reported results by $0.21\% / 2.45\% \approx 12$ times in terms of the gold recovery. This can be explained by the fact that the traditional recycling techniques usually involve grinding followed by the leaching process so that to recover valuable materials, and a significant part of the metals is lost since they are converted into volatile dust-sized particles.

3.6. Preliminary economic and Carbon Footprint analysis (Solvent treatment)

Preliminary economic analysis was performed to evaluate the feasibility of using the new approach for WPCB recycling at a larger scale. The analysis was done based on the cost of WPCBs, organic solvent, and electric power consumed during the treatment processes. To provide more representative data and omit repetition, analysis was done only for WPCB with its unique composition – Milled samples, a RAM, and a Motherboard. While a more detailed description of the calculations can be found in the respective published articles (Tatariants, Yousef, Denafas & Bendikiene, 2018; Tatariants, Yousef, Denafas, Tichonovas & Bendikiene, 2018), the essence of the work is presented here. Firstly, the boundaries of the system were defined as illustrated in **Fig. 3.6.1.** (an example of milled samples). The system boundaries for RAM and MB can be found in **Annexes 15–16.**

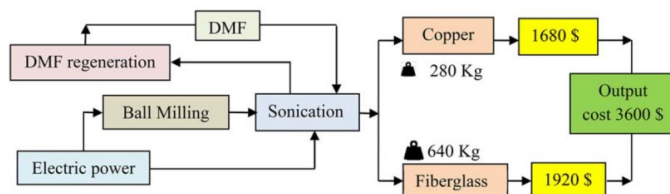


Figure 3.6.1. Boundaries and economic performance of the developed technique (example of milled samples, calculations for 1 tonne of input WPCBs)

After that, the input and output energy/material flows were defined, and the economic balance was calculated for 1 tonne of WPCBs according to the cost of materials found in various sources as shown in **Table 3.6.1.** The cost of Motherboards was presumed to be 600\$/tonne, and RAMs were estimated at 1,300\$/tonne (<https://alibaba.com>). Electric energy consumption was measured with a Kilowatt-hour meter, and its cost was estimated as 0.12\$/kWh (“Energy price statistics,” 2016). The cost of industrial grade DMF and Nitric Acid was estimated according to the price set by

industrial suppliers as 1100\$/ 1000 L for DMF, and 300\$/tonne for Nitric Acid (<https://alibaba.com>). It needs to be added that, since the organic solvent (waste RAM/Solvent ratio 3/10 (wt./v)) can be constantly regenerated and reused during the dissolution process, only losses of DMF (2% wt. per regeneration cycle) were considered during the calculation of the recovery cost. Regarding the cost of the recovered materials, their value was found based on the cost of similar scrap/recycled materials: scrap epoxy resin/fiberglass ~3,000\$/tonne, scrap copper ~ 3,600-6,000\$/tonne, Gold – 40,900\$/kg, metal alloys in THSJ – 3,600\$/tonne (<https://alibaba.com>).

It is also necessary to remark a much higher energy consumption for RAM separation compared to the Motherboard regardless of RAM taking less time to separate. It can be explained by the fact that the energy consumption that was calculated for 1 tonne was a sum of many runs to separate batches of WPCBs. The size of one batch was selected as ~20 WPCBs. Due to the higher mass of the Motherboard, 20 WPCBs of this type would weigh ~ 5 kg, while 20 RAMs would weigh ~ 250 g. Thus the separation of one tonne of RAMs while using such batches would take more time in total.

Overall, our preliminary analysis shows that solvent treatment is denoted by good economic potential, especially for recycling of gold-containing WPCBs, as gold contributes greatly to the value of the recovered materials. Moreover, our economic analysis confirmed that the solvent treatment of full-size WPCBs is a more economically viable option compared to the treatment of milled WPCBs. Obviously, upscaling the balance of the laboratory process cannot provide very accurate data; therefore, to obtain more precise economic evaluation results, it is advisable to perform the solvent treatment of WPCBs on the pilot scale, which is, unfortunately, beyond the dissertation scope.

Table 3.6.1. Summary of preliminary economic analysis for solvent treatment of WPCBs (calculated for one tonne of waste)

Input cost				Output cost					Profit
Solvent	WPCB	Energy	Nitric Acid	Fiberglass	Epoxy Resin	Copper	Gold	Trough-Hole Solder Joints	(Output cost – Input cost)
<i>Milled samples (preliminary experiments)</i>									
(120 L) 132\$	(1 tonne) 1,300\$	(2520 kWh) 302\$	-	(640 kg) 1,920\$	-	(280 kg) 1,680\$	-	-	1,866\$
<i>Random Access Memory (RAM)</i>									
(66.7 L) 73.37\$	(1 tonne) 1,300\$	(7600 kWh) 912\$	(1185 kg) 355.5\$	(620 kg) 1,860\$	(380 kg) 1,850\$	(2.2 kg) 89,980\$	-	-	90,269\$
<i>Motherboard (MB)</i>									
(66.7 L) 73.37\$	(1 tonne) 600\$	(1472 kWh) 177\$	-	(600 kg) 1,770\$	(82 kg) 245\$	(194 kg) 700\$	-	(121 kg) 430\$	2,300\$

Preliminary Carbon Footprint analysis

The GGEs were calculated according to the recovered materials (epoxy resin, fiberglass, and metals); each material had a different GGE value determined according to various literature sources as shown in **Table 3.6.2.** (EEA, 2014; Kočí & Loubal, 2012;

Mudd *et al.*, 2012; PwC – Sustainable Performance and Strategy, 2016; Recycling, 2008). It is important to remark that, according to SEM-EDS analysis, metal alloys were mainly composed of Pb, Sn, Al, and Cu; thus the carbon footprint was determined as the average value of these metals. Based on these values, applying the chemical-ultrasonic-mechanical technology on an industrial scale gives a possibility to decrease GGE by -1868 kg CO₂-eq/t.

Table 3.6.2. GHG emissions from waste Motherboard recycling by the developed approach

Waste material type	Kg or kWh/tonne	Average (kgCO ₂ -eq/t or 1000 kWh)	kgCO ₂ -eq/t of WPCBs
Fiberglass	603	-1500	-904.5
Epoxy resin	82	-4632	-380
Copper foils and wires	194	-5500	-1067
Metal alloys (Al, Cu, Pb, Sn)	121	-3285	-398
Input energy	1472	+600	+882
CO₂-eq reduction of new technique (kgCO₂-eq/t)			-1868

3.7. Indication of the material application field (Solvent treatment)

As a result of treating WPCB composites with a solvent, five main material fractions were received: Brominated Epoxy Resin residue, Fiberglass (sheets and powder), Gold (from RAMs only), Copper (all WPCBs), and Through-Hole Solder Joints (from Video Cards and Motherboards only). Taking into account the results of instrumental analyses (discussed in the previous Sections) for each of the fractions, we can now highlight some potential applications for them. If compared to other recycling approaches, the presently discussed solvent treatment technique is denoted by certain benefits. For instance, the commonly used pyrolysis of WPCBs produces a variety of gases and oils which can be used as a fuel and high purity copper (Liu, Zhang & Zhang, 2016); however, the presence of brominated flame retardants in WPCBs makes their pyrolysis difficult due to environmental risks (Huang *et al.*, 2009).

Fiberglass

Woven fiberglass extracted after WPCB separation can be used as received in a variety of fields, such as pressure vessels and automotive structures, or as a filler material (after pulverization) in composites and sound insulation applications (Astashkin & Mishnev, 2016; Biswal, Jada, Mohanty & Nayak, 2015; Cai, Fu, Long, Liao & Xu, 2017; Mou, Xiang & Duan, 2007). Moreover, pulverized fiberglass can be employed in plastic, wood, and concrete production to improve its properties (Krayushkina, Khymerik, Skrypchenko, Moshkovskiy & Pershakov, 2017; Li, Sun, Liang, Zhong & Yang, 2014; Wang & Ge, 2017; Woltman, Noel & Fam, 2017; Zheng, Shen, Cai, Ma & Xing, 2009b).

Brominated Epoxy Resin

In the current case, brominated epoxy resin can be separated by solvent without heating until decomposition temperatures. Moreover, to purify its solid products, pyrolysis usually requires crushing, classification and calcination stages which reduce

the final recycling rate and generate fiberglass powder while the current method can be used to recover fiberglass sheets. Another option is the Supercritical Fluid (SCF) technology which uses various liquids above their critical points to greatly enhance the rate of organic reactions. SCF demonstrates a high efficiency in terms of debromination; however, this process also requires a high temperature (up to 425 °C) and pressure (up to 36 MPa) (Long *et al.*, 2010) unlike the current solvent treatment technique that operates at 50 °C and normal pressure. The Gasification process can also be applied to recycle WPCBs, but it has drawbacks similar to those of SCF since the temperature needed for the process can be 1150 °C and higher (Yamawaki, 2003) – thus a significant amount of energy is needed for this operation. Therefore, it can be concluded that the reported recycling method provides a promising and viable alternative to the previously reported techniques applied to recycle NMFs of WPCBs, while the recovered epoxy resin can be applied in adhesive and filler material composite applications (Jin *et al.*, 2015).

Gold

Compared to the other recovered materials, Gold flakes are, perhaps, the least difficult material to find application for. As it was shown by SEM-EDS analysis (**Fig. 3.4.12.**), the purity of the recovered Gold was rather high – 94% – while impurities were represented only by organic contaminants (C and O). This means that the recovered Gold can be easily purified by calcination, re-smelted and used in traditional Gold-consuming applications, for instance, electronics, catalysts, etc. (Lewandowski, 2015).

Copper

Copper, being one of the most commonly recycled metals in the world, is also not difficult to find application for. Copper foils obtained from WPCBs after solvent treatment can be directed for refining through melting or the electrochemical process, and the obtained metal can be reused in electronics, thermal conducting, or for anticorrosive applications (Samuelsson & Björkman, 2014).

However, there is another option available for the recovered copper since, as our chemical analysis suggested, it was denoted by remarkably high purity (89–98%, **Fig. 3.4.11.**) and a low amount of metallic inclusions (<1.5 wt.%). Such high purity of copper can be explained by its original purpose, as copper for WPCBs is usually high-grade to ensure its good electrical conductivity. Therefore, regarding the recent achievements in reprocessing WPCBs (see Section 1.3.2. in our literature review), it would be wiser not to simply recycle the copper, but instead to reprocess it into a high-added value material, such as copper nanoparticles. The following Chapters **3.8. Electrospraying of nanoparticles** and **3.9 Green synthesis of nanoparticles** describe the production of such nanoparticles in detail. *We should take note that these Chapters cover already established nanoparticle production methods; therefore, they are focused mostly not on finding the optimum process conditions (as the optimum conditions had already been described by other authors), but instead on proving the feasibility of nanoparticle synthesis from waste material.*

Through-Hole Solder Joints

Through-Hole Solder Joints, as extracted from the Video Card and the Motherboard, were the most challenging to find an application for. The fact that these components contained three main (43 wt.% of Sn, 29 wt.% of Pb, 27 wt.% of Cu, according to **Fig. 3.4.14.**) and four minor metals (Ni, Fe, Al, Pd), it turned direct repurposing of THSJs into a very difficult task. To solve this problem and therefore close the loop of the solvent treatment, Sn and Pb were recovered from the liberated THSJs in the form of SnO₂ nanoparticles and PbO₂ micro cross/cubic structures as high added value products by using a sustainable leaching technique as described in Section 3.10. **Leaching and precipitation of micro/nano particles.**

3.8. Electrospraying of nanoparticles

As described in the respective part of the Materials and Methods Section, to produce nanoparticles by Electrospraying, the recovered copper from WPCBs was converted into copper acetate. Copper acetate was used to produce sol-gel which was spun and, finally, the collected particles were calcined to obtain pure Cu-NPs. This synthesis approach had previously been developed and tested by Khalil *et al.* (Khalil *et al.*, 2014).

3.8.1. Nanoparticle preparation

First of all, the produced Copper Acetate was analysed by FTIR, XRD, and AAS to ensure its quality. While the obtained FTIR and XRD peaks (**Annexes 17, 18**) confirmed that the produced crystals were composed of copper acetate, AAS indicated that Cu was the main element in the prepared powder (26.8%) which also had a very small amount of Ni (0.01%) and Zn (0.015%). In addition, the AAS was repeated for the control sample of Cu (II) acetate supplied by *Sigma Aldrich*; the results were almost identical and showed the following values: Cu (26.5%), Ni (0.01%) Zn (0.19%).

Fig. 3.8.1. elucidates the possible Cu-NP growth mechanism for Electrospraying process

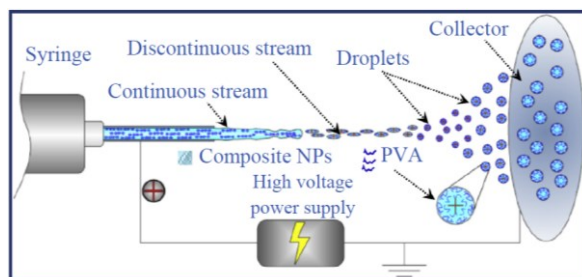


Figure 3.8.1. Composite NP synthesis mechanism for Electrospraying process

As shown, the prepared solution is extruded from a syringe in a continuous stream in the form of laminar flow. When the solution passes through the needle, a high voltage is applied, which causes the solution to become charged. At this point, the forces of electrostatic repulsion begin to counteract the forces of the surface tension acting in sol-gel (Cheng *et al.*, 2011). An evaporation process begins on the surface of sol-gel immediately after it has left the syringe; this leads to the increase of the PVA

concentration in this area and consequently results in the formation of the gel layer when the concentration exceeds the coagulation threshold (Yang *et al.*, 2017). The formed gel layer becomes a grid which keeps the morphology and prevents the sol-gel from distortion and oxidation. As a result of the liquid phase evaporation under the atmospheric ambient, the viscosity of the solution decreases significantly. This causes the charged jet to become discontinuous, and the stream of sol-gel breaks into droplets (Liu *et al.*, 2018). In accordance with that, copper (II) acetate starts to lose water due to the evaporation that steps up the generation of crystal seeds, and, under the effect of a long distance (10 cm), the nanocrystals coated with PVA are formed before reaching the grounded collector. The synthesized composite particles are collected on an aluminium foil as a substrate. Finally, a Scanning Electron Microscope (SEM) is used to determine the optimal synthesis conditions in terms of the voltage. **Figure 3.8.2.** shows the SEM images of composite nanoparticles electrospun at a constant flow rate (0.2 ml/h) and various applied voltages (23, 25, 27, and 29 kV) with a scale of 1 mm except for 27 kV where the scale is 300 nm.

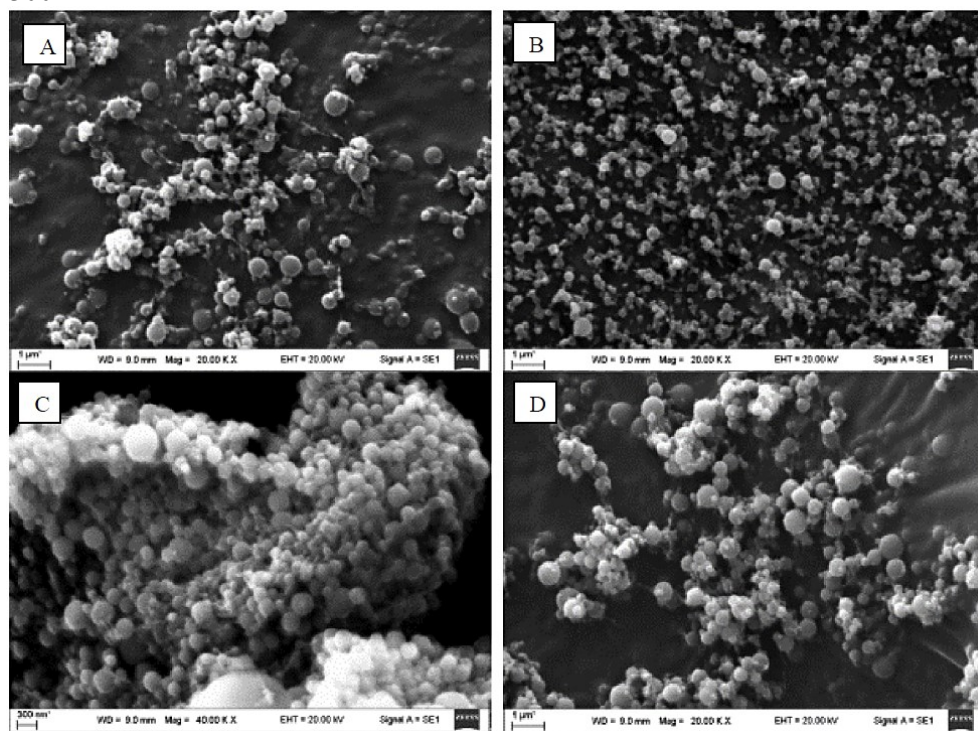


Figure 3.8.2. SEM images of nanoparticles synthesized at A) 23 kV; B) 25 kV; C) 27 kV; and 29 kV

As shown in the Figure, at a lower voltage of 23 kV, the amount of synthesized nanoparticles was very low. By increasing the applied voltage up to 25 kV, the amount of nanoparticles and their disposition density started to grow. By increasing the value of the voltage up to 27 kV, the amount of the obtained nanoparticles grew significantly with a nearly uniform morphology and a high yield. At a higher voltage of 29 kV, the yield

started to decrease again because the solution removal rate exceeded the delivery rate what made the jet discontinuous, leading to deposition of non-uniform particles with a poorly defined shape (Khalil *et al.*, 2014). As it can be seen, the maximum uniformity and optimum shape definition in the particles was observed at a voltage of 27 kV. This indicated that the selection of the optimum voltage is mandatory for producing uniform and defect-free particles. Due to the high salt proportion, the precursor is heavily charged, and the effect of the applied electric field may cause unexpected jet instabilities. Therefore, in the next Section, all the analyses and characterizations focus on the nanoparticles obtained from treatment at 27 kV as the optimum conditions. The samples prepared at the optimum voltage were dried and then calcined in a furnace at 475 °C for 2 hrs. The calcination temperature was based on the PVA decomposition temperature, as determined by TGA analysis. The calcined particles were then reduced in hydrogen atmosphere at 300 °C to obtain pure Cu-NPs.

3.8.2. Analysis of obtained nanoparticles

Figure 3.8.3. shows the morphology of the Cu-NPs synthesized at the optimum conditions after calcination and reduction in hydrogen. As shown in the Figure, the produced Cu-NPs had a uniform size and a high yield. In addition, a small amount of agglomerated particles (indicated with white arrows) was present as a result of the long duration of Electrospraying, which led to accumulation of Cu-NPs and the formation of a new layer.

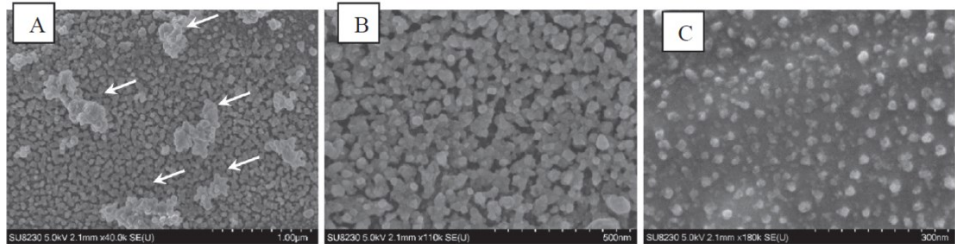


Figure 3.8.3. SEM images of Cu-NPs with scale A) 1 mm; B) 500 nm; and C) 300 nm (Electrospraying)

Figure 3.8.4. shows the EDS mapping of the obtained nanoparticles; as it can be seen, the particles were rich in Cu (83 wt.%) with a small share of oxygen (O) and carbon (C) being present. With regard to the Aluminum (Al) peaks in the EDS analysis, they were produced by Al foil which served as a substrate.

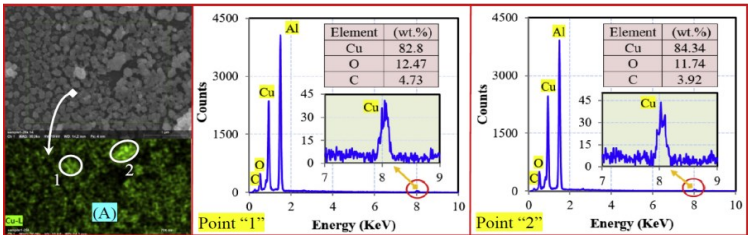


Figure 3.8.4. A) SEM-EDS mapping of Cu-NPs, B, C) EDS analyses at points “1” and “2” (Electrospraying)

The synthesized Cu-NPs were examined by using HRTEM through rinsing the prepared samples with a tiny droplet of fresh sonicated water, after that, the produced water-based Cu-NPs suspension was placed on the mesh of the TEM nickel grid. **Figure 3.8.5.** shows HRTEM images of the synthesized Cu-NPs in different locations with a scale of 20 nm.

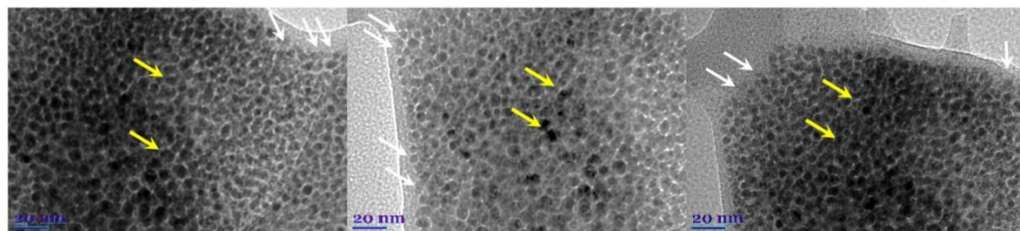


Figure 3.8.5. HRTEM images of Cu-NPs (Electrospraying)

As shown in the Figure, the produced Cu-NPs were regularly distributed forming a honeycomb-like structured layer where particles had a uniform size with average dimensions of ~ 5 nm and high yields, and these results agree with the SEM results. Also, it was observed that some examined NPs appeared to be transparent (indicated by white arrows), whereas, in other places, the particles were darker (indicated by yellow arrows), and, according to Kobayashi (2011), the transparent particles represent single-crystal and single-layer NPs while the dark particles represent single-crystal and multi-layer clusters of NPs (Betancourt-Galindo *et al.*, 2014; Kobayashi, Shirochi, Yasuda, & Morita 2011).

In order to confirm that the chemical and thermal properties of nanoparticles were in accordance with the normal values, TGA, XRD, and FTIR analyses were done (**Annexes 19–21**). TGA indicated that the nanoparticles were relatively stable up to 500 °C since the weight loss was only 6.2% due to the decomposition of surfactant residues remaining from PVA (additional calcination time is needed) and inorganic impurities within copper (II) acetate. The results obtained for the synthesized nanoparticles were almost identical to the results reported in other literature for pure Cu nanoparticles in the same heating range of 25–500 °C and the weight loss of $\sim 6\%$ (Betancourt-Galindo *et al.*, 2014; Kobayashi *et al.*, 2011). Finally, both XRD and FTIR confirmed the presence of all the respective peaks and bands characteristic for Cu-NPs.

3.8.3. Conclusion: Electrospraying of nanoparticles

The results described in this chapter showed that it is indeed possible to produce Cu-NPs by using foils recovered by solvent treatment from WPCBs as a source of raw material. Despite the waste origins of the input material, the properties of the produced nanoparticles were relatively high; the size of the particles was 5–7 nm, which is considered to be a good result for this type of nanomaterial.

Unfortunately, the drawbacks of the employed approach were the yield of the product and the difficult preparation procedure – Electrospraying could produce only ~ 140 mg of nanoparticles per batch (the yield is described in Section 3.11.). In addition, Electrospraying is not a well-scalable approach, which means that the further development of this approach past the laboratory scale would be complicated. To address

this problem, an alternative nanoparticle production approach was used (see the following Section, i.e., 3.9.).

3.9. Green synthesis of nanoparticles

As concluded in the previous Chapter, the alternative synthesis approach was required to replace the lowly-productive Electrospraying. To achieve that, a copper sulphate precursor was produced from the original copper. **Figure 2.9.2.A–C.** illustrates the final color of the CuSO_4 solutions at the end of the reaction process. The refined solution was left for drying at 50°C overnight in order to obtain crystallized CuSO_4 as shown in **Fig. 2.9.2.D–F.** The color of the solutions and the final residue was slightly different due to the different amounts of water used during the preparation and remaining inside the dried samples, as anhydrous Copper Sulphate readily forms a bond with water molecules.

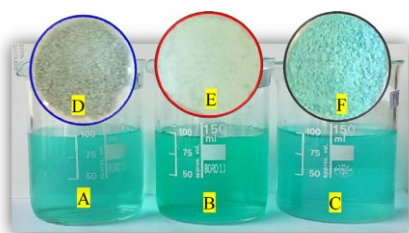


Figure 3.9.1. Copper (II) Sulfate solution produced from: (A, B, C) MB, VC, RAM; The obtained Copper (II) Sulfate from: (D, E, F) MB, VC, RAM sample

Later, copper nanoparticles were produced in aqueous solution by reduction using ascorbic acid and native cyclodextrin as stabilizer. Initial development of this synthesis route was done by other researchers (Suárez-Cerda *et al.*, 2016).

3.9.1. Nanoparticle preparation and synthesis

Similarly to the precursor for Electrospraying, Copper Hydroxide was examined by XRD and Raman Spectroscopy (**Annexes 22, 23**) in order to ensure the identity of its molecular and crystalline structure. Raman Spectroscopy showed strong vibrations in the range from 1004 cm^{-1} to 1006 cm^{-1} that is identical to the Raman spectra of Copper (II) Sulfate. At the same time, the presence of specific peaks found in the XRD pattern provided conclusive evidence that the powder was Copper (II) Sulfate (National Center for Biotechnology Information. PubChem Compound Database; CID=24462, n.d.). In order to confirm that there was no contamination with other elements, ICP analysis was employed to check the chemical composition of the prepared reagents. The ICP analysis showed that Cu was the main element in the prepared reagents of all the samples ($\sim 25.8\text{ wt.}\%$) mixed with a small amount of Ni ($\sim 0.003\text{ wt.}\%$), Zn ($< 0.015\text{ wt.}\%$), Na ($< 0.02\text{ wt.}\%$), and Fe ($< 0.003\text{ wt.}\%$), which is similar to the elements that can be found in the commercial Copper Sulfate reagent.

Figure 3.9.2. shows the morphology and chemical composition (analysed by FE-SEM EDS) of the Cu-NPs synthesized from MB, VC, and RAM samples. As shown in the Figure, the Cu-NPs produced from the RAM sample had a more uniform size

distribution and higher purity in comparison with the other samples. Also, these Cu-NPs were relatively smaller and had a higher yield than VC and MB-derived nanoparticles whereas their shape was closer to a sphere.

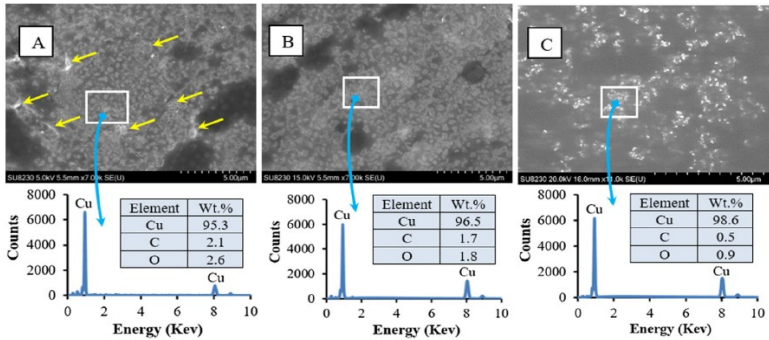


Figure 3.9.2. SEM-EDS images of Cu-NPs synthesized from: (A) MB; (B) VC; and (C) RAM

In addition, small amounts of agglomerated particles (indicated by yellow arrows) were found during the analyses; this was especially noticeable in the MB sample. Finally, the EDS analysis of the obtained nanoparticles showed that all of the samples were rich in Cu whose purity ranged from ~96 to 99 wt.% with a very small fraction of Oxygen (O) and Carbon (C). The results indicated that the Cu-NPs synthesized from MB, VC and RAM by the developed technique were denoted by high purity, whereas the best properties were observed for the RAM sample. The synthesized Cu-NPs were examined by using HRTEM through rinsing the prepared samples with a tiny droplet of sonicated distilled water and by placing the produced water-based Cu-NP suspension on the mesh of a TEM nickel grid. **Figure 3.9.3.** shows HRTEM images of Cu-NPs synthesized from MB, VC, and RAM samples with image scales of 50 and 20 nm.

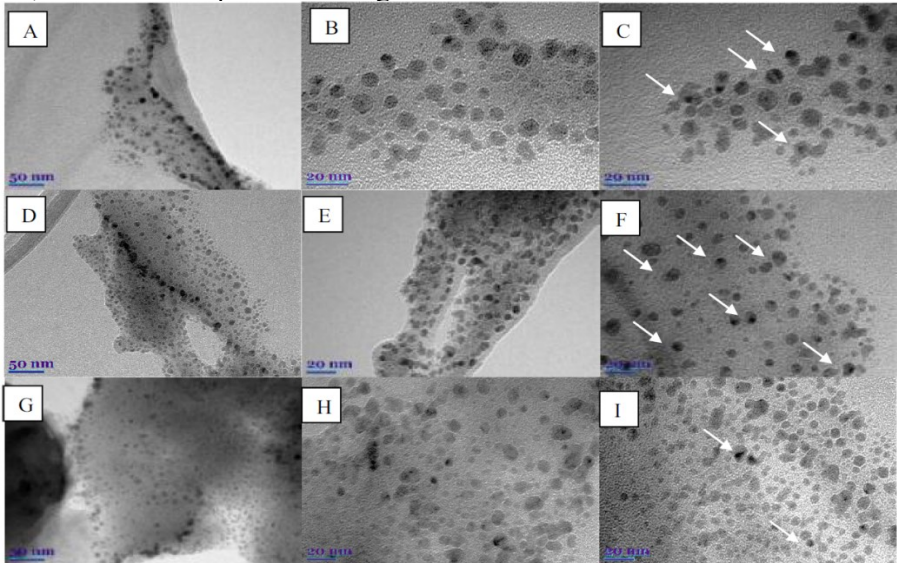


Figure 3.9.3. HRTEM images of Cu-NPs synthesized from: (A–C) MB; (D–F) VC; and (G–I) RAM

As it can be seen in the figure, the produced Cu-NPs were regularly distributed and had quasi-spherical shapes with an average diameter of 7 nm. It needs to be noted that the yield of NPs from RAM was higher than that from MB and VC due to the higher purity of the recovered Cu foils (98.2 wt.%) and the lower amount of the organic residue contained in the recovered metal of RAM. Another important point is that the majority of the observed NPs appeared to be transparent in HRTEM images, whereas a few particles were of a darker color (indicated by yellow arrows), which was a result of the agglomeration or overlapping of several particles in a small volume of space. This is a common phenomenon encountered in TEM imaging of nanoparticles, especially if there is a certain time gap between the NP suspension preparation and the TEM analysis (Kobayashi *et al.*, 2011).

The absence of impurities (such as CuO) in the obtained Cu-NPs was validated by XRD and Raman Spectroscopy (Annexes 24, 25). Raman spectroscopy showed strong vibrations in the range of 1568 cm^{-1} to 1608 cm^{-1} which is identical to the Raman spectra of Cu-NPs (Muniz-Miranda, Gellini & Giorgetti, 2011).

3.9.2. Antimicrobial tests

Figure 3.9.4.A., C., D. shows the antimicrobial activity of the Cu-NPs (synthesized from Cu of MB, VC, and RAM) at different concentrations against *E. coli*, *P. aeruginosa*, and *S. aureus* bacterial cultures. As it can be seen, the antimicrobial activity of Cu-NPs in terms of the absorption data (all the observations were made for the wavelength of 600 nm) increased significantly by increasing the concentration of Cu-NPs in all the cases.

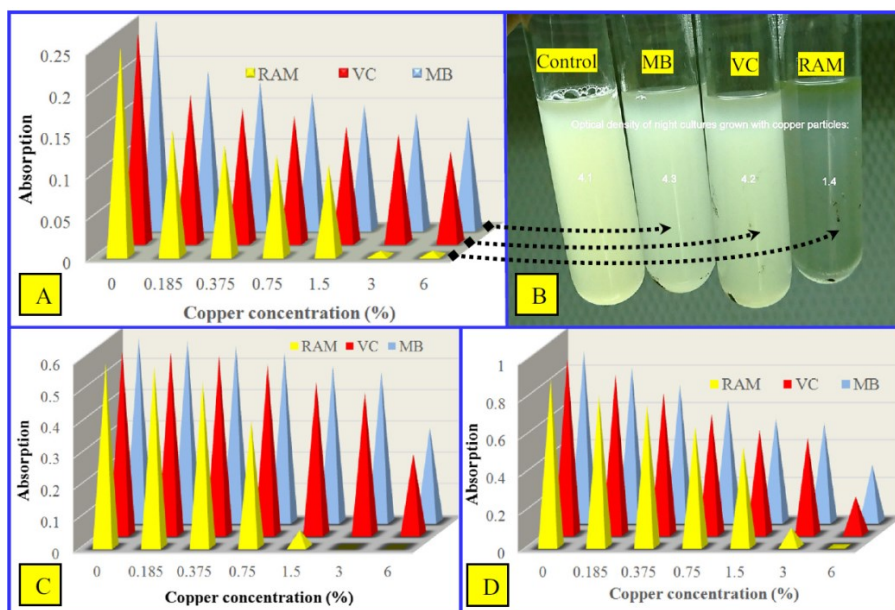


Figure 3.9.4. Representative batch growth profile in the presence of varying concentrations of synthesized Cu-NPs for: A) *E. coli*; B) *P. aeruginosa*; and C) *S. aureus*; D) Optical density of *E. coli* culture grown overnight

It needs to be noted that Ruparelia *et al.* (2008) reported a similar observation in their studies on the effect of Cu-NPs on different types of bacterial cultures (Ruparelia *et al.*, 2008). The absorption measurements for *E. coli*, *P. aeruginosa*, and *S. aureus* revealed almost the same trend for all the NP types; however, there was a significant variation in the absorption values for each type of bacterial cultures, which can be explained by the differences in the bacterial growth patterns (Sondi & Salopek-Sondi, 2004; Zain, Stapley & Shama, 2014). Another point worth noting is some inconsistencies in the absorption trends, which can be a result of gradual NPs agglomeration over time – this is a typical phenomenon for NPs in general (Bueno, 2015). The overall examination of the trends showed that the antimicrobial action of RAM was superior to the one of MB and VC with the Minimum Inhibitory Concentration (MIC) values equalling ~3% for all the types of the bacterial cultures, whereas MIC for other types of Cu-NPs was not reached within the given concentration interval. In the present case, the bactericidal action of NPs had four main influencing parameters: the concentration of NPs, the initial bacterial concentration, the NPs size, and the NP purity (Betancourt-Galindo *et al.*, 2014). Since the concentration of NPs and the initial bacterial concentration were very similar in all the experiments, the Cu-NPs size had a major influence on the final antimicrobial efficacy of the prepared Cu-NP. Smaller particles, as in case of RAM, have a higher surface area: the volume ratio which allows them to interact closely with the microbial membranes and affect microorganisms not merely by the release of metal ions in the solution (Morones *et al.*, 2005). The purity of the prepared Cu-NPs was considered as another factor having a significant impact on the antimicrobial activity. Raffi *et al.* (2010) observed the growth of a bacterial culture in the environment containing NPs by SEM and noted that the interaction of Cu-NPs with *E. coli* resulted in the formation of cavities/pits in the bacterial cell wall (Raffi *et al.*, 2010). The antibacterial property of Cu-NPs in this case was attributed mainly to the adhesion with bacteria because of their opposite electrical charges resulting in a reduction reaction at the bacterial cell wall; such a property has direct dependence on the purity of Cu-NPs, as was observed in the case of RAM (Ojha *et al.*, 2017; Tang, Wang & Gomez, 2017). Finally, in order to confirm the validity of the above listed results, the optical density test was used as an addition to the Broth dilution method. The growth of an *E. coli* bacteria culture left overnight with 0.05% Cu-NPs was examined as shown in **Fig. 3.9.3.B**. It is clear that the RAM sample featured the lowest optical density (1.2) followed by MB (4.3) and VC (4.2) when compared with the control sample. These results agree with the microdilution test data; therefore, Cu-NPs obtained from RAM can be considered promising as an antimicrobial agent.

3.9.3. Conclusion: Green synthesis of nanoparticles

Compared to Electrospraying, Green synthesis produced nanoparticles with a slightly bigger average size (~7 nm), whereas the chemical properties of the particles were very similar. However, the main benefit achieved by Green Synthesis is that it does not involve any hazardous chemicals, high temperatures, or, more importantly, high voltage (unlike Electrospraying). Moreover, a simple preparation procedure requiring only moderate heating and stirring means that this approach is denoted by much better scalability compared to Electrospraying. Additionally, it was shown that the produced

nanoparticles demonstrated notable antimicrobial activity, which suggests that WPCBs with a high purity of copper may be a promising source of antimicrobial nanoparticles.

3.10. Leaching and precipitation of micro/nano particles

The recovery of metals from THSJs was done in the following order (previously described in Section 2.10. of the chapter on Materials and Methods): Leaching by Nitric Acid and Precipitation of $\text{SnO}_2/\text{PbO}_2$ nano/micro particles, filtration of the micro-fraction, separation of the nano-fraction by gravity, and, finally, the recovery of copper from the remaining solution in the hydroxide form.

3.10.1. Optimum leaching conditions

Several trends were observed during the leaching experiments (with the average values for the two THSJ types as shown in Fig. 3.10.1.). First of all, temperature played a crucial role in decreasing the leaching time. It was noted that a major leaching time reduction occurred at all solid-to-liquid ratios by increasing the temperature from 40 to 50 °C (average reduction 5.6 hrs.) and from 50 to 60 °C (average reduction 4.7 hrs.). A further increase of the temperature until 70 and 80 °C did not substantially affect the leaching time (e.g., for the shift from 60 to 70 °C, the average reduction was only 1.2 hrs.). Secondly, the solid-to-liquid ratio also played an important role in shortening the separation time. The increase of the amount of the liquid had an especially strong effect at lower temperatures, for instance, at 40–60 °C, the change of this ratio from 1:15 to 1:40 resulted in shortening the time by 8–12 hrs., whereas at 70 and 80 °C, the same change in the ratio decreased the time by 4–5 hrs.

As a result of all the tests, the optimum values for the subsequent leaching procedures were defined as 1:35 solid/liquid ratio and a temperature of 60°C since the lower temperatures and w/w ratios (50 and 40 °C) did not grant a sufficient leaching rate, whereas the higher temperatures and w/w ratios (70 and 80 °C) did not shorten the process duration significantly, either.

After having determined the optimum conditions, our final leaching experiments were performed by focusing on the stages of the leaching process and the morphology of the leached materials.

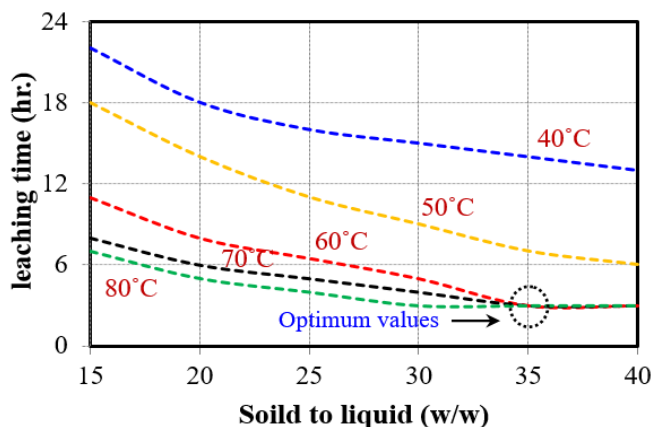


Figure 3.10.1. Relation between solid-to-liquid ratio, temperature and THSJ leaching time

Figure 3.10.2. shows the different stages during the leaching process. As shown in the Figure, once the leaching process had started, the transparent colour of concentrated Nitric Acid (**Fig. 3.10.2.A.**) changed to light green (**Fig. 3.10.2.B.**), and the temperature increased due to the exothermic nature of metal dissolution reactions and the formation of new chemical bonds. After a certain period, the outer layers of THSJs dissolved thus exposing the core while the colour of the solution changed to dark green with a high amount of Nitrogen Dioxide gas as shown in **Fig. 3.10.2.C., D.** After two hours, the solution became darker (**Fig. 3.10.2.E.**), and, if left for several minutes without ultrasonic treatment, a white precipitate was beginning to appear (**Fig. 3.10.2.F.**). At the end of the leaching process (3hrs.), the remaining metal dissolved completely, and the colour of the solution changed again to light blue with a significant increase in the amount of a white-coloured precipitate (**Fig. 3.10.2.G.**). After that, the solution was left for the cooling and stabilization of the precipitate as shown in **Fig. 3.10.2.H.**

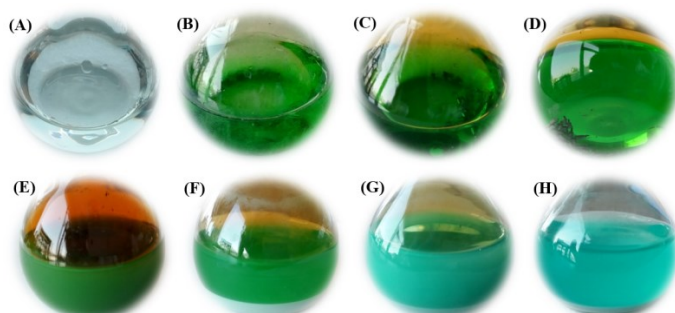


Figure 3.10.2. Images illustrating the leaching steps at different periods of time

In order to study the leaching mechanism of THSJs, SEM was used to observe the changes in the morphology and dimensions of the treated samples, while the changes in the chemical composition were studied by EDS sporadically throughout the process (three times in total). As previously mentioned, the THSJs were mainly composed of three components: legs, solder, and through-hole pads. At the same time, the outer surface of THSJs showed expressed traces of organic contamination in the form of scattered dot-like impurities. Therefore, the observation process focused on these components as well as on the precipitate fraction. The data of our detailed analysis can be found in **Annexes 26–27.**

3.10.2. Analysis of Micro-fraction

The morphology and crystal structure of the microparticles were characterized by conducting SEM analysis. **Figure. 3.10.3.** shows the SEM-EDS analysis of the obtained Micro fraction recovered after the filtration and calcination process for THSJM and THSJV samples. As illustrated, in the THSJM sample, typical precipitate particles had the specific cube shape with well-formed smooth facets in the micrometer scale with the average side length of $\sim 1\ \mu\text{m}$ and uniformly distributed microcrystals. Another peculiar structure with a shape similar to that of a cross was found in the THSJV sample. The EDS analysis (**Fig. 3.10.3.C.**) showed that Pb (45.3 wt.%) and O (33 wt.%) were the main elements of a single crystal for each sample. Also, it was found that the Lead Oxide

crystals were contaminated with a minor amount of Sn (0.8 wt.%) remaining from the washing and filtration steps. As for the Cu peaks in the EDS analysis, they were produced by copper foil which served as a substrate intended to increase the quality of scanning, which is more evident in **Fig. 3.10.3.B₃**, where the cross was marked with the red colour (Pb) and green dots (Cu) highlighting the edges. Also, Pd was present in the THSJ_V particles, yet in a very small amount. This led to difficulties in terms of indicating the accurate concentration by EDS, therefore, ICP measurements were used to confirm these results and to measure the exact quantity of Pd. The results of the ICP analysis showed that the Micro cross particles were composed of (99.862 wt.%), Pd (0.024 wt.%) and Sn (0.114 wt.%). Although there is no data in the literature on the production of Micro Pb from E-waste, several studies have been conducted to synthesize or recover (from waste batteries) similar Lead oxide particles with different structures through solvothermal treatment, electrochemical, direct electrowinning technique, etc. (Liu *et al.*, 2014; Poll & Payne, 2014; Zhi Sun *et al.*, 2017; Xi *et al.*, 2004).

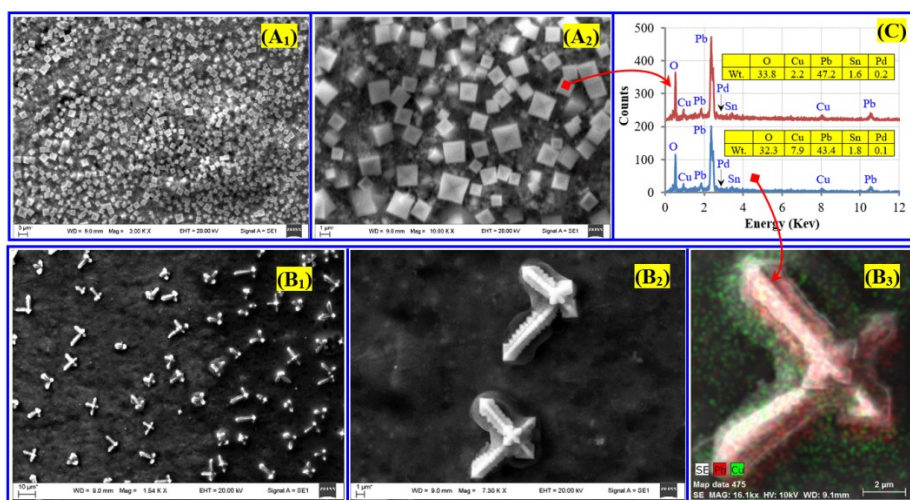


Figure 3.10.3. SEM-EDS images of the Micro-fraction of THSJ_M (A₁–A₂) and THSJ_V (B₁–B₃)

In most of these studies, the grain size and morphology of the produced particles were controlled by the treatment time, the amount of reagents, etc., yet there still was a large variation in the particle size which can adversely affect their performance in the final products because the shape and the size of inorganic nano- or microcrystals determine their widely varying physical and chemical properties (Li *et al.*, 2009). To overcome this problem, doping with different materials was employed to control the size and produce particles with a uniform size distribution where doping did not change the crystal structure, but instead it caused the change of the lattice constant (Shen *et al.*, 2017). Based on this strategy, these microcross and microcube structures were produced as a result of doping by Pd in various concentrations. Since the entire experiment was performed under the same conditions, it can be said that, by controlling the amount of Pd, different particle shapes can be produced (Li *et al.*, 2009).

Copper in the hydroxide form was recovered from THSJ leaching solutions by continuously adding sodium hydroxide (NaOH) so that to elevate the pH of the solutions. Once pH had been raised to 8, a precipitate in the shape of blue flakes started to deposit. **Figure 3.10.4.** shows the SEM-EDS analysis of the precipitate from THSJ_{M, V} samples after filtration and drying at room temperature overnight. As shown in the SEM images, the residue after the filtration process yielded the powder shape with the average particle size of 50µm. Copper was the main element in the two samples with the average share of 50 wt.%. A strong presence of Oxygen was also observed (45 wt.%); the absence of other metals means that copper was recovered selectively. Besides SEM-EDS analysis, FTIR spectroscopy was used to find specific molecular components and structures of the recovered reagent (**Annex 28**).

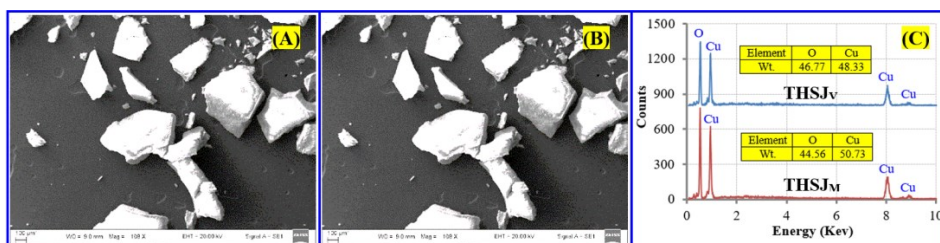


Figure 3.10.4. A) SEM-EDS mapping of precipitated powder; B, C) EDS analysis

3.10.3. Analysis of Nano-fraction

Figure 3.10.5. shows TEM images of the Nano-fraction obtained from THSJM and THSJ_V samples after the filtration process. The nanoparticles of both samples had a spherical shape with the average particle diameter of 7 nm. The particles were regularly distributed with high yield and the EDS analysis of these nanoparticles showed they were rich in Sn and Oxygen, what suggests that the obtained nanoparticles were Tin oxide (SnO₂) which is widely used in semiconductor and gas sensing industries (Borhaninia, Nikfarjam & Salehifar, 2017; Junxia Wang *et al.*, 2017). These industries needed SnO₂ nanoparticles with specific properties which can be reached by doping SnO₂ with other elements; Ni, Fe, and Al are considered the typical doping elements used for such purposes (Gu *et al.*, 2017; Lavanya, Radhakrishnan & Sekar, 2012; Venkateswara Reddy, Venkatramana Reddy & Sankara Reddy, 2016). The results of ICP analysis showed that the nanoparticles were composed of Sn (98.15 wt.%), Ni (0.96 wt.%), Al (0.16 wt.%), and Fe (0.73 wt.%). This means that only a very small share of Ni, Fe, and Al was found during the ICP analysis; this minor share served as a doping agent affecting the morphology of the synthesized SnO₂ and producing nanoparticles with a uniform size distribution. Moreover, FT-IR spectra were used to validate the chemical structure of the prepared SnO₂ nanoparticles (**Annex 29**).

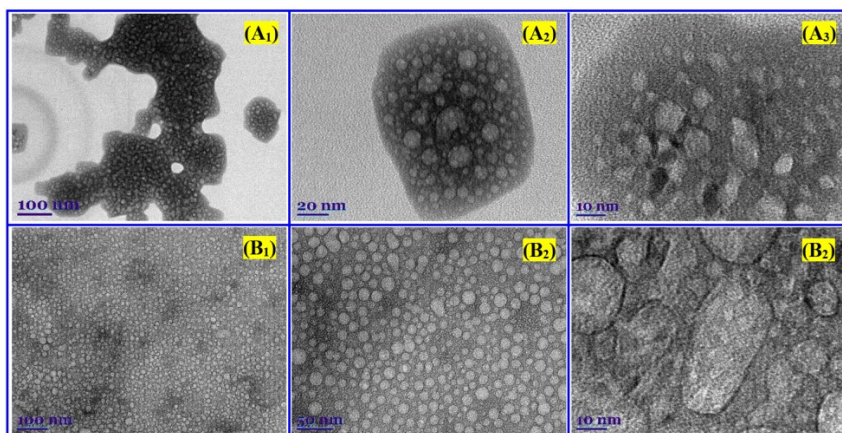


Figure 3.10.5. TEM images of (a) THSJ_M and (b) THSJ_V samples

3.10.4. Conclusion: Leaching and precipitation of micro/nano particles

In conclusion, regarding the results presented in this section, it can be highlighted that the employed treatment including leaching at the optimum conditions (solid-to-liquid ratio 1:35 (wt./wt.), temperature 60 °C) followed by precipitation and filtration was able to recover all the three major metals (Sn, Pb, and Cu) from Through Hole Solder Joint components previously separated from a solvent-treated Motherboard and a Video Card. Lead was recovered as PbO₂ microparticles (average size ~1 μm), Tin was recovered as SnO₂ nanoparticles (average size 7 nm), and copper was recovered as Cu(OH)₂.

3.11. Recycling rate evaluation (Reprocessing)

Yield rate of reprocessing approaches used in the present work was evaluated based on the mass balances of materials throughout the process as shown in **Tab. 3.11.1**. All the used treatment methods required some form of pre-treatment for recovered metal from WPCBs before the actual synthesis of high added value products, therefore, the total yield rate was calculated as a product of Pre-treatment and Synthesis yield rates multiplied.

Table 3.11.1. General recycling rates of the used reprocessing methods

Sample code, element	Pre-treatment			Synthesis			Total yield rate
	Theoretical yield / Initial concentration	Practical yield / Final concentration	Yield rate	Theoretical yield	Practical yield	Yield rate	
Electrospraying							
Cu	1.58 mg (Cu(OAc) ₂)	1.52 mg (Cu(OAc) ₂)	96.2%	160 mg (Cu nanopart.)	140 mg (Cu nanopart.)	87.5%	84%
Green synthesis							
RAM, Cu	1970 mg (Cu(OH) ₂ ·5H ₂ O)	1734 mg (Cu(OH) ₂ ·5H ₂ O)	88%	101 mg (Cu nanopart.)	96 mg (Cu nanopart.)	95%	92.3% × 96.3% = ~ 90%

VC, Cu		1826 mg (Cu(OH) ₂ ·5H ₂ O)	93%		97 mg (Cu nanopart.)	96%	
MB, Cu		1892 mg (Cu(OH) ₂ ·5H ₂ O)	96%		99 mg (Cu nanopart.)	98%	
Avg.		-----	92.3%		-----	96.3%	

Leaching, average values of THSJ_{M,V}

SnO ₂ (Base element Sn)	52451.74 mg/L (Total metal concentration)	281.452 mg/L (Total metal concentration after extraction)	99.5%	11.149 g	10.462 g	93.84%	99.5% × 96.26% = 96%
PbO ₂ (Base element PbO ₂)				7.197 g	6.887 g	95.69%	
Cu(OH) ₂ (Base element Cu)				6.654 g	6.597 g	99.14%	
Avg.				-----		96.23%	

Firstly, evaluation was performed for the products of Electrospraying. The yield of the Cu-NPs obtained by the developed system was calculated based on the weight of electrosprayed Cu (II) acetate/PVA solution and on the weight of the subsequently obtained batch of Cu-NPs that was compared to the weight of the recovered Cu which was considered as the raw material in the present research. The sample for assessment was produced at a constant flow rate (0.2 ml/h) and Electrospraying time (60 min) in order to obtain a noticeable change in the total weight of the composite nanoparticles (Cu-NPs/PVA). Also, the losses during each process were taken into account during the assessment in order to increase the accuracy of the calculation. Based on the results, one kg of the recovered Cu is enough to produce 840g of Cu-NPs and, according to the reported results in the literature, the fraction weight of Cu in WPCBs represents ~22% (He & Xu, 2015), which means that one WPCB may possibly contain ~18% of Cu-NPs if treated with the developed technique.

Secondly, the performance of the Green synthesis technique in terms of the Cu-NP yield was assessed based on the mass balances of Copper (II) Sulfate and the subsequently obtained batch of Cu-NPs that were compared to the weight of the used Cu. At the end of the WPCB dismantling process, it was noted that the quantity of recovered copper foils in the treated samples was 126 mg/cm² (MB), 84 mg/cm² (VC), and 192 mg/cm² (RAM). This large variation in the amount of copper was due to the different structures of WPCBs containing different numbers of copper foils where MB and RAM contained two and four layers, respectively, while VC had only one layer. Due to the large variation in the percentage of copper in each WPCB sample and in order to facilitate the comparison regarding each WPCB type, the yield of Cu-NP was calculated based on a fixed amount of Cu (0.5g) recovered from the MB, RAM, and VC samples which were

considered to serve as our raw material in the present research. The pre-treatment yield was calculated based on the theoretical and factually produced masses of $\text{CuSO}_4 \cdot 5\text{H}_2\text{O}$, while the synthesis yield was calculated based on the theoretical and factually produced masses of Cu-NPs. As it can be seen, there is a high variation in the values of the pre-treatment yield (88 to 96 wt.%) as a result of the mass losses caused by the presence of organic content and the filtration process. The variation in the values of the synthesis yield was notably lower (95 to 98 wt.%) with the yield of Cu-NPs from RAM being higher due to the higher purity of Cu in RAM.

Finally, we can evaluate the efficiency of the Leaching approach. The material recovery efficiency of the pre-treatment was assessed based on the metals concentration in the leaching solution after and before the metal extraction. Thus, ICP analysis was used to determine the exact quantities of the needed elements. As shown in the Table, virtually all the metals were extracted from the spent solution or used as doping agents during the synthesis of micro and nano-fraction with the total leaching rate of >99.6%. The developed leaching approach can produce three different raw materials with different structures and sizes (SnO_2 nanoparticles, PbO_2 microcube/microcross particles, and $\text{Cu}(\text{OH})_2$) while the main losses occur at the end of the leaching process during the steps of filtration and washing. In order to calculate these losses, the yield of each obtained raw material was calculated individually based on the initial and final weight of the metals inside the produced raw materials; the average of the three yields for each material type represents the total recovery rate. The average synthesis rate of SnO_2 and PbO_2 was 93.84% and 95.69%, respectively, while the recovery rate for $\text{Cu}(\text{OH})_2$ was 99.14%. It is worth mentioning that the weight of the Al, Fe, and Ni fraction was included in the SnO_2 nanoparticle yield and that Pd was included in the PbO_2 microcube/microcross particles yield, whereas a single batch was 25g of THSJs. Based on that, the final yield referring to the leaching process was ~96%.

3.12. Preliminary economic and Carbon Footprint analysis (Reprocessing)

While using the values of energy consumption, the mass of the consumed reagents, the mass of the produced high added value products, and the expected cost of all the materials and energy, preliminary economic analysis was conducted for 100 kg of WPCBs as shown in **Table 3.12.1**. It is worth mentioning that most of the values were obtained by using adapted values from the respective publications (Tatariants, Yousef, Sakalauskaitė *et al.*, 2018; Tatariants, Yousef, Skapas *et al.*, 2018; Yousef *et al.*, 2018).

Table 3.12.1. Summary of preliminary economic analysis for reprocessing of WPCBs (calculated for 100 kg of waste)

Input cost		Output cost		Profit (<i>Output cost – Input cost</i>)
Material	Cost	Material	Cost	
Electrospraying				
Separated WPCBs, 100 kg → 23 kg Cu	228 \$	5-7 nm Cu nanoparticles, 19.3 kg	61,760 \$	14,943 \$
PVA, 130.5 kg	196 \$			
Acetic Acid, 145 kg	73\$			
Energy, 386,000 kWh	46,320 \$			

Green synthesis				
Separated WPCBs, 100 kg → 23 kg Cu	228 \$	5-7 nm Cu nanoparticles, 20.7 kg	66,240 \$	59,000 \$
Nitric Acid, 91 kg	27 \$			
Sodium Hydroxide, 29 kg	12 \$			
Sulfuric Acid, 35 kg	14 \$			
Ascorbic Acid, 224 kg	671 \$			
β-cyclodextrin, 52 kg	3,120 \$			
Energy, 26,500 kWh	3,180 \$			
Leaching				
Separated WPCBs, 100 kg → 12 kg THSJs	36 \$	SnO ₂ nanoparticles, 5 kg	400 \$	588 \$
		PbO ₂ microparticles, 3.3 kg	198 \$	
Energy, 5.3 kWh	1 \$	Cu(OH) ₂ , 3.2 kg	26 \$	

As previously noted regarding solvent treatment, the reprocessing evaluation started from defining the system boundaries as shown in **Fig. 3.12.1**.

It is worth remarking that if compared with the commercial prices, the Cu-NPs prepared by the approach developed in this thesis, our costs were 4 times cheaper compared to commercial counterparts. The commercial price is 66\$/5g for particles with the average size of 25 nm (<https://www.sigmaaldrich.com>). The obtained particles with the average size of 5–7 nm and the estimated price of 16\$/5g demonstrate the high potential of the technique we have developed. It is especially important for the Green synthesis approach which can potentially generate a significantly higher profit due to the absence of energy-demanding processes, unlike Electrospraying where only 5 g of product consumes ~100 kWh of energy due to the low production rates.

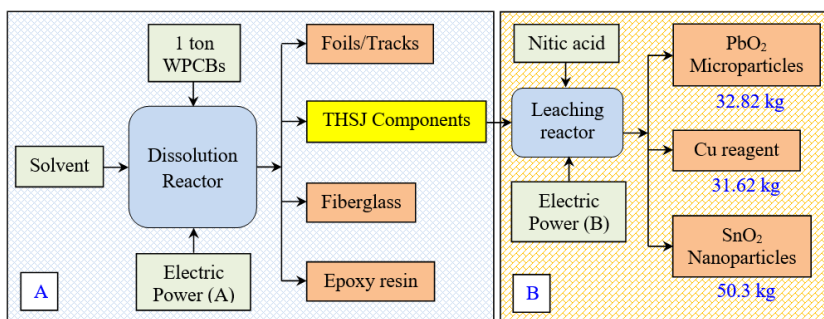


Figure 3.12.1. Boundaries of the developed reprocessing technique (Leaching used as example)

Preliminary Carbon Footprint analysis

Based on the energy consumption and the amount of the recovered metals, Greenhouse Gas Emissions (GGE) were calculated; each material had a specific GGE value determined according to the various literature sources as shown in **Table 3.12.3**. Based on these values and while applying the present technology on the industrial scale, we develop a possibility to decrease GHGE by -787 kg CO₂-eq/t.

Table 3.12.3. GHGE from Leaching treatment of Through-Hole Solder Joints

Recovered material/Energy	Kg or kWh/t of WPCBs	Average (kgCO ₂ -eq/kg or 1000 kWh) (EEA, 2014)	kgCO ₂ -eq /t of WPCBs
Sn	50.3	-13.7	-689.11
Pb	32.82	-1.33	-43.6506
Cu	31.62	-2.75	-86.955
Input energy	53.28	+1472	+32
CO ₂ -eq reduction by the developed approach (kgCO ₂ -eq/t)			-787

3.13. Indication of the material application field (Reprocessing)

The present research started with the separation of metallic components of WPCBs from the non-metallic ones (including copper foils) while using chemical-ultrasonic treatment with a recycling rate of >99% and thus proposing a way to overcome the major challenge for implementing Circular Economy (CE) and achieving the Zero Waste concept for WPCBs by closing their lifecycle loop through efficient recycling. At the same time, the second challenge in CE is in the design stage; at this stage, steps must be taken to improve the condition or quality of the recovered/secondary materials in order to fit the specified application; direct synthesis of high added value products from non-separated WPCBs leads to a decrease in the value of the final product as well as to the loss of other non-metallic fractions of WPCBs, and this is inconsistent with the principles of sustainability (Nekouei, Pahlevani, Rajarao, Golmohammadzadeh & Sahajwalla, 2018b; Shokri *et al.*, 2017).

Therefore, Copper foils and Through-Hole Solder Joints recovered from WPCBs were treated to produce copper sulfate and a leaching solution, respectively, which, in turn, can be used to produce nano- and microparticles. Based on that, this step can be seen not as purification but instead as an experimental design as defined by the CE concept.

The re-manufacturing (or reprocessing) stage is considered to be the third challenge in CE; at this step, the manufacturer should select the optimum remanufacturing process in order to obtain the required product by using the recovered materials constrained by high performance, high yield, environmental and economic benefits (in our case). The reprocessing of Copper foils and Through-Hole Solder Joints yielded three high added value products – Copper nanoparticles, Tin Oxide nanoparticles, and Lead Oxide microparticles. Additionally, Copper Hydroxide was produced from Cu contained in Through Hole Solder Joints.

After that, the remanufactured product is transported to the customer until the end of the product life followed by repeated collection when the loop is expected to start again and thus achieve the sustainability concept as shown in **Fig. 3.13.1**.

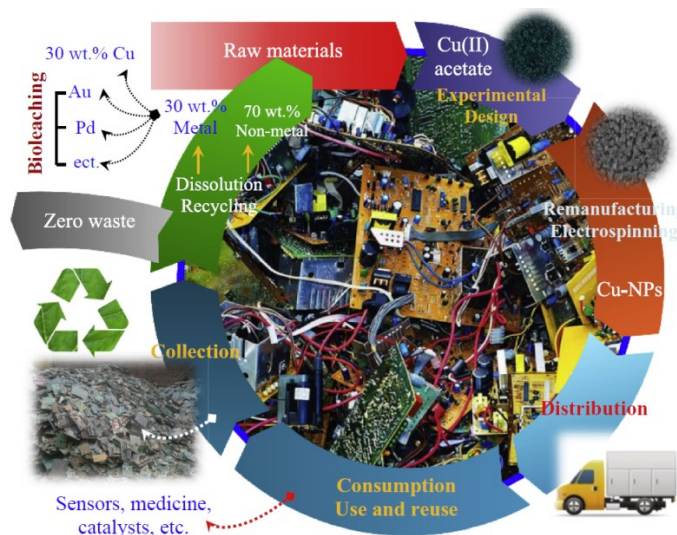


Figure 3.13.1. The developed WPCB recycling/remanufacturing technology as a part of Circular Economy system (example of Copper nanoparticles)

Basing on the steps that were followed in the present research in order to prepare SnO_2 nanoparticles, PbO_2 micro particles and Cu(OH)_2 on the experiential scale, a layout is suggested for the extension of the approach in order to adopt it as an innovative technology suitable for the industrial scale. **Figure 3.13.2.** shows the suggested layout of the new technology; as illustrated in the Figure, the processing starts by mechanical disassembly whose objective is to remove all the electronic components; then, the washing step follows. After that, the dissolution treatment is employed to separate fiberglass, epoxy resin, copper foils/tracks, and THSJs components. At the next step, the leaching process supported with ultrasonic treatment is performed in a glass reactor (a leaching unit). Afterwards, Microparticles of PbO_2 are extracted with a specialized Micro-filtration unit, and the solution containing SnO_2 nanoparticles is stored in an agitation tank in order to prevent nanoparticles from agglomeration. When the needed volume of the nanoparticle-containing solution has been reached, centrifugation is performed to extract SnO_2 nanopowder. The remaining solution is pumped into the Cu(OH)_2 precipitation unit, where water solution of NaOH is added into the unit until the required pH has been reached. The residue consisting of Copper Hydroxide is extracted by performing a further step of centrifugation, and the 'empty' acid solution is directed to the membrane regeneration unit in order to reuse the solution for leaching.

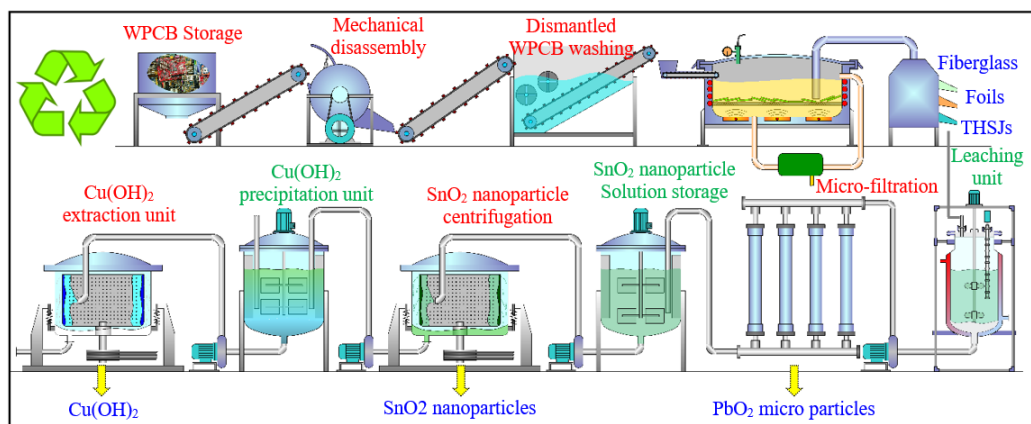


Figure 3.13.2. Industrial technology for mass production of Micro/nano products from WPCBs

Finally, below, we can indicate specific applications suitable for each reprocessed product.

Copper nanoparticles

Nanomaterials usually have a specifically outlined field of application due to their unique properties. Copper Nanoparticles are considered to be the most appropriate choice for high added value product manufacturing, especially since Cu-NPs are widely used in various fields, such as photochemistry, catalysis, electronics, optics, biosensing, gas sensors, electrochemical sensing, solar/photovoltaic energy conversion, lubrication, nano-fluids, etc. (Gawande *et al.*, 2016; Gurav *et al.*, 2014; Khodashenas & Ghorbani, 2014; Zin *et al.*, 2013). Cu Nanoparticles (Cu-NPs) can also be used for high thermal conductivity and high strength alloys as well as for antibacterial and antiviral materials (Din & Rehan, 2017). As it was shown in Section 3.9.2. **Antimicrobial tests**, the produced Nanoparticles indeed manifested notable antimicrobial properties when tested on such common gram-positive and gram-negative microorganisms as *E. coli*, *S. aureus*, and *P. aeruginosa*. This fact shows that WPCBs may have a high potential as a source of antimicrobial nanoparticles in the future.

Tin Oxide nanoparticles

Tin Oxide nanoparticles are currently receiving high attention as they are suitable for many applications due to their peculiar optical, electronic, magnetic and catalytic properties. Such nanoparticles can be used for the production of LED displays, anti-reflective coatings and electrodes in solar cells, photocatalytic degradation of dyes, magnetic data storing, gas sensing, etc. (Chen, Shek, Wu & Lai, 2013).

Lead Oxide microparticles

The use of Lead Oxide microparticles in various applications is less common if compared to Tin Oxide nanoparticles; however, it has been reported that Lead Oxide can serve as a catalyst enhancing the decomposition of certain energetic formulations (Mirzajani, Farhadi & Pourmortazavi, 2018). Obviously, Lead Oxide may be relatively

easily reduced (while using, for example, heating in hydrogen atmosphere) when seeking to obtain Lead microparticles. Lead itself may be used for the production of batteries and lead crystal glass. More advanced applications include the production of lead halide perovskites which are promising materials for solar cell manufacturing (Park, 2015).

Copper Hydroxide

Copper Hydroxide is a common chemical reagent which has a wide variety of potential uses ranging from typical (for instance, cellulose dissolution for the manufacturing of synthetic fiber rayon, pigmentation, dyeing, fungicidal applications, metallurgy, printing, catalysts in various reactions) to advanced (for example, production of nanorods for glucose sensing) (Richardson, 1997; Shackery *et al.*, 2016).

CONCLUSIONS

The work performed within the scope of this thesis was aimed at the development of a novel solvent treatment for the recovery of materials from Waste Printed Circuit Boards and the production of high added value products. It can be summarized by highlighting the following points:

1. Several types of WPCBs were treated with solvent: milled, cut, and full-size WPCBs. It turned out that the treatment of full-size samples was more beneficial if compared to milled or cut samples since the processing of milled samples required higher solvent consumption, and the separation of milled fiberglass/metal was difficult to conduct with a high recovery rate;

2. All the essential characteristics of the separation process were described by the respective regression models. It was determined that the optimum conditions for the treatment with organic solvent Dimethylformamide (DMF) were: temperature 50 °C and solid-to-liquid ratio 3:10 (WPCB wt.: Solvent v.). The optimum time was a varying parameter that was in the range of 22–18 hrs. for smaller WPCB types (Video Card, Random Access Memory) and 80–85 hrs. for the biggest treated WPCBs (Motherboard ~70,000 mm²). In addition, based on the modeling results, it can be concluded that the separation of WPCBs with a surface area larger than 100,000 mm² may be inefficient due to the high probability of the exponential increase of the separation time that would reach >160 hrs.;

3. The recovered metals and non-metals were split into three groups according to their condition and readiness for repeated use in new applications: repurposable, semi-repurposable, and non-repurposable without additional treatment. Repurposable materials included recovered Fiberglass, Epoxy Resin, and Gold flakes. It was discovered that the recovered Fiberglass and Epoxy Resin retained most of their original mechanical and thermochemical properties and can be applied for composite, sound insulation, and adhesive applications, whereas the high purity of Gold (~94%) can be used in those applications which traditionally require high purity Gold, such as electronics, catalysts, etc. The second category of semi-repurposable materials included the recovered Copper foils. Lastly, non-repurposable materials included the so-called Through-Hole Solder Joints (THSJs) composed of several metals and alloys which are not suitable for any application without prior reprocessing;

4. Three reprocessing technologies were implemented to close the loop of the treatment and produce high added value products from the recovered materials: Electro spraying and Green Synthesis for Copper, and Ultrasound-Assisted Leaching for THSJs. Electro spraying at optimum conditions yielded copper nanoparticles with the average size of 5 nm. Electro spraying had some disadvantages, such as a low synthesis rate and high energy consumption. Therefore, Green Synthesis was used to obtain 7 nm-sized copper nanoparticles with lower energy consumption and synthesis rates. In addition, the synthesized nanoparticles were shown to exhibit antimicrobial behavior against *E. coli*, *P. aeruginosa*, and *S. aureus* bacterial cultures, and they showed notable inhibition rates. Finally, the leaching of metals from THSJs produced SnO₂ nanoparticles

and PbO₂ microcubes/microcross particles. Such particles can be used in LED displays, photocatalytic dyes degradation, anti-reflective coatings and electrodes in solar cells, for the production of lead halide perovskites, etc.

REFERENCES

1. Adie, G. U., Sun, L., Zeng, X., Zheng, L., Osibanjo, O., & Li, J. (2017). Examining the evolution of metals utilized in printed circuit boards. *Environmental Technology* (United Kingdom).
2. Afroz, R., Masud, M. M., Akhtar, R., & Duasa, J. B. (2013). Survey and analysis of public knowledge, awareness and willingness to pay in Kuala Lumpur, Malaysia-a case study on household WEEE management. *Journal of Cleaner Production*.
3. Agarwal, T. (2015). Different Types of Printed Circuit Boards. *Elprocus*. Retrieved August 29, 2018, from <https://www.elprocus.com/different-types-printed-circuit-boards/>
4. Akcil, A., Erust, C., Gahan, C. S., Ozgun, M., Sahin, M., & Tuncuk, A. (2015). Precious metal recovery from waste printed circuit boards using cyanide and non-cyanide lixivants - A review. *Waste Management*, 45, 258–271.
5. Alae, M., Arias, P., Sjödin, A., & Bergman, Å. (2003). An overview of commercially used brominated flame retardants, their applications, their use patterns in different countries/regions and possible modes of release. *Environment International*.
6. Argueta-Figueroa, L., Morales-Luckie, R. A., Scougall-Vilchis, R. J., & Olea-Mejia, O. F. (2014). Synthesis, characterization and antibacterial activity of copper, nickel and bimetallic Cu-Ni nanoparticles for potential use in dental materials. *Progress in Natural Science: Materials International*, 24(4), 321–328.
7. Astashkin, V. M., & Mishnev, M. V. (2016). On the Development of the Manufacturing Technology of Fiberglass Cylindrical Shells of Gas Exhaust Trunks by Buildup Winding. *Procedia Engineering* (Vol. 150, pp. 1636–1642).
8. Awasthi, A. K., Wang, M., Wang, Z., Awasthi, M. K., & Li, J. (2018). E-waste management in India: A mini-review. *Waste Management & Research*, 36(5), 408–414. Retrieved from <https://doi.org/10.1177/0734242X18767038>
9. Awasthi, A. K., Zlamparet, G. I., Zeng, X., & Li, J. (2017). Evaluating waste printed circuit boards recycling: Opportunities and challenges, a mini review. *Waste Management & Research*, 35(4), 346–356. Retrieved from <http://journals.sagepub.com/doi/10.1177/0734242X16682607>
10. Baker, S. C. (2005). *Sustainable Development*. Science.
11. Batnasan, A., Haga, K., & Shibayama, A. (2018). Recovery of Precious and Base Metals from Waste Printed Circuit Boards Using a Sequential Leaching Procedure. *JOM*.
12. Behnamfard, A., Salarirad, M. M., & Veglio, F. (2013). Process development for recovery of copper and precious metals from waste printed circuit boards with emphasize on palladium and gold leaching and precipitation. *Waste Management*, 33(11), 2354–2363.
13. Bernstad, A., la Cour Jansen, J., & Aspegren, H. (2011). Property-close source separation of hazardous waste and waste electrical and electronic equipment - A Swedish case study. *Waste Management*.
14. Betancourt-Galindo, R., Reyes-Rodriguez, P. Y., Puente-Urbina, B. A., Avila-Orta, C. A., Rodríguez-Fernández, O. S., Cadenas-Pliego, G., Lira-Saldivar, R. H., et al. (2014). Synthesis of copper nanoparticles by thermal decomposition and their antimicrobial properties. *Journal of Nanomaterials*, 2014.
15. Bi, X., Simoneit, B. R. T., Wang, Z., Wang, X., Sheng, G., & Fu, J. (2010). The major components of particles emitted during recycling of waste printed circuit boards in a typical e-

waste workshop of South China. Atmospheric Environment.

16. Bidini, G., Fantozzi, F., Bartocci, P., D'Alessandro, B., D'Amico, M., Laranci, P., Scozza, E., et al. (2015). Recovery of precious metals from scrap printed circuit boards through pyrolysis. *Journal of Analytical and Applied Pyrolysis*, 111, 140–147.

17. Biffis, A., Gardan, M., & Corain, B. (2006). Homogeneous and supported copper(II) acetate as catalyst for C{single bond}O coupling reactions. *Journal of Molecular Catalysis A: Chemical*, 250(1–2), 1–5.

18. Biswal, M., Jada, N., Mohanty, S., & Nayak, S. K. (2015). Recovery and utilisation of non-metallic fraction from waste printed circuit boards in polypropylene composites. *Plastics, Rubber and Composites*, 44(8), 314–321. Retrieved from <http://www.scopus.com/inward/record.url?eid=2-s2.0-84957666153&partnerID=tZOTx3yl>

19. BORHANINIA, A., NIKFARJAM, A., & SALEHIFAR, N. (2017). Gas sensing properties of SnO₂ nanoparticles mixed with gold nanoparticles. *Transactions of Nonferrous Metals Society of China*, 27(8), 1777–1784. Elsevier. Retrieved July 18, 2018, from <https://www.sciencedirect.com/science/article/pii/S1003632617602000>

20. Bueno, J. (2015). Chapter 2 - Antimicrobial Models in Nanotechnology: From the Selection to Application in the Control and Treatment of Infectious Diseases. In M. Rai & K. Kon (Eds.), *Nanotechnology in Diagnosis, Treatment and Prophylaxis of Infectious Diseases* (pp. 19–38). Boston: Academic Press. Retrieved from <https://www.sciencedirect.com/science/article/pii/B9780128013175000025>

21. Cai, J., Fu, Q., Long, M., Liao, G., & Xu, Z. (2017). The sound insulation property of composite from waste printed circuit board and unsaturated polyester. *Composites Science and Technology*, 145, 132–137.

22. Cayumil, R., Khanna, R., Rajarao, R., Mukherjee, P. S., & Sahajwalla, V. (2016). Concentration of precious metals during their recovery from electronic waste. *Waste Management*, 57, 121–130.

23. Cerchier, P., Dabalà, M., & Brunelli, K. (2017). Synthesis of SnO₂ and Ag Nanoparticles from Electronic Wastes with the Assistance of Ultrasound and Microwaves. *JOM*.

24. Das Chakladar, N., Pal, S. K., & Mandal, P. (2012). Drilling of woven glass fiber-reinforced plastic - An experimental and finite element study. *International Journal of Advanced Manufacturing Technology*.

25. Chang, L. W., Yau, S. S., & Chou, T. W. (1987). Notched strength of woven fabric composites with moulded-in holes. *Composites*.

26. Chang, S.-S. S. (1988). HEAT OF REACTION AND CURING OF EPOXY RESIN. *Journal of Thermal Analysis*, Vol. 34(1), 135–154.

27. Chauhan, G., Jadhao, P. R., Pant, K. K., & Nigam, K. D. P. (2018). Novel technologies and conventional processes for recovery of metals from waste electrical and electronic equipment: Challenges & opportunities – A review. *Journal of Environmental Chemical Engineering*.

28. Chehade, Y., Siddique, A., Alayan, H., Sadasivam, N., Nusri, S., Ibrahim, T., Cui, J., et al. (2014). Metal Extraction Processes for Electronic Waste and Existing Industrial Routes: A Review and Australian Perspective. *Journal of Hazardous Materials*, 33(4), 219–224. Retrieved from

<http://dx.doi.org/10.1016/j.wasman.2013.01.003>
<http://www.sciencedirect.com/science/article/pii/S1877042812007847>
<http://dx.doi.org/10.1016/j.jhazmat.2014.03.043>
<http://linkinghub.elsevier.com/retrieve/pii/S0304389408002161>

29. Chen, M., Huang, J., Ogunseitan, O. A., Zhu, N., & Wang, Y. min. (2015). Comparative study on copper leaching from waste printed circuit boards by typical ionic liquid acids. *Waste Management*.

30. Chen, S., Yang, Y., Liu, C., Dong, F., & Liu, B. (2015). Column bioleaching copper

and its kinetics of waste printed circuit boards (WPCBs) by *Acidithiobacillus ferrooxidans*. *Chemosphere*, 141, 162–168.

31. Chen, Z. W., Shek, C. H., Wu, C. M. L., & Lai, J. K. L. (2013). Recent research situation in tin dioxide nanomaterials: Synthesis, microstructures, and properties. *Frontiers of Materials Science*.

32. Cheng, S., Huang, C. M., & Pecht, M. (2017). A review of lead-free solders for electronics applications. *Microelectronics Reliability*.

33. Cheng, Y., Zou, B., Wang, C., Liu, Y., Fan, X., Zhu, L., Wang, Y., et al. (2011). Formation mechanism of Fe₂O₃ hollow fibers by direct annealing of the electrospun composite fibers and their magnetic, electrochemical properties. *CrystEngComm*, 13(8), 2863. Retrieved from <http://xlink.rsc.org/?DOI=c0ce00379d>

34. Chi, X., Streicher-Porte, M., Wang, M. Y. L., & Reuter, M. A. (2011). Informal electronic waste recycling: A sector review with special focus on China. *Waste Management*, 31(4), 731–742.

35. Chien, Y. C., Paul Wang, H., Lin, K. S., Huang, Y. J., & Yang, Y. W. (2000). Fate of bromine in pyrolysis of printed circuit board wastes. *Chemosphere*.

36. Christie, I. R., & Cameron, B. P. (1994). Gold electrodeposition within the electronics industry. *Gold Bulletin*, 27(1), 12–20.

37. Clsi. (2013). Performance Standards for Antimicrobial Susceptibility Testing; Twenty-Second Informational Supplement. Clinical and Laboratory Standards Institute (Vol. 32).

38. Côrtes, L. N., Tanabe, E. H., Bertuol, D. A., & Dotto, G. L. (2015). Biosorption of gold from computer microprocessor leachate solutions using chitin. *Waste Management*.

39. Cucchiella, F., D'Adamo, I., Lenny Koh, S. C., & Rosa, P. (2016). A profitability assessment of European recycling processes treating printed circuit boards from waste electrical and electronic equipments. *Renewable and Sustainable Energy Reviews*.

40. Cucchiella, F., D'Adamo, I., Rosa, P., & Terzi, S. (2016). Automotive printed circuit boards recycling: An economic analysis. *Journal of Cleaner Production*, 121, 130–141.

41. Cui, J., & Forssberg, E. (2003). Mechanical recycling of waste electric and electronic equipment: A review. *Journal of Hazardous Materials*.

42. Cui, J., & Zhang, L. (2008). Metallurgical recovery of metals from electronic waste: A review. *Journal of Hazardous Materials*.

43. Dang, W., Kubouchi, M., Yamamoto, S., Sembokuya, H., & Tsuda, K. (2002). An approach to chemical recycling of epoxy resin cured with amine using nitric acid. *Polymer*, 43(10), 2953–2958. Retrieved May 11, 2017, from <http://www.sciencedirect.com/science/article/pii/S0032386102001003>

44. Davis, M. E., & Brewster, M. E. (2004). Cyclodextrin-based pharmaceuticals: Past, present and future. *Nature Reviews Drug Discovery*.

45. Dealba-Montero, I., Guajardo-Pacheco, J., Morales-Sánchez, E., Araujo-Martínez, R., Loredó-Becerra, G. M., Martínez-Castañón, G. A., Ruiz, F., et al. (2017). Antimicrobial Properties of Copper Nanoparticles and Amino Acid Chelated Copper Nanoparticles Produced by Using a Soya Extract. *Bioinorganic Chemistry and Applications*, 2017.

46. Dean, K., Krstina, J., Tian, W., & Varley, R. J. (2007). Effect of ultrasonic dispersion methods on thermal and mechanical properties of organoclay epoxy nanocomposites. *Macromolecular Materials and Engineering*.

47. Deng, X., & Chawla, N. (2008). Three-dimensional (3D) modeling of the thermoelastic behavior of woven glass fiber-reinforced resin matrix composites. *Journal of Materials Science*.

48. Dimitrakakis, E., Janz, A., Bilitewski, B., & Gidarakos, E. (2009). Small WEEE: Determining recyclables and hazardous substances in plastics. *Journal of Hazardous Materials*.

49. Din, M. I., & Rehan, R. (2017). Synthesis, Characterization, and Applications of

Copper Nanoparticles. Analytical Letters.

50. Duan, C., Wen, X., Shi, C., Zhao, Y., Wen, B., & He, Y. (2009). Recovery of metals from waste printed circuit boards by a mechanical method using a water medium. *Journal of Hazardous Materials*, 166(1), 478–482.

51. Ebin, B., & Isik, M. I. (2016). Pyrometallurgical Processes for the Recovery of Metals from WEEE. *WEEE Recycling*, 107–137. Elsevier. Retrieved April 8, 2019, from <https://www.sciencedirect.com/science/article/pii/B9780128033630000055>

52. EEA. (2014). EEA greenhouse gas - data viewer. European Environment Agency. Retrieved from <http://www.eea.europa.eu/data-and-maps/data/data-viewers/greenhouse-gases-viewer>

53. Ellis, B. (1993). *Chemistry and Technology of Epoxy Resins*. Springer-Science+Business Media.

54. Energy price statistics. (2016). . Retrieved November 1, 2017, from http://ec.europa.eu/eurostat/statistics-explained/index.php/Energy_price_statistics

55. Ernst, T., Popp, R., Wolf, M., & Van Eldik, R. (2003). Analysis of eco-relevant elements and noble metals in printed wiring boards using AAS, ICP-AES and EDXRF. *Analytical and Bioanalytical Chemistry*.

56. Etches, J., Potter, K., Weaver, P., & Bond, I. (2009). Environmental effects on thermally induced multistability in unsymmetric composite laminates. *Composites Part A: Applied Science and Manufacturing*.

57. European Parliament, C. (2003). DIRECTIVE 2002/95/EC OF THE EUROPEAN PARLIAMENT AND OF THE COUNCIL on the restriction of the use of certain hazardous substances in electrical and electronic equipment. *Official Journal of the European Union*.

58. Evangelopoulos, P., Kantarelis, E., & Yang, W. (2017). Experimental investigation of the influence of reaction atmosphere on the pyrolysis of printed circuit boards. *Applied Energy*.

59. Van Eygen, E., De Meester, S., Tran, H. P., & Dewulf, J. (2016). Resource savings by urban mining: The case of desktop and laptop computers in Belgium. *Resources, Conservation and Recycling*.

60. Fang, W., Yang, Y., & Xu, Z. (2013). PM10 and PM2.5 and health risk assessment for heavy metals in a typical factory for cathode ray tube television recycling. *Environmental Science and Technology*.

61. Fogarasi, S., Imre-Lucaci, F., Egedy, A., Imre-Lucaci, Á., & Ilea, P. (2015). Eco-friendly copper recovery process from waste printed circuit boards using Fe³⁺/Fe²⁺ redox system. *Waste Management*, 40, 136–143.

62. Fogarasi, S., Imre-Lucaci, F., Imre-Lucaci, Á., & Ilea, P. (2014). Copper recovery and gold enrichment from waste printed circuit boards by mediated electrochemical oxidation. *Journal of Hazardous Materials*, 273, 215–221.

63. Fu, J., Wang, Y., Zhang, A., Zhang, Q., Zhao, Z., Wang, T., & Jiang, G. (2011). Spatial distribution of polychlorinated biphenyls (PCBs) and polybrominated biphenyl ethers (PBDEs) in an e-waste dismantling region in Southeast China: Use of apple snail (Ampullariidae) as a bioindicator. *Chemosphere*.

64. Fu, J., Zhou, Q., Liu, J., Liu, W., Wang, T., Zhang, Q., & Jiang, G. (2008). High levels of heavy metals in rice (*Oryza sativa* L.) from a typical E-waste recycling area in southeast China and its potential risk to human health. *Chemosphere*.

65. G. Long, M.E. Meek, M. L. (2001). Concise International Chemical Assessment Document 31. N,N-DIMETHYLFORMAMIDE. Geneva. Retrieved from <http://www.who.int/ipcs/publications/cicad/en/cicad31.pdf?ua=1>

66. Gadd, G. M. (2009). Biosorption: Critical review of scientific rationale, environmental importance and significance for pollution treatment. *Journal of Chemical Technology and*

Biotechnology.

67. Gawande, M. B., Goswami, A., Felpin, F. X., Asefa, T., Huang, X., Silva, R., Zou, X., et al. (2016). Cu and Cu-Based Nanoparticles: Synthesis and Applications in Catalysis. *Chemical Reviews*.

68. Geng, Y., Fujita, T., Park, H. S., Chiu, A. S. F., & Huisinigh, D. (2016). Recent progress on innovative eco-industrial development. *Journal of Cleaner Production*, 114, 1–10.

69. Ghasemi Nejhad, M. N., & Chou, T. W. (1990). Compression behaviour of woven carbon fibre-reinforced epoxy composites with moulded-in and drilled holes. *Composites*.

70. Ghisellini, P., Cialani, C., & Ulgiati, S. (2016). A review on circular economy: The expected transition to a balanced interplay of environmental and economic systems. *Journal of Cleaner Production*.

71. Ghosh, B., Ghosh, M. K., Parhi, P., Mukherjee, P. S., & Mishra, B. K. (2015). Waste Printed Circuit Boards recycling: An extensive assessment of current status. *Journal of Cleaner Production*.

72. Gomes, M. I., Barbosa-Povoa, A. P., & Novais, A. Q. (2011). Modelling a recovery network for WEEE: A case study in Portugal. *Waste Management*.

73. Goosey, M., & Kellner, R. (2003). Recycling technologies for the treatment of end of life printed circuit boards (PCBs). *Circuit World*, 29(3), 33–37. Retrieved from <http://www.emeraldinsight.com/doi/10.1108/03056120310460801>

74. Graedel, T. E., Allwood, J., Jean-Pierre Birat, A.-M., Buchert, M., Hagelüken, C., Reck, B. K., Sibley, S. F., et al. (2011). Recycling rates of metals: A Status Report. International Resource Panel.

75. Grunow, M., & Gobbi, C. (2009). Designing the reverse network for WEEE in Denmark. *CIRP Annals - Manufacturing Technology*.

76. Gu, C., Guan, W., Liu, X., Gao, L., Wang, L., Shim, J. J., & Huang, J. (2017). Controlled synthesis of porous Ni-doped SnO₂ microstructures and their enhanced gas sensing properties. *Journal of Alloys and Compounds*.

77. Gu, W., Bai, J., Dong, B., Zhuang, X., Zhao, J., Zhang, C., Wang, J., et al. (2017). Enhanced bioleaching efficiency of copper from waste printed circuit board driven by nitrogen-doped carbon nanotubes modified electrode. *Chemical Engineering Journal*, 324, 122–129.

78. Guanghan, S., Zhu, X., Wenyi, Y., Chenglong, Z., & Wen, M. (2016). Recycling and Disposal Technology for Non-metallic Materials from Waste Printed Circuit Boards(WPCBs) in China. *Procedia Environmental Sciences*, 31, 935–940. Retrieved from <http://linkinghub.elsevier.com/retrieve/pii/S1878029616001158>

79. Gullett, B. K., Linak, W. P., Touati, A., Wasson, S. J., Gatica, S., & King, C. J. (2007). Characterization of air emissions and residual ash from open burning of electronic wastes during simulated rudimentary recycling operations. *Journal of Material Cycles and Waste Management*.

80. Guo, J., Cao, B., Guo, J., & Xu, Z. (2008). A plate produced by nonmetallic materials of pulverized waste printed circuit boards. *Environmental Science and Technology*.

81. Guo, J. J., Guo, J. J., Wang, S., & Xu, Z. (2009). Asphalt modified with nonmetals separated from pulverized waste printed circuit boards. *Environmental Science and Technology*, 43(2), 503–508.

82. Guo, J., Li, J., Rao, Q., & Xu, Z. (2008). Phenolic molding compound filled with nonmetals of waste PCBs. *Environmental Science and Technology*.

83. Guo, Q., Harrats, C., Groeninckx, G., & Koch, M. H. J. (2001). Miscibility, crystallization kinetics and real-time small-angle X-ray scattering investigation of the semicrystalline morphology in thermosetting polymer blends of epoxy resin and poly(ethylene oxide). *Polymer*, 42(9), 4127–4140.

84. Guo, X., Zhang, Y., & Xu, K. (2016). Metallurgical Recovery of Metals from Waste

Electrical and Electronic Equipment (WEEE) in PRC. Metal Sustainability: Global Challenges, Consequences, and Prospects.

85. Gurav, P., Naik, S. S., Ansari, K., Srinath, S., Kishore, K. A., Setty, Y. P., & Sonawane, S. (2014). Stable colloidal copper nanoparticles for a nanofluid: Production and application. *Colloids and Surfaces A: Physicochemical and Engineering Aspects*, 441, 589–597.

86. Gurgul, A., Szczepaniak, W., & Zabłocka-Malicka, M. (2018). Incineration and pyrolysis vs. steam gasification of electronic waste. *Science of the Total Environment*.

87. Gurung, M., Adhikari, B. B., Kawakita, H., Ohto, K., Inoue, K., & Alam, S. (2013). Recovery of gold and silver from spent mobile phones by means of acidothioureia leaching followed by adsorption using biosorbent prepared from persimmon tannin. *Hydrometallurgy*, 133, 84–93.

88. Hadi, P., Barford, J., & McKay, G. (2014). Selective toxic metal uptake using an e-waste-based novel sorbent-Single, binary and ternary systems. *Journal of Environmental Chemical Engineering*.

89. Hadi, P., Gao, P., Barford, J. P., & McKay, G. (2013). Novel application of the nonmetallic fraction of the recycled printed circuit boards as a toxic heavy metal adsorbent. *Journal of Hazardous Materials*, 252–253, 166–170.

90. Hadi, P., Xu, M., Lin, C. S. K. K., Hui, C. W., & McKay, G. (2015). Waste printed circuit board recycling techniques and product utilization. *Journal of Hazardous Materials*.

91. Hajipour, M. J., Fromm, K. M., Akbar Ashkarran, A., Jimenez de Aberasturi, D., Larramendi, I. R. de, Rojo, T., Serpooshan, V., et al. (2012). Antibacterial properties of nanoparticles. *Trends in Biotechnology*.

92. Hall, W. J., & Williams, P. T. (2007). Separation and recovery of materials from scrap printed circuit boards. *Resources, Conservation and Recycling*.

93. Hanafi, J., Jobiliong, E., Christiani, A., Soenarta, D. C., Kurniawan, J., & Irawan, J. (2012). Material Recovery and Characterization of PCB from Electronic Waste. *Procedia - Social and Behavioral Sciences*.

94. Haraszti, T. P. (2002). *CMOS Memory Circuits*. Springer US.

95. Haugan, E. T., & Dalsjø, P. (2014). Characterization of the material properties of two FR4 printed circuit board laminates.

96. Havlik, T., Orac, D., Petranikova, M., Miskufova, A., Kukurugya, F., & Takacova, Z. (2010). Leaching of copper and tin from used printed circuit boards after thermal treatment. *Journal of Hazardous Materials*, 183(1–3), 866–873.

97. He, J. F., He, Y. Q., Ge, W. S., Duan, C. L., & Wu, X. B. (2010). Research on the Recycling of Valuable Metals from Waste Printed Circuit Boards by Eddy Current Separation. *Advanced Materials Research*.

98. He, Y., & Xu, Z. (2015). Recycling gold and copper from waste printed circuit boards using chlorination process. *RSC Adv.*, 5(12), 8957–8964. Retrieved from <http://xlink.rsc.org/?DOI=C4RA16231E>

99. Hirai, Y., Hamada, H., & Kim, J. K. (1998). Impact response of woven glass-fabric composites - I. Effect of fibre surface treatment. *Composites Science and Technology*.

100. Hischier, R., Wäger, P., & Gaughhofer, J. (2005). Does WEEE recycling make sense from an environmental perspective? The environmental impacts of the Swiss take-back and recycling systems for waste electrical and electronic equipment (WEEE). *Environmental Impact Assessment Review*.

101. Hong, S. G., & Su, S. H. (1996). The use of recycled printed circuit boards as reinforcing fillers in the polyester composite. *Journal of Environmental Science and Health . Part A: Environmental Science and Engineering and Toxicology*.

102. Hu, J., Wang, T., Wang, Y., Huang, D., He, G., Han, Y., Hu, N., et al. (2018).

Enhanced formaldehyde detection based on Ni doping of SnO₂nanoparticles by one-step synthesis. *Sensors and Actuators, B: Chemical*.

103. Huang, K., Guo, J., & Xu, Z. M. (2009). Recycling of waste printed circuit boards: A review of current technologies and treatment status in China. *Journal of Hazardous Materials*, 164(2–3), 399–408.

104. Huang, Z., Yu, L., Dai, Y., & Wang, H. (2011). Hydrogen bonding interactions between N, N-dimethylformamide and cysteine: DFT studies of structures, properties, and topologies. *Structural Chemistry*.

105. Huo, X., Peng, L., Xu, X., Zheng, L., Qiu, B., Qi, Z., Zhang, B., et al. (2007). Elevated blood lead levels of children in Guiyu, an electronic waste recycling town in China. *Environmental Health Perspectives*.

106. Hwan, C. L., Tsai, K. H., Chiu, C. H., & Huang, Y. S. (2014). Strength prediction of woven hybrid composite laminates each with a center hole. *Journal of Composite Materials*.

107. Iji, M. (1998). Recycling of epoxy resin compounds for moulding electronic components. *Journal of Materials Science*, 33(1), 45–53. Retrieved from <http://dx.doi.org/10.1023/A:1004329209623>

108. Ikhlayel, M. (2017). Environmental impacts and benefits of state-of-the-art technologies for E-waste management. *Waste Management*, 68, 458–474.

109. Ilyas, S., & Lee, J. (2014). Biometallurgical Recovery of Metals from Waste Electrical and Electronic Equipment: a Review. *ChemBioEng Reviews*.

110. Imre-Lucaci, Á., Nagy, M., Imre-Lucaci, F., & Fogarasi, S. (2017). Technical and environmental assessment of gold recovery from secondary streams obtained in the processing of waste printed circuit boards. *Chemical Engineering Journal*, 309, 655–662.

111. Işildar, A., van de Vossenberg, J., Rene, E. R., van Hullebusch, E. D., & Lens, P. N. L. (2016). Two-step bioleaching of copper and gold from discarded printed circuit boards (PCB). *Waste Management*, 57, 149–157.

112. Islam, M. T., & Huda, N. (2018). Reverse logistics and closed-loop supply chain of Waste Electrical and Electronic Equipment (WEEE)/E-waste: A comprehensive literature review. *Resources, Conservation and Recycling*.

113. Jie, G., Ying-Shun, L., & Mai-Xi, L. (2008). Product characterization of waste printed circuit board by pyrolysis. *Journal of Analytical and Applied Pyrolysis*.

114. Jin, F. L., Li, X., & Park, S. J. (2015). Synthesis and application of epoxy resins: A review. *Journal of Industrial and Engineering Chemistry*.

115. Jing-ying, L., Xiu-li, X., & Wen-quan, L. (2012). Thiourea leaching gold and silver from the printed circuit boards of waste mobile phones. *Waste Management*, 32(6), 1209–1212.

116. Jinlian, H., Yi, L., & Xueming, S. (2004). Study on void formation in multi-layer woven fabrics. *Composites Part A: Applied Science and Manufacturing*, 35(5), 595–603.

117. Jordens, A., Cheng, Y. P., & Waters, K. E. (2013). A review of the beneficiation of rare earth element bearing minerals. *Minerals Engineering*.

118. Kaksonen, A. H., Boxall, N. J., Gumulya, Y., Khaleque, H. N., Morris, C., Bohu, T., Cheng, K. Y., et al. (2018). Recent progress in biohydrometallurgy and microbial characterisation. *Hydrometallurgy*.

119. Kang, H. Y., & Schoenung, J. M. (2005). Electronic waste recycling: A review of U.S. infrastructure and technology options. *Resources, Conservation and Recycling*.

120. Kansagara, R. (2018). Basics of PCB. *Circuit Digest*. Retrieved from <https://circuitdigest.com/tutorial/basics-of-pcb>

121. Khalil, A., Jouiad, M., Khraisheh, M., & Hashaikheh, R. (2014). Facile Synthesis of Copper Oxide Nanoparticles via Electrospinning. *Journal of Nanomaterials*, 2014.

122. Khandpur, R. S. (2006). Printed Circuit Boards: Design, Fabrication, Assembly and

Testing. Electronic engineering. McGraw-Hill Companies. Retrieved from <https://books.google.lt/books?id=h1RMPgAACAAJ>

123. Khashaba, U. A. (2003). Fracture behavior of woven composites containing various cracks geometry. *Journal of Composite Materials*.

124. Khodashenas, B., & Ghorbani, H. R. (2014). Synthesis of copper nanoparticles: An overview of the various methods. *Korean Journal of Chemical Engineering*.

125. Kim, J. W., Lee, A. S., Yu, S., & Han, J. W. (2018). En masse pyrolysis of flexible printed circuit board wastes quantitatively yielding environmental resources. *Journal of Hazardous Materials*.

126. Kobayashi, Y., Shirochi, T., Yasuda, Y., & Morita, T. (2011). Preparation of metallic copper nanoparticles in aqueous solution and their bonding properties. *Solid State Sciences*, 13(3), 553–558.

127. Kočí, V., & Loubal, T. (2012). LCA of Liquid Epoxy Resin Produced Based on Propylene and on Glycerine. *ACTA ENVIRONMENTALICA UNIVERSITATIS COMENIANAE (BRATISLAVA)*, 20, 62–67.

128. Kolias, K., Hahladakis, J. N., & Gidaracos, E. (2014). Assessment of toxic metals in waste personal computers. *Waste Management*, 34(8), 1480–1487.

129. Kooroshy, J. (2015). The Low Carbon Economy. Goldman Sachs Research.

130. Korhonen, J., Nuur, C., Feldmann, A., & Birkie, S. E. (2018). Circular economy as an essentially contested concept. *Journal of Cleaner Production*.

131. Krayushkina, K., Khmerik, T., Skrypchenko, O., Moshkovskiy, I., & Pershakov, V. (2017). Investigation of Fiber Concrete for Road and Bridge Building. *Procedia Engineering* (Vol. 187, pp. 620–627).

132. Kuang, G. C., Michaels, H. A., Simmons, J. T., Clark, R. J., & Zhu, L. (2010). Chelation-assisted, copper(II)-acetate-accelerated azide-alkyne cycloaddition. *Journal of Organic Chemistry*, 75(19), 6540–6548.

133. Kumar, A., Saini, H. S., & Kumar, S. (2017). Bioleaching of Gold and Silver from Waste Printed Circuit Boards by *Pseudomonas balearica* SAE1 Isolated from an e-Waste Recycling Facility. *Current Microbiology*, 1–8.

134. Lago, A. B., Carballo, R., Rodríguez-Hermida, S., & Vázquez-López, E. M. (2014). Copper(II) acetate/bis(4-pyridylthio)methane system: Synthesis, structural diversity, and single-crystal to single-crystal transformation. *Crystal Growth and Design*, 14(6), 3096–3109.

135. Lavanya, N., Radhakrishnan, S., & Sekar, C. (2012). Fabrication of hydrogen peroxide biosensor based on Ni doped SnO₂ nanoparticles. *Biosensors & bioelectronics*.

136. Leung, A. O. W., Duzgoren-Aydin, N. S., Cheung, K. C., & Wong, M. H. (2008). Heavy metals concentrations of surface dust from e-waste recycling and its human health implications in southeast China. *Environmental Science and Technology*.

137. Leung, A. O. W., Zheng, J., Yu, C. K., Liu, W. K., Wong, C. K. C., Cai, Z., & Wong, M. H. (2011). Polybrominated diphenyl ethers and polychlorinated dibenzo- P -dioxins and dibenzofurans in surface dust at an E-waste processing site in southeast China. *Environmental Science and Technology*.

138. Lewandowski, C. M. (2015). Gold, science and applications. CRC Press.

139. Lewis, H., & Ryan, A. (2010). Printing as an Alternative Manufacturing Process for Printed Circuit Boards, *New Trends in Technologies: Devices, Computer, Communication and Industrial Systems*. In M. J. Er (Ed.), *New Trends in Technologies: Devices, Computer, Communication and Industrial Systems*. InTech.

140. Li, F., Huang, X., Kong, T., Liu, X., Qin, Q., & Li, Z. (2009). Synthesis and characterization of PbS crystals via a solvothermal route. *Journal of Alloys and Compounds*.

141. Li, J., Lu, H., Guo, J., Xu, Z., & Zhou, Y. (2007). Recycle technology for recovering

resources and products from waste printed circuit boards. *Environmental Science and Technology*, 41(6), 1995–2000.

142. Li, J., Xu, Z., & Zhou, Y. (2007). Application of corona discharge and electrostatic force to separate metals and nonmetals from crushed particles of waste printed circuit boards. *Journal of Electrostatics*.

143. Li, J., Zhao, M., Gao, X., Wan, X., & Zhou, J. (2014). Modeling the stiffness, strength, and progressive failure behavior of woven fabric-reinforced composites. *Journal of Composite Materials*, 48(6), 735–747. Retrieved from [http://jcm.sagepub.com/content/48/6/735%5Cnfiles/20/Li ?](http://jcm.sagepub.com/content/48/6/735%5Cnfiles/20/Li%20et%20al%20-%20Modeling%20the%20stiffness%20and%20progressive%20failure%20behavior%20of%20woven%20fabric%20reinforced%20composites.pdf%5Cnfiles/24/735.html). - 2014 - Modeling the stiffness, strength, and progressive .pdf%5Cnfiles/24/735.html

144. Li, S., Sun, S., Liang, H., Zhong, S., & Yang, F. (2014). Production and characterization of polypropylene composites filled with glass fibre recycled from pyrolysed waste printed circuit boards. *Environmental Technology*, 35(21), 2743–2751. Retrieved from <http://www.tandfonline.com/doi/abs/10.1080/09593330.2014.920049>

145. Liang, G., Mo, Y., & Zhou, Q. (2010). Novel strategies of bioleaching metals from printed circuit boards (PCBs) in mixed cultivation of two acidophiles. *Enzyme and Microbial Technology*.

146. Lin, K. H., & Chiang, H. L. (2014). Liquid oil and residual characteristics of printed circuit board recycle by pyrolysis. *Journal of Hazardous Materials*, 271, 258–265.

147. Lin, Z., Li, N., Chen, Z., & Fu, P. (2017). The effect of Ni doping concentration on the gas sensing properties of Ni doped SnO₂. *Sensors and Actuators, B: Chemical*.

148. Liu, K., Zhang, Z., & Zhang, F. S. (2016). Advanced degradation of brominated epoxy resin and simultaneous transformation of glass fiber from waste printed circuit boards by improved supercritical water oxidation processes. *Waste Management*.

149. Liu, Q., Zhu, J., Zhang, L., & Qiu, Y. (2018). Recent advances in energy materials by electrospinning. *Renewable and Sustainable Energy Reviews*.

150. Liu, Y., Gao, P., Bu, X., Kuang, G., Liu, W., & Lei, L. (2014). Nanocrosses of lead sulphate as the negative active material of lead acid batteries. *Journal of Power Sources*.

151. Loftsson, T., & Duchêne, D. (2007). Cyclodextrins and their pharmaceutical applications. *International Journal of Pharmaceutics*.

152. Long, L., Sun, S., Zhong, S., Dai, W., Liu, J., & Song, W. (2010). Using vacuum pyrolysis and mechanical processing for recycling waste printed circuit boards. *Journal of Hazardous Materials*, 177(1–3), 626–632.

153. Long, Y. Y., Feng, Y. J., Cai, S. S., Ding, W. X., & Shen, D. S. (2013). Flow analysis of heavy metals in a pilot-scale incinerator for residues from waste electrical and electronic equipment dismantling. *Journal of Hazardous Materials*.

154. Longobardo, A. V. (2010). Glass Fibers for Printed Circuit Boards. In F. T. Wallenberger & P. A. Bingham (Eds.), *Fiberglass and Glass Technology: Energy-Friendly Compositions and Applications* (pp. 175–196). Boston, MA: Springer US. Retrieved from https://doi.org/10.1007/978-1-4419-0736-3_4

155. Lu, Y., & Xu, Z. (2016). Precious metals recovery from waste printed circuit boards: A review for current status and perspective. *Resources, Conservation and Recycling*.

156. Luo, C., Liu, C., Wang, Y., Liu, X., Li, F., Zhang, G., & Li, X. (2011). Heavy metal contamination in soils and vegetables near an e-waste processing site, south China. *Journal of Hazardous Materials*.

157. M.H.H. Al-Kuwaiti and A-H.I. Mourad. (2015). Effect of Different Environmental Conditions on the Mechanical Behavior of Plain Weave Woven Laminated Composites. *Procedia Engineering*.

158. Maguyon, M. C. C., Alfafara, C. G., Migo, V. P., Movillon, J. L., & Rebancos, C.

M. (2012). Recovery of copper from spent solid printed-circuit-board (PCB) wastes of a PCB manufacturing facility by two-step sequential acid extraction and electrochemical deposition. *Journal of Environmental Science and Management*.

159. De Marco, I., Caballero, B. M., Chomôn, M. J., Laresgoiti, M. F., Torres, A., Fernández, G., & Arnaiz, S. (2008). Pyrolysis of electrical and electronic wastes. *Journal of Analytical and Applied Pyrolysis*.

160. Materion Corporation. (2011). Surface Coating of Copper Alloy Strip for Electrical Connector Applications. Retrieved from <https://materion.com/-/media/files/pdfs/alloy/tech-briefs/at0017-0311---tech-briefs---surface-coating-of-copper-alloy-strip.pdf>

161. Matsumoto, Y., & Oshima, Y. (2014). Au and Cu recovery from printed boards by decomposition of epoxy resin in supercritical water. *Journal of Supercritical Fluids*, 95, 462–467.

162. Mavrokefalos, C. K., Hasan, M., Khunsin, W., Schmidt, M., Maier, S. A., Rohan, J. F., Compton, R. G., et al. (2017). Electrochemically modified boron-doped diamond electrode with Pd and Pd-Sn nanoparticles for ethanol electrooxidation. *Electrochimica Acta*.

163. Mei, C., Liu, J., Chuang, P. Y., Song, T. T., Tang, F. L., Su, H. L., Huang, J. C. A., et al. (2017). High-temperature ferromagnetism of Ni-doped PbPdO₂nanograin films synthesized by sol-gel spin-coating method. *Ceramics International*.

164. Meng, L., Wang, Z., Zhong, Y., Guo, L., Gao, J., Chen, K., Cheng, H., et al. (2017). Supergravity separation for recovering metals from waste printed circuit boards. *Chemical Engineering Journal*.

165. Menon, S., George, E., Osterman, M., & Pecht, M. (2015). High lead solder (over 85 %) solder in the electronics industry: RoHS exemptions and alternatives. *Journal of Materials Science: Materials in Electronics*.

166. Methods, S. T. (2015). ASTM-D5035 Standard Test Methods for Breaking Force and Elongation of Textile Fabrics (Strip Method). *Astm*.

167. Mirzajani, V., Farhadi, K., & Pourmortazavi, S. M. (2018). Catalytic effect of lead oxide nano- and microparticles on thermal decomposition kinetics of energetic compositions containing TEGDN/NC/DAG. *Journal of Thermal Analysis and Calorimetry*.

168. Mishra, D., & Rhee, Y.-H. (2010). Current research trends of microbiological leaching for metal recovery from industrial wastes. *Curr Res Technol Educ Topics Appl Microbiol Microb Biotechnol*.

169. Moriwaki, H., Yamada, K., & Usami, H. (2017). Electrochemical extraction of gold from wastes as nanoparticles stabilized by phospholipids. *Waste Management*, 60, 591–595.

170. Morones, J. R., Elechiguerra, J. L., Camacho, A., Holt, K., Kouri, J. B., Ramírez, J. T., & Yacaman, M. J. (2005). The bactericidal effect of silver nanoparticles. *Nanotechnology*, 16(10), 2346–2353.

171. Moroydor Derun, E., Tugrul, N., Senberber, F. T., Kipcak, A. S., & Piskin, S. (2014). The Optimization of Copper Sulfate and Tincalconite Molar Ratios on the Hydrothermal Synthesis of Copper Borates. *International Journal of Chemical, Molecular, Nuclear, Materials and Metallurgical Engineering*, 8(10), 1152–1156.

172. Mou, P., Xiang, D., & Duan, G. (2007). Products Made from Nonmetallic Materials Reclaimed from Waste Printed Circuit Boards. *Tsinghua Science and Technology*, 12(3), 276–283.

173. MSI MS-6163 Motherboard Manual, MSI Computer Corp. (2001). . Retrieved from http://pcrebuilding.altervista.org/9/download/55d5c664cee64_msi_mb_ms-6163.pdf

174. Mudd, G. M., Weng, Memary, Z. R., Northey, S. A., Giurco, D., Mohr, S., & Mason, L. (2012). Future Greenhouse Gas Emissions from Copper Mining: Assessing Clean Energy Scenarios. Sydney. Retrieved from <http://cfsites1.uts.edu.au/find/isf/publications/muddetal2012copperemissionscleanenergy.pdf>

175. Mulvaney, D. (2011). *Green Technology: An A-to-Z Guide*. Thousand Oaks, California. Retrieved from <http://sk.sagepub.com/reference/greentechnology>
176. Muniz-Miranda, M., Gellini, C., & Giorgetti, E. (2011). Surface-Enhanced Raman Scattering from Copper Nanoparticles Obtained by Laser Ablation. *The Journal of Physical Chemistry C*, 115(12), 5021–5027. Retrieved from <http://pubs.acs.org/doi/abs/10.1021/jp1086027>
177. Naik, N. K., & Shembekar, P. S. (1992). Notched strength of fabric laminates I: Prediction. *Composites Science and Technology*, 44(1), 1–12. Elsevier. Retrieved July 11, 2018, from <https://www.sciencedirect.com/science/article/pii/0266353892900204>
178. Nasrollahzadeh, M., Momeni, S. S., & Sajadi, S. M. (2017). Green synthesis of copper nanoparticles using *Plantago asiatica* leaf extract and their application for the cyanation of aldehydes using $K_4Fe(CN)_6$. *Journal of Colloid and Interface Science*, 506, 471–477.
179. National Center for Biotechnology Information. PubChem Compound Database; CID=24462. (n.d.). Retrieved November 29, 2017, from <https://pubchem.ncbi.nlm.nih.gov/compound/24462>
180. Nekouei, R. K., Pahlevani, F., Rajarao, R., Golmohammadzadeh, R., & Sahajwalla, V. (2018a). Two-step pre-processing enrichment of waste printed circuit boards: Mechanical milling and physical separation. *Journal of Cleaner Production*.
181. Nekouei, R. K., Pahlevani, F., Rajarao, R., Golmohammadzadeh, R., & Sahajwalla, V. (2018b). Direct transformation of waste printed circuit boards to nano-structured powders through mechanical alloying. *Materials and Design*, 141, 26–36.
182. Ning, C., Lin, C. S. K., Hui, D. C. W., & McKay, G. (2017). Waste Printed Circuit Board (PCB) Recycling Techniques. *Topics in Current Chemistry*.
183. Oh, C. J., Lee, S. O., Yang, H. S., Ha, T. J., & Kim, M. J. (2003). Selective leaching of valuable metals from waste printed circuit boards. *Journal of the Air & Waste Management Association* (1995).
184. Ojha, N. K., Zyryanov, G. V., Majee, A., Charushin, V. N., Chupakhin, O. N., & Santra, S. (2017). Copper nanoparticles as inexpensive and efficient catalyst: A valuable contribution in organic synthesis. *Coordination Chemistry Reviews*, 353, 1–57. Retrieved from <http://linkinghub.elsevier.com/retrieve/pii/S0010854517303296>
185. Ozbay, K., Jawad, D., Parker, N., & Hussain, S. (2003). *Guidelines for Life Cycle Cost Analysis*. October.
186. Pantaleo A., F. D. R. D. P. A. (2013). Structural silicone sealant modelling for wood frames: Influence of adhesion on bonding strength. *Journal of Adhesion Science and Technology*, 27(11), 1259–1277.
187. Panyakapo, P., & Panyakapo, M. (2008). Reuse of thermosetting plastic waste for lightweight concrete. *Waste Management*.
188. Park, N. G. (2015). Perovskite solar cells: An emerging photovoltaic technology. *Materials Today*.
189. Park, Y. J., & Fray, D. J. (2009). Recovery of high purity precious metals from printed circuit boards. *Journal of Hazardous Materials*, 164(2–3), 1152–1158.
190. Perkins, D. N., Brune Drisse, M. N., Nxele, T., & Sly, P. D. (2014). E-waste: A global hazard. *Annals of Global Health*.
191. Permatex. (n.d.). Permatex® Clear RTV Silicone Adhesive Sealant. Retrieved March 13, 2018, from <https://www.permatex.com/products/adhesives-sealants/sealants/permatex-clear-rtv-silicone-adhesive-sealant/>
192. Petter, P. M. H., Veit, H. M., & Bernardes, A. M. (2014). Evaluation of gold and silver leaching from printed circuit board of cellphones. *Waste Management*.
193. Poll, C. G., & Payne, D. J. (2014). Electrochemical synthesis of PbO_2 , Pb_3O_4 and

PbO films on a transparent conducting substrate. *Electrochimica Acta*.

194. Pomponi, F., & Moncaster, A. (2017). Circular economy for the built environment: A research framework. *Journal of Cleaner Production*.

195. Pradhan, J. K., & Kumar, S. (2014). Informal e-waste recycling: Environmental risk assessment of heavy metal contamination in Mandoli industrial area, Delhi, India. *Environmental Science and Pollution Research*.

196. Printed Circuit Board Introduction & PCB Types. (2018). PCBCART. Retrieved from <https://www.pcbcart.com/article/content/PCB-introduction.html>

197. Priya, A., & Hait, S. (2018). Toxicity characterization of metals from various waste printed circuit boards. *Process Safety and Environmental Protection*.

198. Puckett, J., Byster, L., Westervelt, S., Gutierrez, R., Davis, S., Hussain, A., Dutta, M., et al. (2002). Exporting harm: the high-tech trashing of Asia. The Basel Action Network, Seattle.

199. PwC – Sustainable Performance and Strategy. (2016). Life cycle assessment of CFGF – Continuous Filament Glass Fibre Products. Retrieved from http://www.glassfibreurope.eu/wp-content/uploads/2016/11/LCA-report-CFGF-products_20161031_PwC.pdf

200. Quan, C., Li, A., & Gao, N. (2010). Synthesis of carbon nanotubes and porous carbons from printed circuit board waste pyrolysis oil. *Journal of Hazardous Materials*, 179(1–3), 911–917.

201. Quan, C., Li, A., Gao, N., & Dan, Z. (2010). Characterization of products recycling from PCB waste pyrolysis. *Journal of Analytical and Applied Pyrolysis*.

202. Raffi, M., Mehrwan, S., Bhatti, T. M., Akhter, J. I., Hameed, A., Yawar, W., & Ul Hasan, M. M. (2010). Investigations into the antibacterial behavior of copper nanoparticles against *Escherichia coli*. *Annals of Microbiology*, 60(1), 75–80.

203. Rafique, M., Shaikh, A. J., Rasheed, R., Tahir, M. B., Bakhat, H. F., Rafique, M. S., & Rabbani, F. (2017). A Review on Synthesis, Characterization and Applications of Copper Nanoparticles Using Green Method. *Nano*, 12(04), 1750043. Retrieved from <http://www.worldscientific.com/doi/abs/10.1142/S1793292017500436>

204. Rajagopal, R. R., Rajarao, R., Cholake, S. T., & Sahajwalla, V. (2017). Sustainable composite panels from non-metallic waste printed circuit boards and automotive plastics. *Journal of Cleaner Production*.

205. Rath, M. K., & Sahu, S. K. (2011). Static behavior of woven fiber-laminated composites in hygrothermal environment. *Journal of Reinforced Plastics and Composites*, 30(21), 1771–1781. Retrieved from <https://doi.org/10.1177/0731684411426811>

206. Recycling, I. (2008). Report on the Environmental Benefits of Recycling. October, (April), 49. Retrieved from <http://www.thenbs.com/topics/DesignSpecification/articles/benefitsMasterSpecifications.asp>

207. Richardson, H. W. (1997). Handbook of Copper Compounds and Applications. *Journal of neurology, neurosurgery, and psychiatry*.

208. Robinson, B. H. (2009). E-waste: An assessment of global production and environmental impacts. *Science of the Total Environment*.

209. Rocchetti, L., Amato, A., & Beolchini, F. (2018). Printed circuit board recycling: A patent review. *Journal of Cleaner Production*. Retrieved January 29, 2018, from <http://linkinghub.elsevier.com/retrieve/pii/S0959652618300842>

210. La Rosa, A. D., Banatao, D. R., Pastine, S. J., Latteri, A., & Cicala, G. (2016). Recycling treatment of carbon fibre/epoxy composites: Materials recovery and characterization and environmental impacts through life cycle assessment. *Composites Part B: Engineering*, 104, 17–25. Elsevier. Retrieved May 11, 2017, from

<http://www.sciencedirect.com/science/article/pii/S1359836816306898>

211. Ruparelia, J. P., Chatterjee, A. K., Duttagupta, S. P., & Mukherji, S. (2008). Strain specificity in antimicrobial activity of silver and copper nanoparticles. *Acta Biomaterialia*, 4(3), 707–716.
212. Samuelsson, C., & Björkman, B. (2014). Copper Recycling. *Handbook of Recycling: State-of-the-art for Practitioners, Analysts, and Scientists*.
213. Shackery, I., Patil, U., Pezeshki, A., Shinde, N. M., Kang, S., Im, S., & Jun, S. C. (2016). Copper Hydroxide Nanorods Decorated Porous Graphene Foam Electrodes for Non-enzymatic Glucose Sensing. *Electrochimica Acta*.
214. Shen, J., Li, F., Yin, B., Sun, L., Chen, C., Wen, S., Chen, Y., et al. (2017). Enhanced ethyl acetate sensing performance of Al-doped In₂O₃ microcubes. *Sensors and Actuators, B: Chemical*.
215. Shen, Y., Chen, X., Ge, X., & Chen, M. (2018a). Thermochemical treatment of non-metallic residues from waste printed circuit board: Pyrolysis vs. combustion. *Journal of Cleaner Production*.
216. Shen, Y., Chen, X., Ge, X., & Chen, M. (2018b). Chemical pyrolysis of E-waste plastics: Char characterization. *Journal of Environmental Management*.
217. Shokri, A., Pahlevani, F., Levick, K., Cole, I., & Sahajwalla, V. (2017). Synthesis of copper-tin nanoparticles from old computer printed circuit boards. *Journal of Cleaner Production*, 142, 2586–2592.
218. Sichina, W. J. (2000). Application note: Prediction of Epoxy Cure Properties Using Pyris DSC Scanning Kinetics Software. *Thermal Analysis, PerkinElmer Instruments*.
219. Silvas, F. P. C., Jiménez Correa, M. M., Caldas, M. P. K., de Moraes, V. T., Espinosa, D. C. R., & Tenório, J. A. S. (2015). Printed circuit board recycling: Physical processing and copper extraction by selective leaching. *Waste Management*.
220. Silverstein, R. M., Webster, F. X., Kiemle, D., & Einholm, E. J. (2005). *Spectrometric Identification of Organic Compounds*, 7th Edition. *Journal of Magnetic Resonance, Series A*. Retrieved from <http://linkinghub.elsevier.com/retrieve/pii/S106418589690145X%5Cnhttps://books.google.com/books?id=mQ8cAAAAQBAJ&pgis=1>
221. Singho, N. D., Lah, N. A. C., Johan, M. R., & Ahmad, R. (2012). FTIR studies on silver-poly(methylmethacrylate) nanocomposites via in-situ polymerization technique. *International Journal of Electrochemical Science*, 7(6), 5596–5603.
222. Smith, A. C. (1985). The thermal characterization of epoxide resins. (G. E. Company, Ed.) *GEC journal of research*, 3(3), 162–166. Retrieved from <http://www.refdoc.fr/Detailnotice?idarticle=12508877>
223. SonDI, I., & Salopek-SonDI, B. (2004). Silver nanoparticles as antimicrobial agent: A case study on *E. coli* as a model for Gram-negative bacteria. *Journal of Colloid and Interface Science*, 275(1), 177–182.
224. Song, Q., & Li, J. (2015). A review on human health consequences of metals exposure to e-waste in China. *Environmental Pollution*.
225. Song, Q., Li, J., & Zeng, X. (2015). Minimizing the increasing solid waste through zero waste strategy. *Journal of Cleaner Production*, 104, 199–210.
226. Suárez-Cerda, J., Espinoza-Gómez, H., Alonso-Núñez, G., Rivero, I. A., Gochi-Ponce, Y., & Flores-López, L. Z. (2016). A green synthesis of copper nanoparticles using native cyclodextrins as stabilizing agents. *Journal of Saudi Chemical Society*, 341–348.
227. Sun, Z., Cao, H., Zhang, X., Lin, X., Zheng, W., Cao, G., Sun, Y., et al. (2017). Spent lead-acid battery recycling in China – A review and sustainable analyses on mass flow of lead. *Waste Management*.

228. Sun, Z., Shen, Z., Ma, S., & Zhang, X. (2015). Sound absorption application of fiberglass recycled from waste printed circuit boards. *Materials and Structures/Materiaux et Constructions*, 48(1–2), 387–392.
229. Suresha, B., Chandramohan, G., Renukappa, N. M., & Siddaramaiah. (2007). Mechanical and tribological properties of glass-epoxy composites with and without graphite particulate filler. *Journal of Applied Polymer Science*.
230. Szejtli, J. (2005). Past, Present, and Future of Cyclodextrin Research. *ChemInform*, 36(17). Retrieved from <http://doi.wiley.com/10.1002/chin.200517261>
231. Tang, J., Wang, H., & Gomez, A. (2017). Controlled nanoparticle synthesis via opposite-polarity electrospray pyrolysis. *Journal of Aerosol Science*, 113, 201–211.
232. Tatariants, M., Yousef, S., Denafas, G., & Bendikiene, R. (2018). Separation and purification of metal and fiberglass extracted from waste printed circuit boards using milling and dissolution techniques. *Environmental Progress and Sustainable Energy*.
233. Tatariants, M., Yousef, S., Denafas, G., Tichonovas, M., & Bendikiene, R. (2018). Recovery of gold, other metallic and non-metallic components of full-size waste random access memory. *Journal of Cleaner Production*, 172, 2811–2823. Retrieved from <https://www.sciencedirect.com/science/article/pii/S0959652617328056>
234. Tatariants, M., Yousef, S., Sakalauskaitė, S., Daugelavičius, R., Denafas, G., & Bendikiene, R. (2018). Antimicrobial copper nanoparticles synthesized from waste printed circuit boards using advanced chemical technology. *Waste Management*, 78, 521–531. Pergamon. Retrieved July 27, 2018, from <https://www.sciencedirect.com/science/article/pii/S0956053X18303702>
235. Tatariants, M., Yousef, S., Sitaraviciute, R., Denafas, G., & Bendikiene, R. (2017). Characterization of waste printed circuit boards recycled using a dissolution approach and ultrasonic treatment at low temperatures. *RSC Adv.*, 7(60), 37729–37738. The Royal Society of Chemistry. Retrieved from <http://xlink.rsc.org/?DOI=C7RA07034A>
236. Tatariants, M., Yousef, S., Skapas, M., Juskenas, R., Makarevicius, V., Lukošiušė, S. I., & Denafas, G. (2018). Industrial technology for mass production of SnO₂ nanoparticles and PbO₂ microcube/microcross structures from electronic waste. *Journal of Cleaner Production*.
237. The European Parliament, & The Council Of The European Union. (2003). Directive 2002/96/EC Of The European Parliament And Of The Council of 27 January 2003 on waste electrical and electronic equipment (WEEE). *Official Journal of the European Union*, L37, 24–38.
238. The International Standards Organisation. (2006). Environmental management — Life cycle assessment — Principles and framework. Iso 14040.
239. Torres, R., & Lapidus, G. T. (2016). Copper leaching from electronic waste for the improvement of gold recycling. *Waste Management*, 57, 131–139.
240. Tuncuk, A., Stazi, V., Akcil, A., Yazici, E. Y. Y., & Deveci, H. (2012). Aqueous metal recovery techniques from e-scrap: Hydrometallurgy in recycling. *Minerals Engineering*, 25(1), 28–37. Pergamon. Retrieved April 8, 2019, from <https://www.sciencedirect.com/science/article/pii/S0892687511003669#b0345>
241. Turner, D. A., Williams, I. D., & Kemp, S. (2015). Greenhouse gas emission factors for recycling of source-segregated waste materials. *Resources, Conservation and Recycling*, 105, 186–197.
242. Umair, S., Björklund, A., & Petersen, E. E. (2015). Social impact assessment of informal recycling of electronic ICT waste in Pakistan using UNEP SETAC guidelines. *Resources, Conservation and Recycling*, 95, 46–57.
243. Veit, H. M., & Bernardes, A. M. (2015). Electronic waste: Generation and management. *Electronic Waste: Recycling Techniques*.

244. Veit, H. M., Bernardes, A. M., Ferreira, J. Z., Tenório, J. A. S., & Malfatti, C. de F. (2006). Recovery of copper from printed circuit boards scraps by mechanical processing and electrometallurgy. *Journal of Hazardous Materials*.
245. Venkateswara Reddy, P., Venkatramana Reddy, S., & Sankara Reddy, B. (2016). Synthesis and properties of (Fe, Al) co-doped SnO₂ nanoparticles. *Materials Today: Proceedings*, 3(6), 1752–1761. Elsevier. Retrieved July 18, 2018, from <https://www.sciencedirect.com/science/article/pii/S2214785316300876>
246. Verma, H. R., Singh, K. K., & Basha, S. M. (2018). Effect of Milling Parameters on the Concentration of Copper Content of Hammer-Milled Waste PCBs: A Case Study. *Journal of Sustainable Metallurgy*, 4(2), 187–193. Retrieved from <https://doi.org/10.1007/s40831-018-0179-z>
247. Verma, H. R., Singh, K. K., & Mankhand, T. R. (2016). Dissolution and separation of brominated epoxy resin of waste printed circuit boards by using di-methyl formamide. *Journal of Cleaner Production*, 139, 586–596.
248. Verma, H. R., Singh, K. K., & Mankhand, T. R. (2017a). Delamination mechanism study of large size waste printed circuit boards by using dimethylacetamide. *Waste Management*, 65, 139–146.
249. Verma, H. R., Singh, K. K., & Mankhand, T. R. (2017b). Liberation of metal clads of waste printed circuit boards by removal of halogenated epoxy resin substrate using dimethylacetamide. *Waste Management*, 60, 652–659.
250. Verma, H. R., Singh, K. K., & Mankhand, T. R. (2017c). Comparative study of printed circuit board recycling by cracking of internal layers using organic solvents-dimethylformamide and dimethylacetamide. *Journal of Cleaner Production*, 142, 1721–1727.
251. VGA Legacy MKIII - graphic cards since 1981! (2015). . Retrieved March 13, 2018, from <http://www.vgamuseum.info/index.php/component/k2/item/445-trident-tvga9000i-3>
252. Wang, H., Hirahara, M., Goto, M., & Hirose, T. (2004). Extraction of flame retardants from electronic printed circuit board by supercritical carbon dioxide. *The Journal of Supercritical Fluids*.
253. Wang, H., Zhang, G., Hao, J., He, Y., Zhang, T., & Yang, X. (2018). Morphology, mineralogy and separation characteristics of nonmetallic fractions from waste printed circuit boards. *Journal of Cleaner Production*.
254. Wang, H., Zhang, S., Li, B., Pan, D., Wu, Y., & Zuo, T. (2017). Recovery of waste printed circuit boards through pyrometallurgical processing: A review. *Resources, Conservation and Recycling*.
255. Wang, J., Guo, J., & Xu, Z. (2015). An environmentally friendly technology of disassembling electronic components from waste printed circuit boards. *Waste Management*, 53, 218–224. Retrieved from <http://dx.doi.org/10.1016/j.wasman.2016.03.036>
256. Wang, J., Lu, C., Liu, X., Wang, Y., Zhu, Z., & Meng, D. (2017). Synthesis of tin oxide (SnO & SnO₂) micro/nanostructures with novel distribution characteristic and superior photocatalytic performance. *Materials and Design*.
257. Wang, J., & Xu, Z. (2015). Disposing and recycling waste printed circuit boards: Disconnecting, resource recovery, and pollution control. *Environmental Science and Technology*.
258. Wang, L., & Ge, H. (2017). Effect of air leakage on the hygrothermal performance of highly insulated wood frame walls: Comparison of air leakage modelling methods. *Building and Environment*, 123, 363–377.
259. Wang, R., Zhang, T., & Wang, P. (2012). Waste printed circuit boards nonmetallic powder as admixture in cement mortar. *Materials and Structures/Materiaux et Constructions*.
260. Wath, S. B., Katariya, M. N., Singh, S. K., Kanade, G. S., & Vaidya, A. N. (2015). Separation of WPCBs by dissolution of brominated epoxy resins using DMSO and NMP: A

comparative study. *Chemical Engineering Journal*, 280, 391–398. Retrieved from <http://linkinghub.elsevier.com/retrieve/pii/S1385894715008463>

261. Wills, B. a, & Napier-munn, T. (2006). *Mineral Processing Technology:An Introduction to the Practical Aspects of Ore Treatment and Mineral Recovery*. October.

262. Woltman, G., Noel, M., & Fam, A. (2017). Experimental and numerical investigations of thermal properties of insulated concrete sandwich panels with fiberglass shear connectors. *Energy and Buildings*, 145, 22–31.

263. Wong, C. S. C., Duzgoren-Aydin, N. S., Aydin, A., & Wong, M. H. (2007). Evidence of excessive releases of metals from primitive e-waste processing in Guiyu, China. *Environmental Pollution*.

264. Xi, G., Peng, Y., Xu, L., Zhang, M., Yu, W., & Qian, Y. (2004). Selected-control synthesis of PbO₂ submicrometer-sized hollow spheres and Pb₃O₄ microtubes. *Inorganic Chemistry Communications*.

265. Xing, M., & Zhang, F. S. (2013). Degradation of brominated epoxy resin and metal recovery from waste printed circuit boards through batch sub/supercritical water treatments. *Chemical Engineering Journal*, 219, 131–136.

266. Xiu, F. R., Weng, H., Qi, Y., Yu, G., Zhang, Z., Zhang, F. S., & Chen, M. (2017). A novel recovery method of copper from waste printed circuit boards by supercritical methanol process: Preparation of ultrafine copper materials. *Waste Management*, 60, 643–651.

267. Xiu, F. R., & Zhang, F. S. (2009). Preparation of nano-Cu₂O/TiO₂ photocatalyst from waste printed circuit boards by electrokinetic process. *Journal of Hazardous Materials*, 172(2–3), 1458–1463.

268. Xiu, F. R., & Zhang, F. S. (2010). Materials recovery from waste printed circuit boards by supercritical methanol. *Journal of Hazardous Materials*, 178(1–3), 628–634.

269. Xu, B., Lin, Z., Xian, J., Huo, Z., Cao, L., Wang, Y., Gaosun, W., et al. (2016). Preparation and characterization of polypropylene composites with nonmetallic materials recycled from printed circuit boards. *Journal of Thermoplastic Composite Materials*.

270. Xue, M., Yang, Y., Ruan, J., & Xu, Z. (2012). Assessment of noise and heavy metals (Cr, Cu, Cd, Pb) in the ambience of the production line for recycling waste printed circuit boards. *Environmental science & technology*.

271. Yamawaki, T. (2003). The gasification recycling technology of plastics WEEE containing brominated flame retardants. *Fire and Materials*.

272. Yang, C., Li, J., Tan, Q., Liu, L., & Dong, Q. (2017). Green Process of Metal Recycling: Coprocessing Waste Printed Circuit Boards and Spent Tin Stripping Solution. *ACS Sustainable Chemistry and Engineering*.

273. Yang, G., Wang, L., Wang, J., & Yan, W. (2017). Fabrication and formation mechanism of Li₂MnO₃ultrathin porous nanobelts by electrospinning. *Ceramics International*, 43(1), 71–76.

274. Yang, S., Bai, S., & Wang, Q. (2015). Preparation of fine fiberglass-resin powders from waste printed circuit boards by different milling methods for reinforcing polypropylene composites. *Journal of Applied Polymer Science*, 132(35). Wiley Online Library. Retrieved from <http://dx.doi.org/10.1002/app.42494>

275. Yang, X., Sun, L., Xiang, J., Hu, S., & Su, S. (2013). Pyrolysis and dehalogenation of plastics from waste electrical and electronic equipment (WEEE): A review. *Waste Management*.

276. Yazici, E. Y., & Deveci, H. (2015). Cupric chloride leaching (HCl-CuCl₂-NaCl) of metals from waste printed circuit boards (WPCBs). *International Journal of Mineral Processing*, 134, 89–96.

277. Ye, Z., Yang, F., Qiu, Y., Chen, N., Lin, W., & Sun, S. (2018). The debrominated

and lightweight oil generated from two stage pyrolysis of WPCBs by using compound chemical additives. *Process Safety and Environmental Protection*.

278. Yin, J., Li, G., He, W., Huang, J., & Xu, M. (2011). Hydrothermal decomposition of brominated epoxy resin in waste printed circuit boards. *Journal of Analytical and Applied Pyrolysis*, 92(1), 131–136.

279. Ylä-Mella, J., Poikela, K., Lehtinen, U., Keiski, R. L., & Pongrácz, E. (2014). Implementation of Waste Electrical and Electronic Equipment Directive in Finland: Evaluation of the collection network and challenges of the effective WEEE management. *Resources, Conservation and Recycling*.

280. Yoshida, A., Terazono, A., Ballesteros, F. C., Nguyen, D. Q., Sukandar, S., Kojima, M., & Sakata, S. (2016). E-waste recycling processes in Indonesia, the Philippines, and Vietnam: A case study of cathode ray tube TVs and monitors. *Resources, Conservation and Recycling*, 106, 48–58.

281. Yousef, S., Tatariants, M., Makarevicius, V., Lukošiušė, S.-I., Bendikiene, R., Denafas, G., Makarevičius, V., et al. (2018). A strategy for synthesis of copper nanoparticles from recovered metal of waste printed circuit boards. *Journal of Cleaner Production*, 185, 653–664. Elsevier. Retrieved May 5, 2018, from <https://www.sciencedirect.com/science/article/pii/S0959652618306875>

282. Yuhana, N. Y., Ahmad, S., & Bahri, A. R. S. (2012). The effect of ultrasonic treatment on thermal stability of the cured epoxy/layered silicate nanocomposite. *Advances in Materials Science and Engineering*.

283. Yung, K. C., Zhu, B. L., Wu, J., Yue, T. M., & Xie, C. S. (2007). Effect of AlN content on the performance of brominated epoxy resin for printed circuit board substrate. *Journal of Polymer Science, Part B: Polymer Physics*, 45(13), 1662–1674. Wiley Subscription Services, Inc., A Wiley Company. Retrieved June 7, 2017, from <http://doi.wiley.com/10.1002/polb.21201>

284. Zain, N. M., Stapley, A. G. F., & Shama, G. (2014). Green synthesis of silver and copper nanoparticles using ascorbic acid and chitosan for antimicrobial applications. *Carbohydrate Polymers*, 112, 195–202.

285. Zaman, A. U. (2014). Identification of key assessment indicators of the zero waste management systems. *Ecological Indicators*.

286. Zeng, X., & Li, J. (2016). Measuring the recyclability of e-waste: An innovative method and its implications. *Journal of Cleaner Production*, 131, 156–162.

287. Zeng, X., Yang, C., Chiang, J. F., & Li, J. (2017). Innovating e-waste management: From macroscopic to microscopic scales. *Science of the Total Environment*.

288. Zhan, L., Xiang, X., Xie, B., & Sun, J. (2016). A novel method of preparing highly dispersed spherical lead nanoparticles from solders of waste printed circuit boards. *Chemical Engineering Journal*, 303, 261–267.

289. Zhang, G., Wang, H., He, Y., Yang, X., Peng, Z., Zhang, T., & Wang, S. (2017). Triboelectric separation technology for removing inorganics from non-metallic fraction of waste printed circuit boards: Influence of size fraction and process optimization. *Waste Management*.

290. Zhang, L., & Xu, Z. (2016). A review of current progress of recycling technologies for metals from waste electrical and electronic equipment. *Journal of Cleaner Production*.

291. Zhang, S., Ding, Y., Liu, B., & Chang, C. chi. (2017). Supply and demand of some critical metals and present status of their recycling in WEEE. *Waste Management*.

292. Zhang, X., Guan, J., Guo, Y., Yan, X., Yuan, H., Xu, J., Guo, J., et al. (2015). Selective Desoldering Separation of Tin-Lead Alloy for Dismantling of Electronic Components from Printed Circuit Boards. *ACS Sustainable Chemistry and Engineering*.

293. Zheng, J., Chen, K. hui, Yan, X., Chen, S. J., Hu, G. C., Peng, X. W., Yuan, J. gang, et al. (2013). Heavy metals in food, house dust, and water from an e-waste recycling area in South

China and the potential risk to human health. *Ecotoxicology and Environmental Safety*.

294. Zheng, Y., Shen, Z., Cai, C., Ma, S., & Xing, Y. (2009a). Influence of nonmetals recycled from waste printed circuit boards on flexural properties and fracture behavior of polypropylene composites. *Materials and Design*.

295. Zheng, Y., Shen, Z., Cai, C., Ma, S., & Xing, Y. (2009b). The reuse of nonmetals recycled from waste printed circuit boards as reinforcing fillers in the polypropylene composites. *Journal of Hazardous Materials*, 163(2–3), 600–606.

296. Zhou, X., Guo, J., Lin, K., Huang, K., & Deng, J. (2013). Leaching characteristics of heavy metals and brominated flame retardants from waste printed circuit boards. *Journal of Hazardous Materials*.

297. Zhu, L., Zhou, J., Guo, Z., & Sun, Z. (2015). An overview of materials issues in resistive random access memory. *Journal of Materiomics*.

298. Zhu, N., Xiang, Y., Zhang, T., Wu, P., Dang, Z., Li, P., & Wu, J. (2011). Bioleaching of metal concentrates of waste printed circuit boards by mixed culture of acidophilic bacteria. *Journal of Hazardous Materials*.

299. Zhu, P., Chen, Y., Wang, L., Qian, G., Zhang, W. J., Zhou, M., & Zhou, J. (2013). Dissolution of brominated epoxy resins by dimethyl sulfoxide to separate waste printed circuit boards. *Environmental Science and Technology*, 47(6), 2654–2660.

300. Zhu, P., Chen, Y., Wang, L. Y., Qian, G. R., Zhou, M., & Zhou, J. (2013). A novel approach to separation of waste printed circuit boards using dimethyl sulfoxide. *International Journal of Environmental Science and Technology*, 10(1), 175–180.

301. Zhu, P., Chen, Y., Wang, L. Y., Qian, G. Y., Zhou, M., & Zhou, J. (2012). A new technology for separation and recovery of materials from waste printed circuit boards by dissolving bromine epoxy resins using ionic liquid. *Journal of Hazardous Materials*, 239–240, 270–278.

302. Zhu, P., Chen, Y., Wang, L. Y., Zhou, M., & Zhou, J. (2013). The separation of waste printed circuit board by dissolving bromine epoxy resin using organic solvent. *Waste Management*, 33(2), 484–488.

303. Zin, V., Agresti, F., Barison, S., Colla, L., Gondolini, A., & Fabrizio, M. (2013). The synthesis and effect of copper nanoparticles on the tribological properties of lubricant oils. *IEEE Transactions on Nanotechnology*, 12(5), 751–759.

304. Žiukaite, S., Ivanauskas, R., Tatariants, M., & Denafas, G. (2017). Feasibilities for hydrometallurgical recovery of precious metals from waste printed circuit boards in Lithuania. *Chemija*, 28(2), 109–116.

LIST OF SCIENTIFIC PUBLICATIONS ON THE DISSERTATION TOPIC

Publications, listed in Web of Science database:

1. Tatariants, M., Yousef, S., Denafas, G., & Bendikiene, R. (2018). Separation and purification of metal and fiberglass extracted from waste printed circuit boards using milling and dissolution techniques. *Environmental Progress and Sustainable Energy* [IF 2017: 1.326];
2. Tatariants, M., Yousef, S., Denafas, G., Tichonovas, M., & Bendikiene, R. (2018). Recovery of gold, other metallic and non-metallic components of full-size waste random access memory. *Journal of Cleaner Production*, 172, 2811–2823. [IF 2017: 5.651];
3. Tatariants, M., Yousef, S., Sakalauskaitė, S., Daugelavičius, R., Denafas, G., & Bendikiene, R. (2018). Antimicrobial copper nanoparticles synthesized from waste printed circuit boards using advanced chemical technology. *Waste Management*, 78, 521–531. [IF 2017: 4.723];
4. Tatariants, M., Yousef, S., Sidaraviciute, R., Denafas, G., & Bendikiene, R. (2017). Characterization of waste printed circuit boards recycled using a dissolution approach and ultrasonic treatment at low temperatures. *RSC Adv.*, 7(60), 37729–37738. [IF 2017: 2.936];
5. Tatariants, M., Yousef, S., Skapas, M., Juskenas, R., Makarevicius, V., Lukošiuūtė, S. I., & Denafas, G. (2018). Industrial technology for mass production of SnO₂ nanoparticles and PbO₂ microcube/microcross structures from electronic waste. *Journal of Cleaner Production*. [IF 2017: 5.651];
6. Yousef, S., Tatariants, M., Bendikiene, R., & Denafas, G. (2017). Mechanical and thermal characterizations of non-metallic components recycled from waste printed circuit boards. *Journal of Cleaner Production*, 167(Supplement C), 271–280. [IF 2017: 5.651];
7. Yousef, S., Tatariants, M., Makarevicius, V., Lukošiuūtė, S.-I., Bendikiene, R., Denafas, G., Makarevičius, V., et al. (2018). A strategy for synthesis of copper nanoparticles from recovered metal of waste printed circuit boards. *Journal of Cleaner Production*, 185, 653–664. [IF 2017: 5.651];
8. Yousef, S., Tatariants, M., Tichonovas, M., Bendikiene, R., & Denafas, G. (2018). Recycling of bare waste printed circuit boards as received using an organic solvent technique at a low temperature. *Journal of Cleaner Production*. [IF 2017: 5.651];
9. Žiukaite, S., Ivanauskas, R., Tatariants, M., & Denafas, G. (2017). Feasibilities for hydrometallurgical recovery of precious metals from waste printed circuit boards in Lithuania. *Chemija*, 28(2), 109–116. [IF 2017: 0.394].

Publications, listed in conferences:

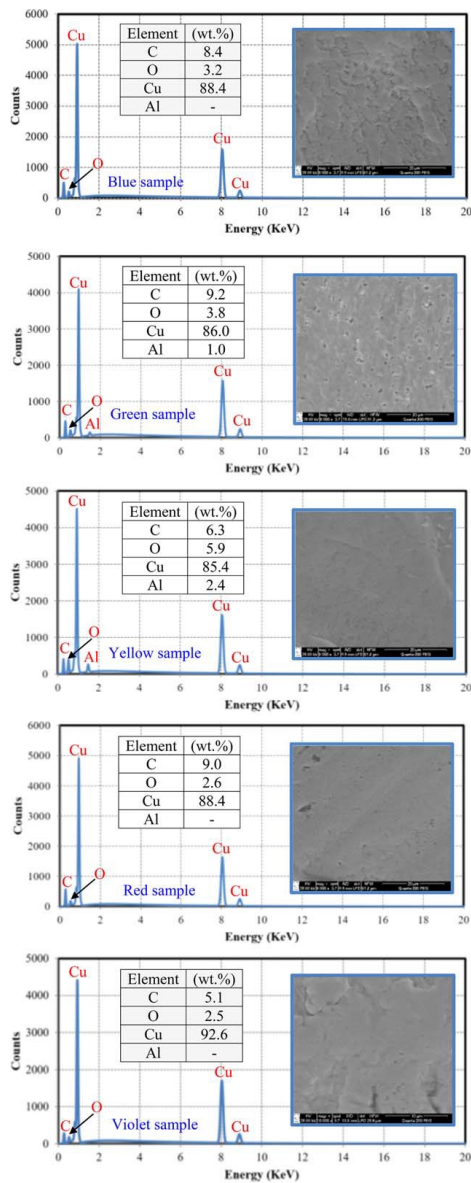
1. Tatariants M., Yousef S., Denafas G., & Bendikienė R. (2017). Recycling of full-size waste printed circuit boards using an organic solvent, *Chemistry and chemical technology 2017 : proceedings of the international conference*, Kaunas. Kaunas : Kauno technologijos universitetas. ISSN 2538-7359, p. 109;
2. Tatariants, M.; Yousef, S.; Denafas, G., & Bendikiene, R. (2018). Environmentally-friendly and efficient technology for recycling of waste printed circuit boards, Актуальные проблемы экологии: сборник научных статей по материалам XIII международной научно-практической конференции, Гродно, 3–5 октября 2018 г. / Гродненский государственный университет имени Янки Купалы (Беларусь), ISBN 9789857134426, , p. 255-256;
3. Yousef S., Tatariants M., Bendikienė R., & G. Denafas. (2017). Recycling and characterization of printed circuit boards, *Materials Engineering 2017: 26th international Baltic conference*, October 26-27, Kaunas, Lithuania : conference book. Kaunas : Kauno technologijos universitetas. ISSN 2029-8307, p. 37.

ANNEXES

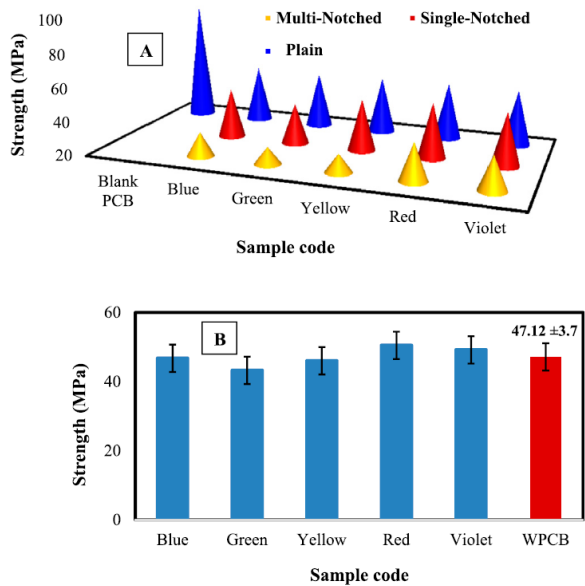
Annex 1 Potential environmental contaminants arising from E-waste disposal or recycling (Robinson, 2009)

Contaminant	Relationship with E-waste	Typical E-waste concentration (mg/kg)	Annual global emission in E-waste (tons)
Polybrominated diphenyl ethers (PBDEs) polybrominated biphenyls (PBBs) tetrabromobisphenol-A (TBBPA)	Flame retardants		
Polychlorinated biphenyls (PCB)	Condensers, transformers	14	280
Chlorofluorocarbon (CFC)	Cooling units, insulation foam		
Polycyclic aromatic hydrocarbons (PAHs)	Product of combustion		
Polyhalogenated aromatic hydrocarbons (PHAHs)	Product of low-temperature combustion		
Polychlorinated dibenzo- <i>p</i> -dioxins (PCDDs), polychlorinated dibenzofurans (PCDFs)	Product of low-temperature combustion of PVCs and other plastics		
Americium (Am)	Smoke detectors		
Antimony (Sb)	Flame retardants, plastics (Ernst, Popp, Wolf, & Van Eldik, 2003)	1700	34,000
Arsenic (As)	Doping material for Si		
Barium (Ba)	Getters in cathode ray tubes (CRTs)		
Beryllium (Be)	Silicon-controlled rectifiers		
Cadmium (Cd)	Batteries, toners, plastics	180	3600
Chromium (Cr)	Data tapes and floppy disks	9900	198,000
Copper (Cu)	Wiring	41,000	820,000
Gallium (Ga)	Semiconductors		
Indium (In)	LCD displays		
Lead (Pb)	Solder (Kang & Schoenung, 2005), CRTs, batteries	2900	58,000
Lithium (Li)	Batteries		
Mercury (Hg)	Fluorescent lamps, batteries, switches	0.68	13.6
Nickel (Ni)	Batteries	10,300	206,000
Selenium (Se)	Rectifiers		
Silver (Ag)	Wiring, switches		
Tin (Sn)	Solder (Kang & Schoenung, 2005), LCD screens	2400	48,000
Zinc (Zn)		5100	102,000
Rare earth elements	CRT screens		

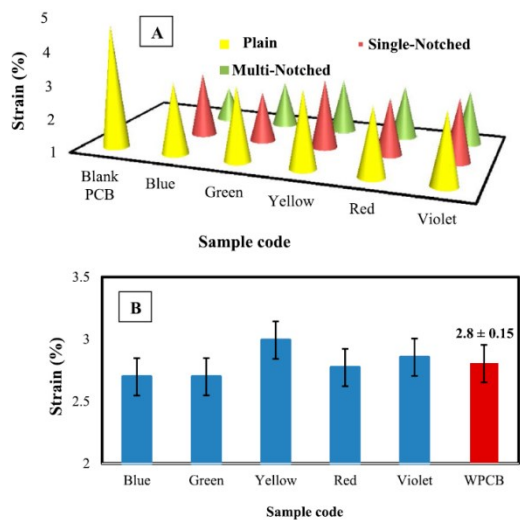
Annex 2 SEM images and EDS analysis of recovered metal powder



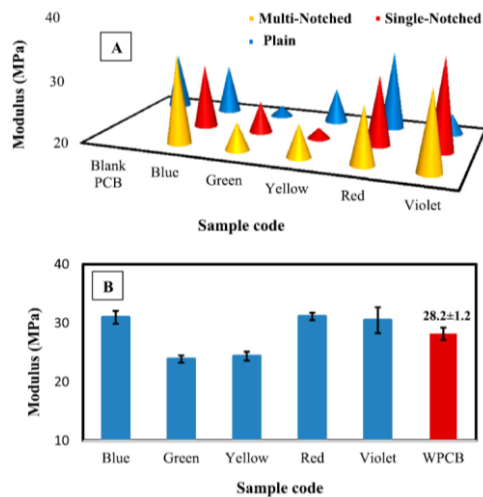
Annex 3 A) Variations in strength of WPCB samples and B) Average strength of WPCB samples



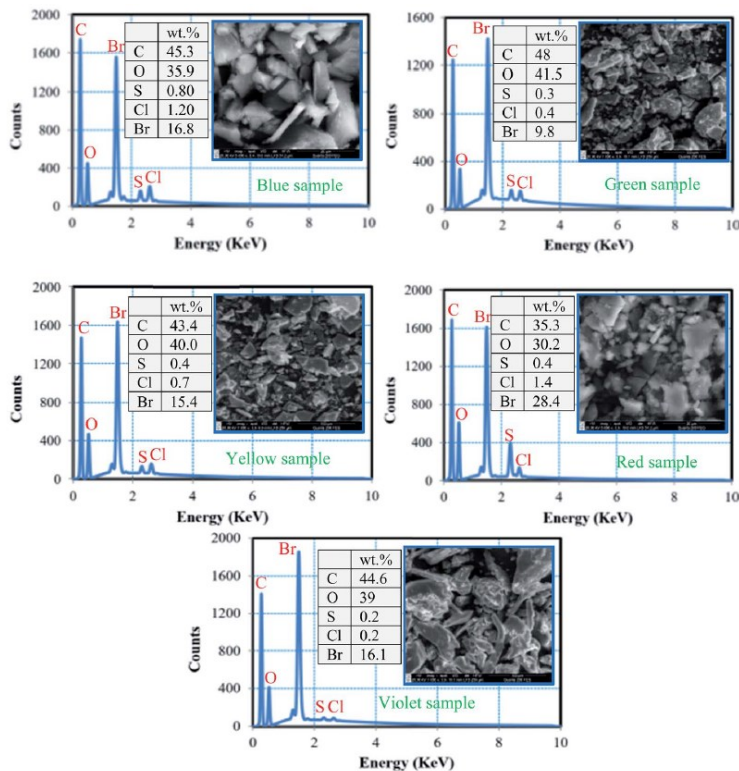
Annex 4 A) Variations in strain of WPCB samples and B) Average strain of WPCB samples.



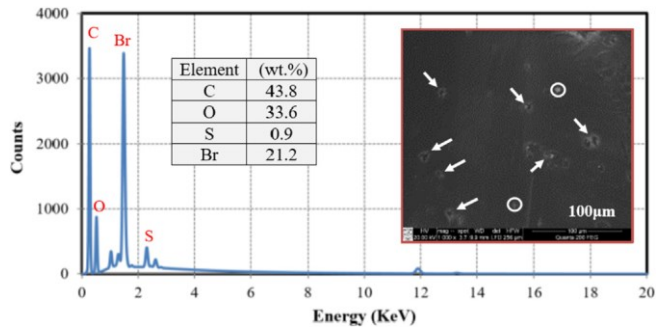
Annex 5 A) Variation in Young’s modulus of WPCB samples and B) Average Young’s modulus of WPCB samples



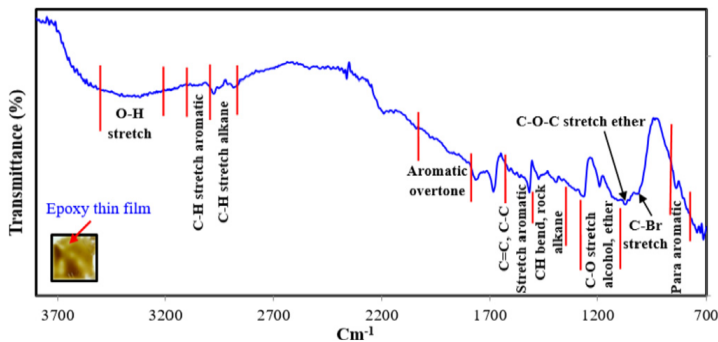
Annex 6 SEM-EDS analysis of recovered Brominated Epoxy Resin (Motherboards, sample codes in Table 2.4.1.)



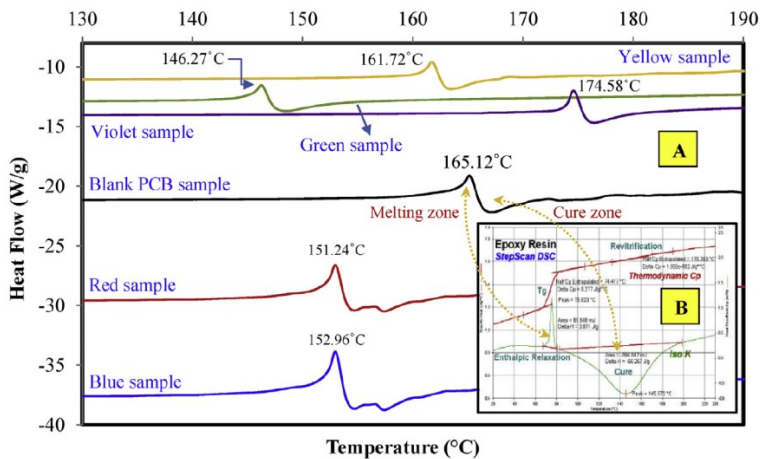
Annex 7 SEM-EDS analysis of recovered Brominated Epoxy Resin (Video Card)



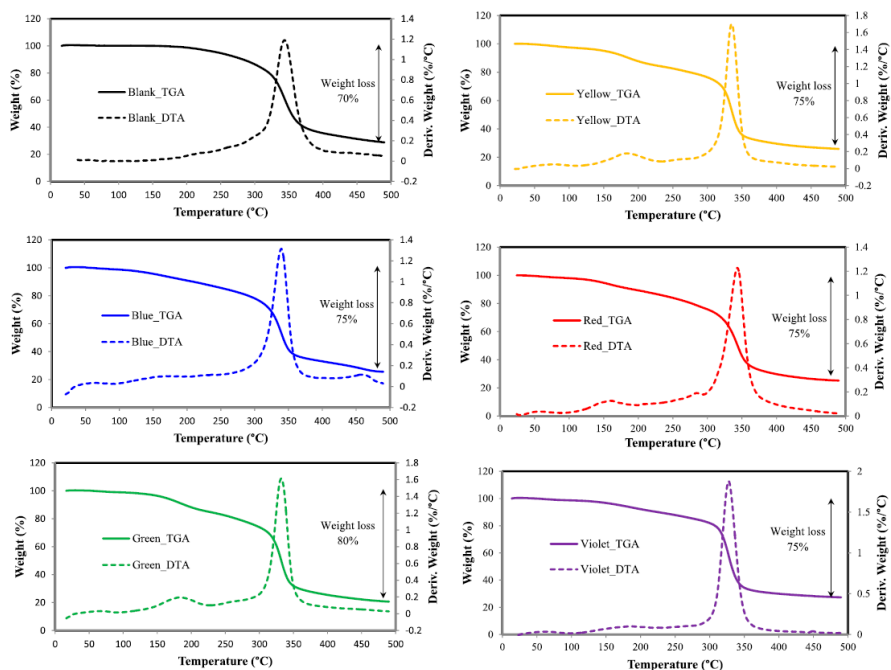
Annex 8 FTIR spectra of thin epoxy residue film (Video Card)



Annex 9 FTIR spectra A) Typical DSC curves of blank PCB and WPCB samples and B) Analyzed results for the StepScan DSC data for the epoxy resin (Sichina, 2000) (motherboards, sample codes in Table 2.5.1.)



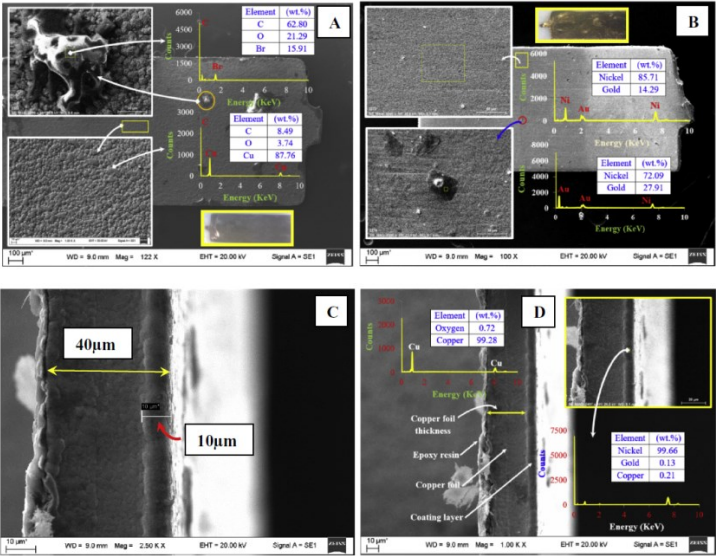
Annex 10 TGA-DTG analysis of recovered epoxy resin (motherboards, sample codes in Table 2.5.1.)



Annex 11 Chemical composition of the recovered metal foils

Sample type	Metal impurities, mg/kg								
	Al	Cd	Co	Fe	Mg	Mn	Ni	Pb	Zn
MB	136	86	72	260	221	96	168	210	249
VC	83	62	56	238	198	62	96	186	220
RAM	26	29	21	100	71	39	36	78	100

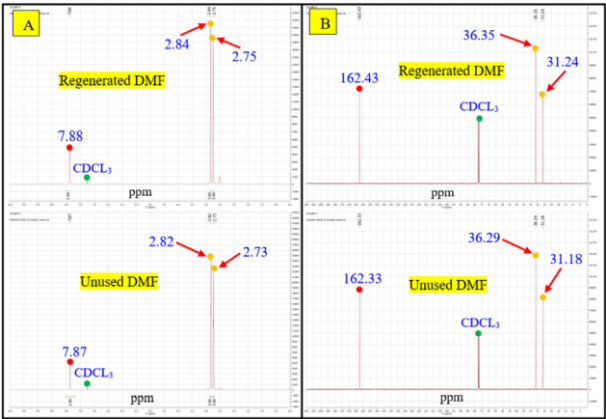
Annex 12 SEM-EDS images of RAM contact: A) Base metal side with adhered BER particles, B) Coating metal side, C) Cross section – thickness of layers, D) Cross section – elemental composition of base metal and undercoating layers



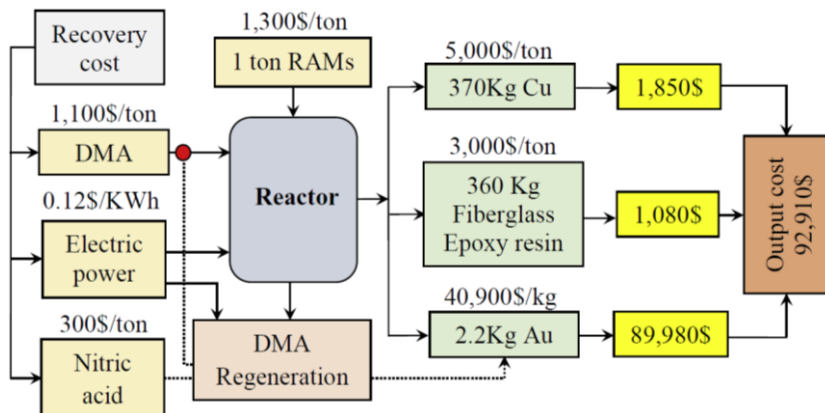
Annex 13 Composition of the liberated THSJ samples

Sample code	Element (mg/L)							Sum (mg/L)
	Al	Cu	Fe	Ni	Pb	Sn	Pd	
THSJ _M	84.0415	13985	637.65	99.21	15124	22686	2.326	52451.74
THSJ _V	52.3585	13935	-----	620.20	15070	22605	2.403	
Average	68.2	13960	318.825	359.705	15097	22645.5	2.5145	

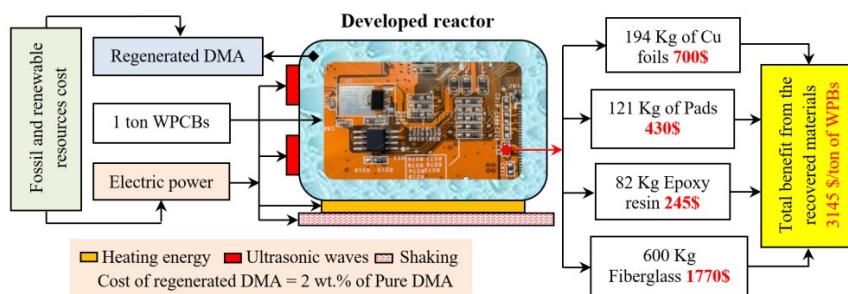
Annex 14 A) ¹H-NMR B) ¹³C-NMR spectra of unused and regenerated DMF



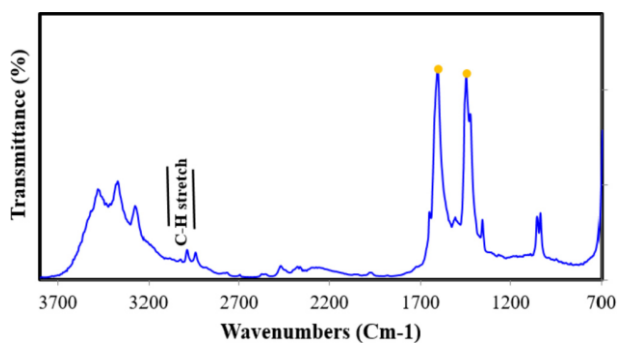
Annex 15 Boundaries and economic performance of the developed technique (RAM)



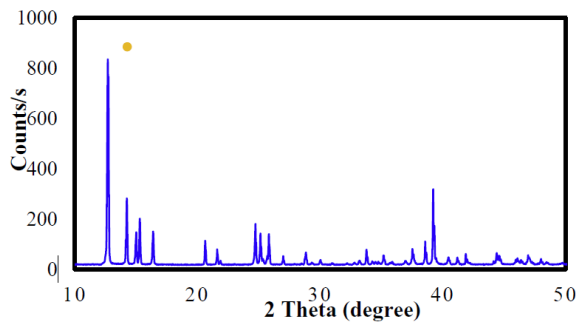
Annex 16 Boundaries and economic performance of the developed technique (MB)



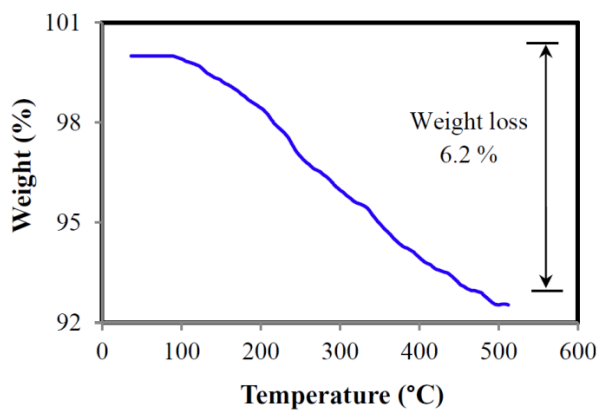
Annex 17 FTIR spectra of produced copper (II) acetate



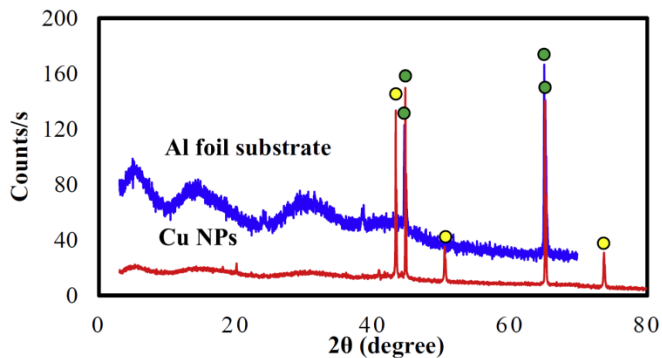
Annex 18 XRD pattern of copper (II) acetate



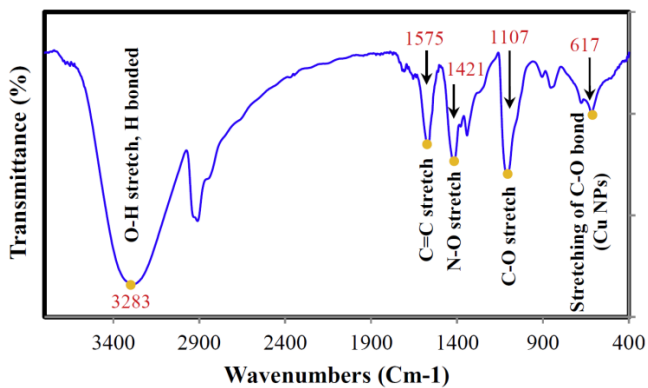
Annex 19 TGA analysis of the synthesized Cu-NPs (Electrospinning)



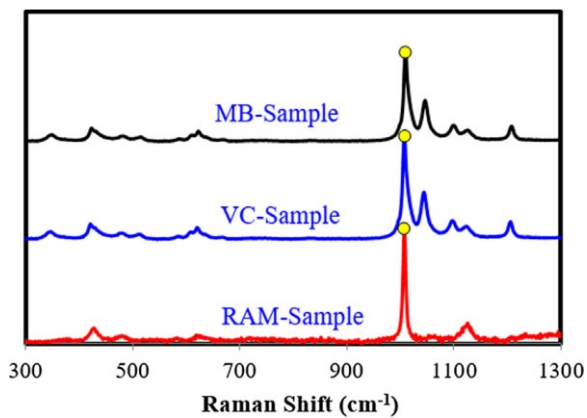
Annex 20 XRD patterns of substrate and synthesized Cu-NPs (Electrospinning)



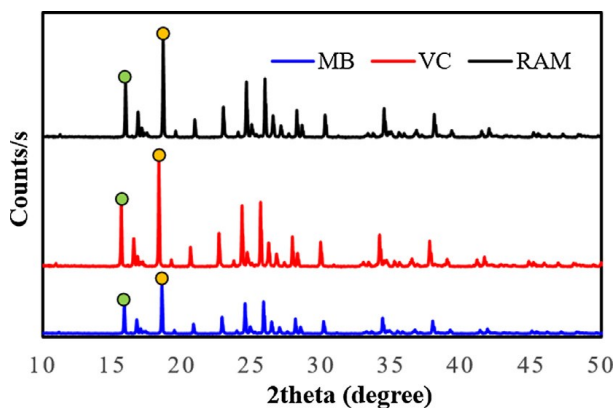
Annex 21 FTIR spectra of the obtained Cu-NPs (Electrospinning)



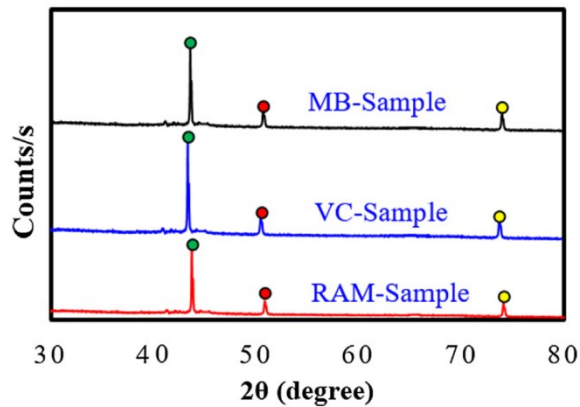
Annex 22 Raman Spectra of the produced Copper (II) Sulfate (Green synthesis)



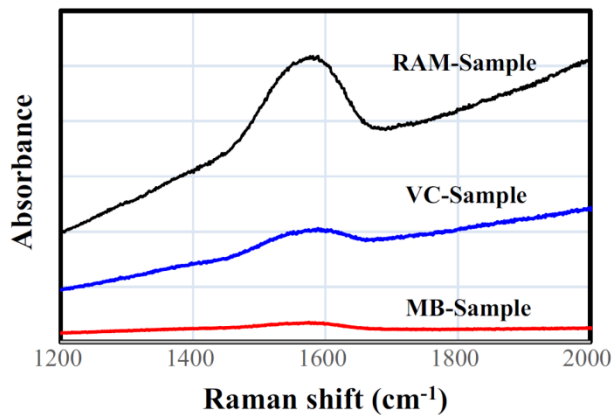
Annex 23 XRD pattern of the produced Copper (II) Sulfate (Green synthesis)



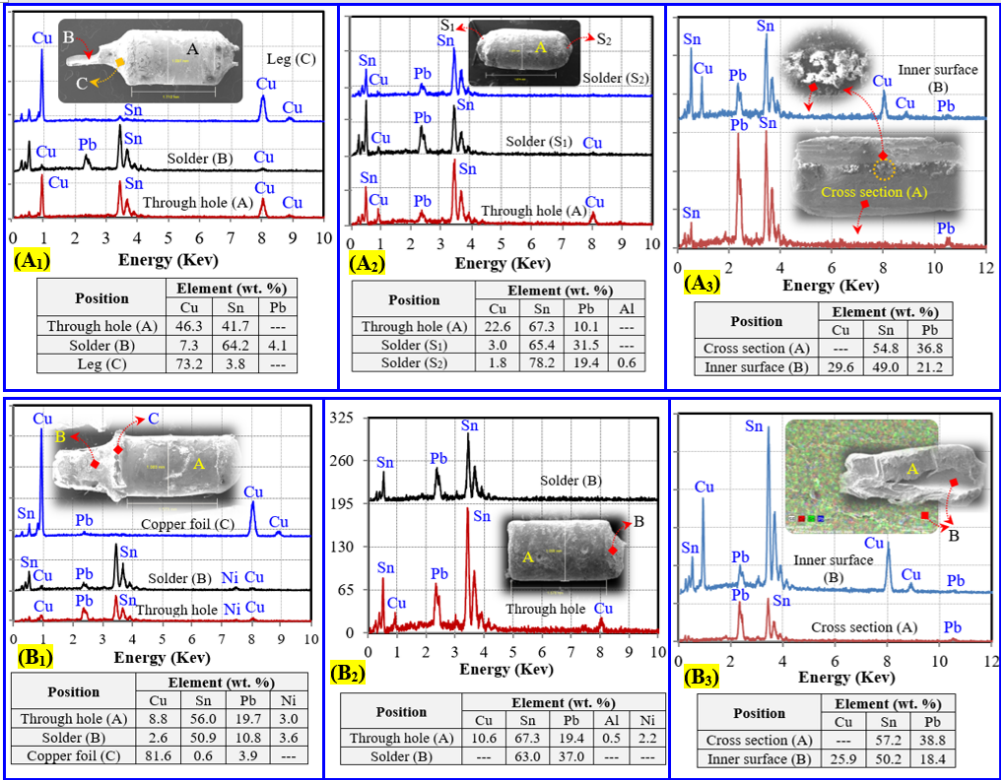
Annex 24 XRD patterns of Cu-NPs synthesized from metal of MB, VC and RAM (Green synthesis)



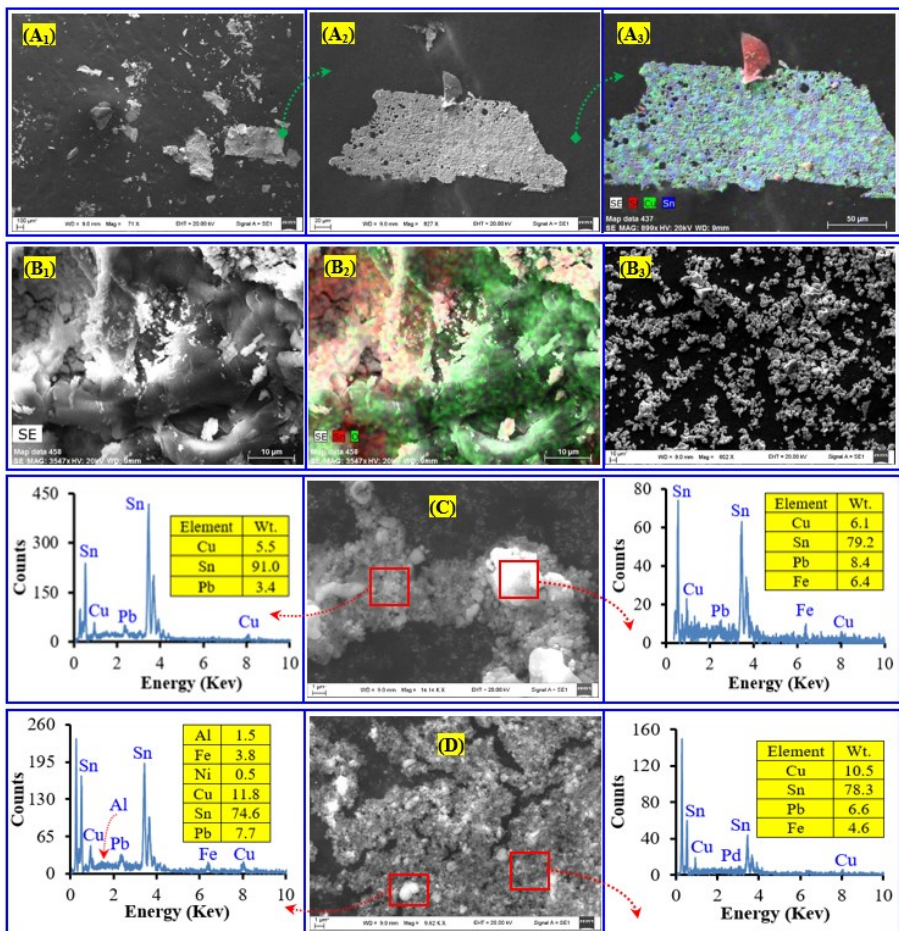
Annex 25 Raman spectra of Cu-NPs synthesized from metal of MB, VC and RAM (Green synthesis)



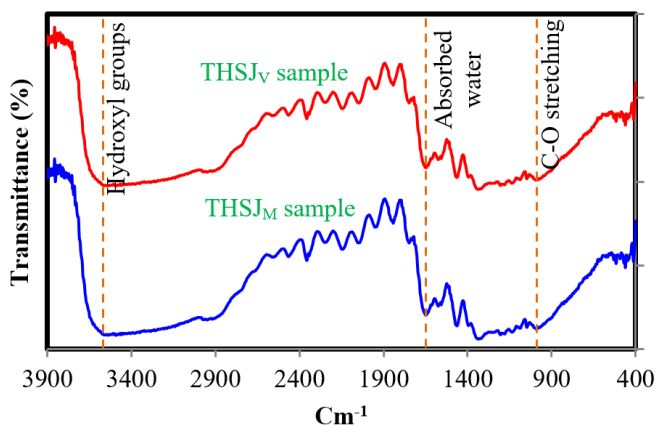
Annex 26 Images illustrating Trough-Hole Solder Joint leaching steps at different periods of time: A₁₋₃ – Motherboard, B₁₋₃ – Video Card



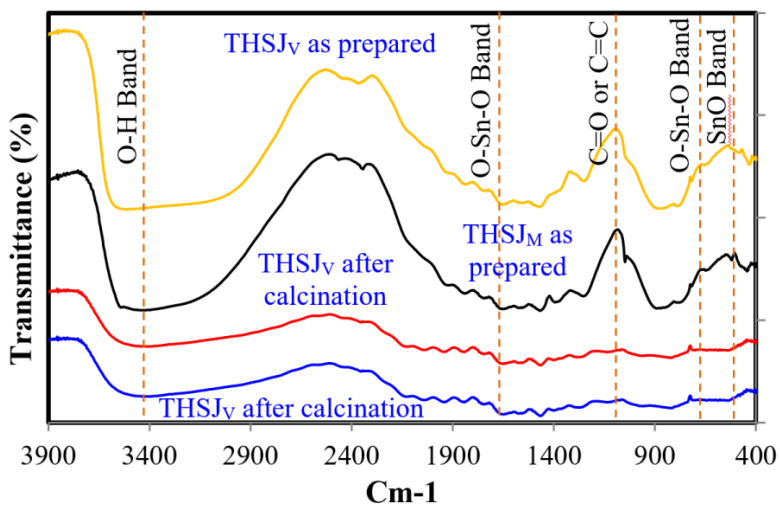
Annex 27 SEM-EDs analysis of the leached THSJs precipitate: A₁₋₃ – Motherboard, B₁₋₃ – Video Card, C, D – metallic precipitate from Motherboard and Video Card



Annex 28 FTIR spectra of the recovered $\text{Cu}(\text{OH})_2$



Annex 29 FTIR spectra of the prepared SnO_2 nanoparticles after and before calcination



SL344. 2019-05-31, 21,75 leidyb. apsk. l. Tiražas 14 egz. Užsakymas 121.
Išleido Kauno technologijos universitetas, K. Donelaičio g. 73, 44249 Kaunas
Spausdino leidyklos „Technologija“ spaustuvė, Studentų g. 54, 51424 Kaunas